

NASA Conference Publication 10087
Part 4

First Annual High-Speed Research Workshop

(NASA-CP-10087-Pt-4) FIRST ANNUAL
HIGH-SPEED RESEARCH WORKSHOP, PART
4 (NASA. Langley Research Center)
390 p

N94-33517
--THRU--
N94-33531
Unclass

G3/02 0011975

Compiled by
Allen H. Whitehead, Jr.
Langley Research Center
Hampton, Virginia

Proceedings of a workshop sponsored by the
National Aeronautics and Space Administration,
Washington, D.C., and held in
Williamsburg, Virginia
May 14-16, 1991

APRIL 1992

Date for general release April 30, 1994

NASA

National Aeronautics and
Space Administration

Langley Research Center
Hampton, Virginia 23665-5225

1
 2
 3

•

—

■

●

▽

—

—

10

10

100

...

—

...

10

1

2

10

⋮

—

100

• • • •

1

FOREWORD

The First Annual High-Speed Research (HSR) Workshop was hosted by NASA Langley Research Center and was held May 14-16, 1991, in Williamsburg, Virginia. The purpose of the workshop was to provide a national forum for the government, industry and university participants in the program to present and discuss important technology issues related to the development of a commercially viable, environmentally compatible U.S. High-Speed Civil Transport. The workshop sessions and this publication are organized around the major task elements in NASA's Phase I - High-Speed Research Program which basically addresses the environmental issues of atmospheric emissions, community noise and sonic boom.

The opening Plenary Session provided program overviews and summaries by senior management from NASA and industry. The remaining twelve technical sessions were organized to preview the content of each program element, to discuss planned activities and to highlight recent accomplishments.

Attendance at the workshop was by invitation only and included only industry, academic and government participants who were actively involved in the High-Speed Research Program. The technology presented at the meeting is considered commercially sensitive, and as such, the conference results and this publication are protected by the NASA designation **LIMITED DISTRIBUTION**.

THIS PAGE INTENTIONALLY BLANK

TABLE OF CONTENTS

Part I*

FOREWORD	i
TABLE OF CONTENTS	iii
SESSION I. -- Plenary Session	
A. Headquarters Perspective	3
<i>Robert E. Anderson, NASA Headquarters, Code RJ</i>	
B. Boeing HSCT Program Summary	25
<i>Michael L. Henderson, Boeing Commercial Airplane Group</i>	
C. Update on Douglas' High-Speed Civil Transport Studies	93
<i>Bruce L. Bunin, Douglas Aircraft Company</i>	
D. General Electric/Pratt & Whitney Summary Report	135
<i>Samuel C. Gilkey, GE Aircraft Engines</i>	
<i>Richard W. Hines, Pratt & Whitney Aircraft</i>	
E. NASA Headquarter's Summary Reports	197
<i>Howard L. Wesoky, Code RJ, Dr. Michael J. Prather, Code EEU, John R. Facey,</i>	
<i>Code RP, George F. Unger, Code RF, and Samuel L. Venneri, Code RM</i>	
SESSION II. -- Airframe Systems Studies	
A. NASA High-Speed Civil Transport Studies--Airframe Systems Studies Review	303
<i>Frank D. Neumann, Boeing Commercial Airplane Group</i>	
B. Douglas Aircraft HSCT--Status and Future Research Needs	359
<i>H. Robert Welge, Douglas Aircraft Company</i>	
C. High-Speed Research Program Systems Analysis Activities at Ames Research Center	385
<i>George H. Kidwell, NASA Ames Research Center</i>	
D. Overview of Langley Systems Studies	421
<i>Samuel D. Dollyhigh, NASA Langley Research Center</i>	
SESSION III. -- Atmospheric Effects	
A. Stratospheric Models and Measurements: A Critical Comparison	459
<i>Dr. Ellis E. Remsberg, NASA Langley Research Center</i>	
B. Previous Model Comparisons	465
<i>Charles H. Jackman, NASA Goddard Space Flight Center</i>	
C. Model Capabilities, 3-D	469
<i>Dr. William L. Grose, NASA Langley Research Center</i>	
D. Model Capabilities, 2-D	471
<i>Charles H. Jackman, NASA Goddard Space Flight Center</i>	

*Published under separate cover.

SESSION III. -- Atmospheric Effects (continued)

E. Quality of Existing Data Sets - Total Ozone and Chemical Species	477
<i>Dr. Richard McPeters, NASA Goddard Space Flight Center</i>	
<i>Dr. Stephen R. Kawa, NOAA</i>	
F. Comparison of the Impact of Volcanic Eruptions and Aircraft Emissions on the Aerosol ...	479
Mass Loading and Sulfur Budget in the Stratosphere	
<i>Dr. Glenn K. Yue and Dr. Lamont R. Poole, NASA Langley Research Center</i>	
G. High Resolution Infrared Datasets Useful for Validating Stratospheric Models	497
<i>Curtis P. Rinsland, NASA Langley Research Center</i>	

Part II*

SESSION IV. -- Source Noise

A. NASA HSR Phase I Low Noise Nozzle Technology Program Overview	507
<i>Bernard J. Blaha, NASA Lewis Research Center</i>	
B. High-Speed Jet Noise Research at NASA Lewis	517
<i>Eugene A. Krejsa, B. A. Cooper and C. M. Kim, NASA Lewis Research Center</i>	
<i>Abbas Khavaran, Sverdrup Technology, Inc.</i>	
C. HSCT Nozzle Source Noise Programs at Pratt & Whitney	533
<i>Alfred M. Stern, Pratt & Whitney Aircraft</i>	
D. HSCT Noise Reduction Technology Development at General Electric Aircraft Engines	551
<i>Rudramuni K. Majjigi, GE Aircraft Engines</i>	
E. Community Noise Sources and Noise Control Issues	591
<i>Gene L. Nihart, Boeing Commercial Airplane Group</i>	
F. NASA LaRC Jet Plume Research	607
<i>Dr. John M. Seiner, Michael K. Ponton and James C. Manning, NASA Langley Research Center</i>	
G. Theoretical Aspects of Supersonic Jet Noise	645
<i>Dr. Christopher K. W. Tam, Florida State University</i>	

SESSION V. -- Sonic Boom (Aerodynamic Performance)

A. Sonic Boom Program Overview and Sonic Boom Source Design/Prediction/Performance ..	665
Overview	
<i>Dr. Christine M. Darden, NASA Langley Research Center</i>	
B. Design and Analysis of Low Boom Concepts at Langley Research Center	673
<i>Dr. Christine M. Darden, Robert J. Mack, Kathy E. Needleman, Daniel G. Baize,</i>	
<i>Peter G. Coen, Raymond L. Barger, N. Duane Melson, Mary S. Adams, Elwood W. Shields</i>	
<i>and Marvin E. McGraw, Jr., NASA Langley Research Center</i>	
C. HSCT Design for Reduced Sonic Boom	701
<i>George T. Haglund, Boeing Commercial Airplane Group</i>	

*Published under separate cover.

SESSION V. -- Sonic Boom (Aerodynamic Performance)(continued)

D. Sonic Boom Prediction and Minimization Using Computational Fluid Dynamics	721
<i>Dr. Thomas A. Edwards and Raymond Hicks, NASA Ames Research Center</i>	
<i>Samson Cheung, MCAT Institute</i>	
<i>Susan Cliff-Hovey, Mike Madson and Joel Mendoza, NASA Ames Research Center</i>	
E. Sonic Boom Configuration Minimization	739
<i>Robert A. Sohn, Douglas Aircraft Company</i>	
F. Sonic Boom Predictions Using a Modified Euler Code	757
<i>Dr. Michael J. Siclari, Grumman Corporate Research Center</i>	
G. Overview of Feasibility Study on Conducting Overflight Measurements of Shaped	785
Sonic Boom Signatures Using RPV's	
<i>Domenic J. Maglieri, Victor E. Sothcott, Thomas N. Keefer and Percy J. Bobbitt, Eagle Engineering, Inc. - Hampton Division</i>	

SESSION VI. -- Propulsion Systems Studies

A. The NASA Sponsored HSCT Propulsion Studies	811
<i>William C. Strack, NASA Lewis Research Center</i>	
B. A NASA Lewis Comparative Propulsion System Assessment for the High-Speed Civil	829
Transport	
<i>Jeffrey J. Berton, William J. Haller, Jonathon A. Seidel and Paul F. Senick, NASA Lewis Research Center</i>	
C. Pratt & Whitney/General Electric Propulsion Systems Studies Introduction	867
<i>Samuel C. Gilkey, GE Aircraft Engines; and Richard W. Hines, Pratt & Whitney Aircraft</i>	
D. Results of GEAE HSCT Propulsion System Studies	879
<i>Fred H. Krause, GE Aircraft Engines</i>	
E. Pratt & Whitney Propulsion Systems Studies Results/Status	919
<i>Martin G. Smith, Jr. and George A. Champagne, Pratt & Whitney Aircraft</i>	

SESSION VII. -- Emission Reduction

A. Low Emissions Combustor Technology for High-Speed Civil Transport Engines	951
<i>Richard W. Niedzwiecki, NASA Lewis Research Center</i>	
B. Theoretical Study of Thermodynamic Properties and Reaction Rates of Importance	965
in the High-Speed Research Program	
<i>Stephen Langhoff, Dr. Charles W. Bauschlicher, Jr. and Richard Jaffe, NASA Ames Research Center</i>	
C. HSR Combustion Analytical Research	981
<i>Dr. H. Lee Nguyen, NASA Lewis Research Center</i>	
D. LeRC In-House Experimental Research	997
<i>Dr. Valerie J. Lyons, NASA Lewis Research Center</i>	
E. Lean Burn Combustor Technology at GE Aircraft Engines	1025
<i>Willard J. Dodds, GE Aircraft Engines</i>	
F. Rich Burn Combustor Technology at Pratt & Whitney	1043
<i>Robert P. Lohmann, Pratt & Whitney Aircraft</i>	
<i>T. J. Rosfford, United Technologies Research Center</i>	

SESSION VII. -- Emission Reduction (continued)

G. Low NO _x Combustor Design	1057
<i>Dr. Hukam Mongia, Allison</i>	
H. Low NO _x Mixing Research	1059
<i>Professor Scott Samuelson, University of California-Irvine</i>	

Part III*

SESSION VIII. -- Aeroacoustic Analysis and Community Noise

A. Aeroacoustics Analysis and Community Noise Overview	1063
<i>Robert A. Golub, NASA Langley Research Center</i>	
<i>Paul T. Soderman, NASA Ames Research Center</i>	
B. New Broadband Shock Noise Model and Computer Code for ANOPP	1073
<i>N. N. Reddy, Lockheed Aeronautical Systems Company</i>	
C. Community Noise Technology Needs - Boeings Perspective	1103
<i>Gene L. Nihart, Boeing Commercial Airplane Group</i>	
D. HSCT Climb to Cruise Noise Assessment	1121
<i>Alan K. Mortlock, Douglas Aircraft Company</i>	
E. ANOPP/VMS HSCT Ground Contour System	1135
<i>John W. Rawls, Jr. and Louis J. Glaab, Lockheed Engineering and Sciences Company</i>	
F. High Performance Jet-Engine Flight Test Data Base for HSR	1159
<i>Jeffrey Kelly, Lockheed Engineering and Sciences Company</i>	
G. Status and Plans for the ANOPP/HSR Prediction System	1179
<i>Sandra K. Nolan, Lockheed Engineering and Sciences Company</i>	

SESSION IX. -- Sonic Boom (Human Response and Atmospheric Effects)

A. Atmospheric Effects on Sonic Boom--A Program Review	1199
<i>Dr. Gerry L. McAninch, NASA Langley Research Center</i>	
B. Relaxation and Turbulence Effects on Sonic Boom Signatures	1209
<i>Dr. Allan D. Pierce and Victor W. Sparrow, Pennsylvania State University</i>	
C. The Effect of Turbulence and Molecular Relaxation on Sonic Boom Signatures	1241
<i>Dr. Kenneth J. Plotkin, Wyle Laboratories</i>	
D. Statistical and Numerical Study of the Relation Between Weather and Sonic Boom	1263
Characteristics	
<i>Lixin Yao, Dr. Henry E. Bass and Richard Raspet, The University of Mississippi</i>	
<i>Walton E. McBride, Planning Systems, Inc.</i>	
E. Overview of NASA Human Response to Sonic Boom Program	1285
<i>Dr. Kevin P. Shepherd, NASA Langley Research Center</i>	
F. Sonic Boom Acceptability Studies	1293
<i>Dr. Kevin P. Shepherd, NASA Langley Research Center</i>	
<i>Brenda M. Sullivan, Lockheed Engineering and Sciences Company</i>	
<i>Dr. Jack E. Leatherwood and David A. McCurdy, NASA Langley Research</i>	

*Published under separate cover.

SESSION IX. -- Sonic Boom (Human Response and Atmospheric Effects)(continued)

G. Georgia Tech Sonic Boom Simulator	1313
<i>Dr. Krish K. Ahuja, Georgia Institute of Technology</i>	
H. Sonic Boom (Human Response and Atmospheric Effects) Outdoor-to-Indoor Response ...	1343
to Minimized Sonic Booms	
<i>David Brown, Wyle Research</i>	
<i>Louis C. Sutherland, Consultant to Wyle</i>	

SESSION X. -- Airframe/Propulsion Integration

A. PAI Session Overview and Review of Lewis PAI Efforts	1367
<i>Peter G. Batterton, NASA Lewis Research Center</i>	
B. Nacelle-Wing Integration	1381
<i>Gelsomina Cappuccio, NASA Ames Research Center</i>	
C. HSCT Inlet Development Issues	1401
<i>Joseph L. Koncsek, Boeing Commercial Airplane Group</i>	
D. Status of an Inlet Configuration Trade Study for the Douglas HSCT	1423
<i>Jay R. Jones and H. Robert Welge, Douglas Aircraft Company</i>	
E. Transonic Airframe Propulsion Integration	1437
<i>Robert E. Coltrin and Bobby W. Sanders, NASA Lewis Research Center</i>	
<i>Daniel P. Bencze, NASA Ames Research Center</i>	
F. Results of a Preliminary Investigation of Inlet Unstart on a High-Speed Civil	1461
Transport Airplane Concept	
<i>Christopher S. Domack, Lockheed Engineering and Sciences Company</i>	
G. Status of the Variable Diameter Centerbody Inlet Program	1481
<i>John E. Saunders and A. A. Linne, NASA Lewis Research Center</i>	
H. HSCT Integrated Propulsion Control Issues	1505
<i>Christopher M. Carlin, Boeing Commercial Airplane Group</i>	

SESSION XI. -- Airframe and Engine Materials

A. Enabling Propulsion Materials for High-Speed Civil Transport Engines	1521
<i>Joseph R. Stephens and Dr. Thomas P. Herbell, NASA Lewis Research Center</i>	
B. Combustor Materials Requirements and Status of Ceramic Matrix Composites	1547
<i>Ralph J. Hecht, Pratt & Whitney Aircraft</i>	
<i>Andrew M. Johnson, GE Aircraft Engines</i>	
C. Nozzle Material Requirements and the Status of Intermetallic Matrix Composites	1565
<i>Andrew M. Johnson, GE Aircraft Engines</i>	
<i>Ralph J. Hecht, Pratt & Whitney Aircraft</i>	
D. Airframe Materials for HSR	1583
<i>Thomas T. Bales, NASA Langley Research Center</i>	
E. HSR Airframe Materials - The Boeing Perspective	1607
<i>Donald L. Grande, Boeing Commercial Airplane Group</i>	
F. HSCT Materials and Structures - An MDC Perspective	1623
<i>Jay O. Sutton, Douglas Aircraft Company</i>	

Part IV

SESSION XII. -- High Lift

A. Overview of NASA HSR High-Lift Program	1645	-1
<i>William P. Gilbert, NASA Langley Research Center</i>		
B. Status of LaRC HSR High-Lift Research	1661	-2
<i>Dr. Paul L. Coe, Jr., NASA Langley Research Center</i>		
C. Status of CFD for LaRC's HSR High-Lift Program	1693	-3
<i>Edgar G. Waggoner and Jerry C. South, Jr., NASA Langley Research Center</i>		
D. HSR High Lift Research Program--Status and Plans	1719	-4
<i>Jim Rose, NASA Ames Research Center</i>		
E. HSCT High Lift System Aerodynamic Requirements	1739	-5
<i>John A. Paulson, Boeing Commercial Airplane Group</i>		
F. HSCT High-Lift Technology Requirements	1765	-6
<i>D. L. Antani and J. M. Morgenstern, Douglas Aircraft Company</i>		
G. Lift Enhancement by Trapped Vortex	1789	-7
<i>Vernon J. Rossow, NASA Ames Research Center</i>		

SESSION XIII. -- Supersonic Laminar Flow Control

A. NASA F-16XL Supersonic Laminar Flow Control Program Overview	1809	-8
<i>Dr. Michael C. Fischer, NASA Langley Research Center</i>		
B. Supersonic Laminar Flow Control - Challenges and Opportunities	1821	-9
<i>Arthur G. Powell, Douglas Aircraft Company</i>		
C. Status of the F-16XL Supersonic Laminar Flow Control Numerical Design Validation	1841	-10
<i>Mike George, Rockwell International</i>		
<i>Marta Bohn-Meyer and Bianca Anderson, NASA Ames-Dryden Flight Research Facility</i>		
D. Code Validation for the Simulation of Supersonic Viscous Flow About the F-16XL	1891	-11
<i>Jolen Flores, Eugene Tu and Lyndell King, NASA Ames Research Center</i>		
E. Inviscid and Viscous Flow Calculations for the F-16XL Configuration	1909	-12
<i>Dr. Vinket Iyer, Vigyan, Inc.</i>		
F. Linear Stability Theory and Three-Dimensional Boundary Layer Transition	1975	-13
<i>Robert E. Spall and Mujeeb Malik, High Technology Corporation</i>		
G. Supersonic HLFC: Potential Benefits and Technology Development Requirements	2001	-14
<i>Frank Neumann, Boeing Commercial Airplane Group</i>		

omit

Session XII. High Lift

THIS PAGE INTENTIONALLY BLANK

Session XII. High Lift

Overview of NASA HSR High-Lift Program

William P. Gilbert, NASA Langley Research Center

THIS PAGE INTENTIONALLY BLANK

OVERVIEW OF NASA HSR HIGH-LIFT PROGRAM

51-02
11976

W. P. Gilbert
NASA Langley Research Center
Hampton, VA

First Annual High-Speed Research Workshop
May 14-16, 1991

INTRODUCTION

The NASA High-Speed Research Program is being conducted to develop the technologies essential for the successful U.S. development of a commercial supersonic air transport in the 2005 timeframe. The HSR program is being conducted in two phases, with the first phase stressing technology to ensure environmental acceptability and the second phase stressing technology to make the vehicle economically viable (in contrast to the current Concorde design). During Phase I of the program, a key element of the environmental emphasis is minimization of community noise through effective engine nozzle noise suppression technology and through improving the performance of high-lift systems.

This presentation presents an overview of the current Phase I High-Lift Program which is directed at technology for community noise reduction. The total target for takeoff engine noise reduction to meet expected regulations is believed to be about 20 EPNdB. As noted in Figure 1, the high-lift research is stressing the exploration of innovative high-lift concepts and advanced flight operations procedures to achieve a substantial (approximately 6 EPNdB) reduction in community noise to supplement the reductions expected from engine nozzle noise suppression concepts; primary concern is focused on the takeoff and climbout operations where very high engine power settings are used. Significant reductions in aerodynamic drag in this regime will allow substantial reductions in the required engine thrust levels and therefore reductions in the noise generated.

HIGH-LIFT REDUCES COMMUNITY NOISE

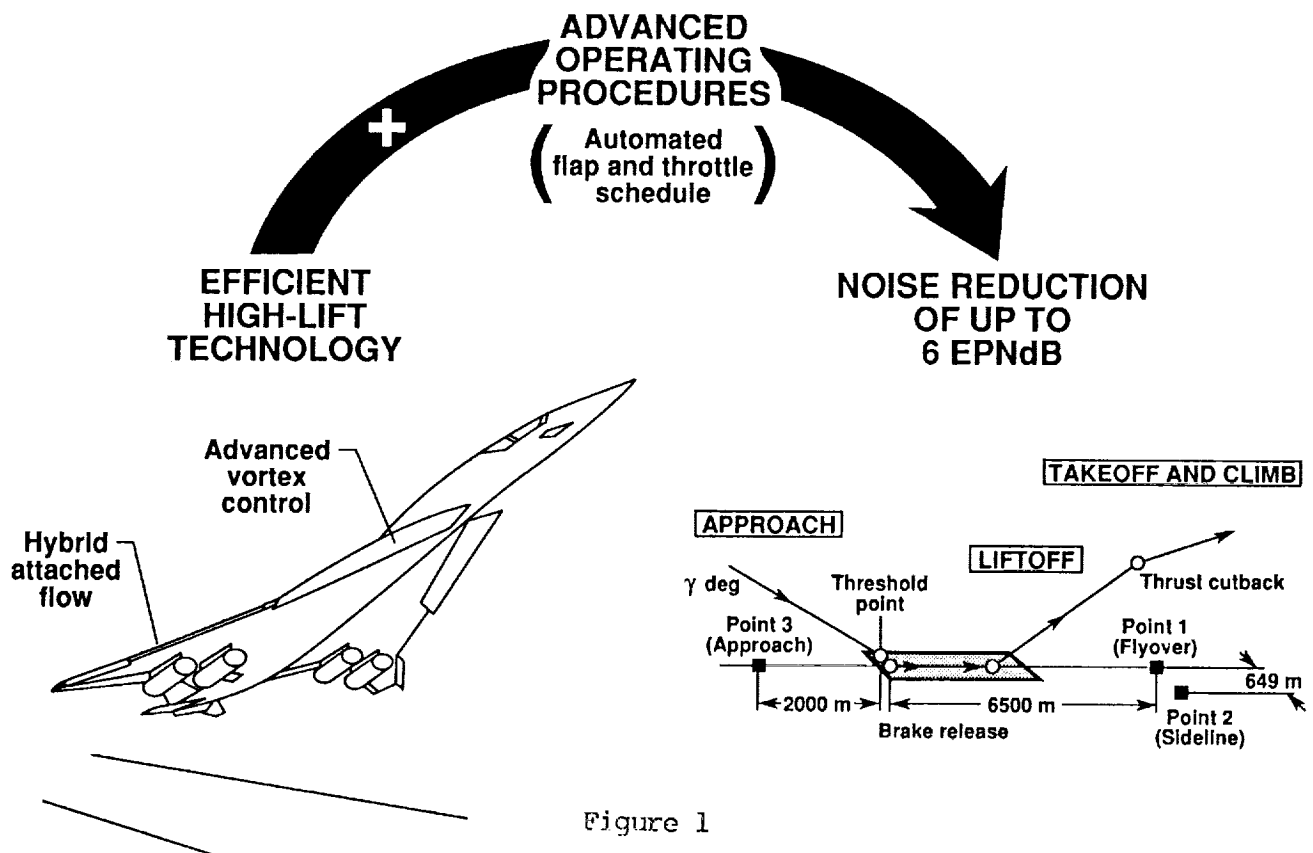


Figure 1

AERODYNAMIC POTENTIAL (Takeoff and Climb)

To achieve the objective of lower thrust (and therefore noise), the high-lift work is examining not only obtaining high values of useful lift but also getting these levels with the best possible aerodynamic efficiency (L/D). As illustrated in figure 2, the desired speeds for takeoff and climb place a highly swept-wing airplane like a supersonic transport in the lift coefficient range near and above the maximum values of L/D . In this regime, extensive flow separation is inevitable and both attached flow and separated flow high-lift concepts must be explored to successfully address the strong separated and vortical flows.

However, as noted in figure 2, there exists substantial room for improving L/D if one considers the difference in performance from a basic untreated swept wing to that ideally possible with fully attached flow. The goal in this program is to achieve levels of leading edge suction in the 80 to 85 percent range; this will produce the substantial improvements sought in L/D .

AERODYNAMIC POTENTIAL (Takeoff and Climb)

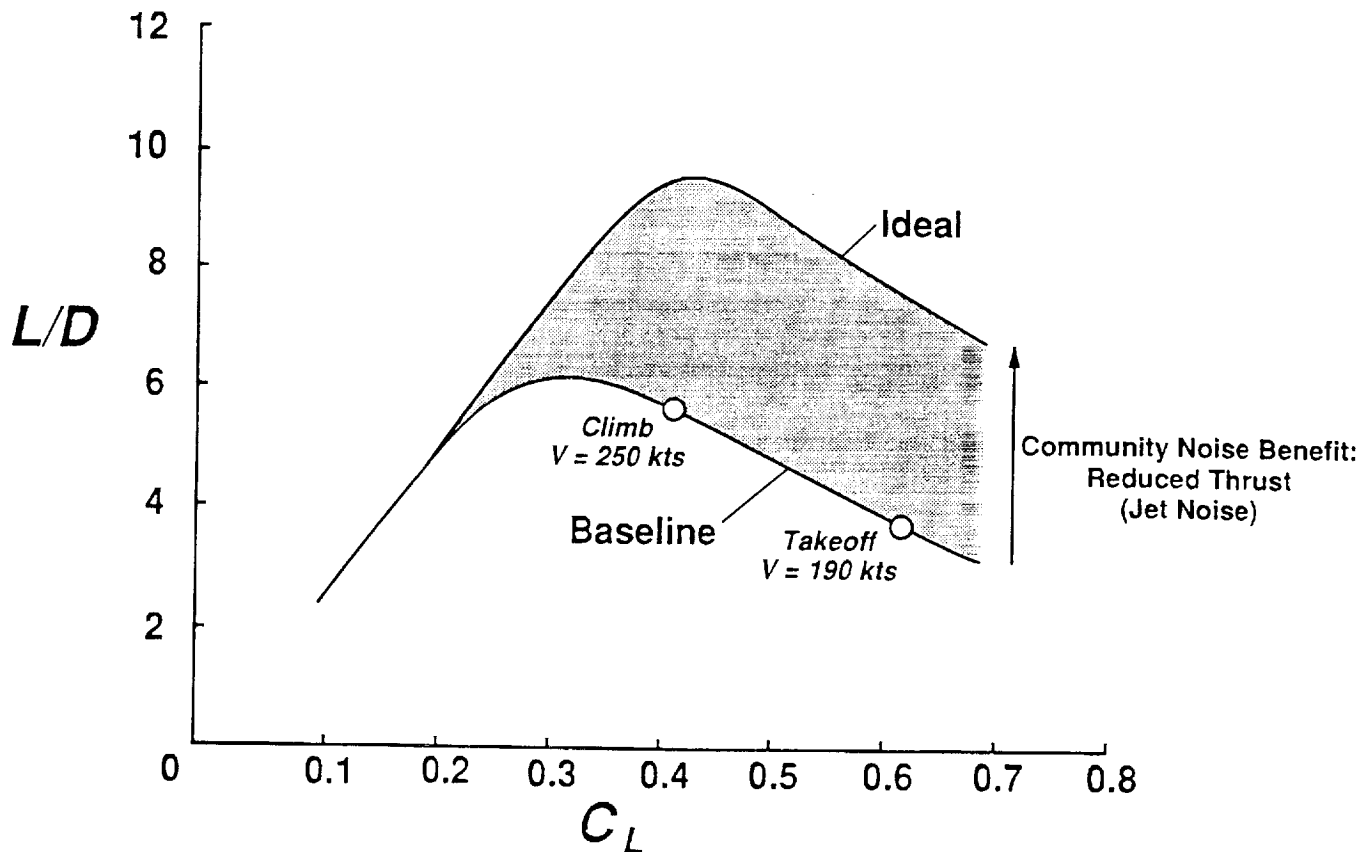


Figure 2

OBJECTIVES

The objectives of the HSR High-Lift research are outlined in figure 3 for both Phase I and Phase II. As already noted, in Phase I the principal emphasis of the high-lift work is to reduce the community noise. This effort involves exploration of high-lift concepts for both attached and separated flow control for both the leading edge and the trailing edge of the wing. During this research, the experimental and analytical efforts will be closely integrated to ensure good analyses codes are available to the designer for use in conducting the design trades during configuration integration. In addition, a key objective in Phase I is to quantify the possible gains in noise reduction from not only the aerodynamic concepts, but also the combination of these with new automated flight management procedures during landing, takeoff, and climbout.

Phase two objectives begin to shift the program focus to more detailed configuration integration efforts and toward extended concept validation tests involving large-scale testing and flight tests.

NASA HSR
HIGH LIFT
PROGRAM

OBJECTIVES

PHASE I - NOISE REDUCTION

- Concept exploration
- Method development & validation
- Payoff of specific concepts

PHASE II - PERFORMANCE

- Configuration integration trades
- Flight verification
 - methods
 - concepts

Figure 3

VORTEX FLAP FLIGHT EXPERIMENT

Completion of the recent vortex flap flight experiment on the F-106 airplane (shown in figure 4 below) at Langley has greatly increased confidence in the potential aerodynamic performance gains possible on highly swept wings operating at high values of lift. Gains predicted for this experiment were realized and correlated well with experiment and theory; much was learned during the indepth flight studies about the wing loading and flow field which was not evident from the earlier ground tests. The challenge now is to extend this type of technology to the more highly-swept, cranked planforms expected for the next generation of high-speed civil transports.

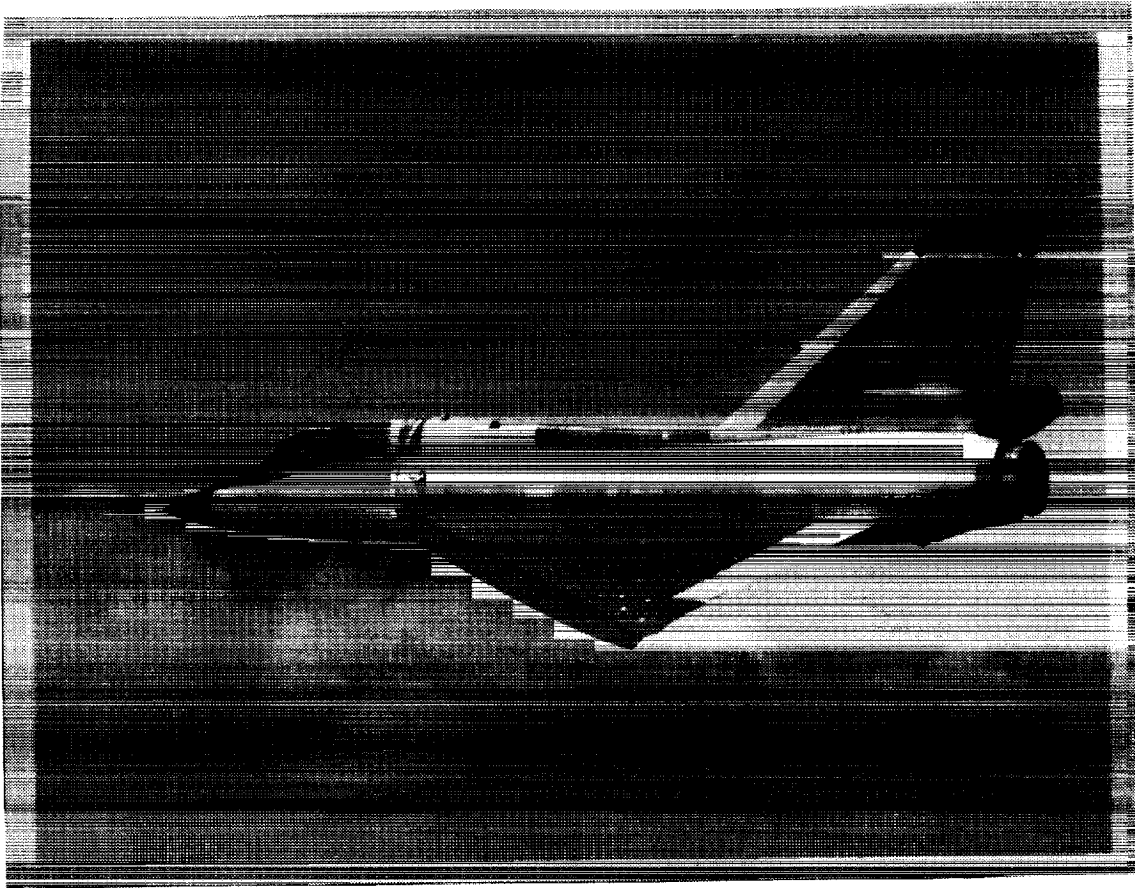
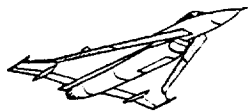


Figure 4

ORIGINAL PAGE
BLACK AND WHITE PHOTOGRAPH

F-16XL MODIFICATIONS FOR HIGH-LIFT RESEARCH

The range of high-lift concepts being studied in the current program is illustrated in the sketch shown in figure 5. The F-16XL will be used as a testbed in Phase II of the program to provide flight validation of both concepts and key aerodynamic prediction methods.



F-16XL MODIFICATIONS FOR HIGH-LIFT RESEARCH

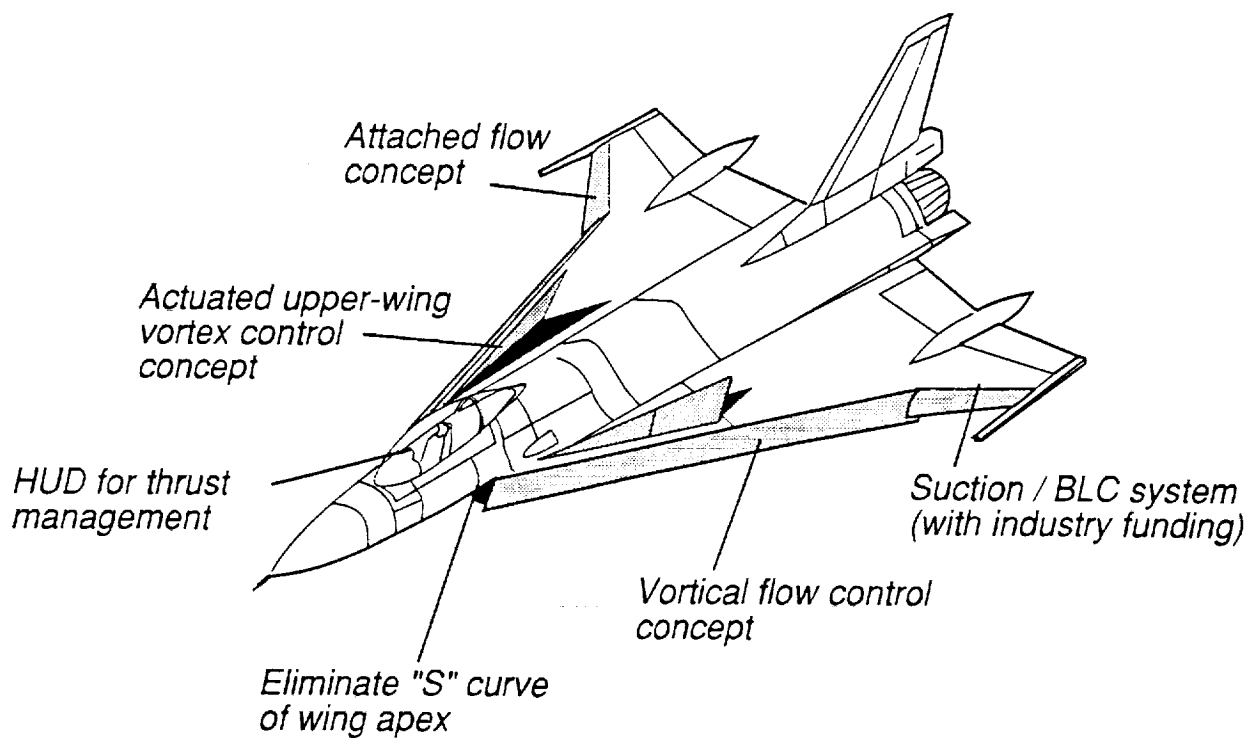


Figure 5

PROGRAM SCOPE AND APPROACH (FIGURE 6)

The NASA High-Speed Research (HSR), High-Lift Program scope ranges from CFD (Computational Fluid Dynamics) code development and application to High-Speed Civil Transport (HSCT) concepts, through extensive experimental investigations in wind-tunnels (and possibly flight tests), and to comprehensive piloted simulations to integrate aerodynamic gains with advanced flight procedures. The approach is to take maximum advantage of the extensive experience gained in the NASA Supersonic Cruise Aircraft Research (SCAR) program in selecting the high-lift concepts to explore and refine. This time around, we have much more powerful research tools in the CFD area and in wind tunnels (with facilities such as NTF).

A prime element in the approach for this program is the careful coordinated development of both promising high-lift concepts and the analysis and prediction methods needed for application of these concepts to various HSCT designs.

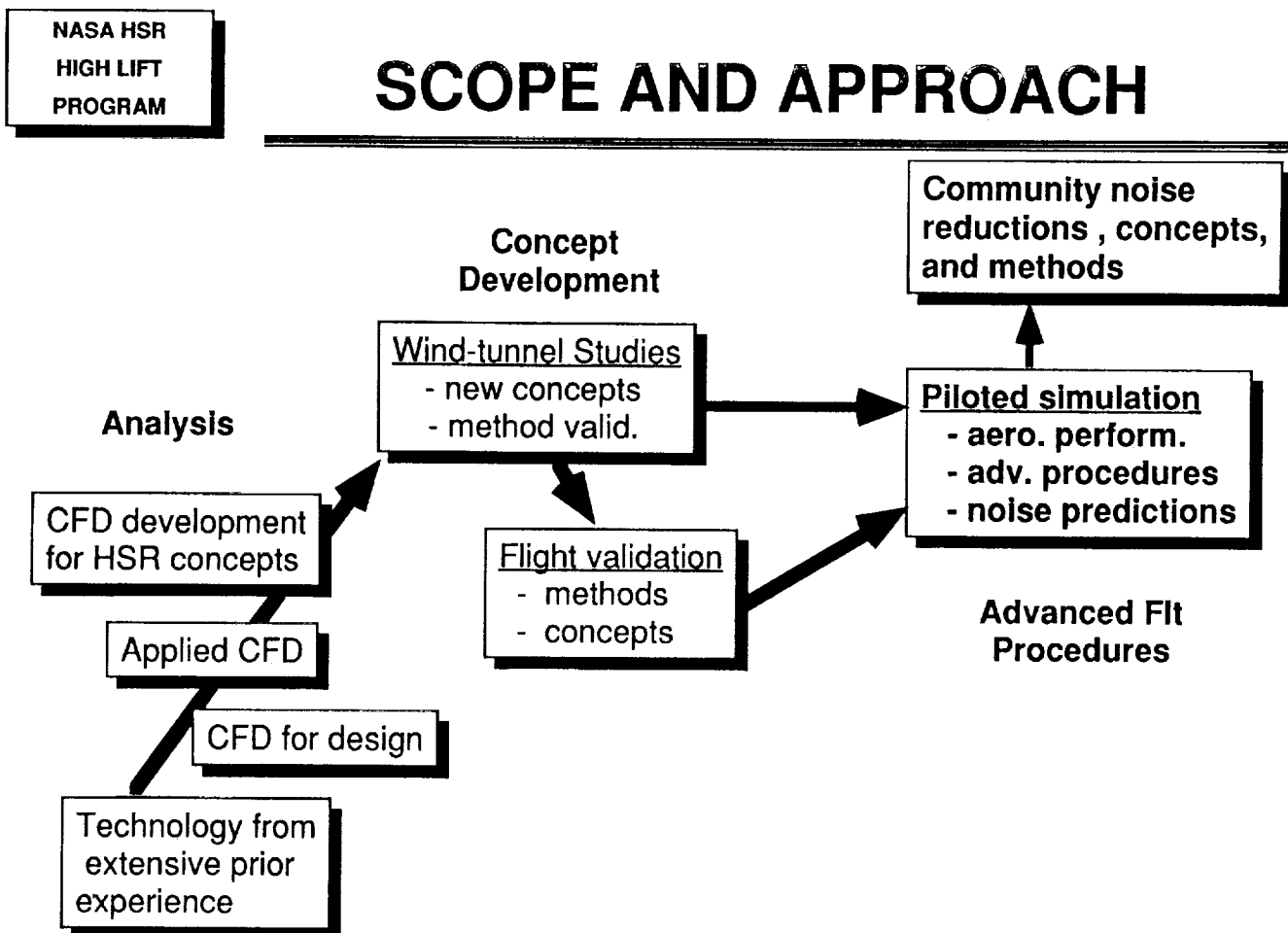


Figure 6

MODIFIED SCAR MODEL

As shown in figure 7, maximum advantage is being taken of the numerous wind-tunnel models available from the previous SCAR program. These models have been modified to refine concepts identified in the prior program and to explore new ideas. Shown in figure 7 is a NASA free-flight model developed during the SCAR effort.

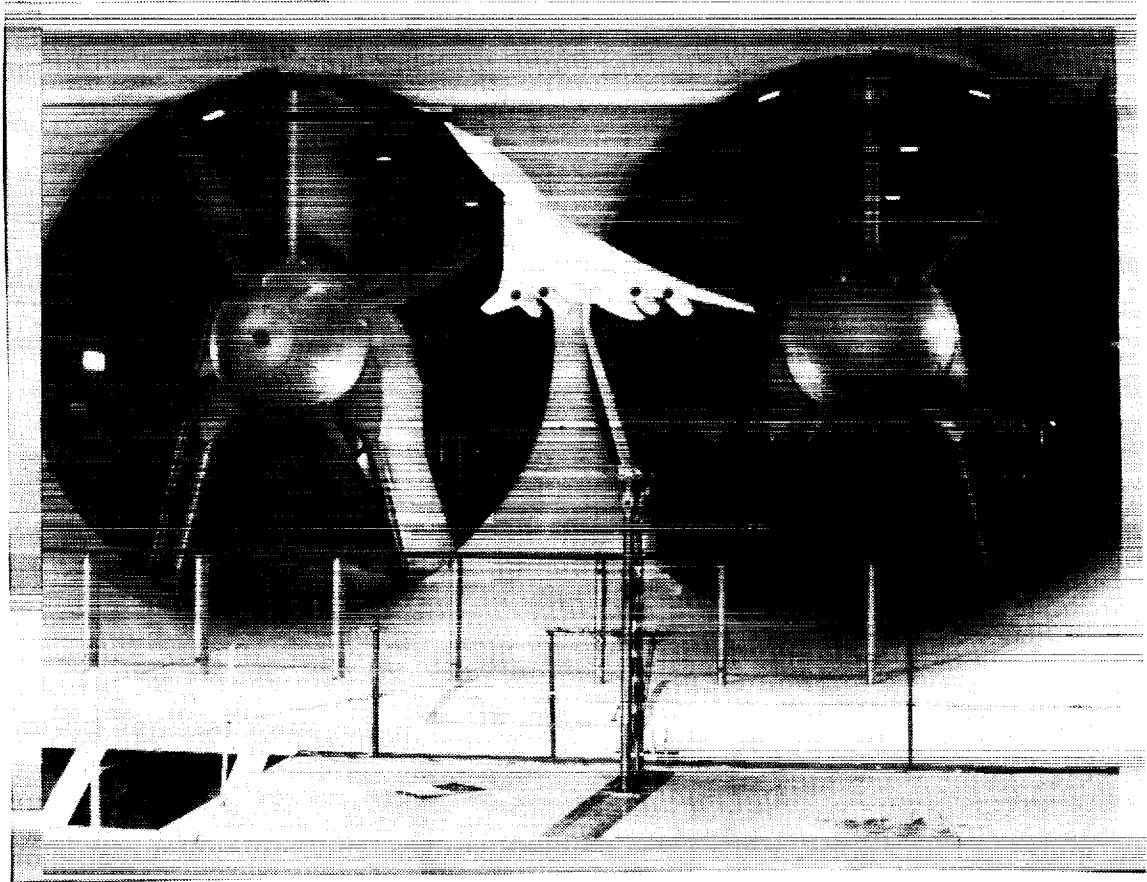


Figure 7

ORIGINAL PAGE
BLACK AND WHITE PHOTOGRAPH

PARTICIPANTS & ROLES

The organizations participating in the current HSR high-lift research are outlined in figure 8. The HSR high-lift program manager is located in NASA Headquarters (Office of Aeronautics, Exploration and Technology) in the Aerodynamics Division where he reports to the HSR program manager in the Office of Aeronautics. Both the Langley and Ames research centers are conducting high-lift research for the HSR program. Both centers are addressing CFD and experimental aerodynamics testing. The work at Langley also includes flight dynamics piloted simulation, and the prediction of community noise reductions provided by improved high-lift concepts. The teams at the two centers are working in a cooperative fashion to ensure the best high-lift concepts are identified, properly understood, and refined for effective application to realistic HSCT concepts. A concerted effort is being made at both centers to maintain a high level of cooperative work with industry.

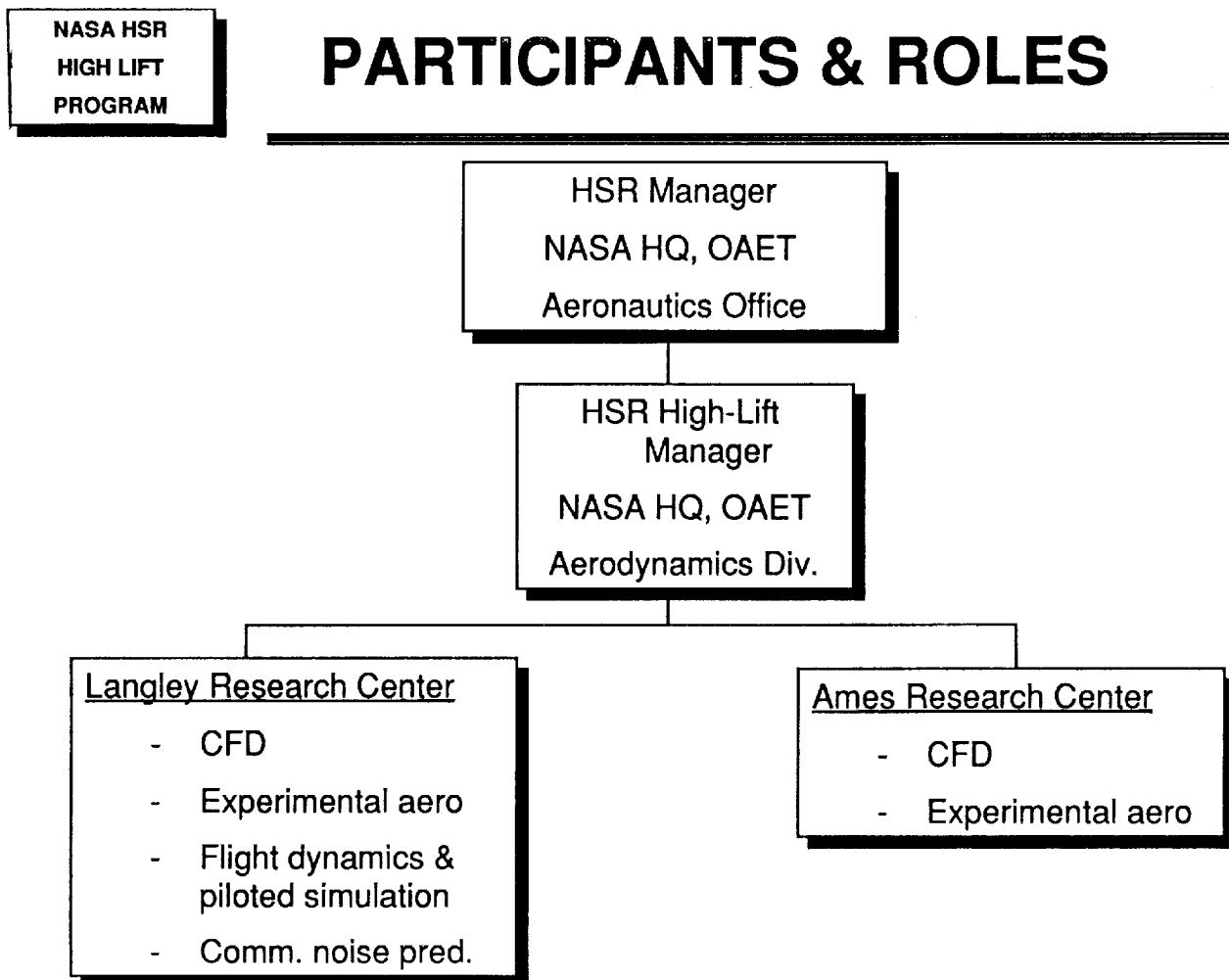


Figure 8

PHASE 1 SCHEDULE

The approximate timing for the research efforts in Phase I is shown in figure 9 for each of the three primary thrusts: simulation and analysis, supporting experiments (wind-tunnel studies), and concept verification (large-scale, high Reynolds number confirmation of most promising concepts). Also shown is the planned funding for this program phase.

The schedule is characterized by broad exploratory work early in the program and by increased focus on the most promising concepts and methods toward the end of the program.

NASA HSR
HIGH LIFT
PROGRAM

PHASE 1 SCHEDULE

	FY91	FY92	FY93	FY94	FY95	\$LaRC/ARC
SIMULATION AND ANALYSIS	CFD on AST's					.7/.3 M
	CFD DEVELOPMENT					
	PILOTED SIMULATION - PERFORMANCE AND PROCEDURES					
SUPPORTING EXPERIMENTS	Rn & LE RAD EFF					2.5/.7 M
	CONCEPT EVALUATION - EXISTING MODELS					
	CODE/TEST METH CALIB		2nd GENERATION CONCEPTS			
CONCEPT VERIFICATION	CODE VERIFICATION FOR ADVANCED CONCEPTS					1.3/.2 M
	VERIFY NOISE REDUCTION DUE TO HIGH LIFT					
\$LaRC/ARC	.5/.3 M	1.5/.5 M	1.5/.1 M	.5/.1 M	.5/.2 M	4.5/1.2 M

Figure 9

PHASE 1 MILESTONES

Key milestones for the Phase I effort are summarized in figure 10 in each of the three primary thrusts. Essential milestones will include proof of effective high-lift concepts, validation of the experimental and CFD methods capable of predicting the performance of these concepts, and prediction of the community noise benefits expected from these concepts.

An important message in this figure is that our program will begin developing a new series of HSCT wind-tunnel models in FY 1992 to carry the most promising ideas into more refined studies or representative wing platforms.

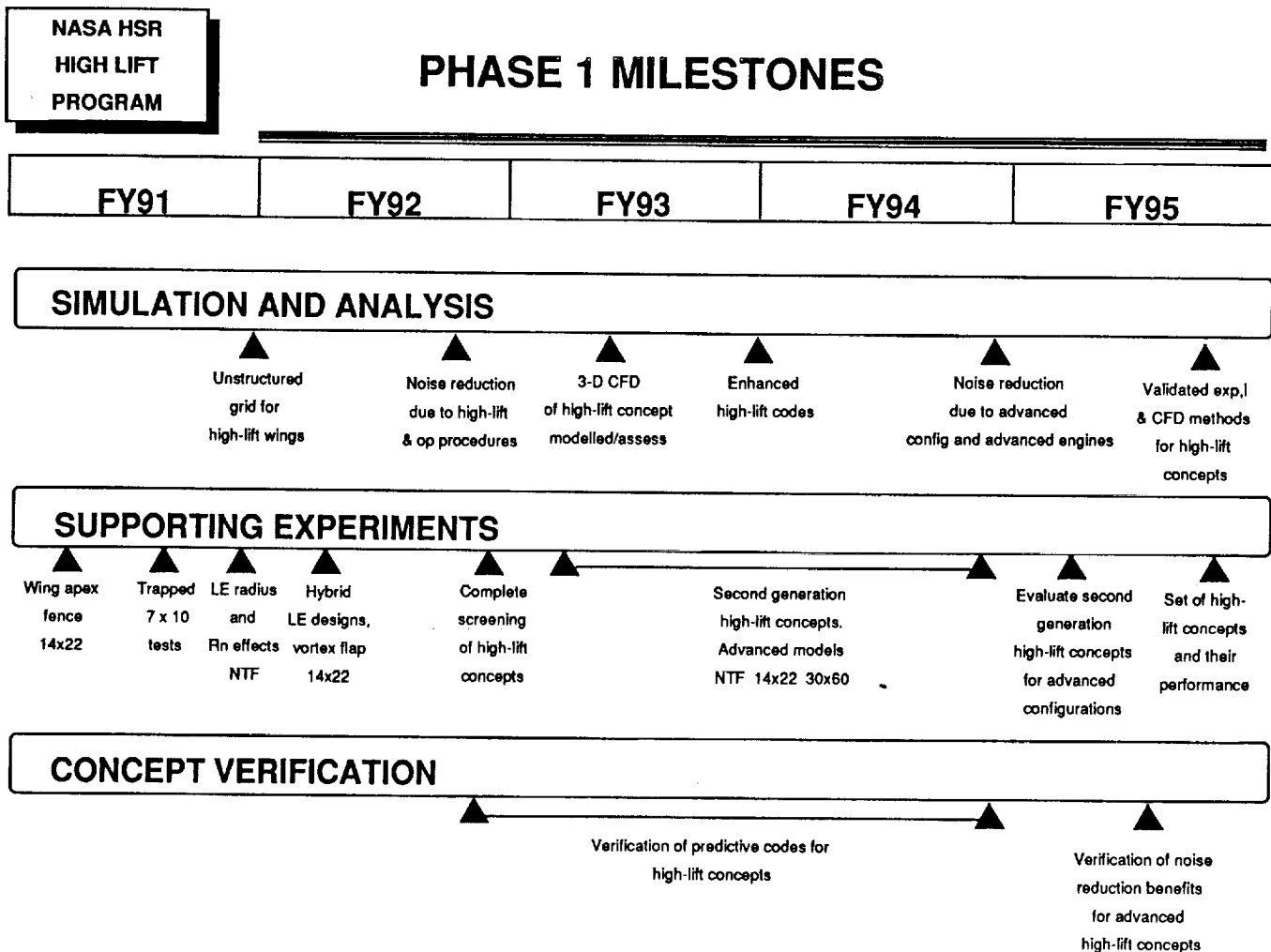


Figure 10

WORKSHOP OBJECTIVES (FIGURE 11)

The present workshop for the high-lift research is intended to give the U.S. technical community a good update on NASA plans for Phase I, NASA progress to date, and industry perspectives and priority technology need. A principal purpose of the workshop is to achieve a good interaction of key technologists to ensure the current program plan is relevant, and the results are apparent to those who need them. All workshop participants should feel free to make constructive criticisms and suggestions for improving the ongoing program.

**NASA HSR
HIGH LIFT
PROGRAM**

WORKSHOP OBJECTIVES

- Provide HSR community an update on
 - NASA plans and progress with emphasis on Phase I
 - Industry plans, progress, and priority needs
- Provide forum for interaction of key techologists and sharing of ideas
- Accomplish constructive critique of high-lift program to improve value and timeliness for industry

Figure 11

AGENDA

The agenda for the high-lift workshop is shown in figure 12. After my overview, the session will first hear about the NASA efforts at Langley and Ames. Our industry colleagues will then brief Boeing and Douglas elements of our workshop.

We will close the workshop with a discussion period led by my Ames colleague, Dr. Jim Ross. I strongly encourage all attendees to give this session your best effort, and please share your concerns and ideas.

NASA HSR
HIGH LIFT
PROGRAM

AGENDA

8:30 - 8:45	Overview	Gilbert
8:45 - 9:15	Langley experimental results & plans	Coe
9:15 - 9:45	Langley computational results & plans	Waggoner
9:45 - 10:30	Ames results and plans	Ross/Rossow
10:30 - 10:40	Break	
10:40 - 11:05	Boeing status	Paulson
11:05 - 11:30	Douglas status	Antani/Morgenstern
11:30 - 12:00	Discussion	Ross/Gilbert

Figure 12

THIS PAGE INTENTIONALLY BLANK

Session XII. High Lift

OMIT

Status of LaRC HSR High-Lift Research

Dr. Paul L. Coe, Jr., NASA Langley Research Center

PRECEDING PAGE BLANK NOT FILMED

THIS PAGE INTENTIONALLY BLANK

**STATUS OF LaRC HSCT
HIGH-LIFT RESEARCH**

*52-02
11977*

By

Paul L. Coe
NASA Langley Research Center

Presented at

First Annual High-Speed Research Workshop
May 14-16, 1991
Williamsburg, Virginia



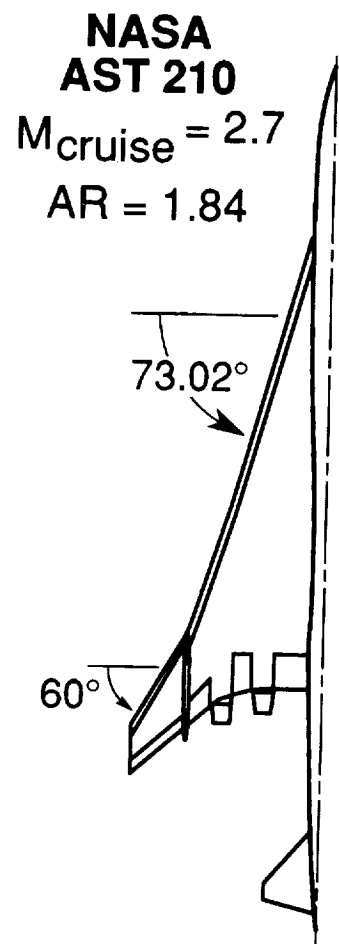
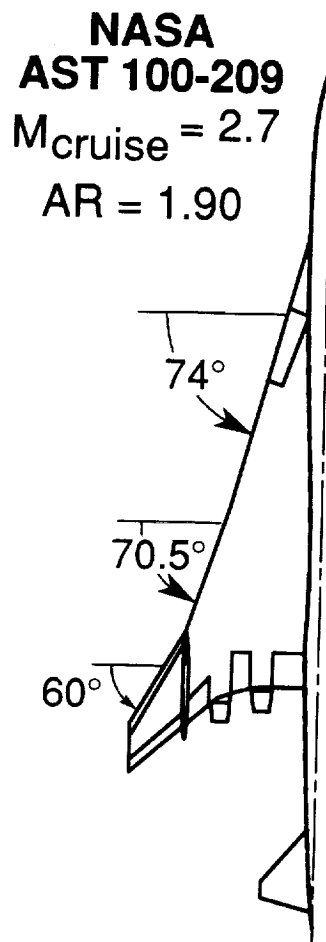
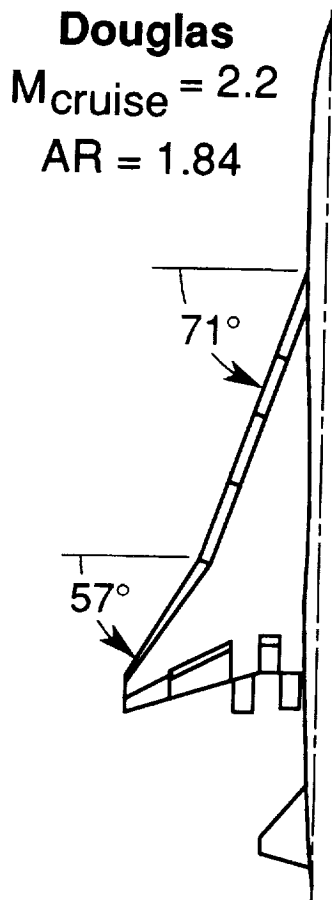
HSCT HIGH-LIFT RESEARCH

The discussion contained herein is intended to provide a status update of the NASA LaRC HSCT High-Lift Research Program. The areas of discussion are shown in the accompanying outline.

- Existing models
- Recent Wind tunnel studies
- Piloted simulation
- Near term plans

HSCT HIGH-LIFT RESEARCH Existing Models

Wind-tunnel models fabricated for the NASA Supersonic Technology Program of the 1970's and early 1980's are representative of current HSCT conceptual designs. Due to their availability, these models are being modified to explore advanced high-lift concepts. Three of these currently available model geometries are shown.



HSCT HIGH-LIFT RESEARCH Existing Models

A listing of currently available models is presented. Detailed geometric characteristics and aerodynamic data for specific models are contained in the reference indicated. These references are listed at the end of this paper.

DESIGNATION	SCALE	CONFIG.	LENGTH (ft)	SPAN (ft)	q_{max} (psf)	COMPONENT VARIABLES	REF.
AST-210 (1979)	0.03259	Wing-Body	8.16	4.133	110	L.E., T.E., outboard panel	1,2
AST-210 (1979)	0.025	Wing-Body	6.26	3.17	780	L.E.	3
AST-105 (1974)	0.10	Complete	31.75	13.78	26	L.E. (apex & outboard panel), powered nacelles, T.E. (hinge line BLC)	4,5
AST-105 (1974) Dynamic Model	0.045	Complete	14.29	6.20	10	L.E., T.E.	6,7,8,9
AST-200	0.03259	Wing-Body thickness distribution	8.16	4.133	110	L.E., T.E., pressures	10
DAC 2.2	0.10	Complete	31.00	13.55	26	L.E., T.E., pressures	11
733-336C Follow-on 2	0.03	Wing-Body	7.69	4.133	30	L.E., wing dihedral	12

HSCT HIGH-LIFT RESEARCH

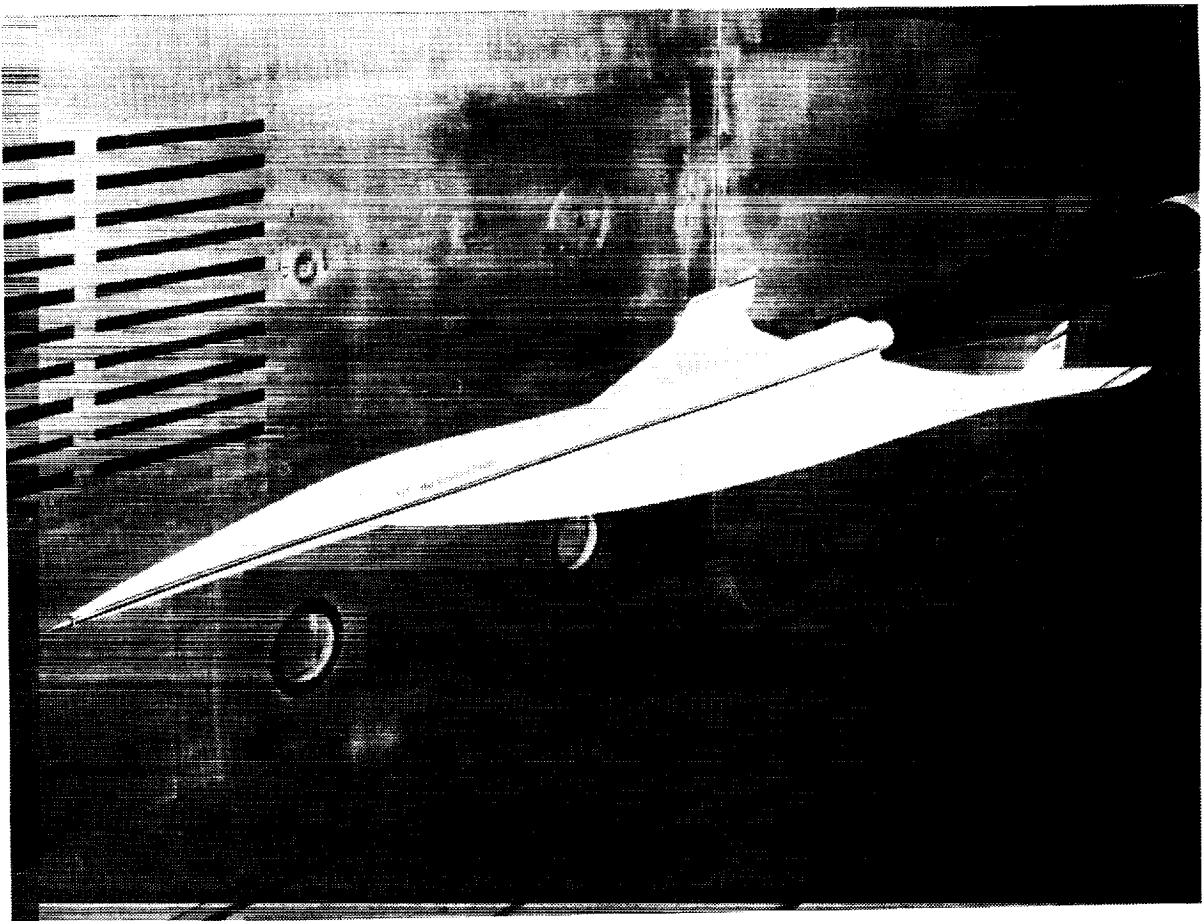
Recent Wind-Tunnel Studies

Three low-speed wind-tunnel studies have recently been conducted. The responsible researchers and principle objectives are as indicated.

- **AST-210** NTF investigation to explore Reynolds number effects on performance.
(Julio Chu (804) 864-5136)
- **AST-210** 14 X 22 Foot Wind Tunnel investigation for CFD correlation and exploratory study of innovative concepts.
(Bryan Campbell (804) 864-5069)
- **AST-105** 30 X 60 Foot Wind Tunnel investigation to explore effect of fuselage forebody fineness ratio on static directional stability.
(E. Richard White (804) 864-1147)

HSCT HIGH-LIFT RESEARCH NTF Model

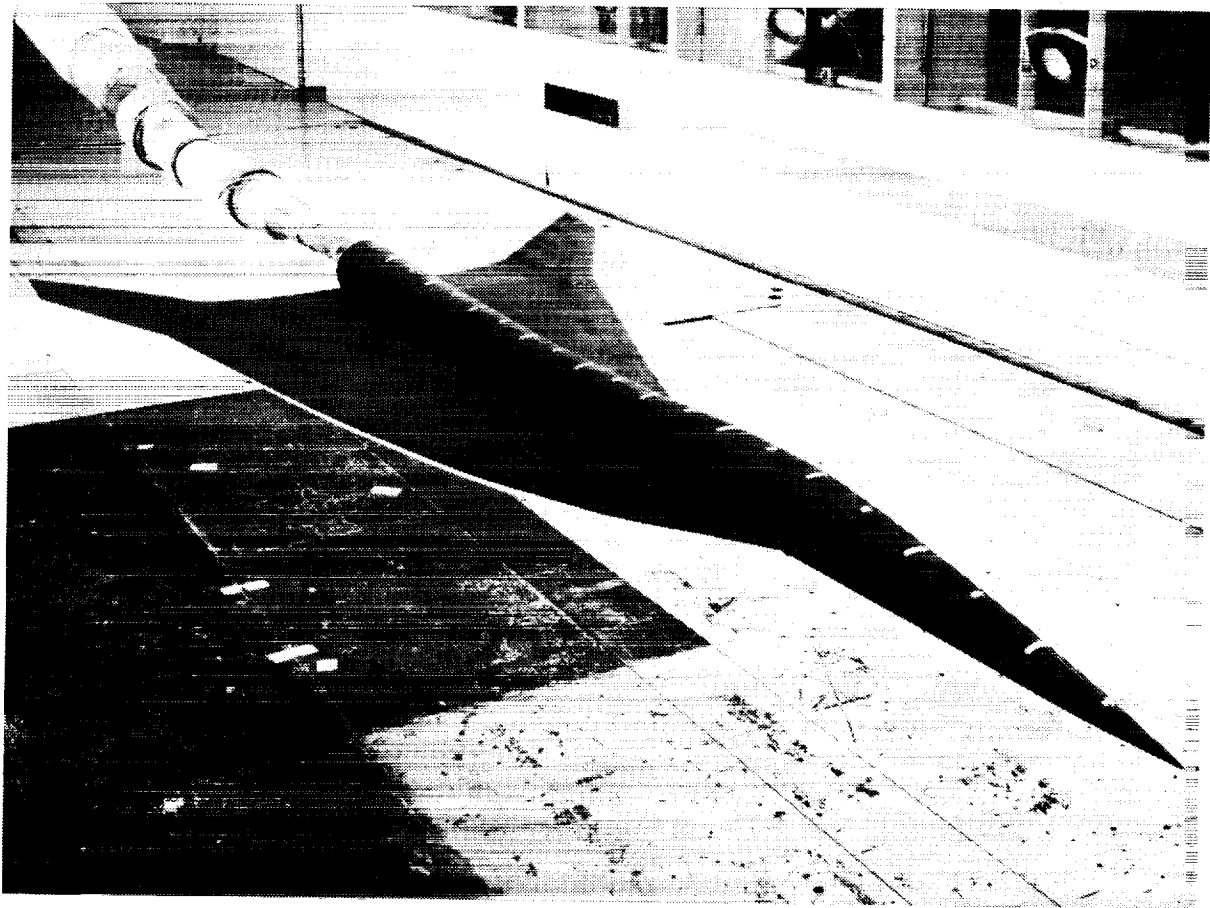
Photograph of the 0.025-scale AST 210 model mounted in the NTF for low-speed tests.



ORIGINAL PAGE
BLACK AND WHITE PHOTOGRAPH

HSCT HIGH-LIFT RESEARCH 14- by 22-Foot Subsonic Tunnel Model

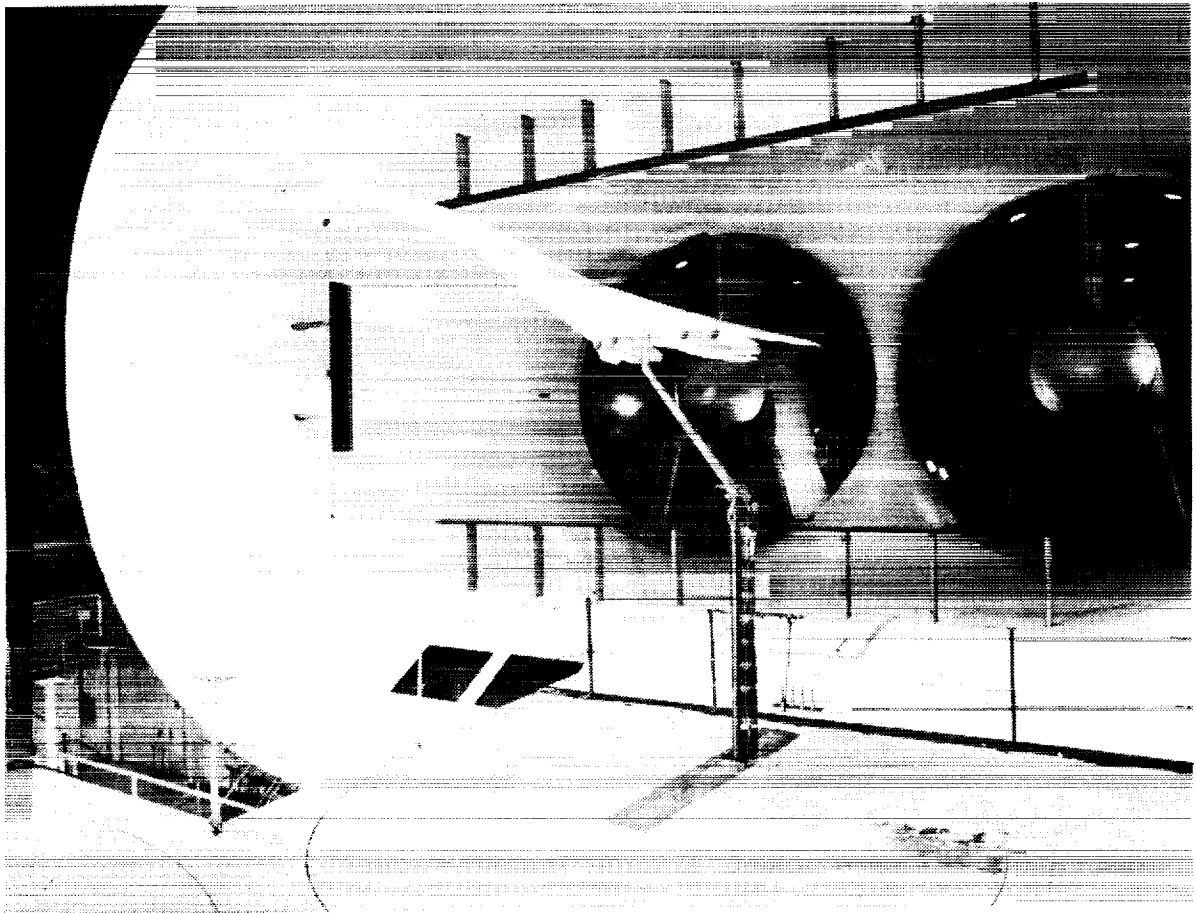
Photograph of the 0.03259-scale AST-210 model mounted in the 14- by 22-Foot Subsonic Tunnel for low-speed tests.



ORIGINAL PAGE
BLACK AND WHITE PHOTOGRAPH

HSCT HIGH-LIFT RESEARCH 30- by 60-Foot Tunnel Model

Photograph of the 0.045-scale AST-105 model mounted in the 30- by 60-Foot Tunnel for tests.



ORIGINAL PAGE
BLACK AND WHITE PHOTOGRAPH

HSCT HIGH-LIFT RESEARCH Piloted Simulation Background

The piloted simulation effort resulted from the projected inability of current HSCT concepts to meet proposed noise regulations.

Previous studies have shown reductions in airport-community noise resulting from:

- Increases in C_L
- Advanced takeoff and landing operating procedures
- Modifications to engine characteristics

HSCT HIGH-LIFT RESEARCH Piloted Simulation Objectives

The objectives of the piloted simulation program are as indicated.

- Document noise reduction resulting from increase in C_L and L/D and modifications to engine characteristics
- Develop and evaluate advanced takeoff and landing pilot operating procedures, which fully exploit noise reduction benefits without compromising safety

Responsible Researchers

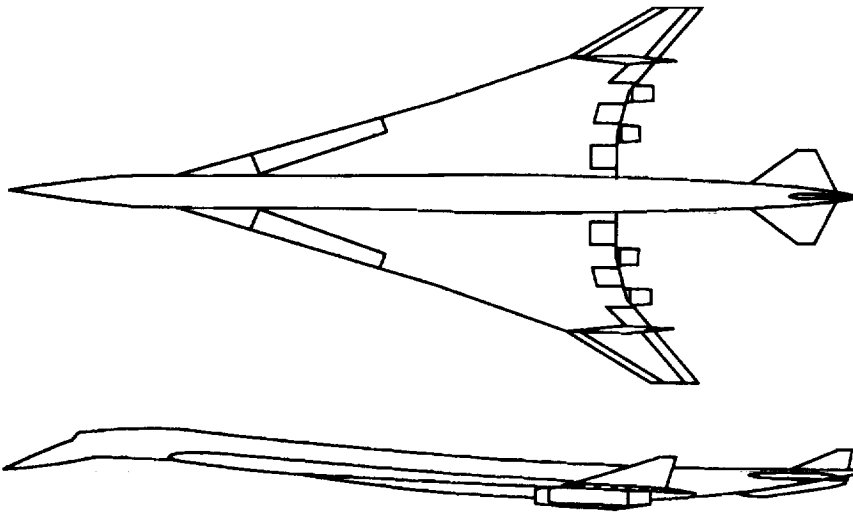
Donald R. Riley (804 864-1148)

Louis J. Glaab (804 864-1159)

HSCT HIGH-LIFT RESEARCH

Piloted Simulation Baseline Configuration

Due to the existence of a comprehensive data base the AST-105 configuration was selected as a simulation model. Although this configuration was developed in the late 1970's it is representative of current HSCT conceptual designs.



Airframe AST-105-1 (1979)

$W_{T.O.}$ (lbf) = 686,000

$W_{App.}$ (lbf) = 392,250

S (ft²) = 8366

b (ft) = 126.215

c (ft) = 88.162

$\Lambda_{L.E.}$ (deg) = 74/70.3/60

Range (n. mi.) = 4500

M_{cruise} = 2.7

T/W = 0.254

L/D_{max} = 9.39

Engine (4) VSCE-516 (1979)

Bypass ratio = 1.3:1

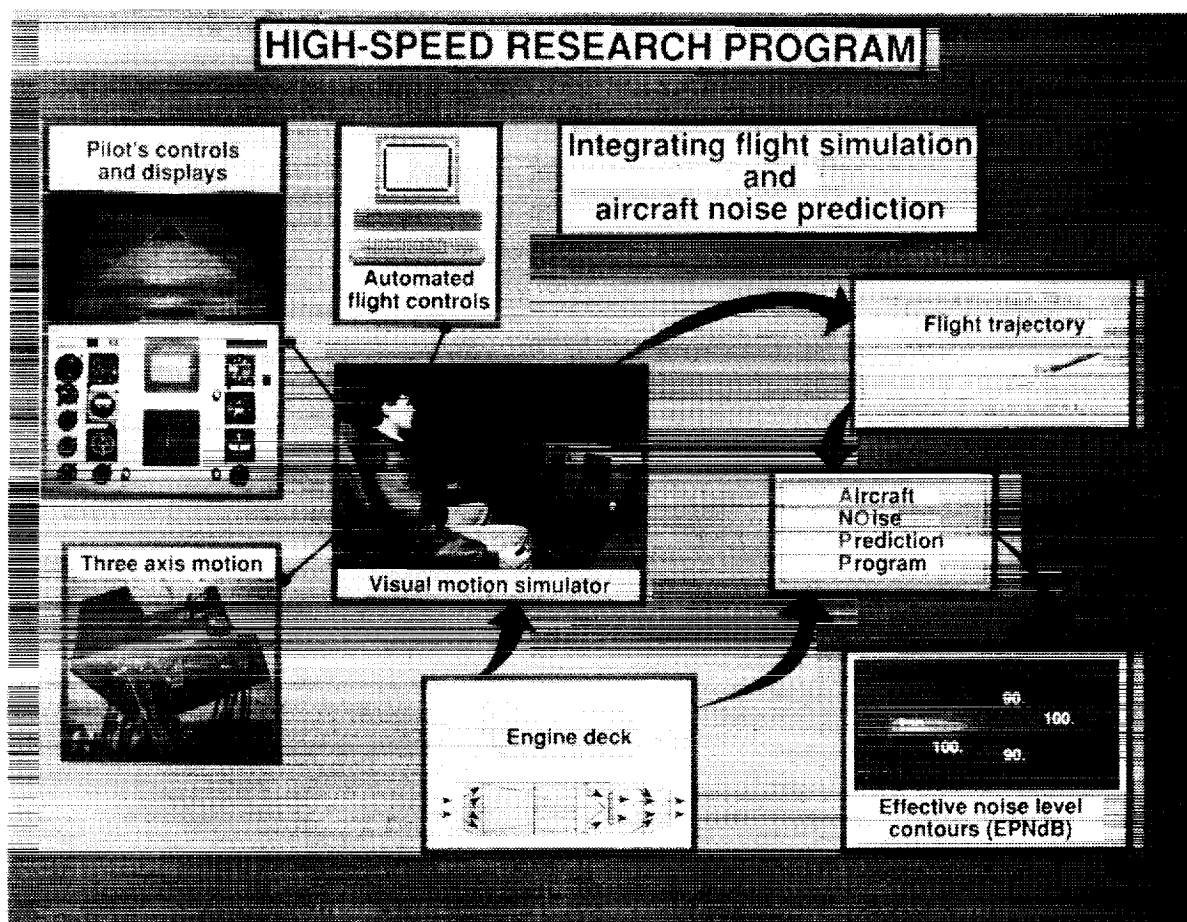
OPR = 16:1

W_a (lbm/sec) = 608

V_f/V_p = 1.7:1

HSCT HIGH-LIFT RESEARCH Piloted Simulation Approach

The approach to noise prediction is shown on the accompanying chart. The research uses the Langley Visual Motion Simulator (VMS) which has three axis motion capability (three axis translation and three axis rotation). The pilot has a standard display panel and controls, and a computer graphics image of the runway and airport surroundings. The simulation provides automated flight control capability and allows different levels of stability augmentation systems to be considered. The pilot can perform take-off and landing procedures and the resulting flight trajectories (coupled with the engine characteristics) are input to the Aircraft Noise Prediction Program (ANOPP) which is then used to compute noise contours. An initial objective of this research effort was to develop the VMS/ANOPP interface. To permit rapid accomplishment of this objective, the AST-105 configuration (because of the available and comprehensive data base) was selected for initial study.



HSCT HIGH-LIFT RESEARCH Piloted Simulation Status

The status of the piloted simulation research is as indicated. Future plans for this activity are presented in a subsequent section.

- AST-105 aerodynamic data base and VSCE-516 engine deck incorporated in Visual Motion Simulation
- VMS/ANOPP interface developed
- AST baseline noise characteristics evaluated
- Advanced engine and advanced operating procedures investigations in progress

HSCT HIGH-LIFT RESEARCH Near-Term Plans

The HSCT High-Lift Research plans are as listed and will be discussed individually.

1. Piloted simulation
2. Planform/L.E. modifications (AST-200 → HSCT 71/50)
3. L.E. BLC-suction/wing apex blowing/ L.E. radius mod (AST-210)
4. L.E. sweep/outboard panel parametric study
5. HSCT baseline configuration
6. DAC-2.2 Advanced L.E. concepts
7. F-16XL model modifications

HSCT HIGH-LIFT RESEARCH Cooperative Programs

The LaRC High-Lift Research Program reflects a highly cooperative effort between NASA LaRC and industry. This cooperative spirit is further evidenced by joint LaRC-ARC-LeRC research as well as a significant number of multi-Division, multi-Branch research activities at LaRC.

		Near term plan
● Piloted simulation of advanced aero and operating procedures	(LaRC/Boeing/DAC)	1
● Community noise	(LaRC-FAD/FDB, ANRD/AB&SAB)	1
● Advanced engines/community noise	(LaRC/LeRC)	1
● Wing apex flap concepts	(LaRC/Boeing)	2, 4
● Trapped vortex concepts	(LaRC/ARC)	2, 4
● Leading-edge BLC/suction	(LaRC/Boeing)	3
● Leading-edge radius effects	(LaRC/Boeing)	3
● Wing apex blowing	(LaRC/DAC)	3
● HSCT baseline configuration	(LaRC-FAD, AVD, AAD/Boeing/DAC/ARC)	5
● High-lift design methods	(LaRC/DAC)	6
● High-lift impact on ejector acoustics	(LaRC/LeRC)	6
● Fuselage foerbody effects	(LaRC/Boeing)	Completed

HSCT HIGH-LIFT RESEARCH Piloted Simulation Plans

Near term plans for the piloted simulation are as indicated. This study is intended to be a long term activity and will be updated to reflect current HSCT concepts as the experimental and computational data become available.

- Complete community noise evaluation of (AST-105) configuration, assess impact of advanced engines, advanced piloting procedures
- Enhance high-lift aerodynamics and evaluate community noise
 - C_L - Assume potential flow
 - C_D - Assume 90-percent suction
 - C_m - No pitchup, alternate trim concepts
- Evaluate community noise characteristics for NASA advanced baseline HSCT configuration

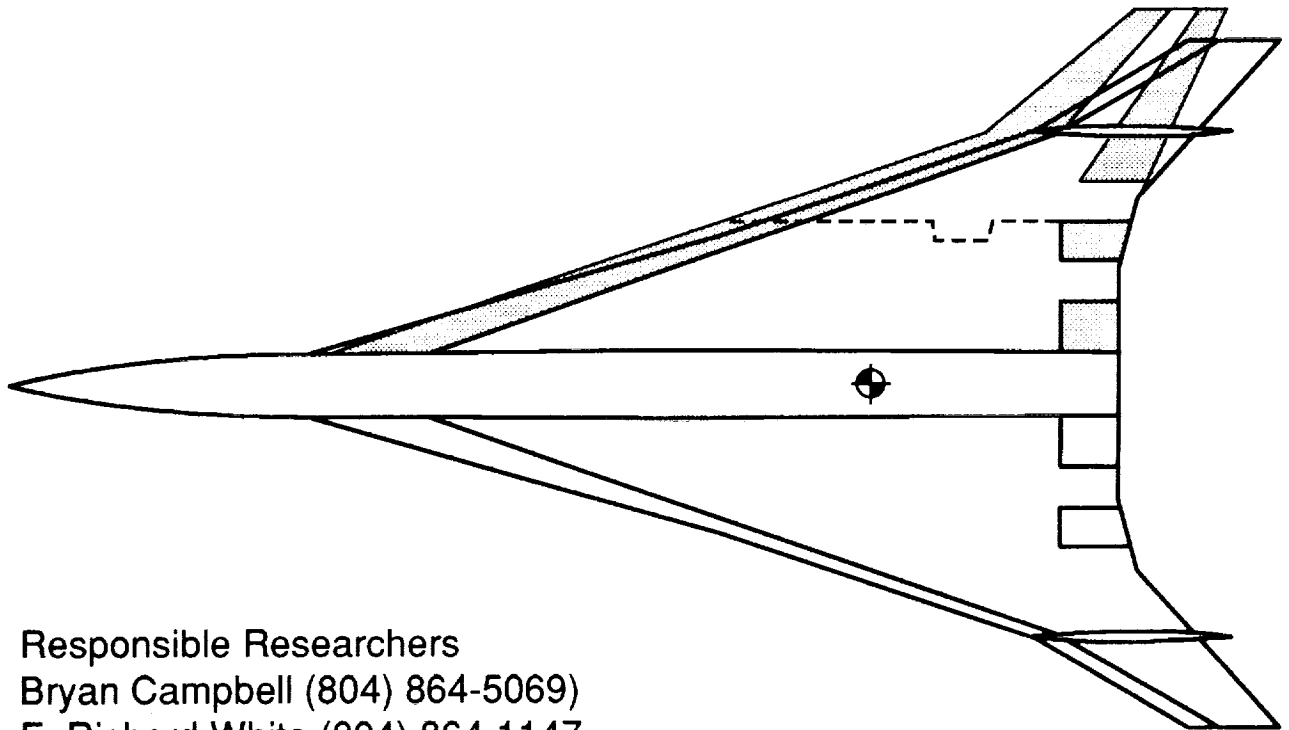
HSCT HIGH-LIFT RESEARCH Planform/L.E. Modifications

The existing AST-200 model will be modified to reduce the leading-edge sweep and increase the span. Advanced leading-edge design will be fabricated and tested in the 14- by 22-Foot Subsonic Tunnel.

- Modify AST-200 planform (0.03259-scale model) from $\Lambda = 74^\circ/70.5^\circ/60^\circ$ to $\Lambda = 71^\circ/50^\circ$
- Incorporate advanced leading edge flap design
 - Carlson design method
 - Frink vortex flap design
- 14 X 22 Foot Tunnel tests

HSCT HIGH-LIFT RESEARCH AST-200 -- HSCT 71/50

The shaded area represents the high-lift system for the revised AST-200 model. The model will incorporate a separate balance system to isolate the aerodynamic loads on the outboard wing panels. A limited number of pressure taps will be installed to evaluate the leading-edge flow characteristics.



Responsible Researchers
Bryan Campbell (804) 864-5069
E. Richard White (804) 864-1147

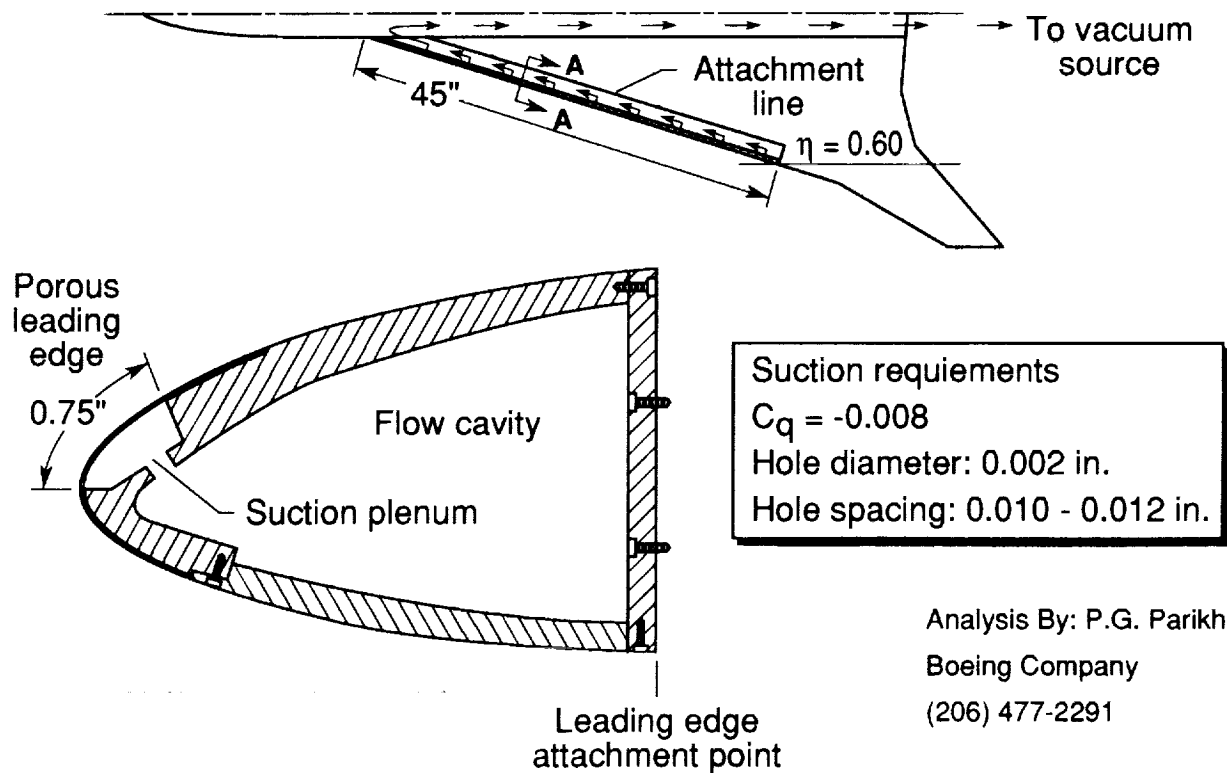
HSCT HIGH-LIFT RESEARCH AST-210 Modifications

Both the 0.025- and 0.03259-scale models of the AST-210 configuration are being modified. The 0.025-scale model is having the leading-edge radius increased by a factor of about 2 and will be tested in the NTF. The larger 0.03259-scale model is having a correspondingly increased leading-edge radius. In addition, a porous leading-edge BLC-suction system will be tested in the 14- by 22-Foot Tunnel. This system is intended to alleviate low speed wing leading-edge flow separation and is designed to be compatible with Supersonic Laminar Flow Control designs. A further consideration of pneumatic devices is the apex blowing concept which is intended for vortex control/amplification.

- **Modify AST-210 L.E. radius (0.025-scale model)**
- NTF tests
- **Modify AST-210 (0.03259-scale model) to incorporate porous L.E. for BLC-suction**
- 14 X 22 Foot Tunnel tests
- **Modify AST-210 fuselage to incorporate wing apex blowing for vortex control/amplification**
- 14 X 22 Foot Tunnel tests

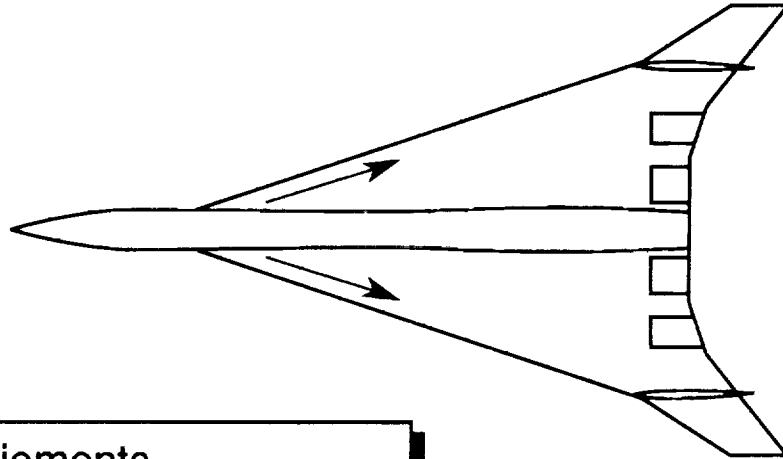
HSCT HIGH-LIFT RESEARCH L.E. BLC-Suction

Leading-Edge Boundary Layer Control (BLC)-Suction system for 0.03259-scale
AST-210 model.



HSCT HIGH-LIFT RESEARCH Apex Blowing

Apex blowing concept for 0.03259-scale AST-210 model.



Blowing requirements

$$C_{\mu} = 0.0075 - 0.04$$

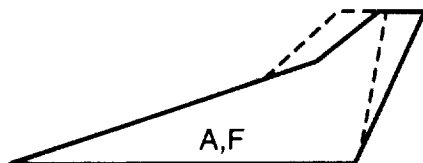
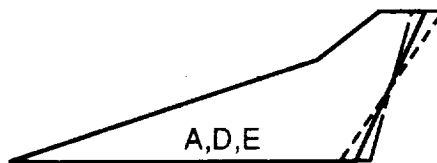
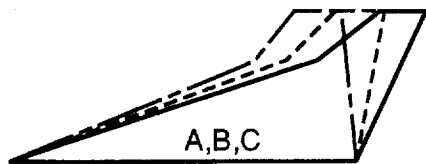
Nozzle diameter = 0.66 in., 1.2 in.

Analysis By: J. Morgenstern
Douglas Aircraft Company
(213) 496-9151

HSCT HIGH-LIFT RESEARCH L.E. Sweep/Outboard Panel Parametric Study

A parametric series of wind-tunnel models is being designed and fabricated.

- These models are intended for parametric study of the effect of L.E. sweep and outboard panel geometry on high-lift performance and high lift system complexity. Models will be sized for tests in LaRC 12-Foot Low-Speed Tunnel, BART, Vigyan and N.C. State University Low-Speed Tunnels.



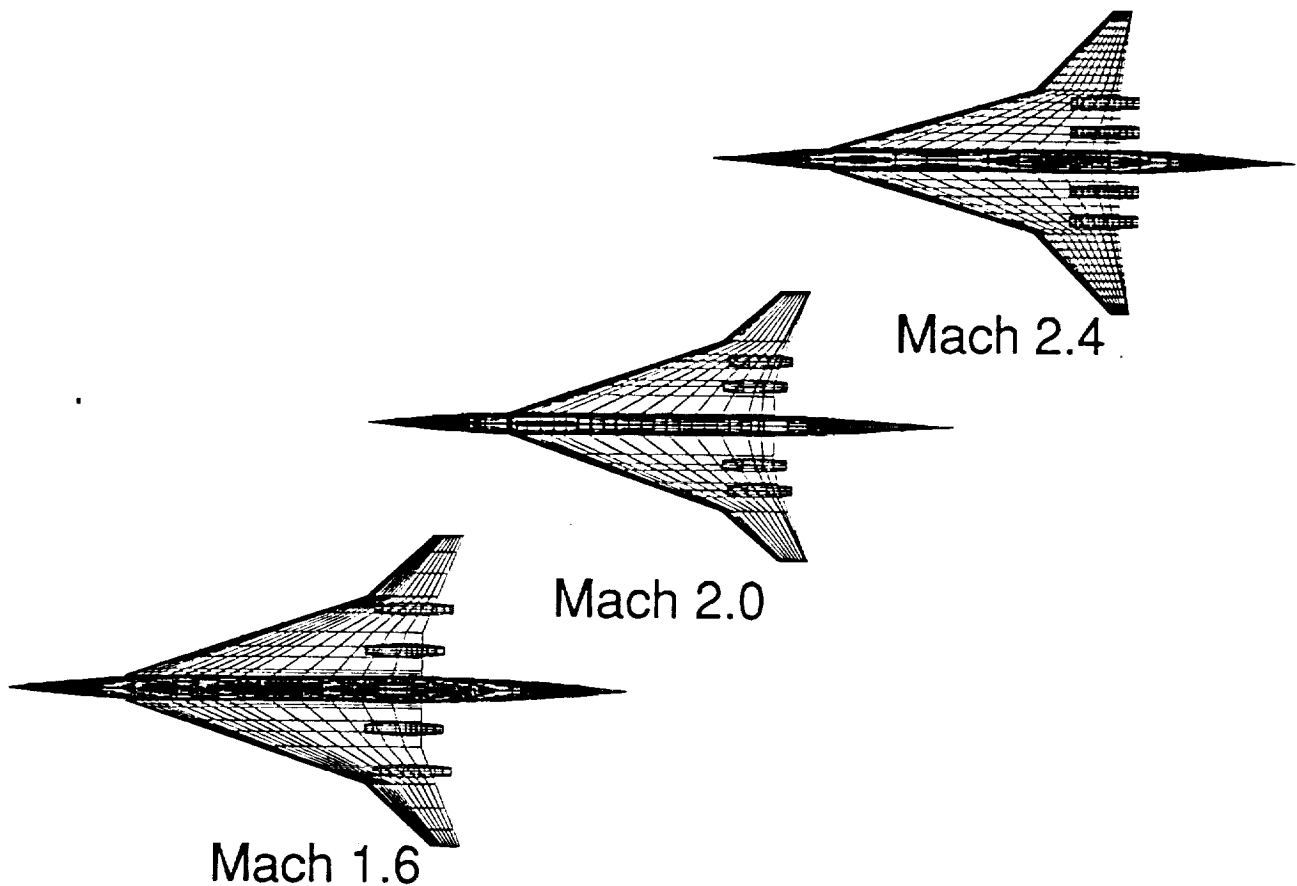
Planform	Δ L.E., deg
A	71/50
B	69/41.8
C	67/32.8
D	71/50
E	71/50
F	71/50

*Note: Each planform has L.E./T.E.
high-lift system*

Responsible Researcher
E. Richard White (804) 864-1147

HSCT HIGH-LIFT RESEARCH Langley Baseline Concepts

A configuration study has been conducted by the NASA LaRC Vehicle Integration Branch of the Advanced Vehicle Division. Preliminary planform views of three Mach number designs are presented. The study will be completed in Summer '91 and design and fabrication of a new model series will be initiated in FY'92.



HSCT HIGH-LIFT RESEARCH

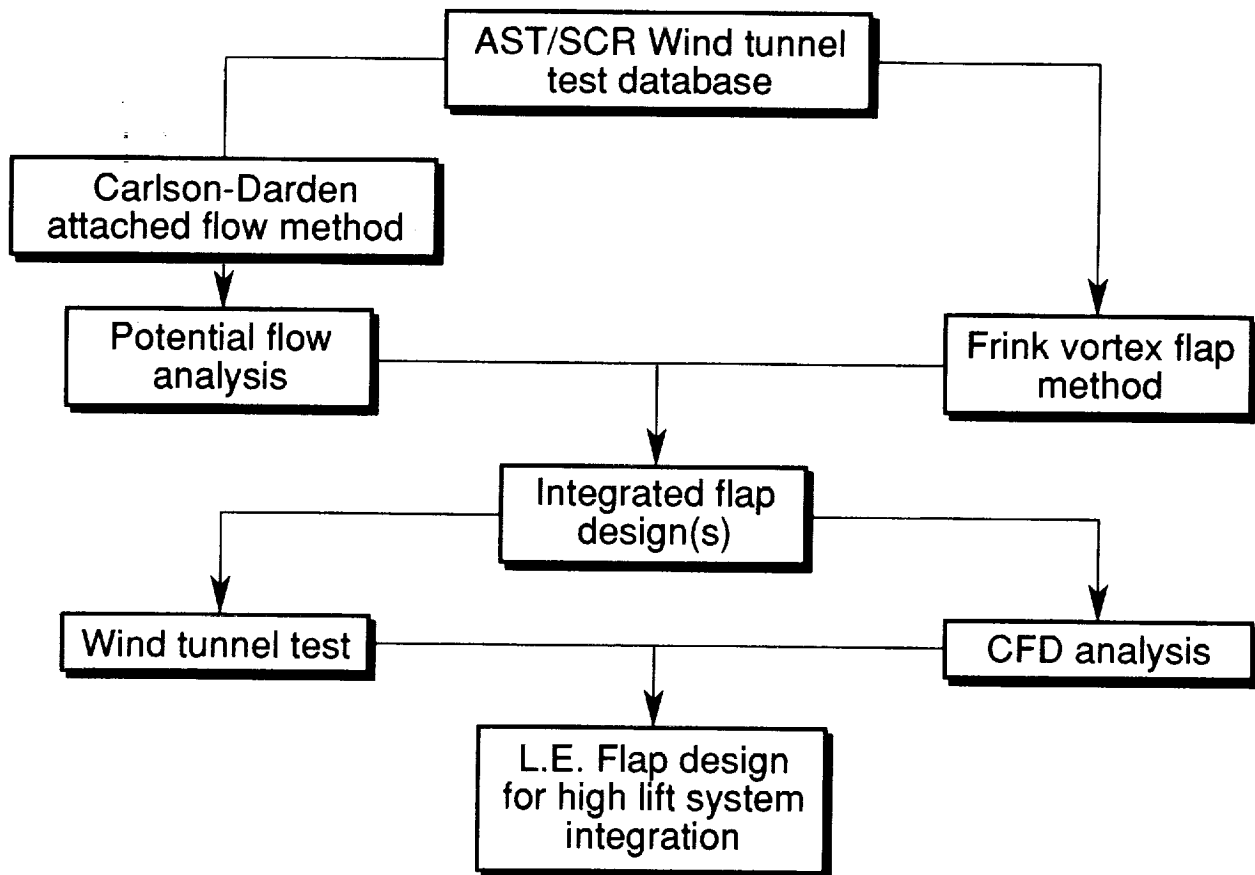
HSCT Baseline Configuration Models

Three models of the NASA LaRC baseline HSCT concept will be designed and fabricated. These models will be the subject of numerous cooperative research programs and are being designed so as to be compatible with a number of wind tunnel facilities.

<u>MODEL SCALE</u>	<u>FACILITY</u>	<u>MACH RANGE</u>	<u>TEST SECTION</u>
0.02	NTF	0.2 - 0.5	8' X 8'
↓	BSWT	0.4 - 4.5	4' X 4'
	BTWT	0.3 - 1.1	8' X 12'
0.035	14 X 22	0.05 - 0.3	14' X 22'
↓	BTWT	0.3 - 1.1	8' X 12'
	ARC 9 X 7	1.5 - 2.5	9' X 7'
	ARC 11'	0.5 - 1.4	11' X 11'
	ARC 7 X 10	0.05 - 0.34	7' X 10'
↓	UWAL	0.05 - 0.27	8' X 12'
0.045	30 X 60	0 - 0.1	30' X 60'

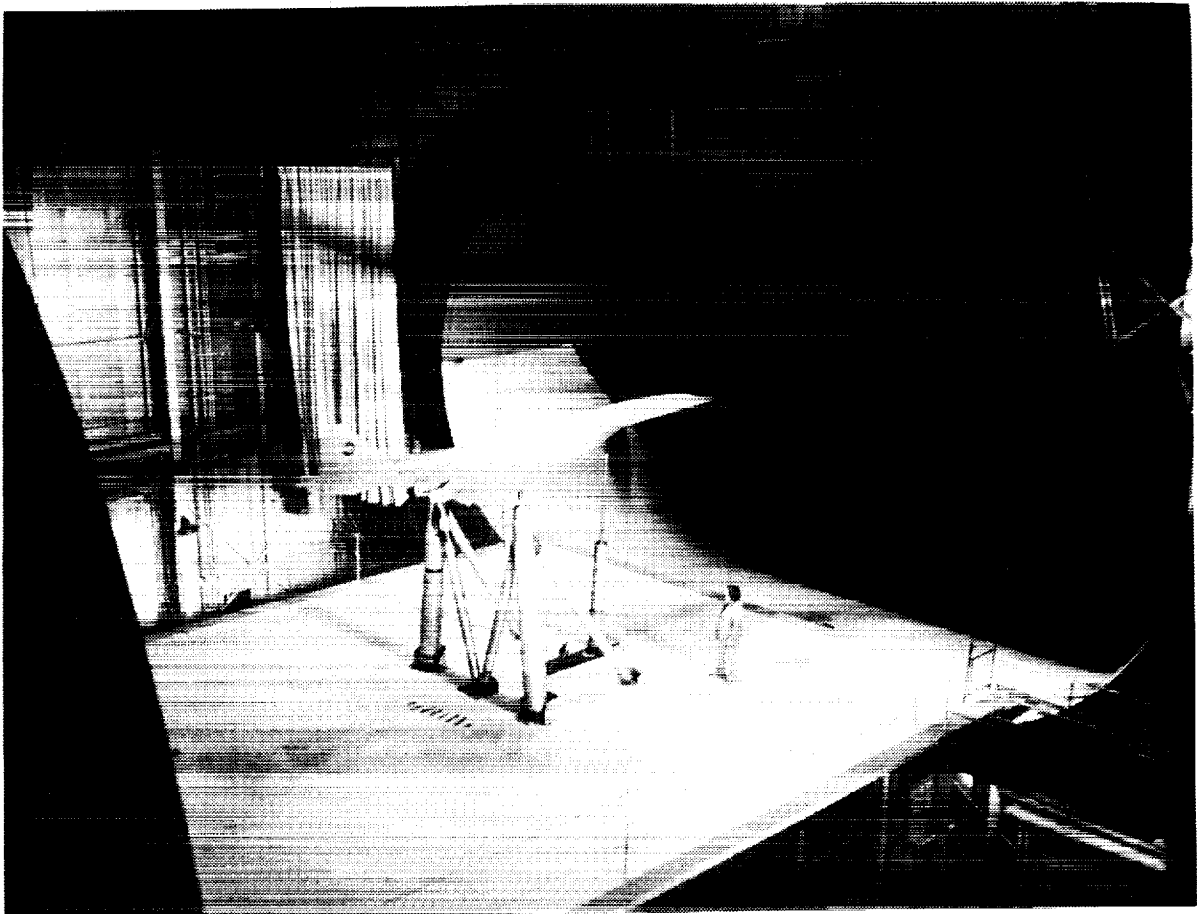
HSCT HIGH-LIFT RESEARCH NASA/Industry L.E. Flap Design Methodology

NASA/Industry teams are using advanced design methods, as shown, to develop integrated high-lift system designs which will be wind tunnel tested and CFD analyzed.



HSCT HIGH-LIFT RESEARCH DAC 2.2 Model

Members of the Douglas design team are using the design method discussed on the previous chart to develop advanced high-lift systems for a 1970's wind-tunnel model of a conceptual design designated DAC 2.2. Although from a previous program, this configuration does aerodynamically represent current HSCT concepts. Owing to the availability of the model, the research can be readily accomplished in the 30- by 60-Foot Tunnel.

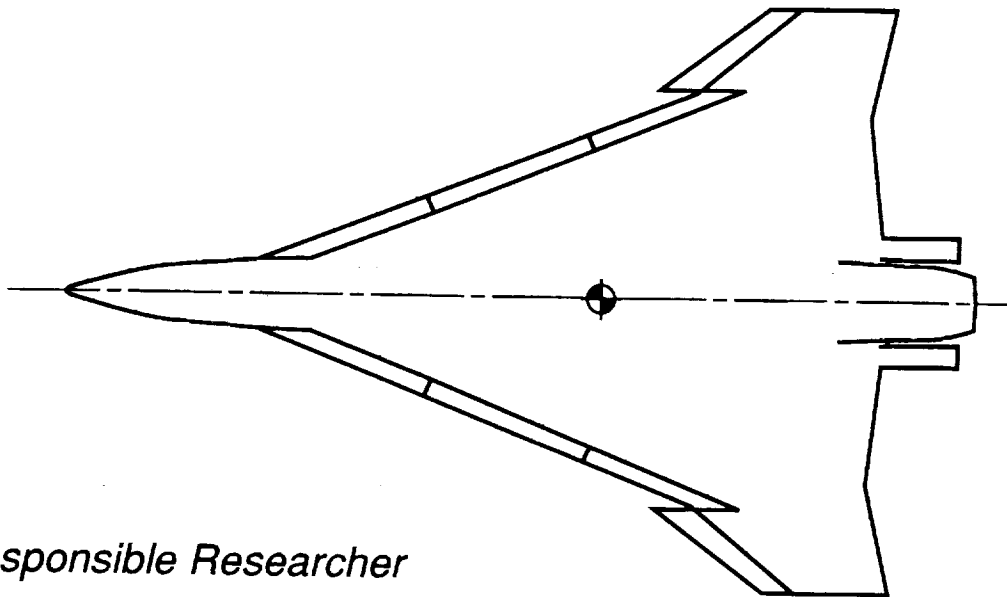


ORIGINAL PAGE
BLACK AND WHITE PHOTOGRAPH

HSCT HIGH-LIFT RESEARCH F-16XL Model Modifications

Low-speed wind-tunnel studies are planned using an existing 0.18-scale model of the F-16XL. These tests are planned for the 30- by 60-Foot Tunnel and will explore wing leading-edge modifications which include the return to a constant sweep inboard wing panel and leading-edge flaps. This research may ultimately lead to full-scale testing of advanced leading-edge devices.

- Wing leading-edge sweep modified in apex region
- Design, fabricate, test advanced L.E. flaps



Responsible Researcher
David E. Hahne (804) 864-1162

HSCT HIGH-LIFT RESEARCH

Concluding Remarks

- Initial experimental/code calibration wind tunnel tests conducted using existing models from prior supersonic technology programs. Results from initial tests valuable in current design process
- Piloted simulation, for community noise reduction, initiated from existing supersonic technology data base due to availability and completeness. Updates planned as experimental/computation results for advanced designs become available
- Near term plans heavily emphasize cooperative programs

REFERENCES

1. **Scott, Samuel J.; Nicks, Oran, W.; and Imbrie, P.K.:** Effects of Leading-Edge Devices on the Low-Speed Aerodynamic Characteristics of a Highly-Swept Arrow-Wing. *NASA CR 172531, 1985.*
2. **Campbell, Bryan; et al:** 14 X 22 Foot Wind Tunnel Tests, *January 1991.*
3. **Lawing, Pierce L.; and Chu, Julio:** NTF Tests, *October 1990.*
4. **Coe, Paul L. Jr.; McLemore, H. Clyde; and Shivers, James P.:** Effects of Upper-Surface Blowing and Thrust Vectoring on Low-Speed Aerodynamic Characteristics of a Large-Scale Supersonic Transport Model. *NASA TND-8296, 1976.*
5. **Shivers, James P.; McLemore, H. Clyde; and Coe, Paul L. Jr.:** Low-Speed Wind-Tunnel Investigation of a Large-Scale Advanced Arrow-Wing Supersonic Transport Configuration with Engines Mounted Above Wing for Upper-Surface Blowing. *NASA TND-8350, December 1976.*
6. **Coe, Paul L. Jr.; and Weston, Robert P.:** Effects of Wing Leading-Edge Deflection on Low-Speed Aerodynamic Characteristics of a Low-Aspect-Ratio Highly Swept Arrow-Wing Configuration. *NASA TP-1434, 1979.*
7. **Coe, Paul L. Jr.; and Thomas, James L.:** Theoretical and Experimental Investigation of Ground-Induced Effects for a Low-Aspect-Ratio Highly Swept Arrow-Wing Configuration. *NASA TP 1508, 1979.*
8. **Coe, Paul L. Jr.; Smith, Paul M.; and Parlett, Lysle P.:** Low-Speed Wind-Tunnel Investigation of an Advanced Supersonic Cruise Arrow-Wing Configuration. *NASA TM 74043, 1977.*
9. **Gentry, Garl L., Jr.; and Coe, Paul L. Jr.:** Low-Speed Aerodynamic Characteristics of a Highly Swept Arrow-Wing Configuration with Several deflected Leading-Edge Concepts. *NASA TM 80180, 1980.*
10. **Coe, Paul L. Jr.; Kjelgaard, Scott O.; and Gentry, Garl L., Jr.:** Low-Speed Aerodynamic Characteristics of a Highly Swept, Untwisted, Uncambered Arrow Wing. *NASA TP 2176, 1983.*
11. **Yip, Long P.; and Parlett, Lysle P.:** Low-Speed Wind-Tunnel Tests of a 1/10-Scale Model of an Advanced Arrow-Wing Supersonic Cruise Configuration Designed for Cruise at Mach 2.2. *NASA TM 80152, 1979.*
12. **Coe, Paul L. Jr.; Huffman, Jarrett K.; and Fenbert, James W.:** Leading-Edge Deflection Optimization for a Highly Swept Arrow-Wing Configuration. *NASA TP-1777, 1980.*

THIS PAGE INTENTIONALLY BLANK

omit

Session XII. High Lift

Status of CFD for LaRC's HSR High-Lift Program

Edgar G. Waggoner and Jerry C. South, Jr., NASA Langley Research Center

PRECEDING PAGE BLANK NOT FILMED

THIS PAGE INTENTIONALLY BLANK

**Status of CFD for LaRC's HSR
High-Lift Program**

**Edgar G. Waggoner
Subsonic Aerodynamics Branch**

**Jerry C. South, Jr.
Computational Aerodynamics Branch**

NASA - Langley Research Center

Presented at the

**First Annual High-Speed Research Workshop
Williamsburg, Virginia
May 14-16, 1991**

*53-02
11978*

N94- 33520

OUTLINE

Objectives of CFD Applications

Approach

Dominant Flow Mechanisms

Candidate Codes

Analysis Results and Experimental Comparisons

Emerging Unstructured Grid Technology

Plans

OBJECTIVES OF CFD APPLICATIONS

- Increased insight into flow physics and fluid mechanisms "driving" the flowfield
- Complement to ground based experiments
 - Improved testing efficiency
 - Aid in parametric interpolation and extrapolation
- Used for design and analysis of high-lift concepts

APPROACH

- Identify candidate computational methods
- Calibrate/validate candidate codes using available experimental data
 - Cruise configuration
 - High-lift concepts
- Determine areas/regions of applicability, resource requirements, etc. for candidate codes.
- Develop new technologies (algorithms, grid generation, etc.) where gaps are identified.

DOMINANT FLOW MECHANISMS

- Vortex formation
 - Large radius separation (forebodies)
 - Small radius separation (wing leading-edges)
- Vortex interaction
- Boundary layer separation and confluent boundary layers
- Ground effects
- Engine/airframe integration

CANDIDATE "PRODUCTION" ANALYSIS CODES

CFL3D

- Upwind-biased differencing
- Multi-block gridding with generalized patching
- Multi-grid
- Balwin-Lomax algebraic turbulence model

TLNS3D

- Central differencing
- Single block grid
- Multi-grid
- Balwin-Lomax algebraic and Johnson-King turbulence models

FMC1

- Incompressible
- Total variation diminishing
- Single block grid
- Shock fitting
- Balwin-Lomax (and extensions) turbulence model

HSCT Configuration

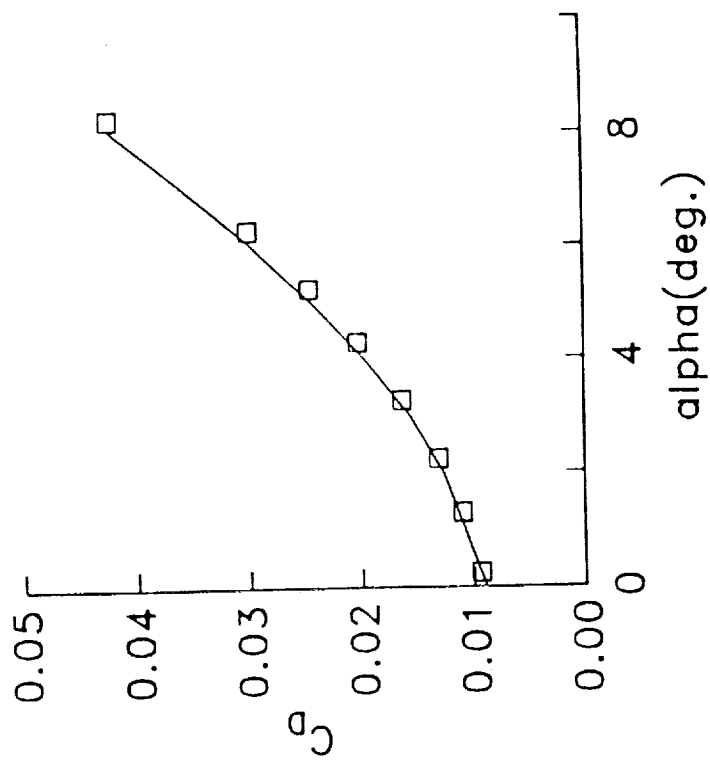
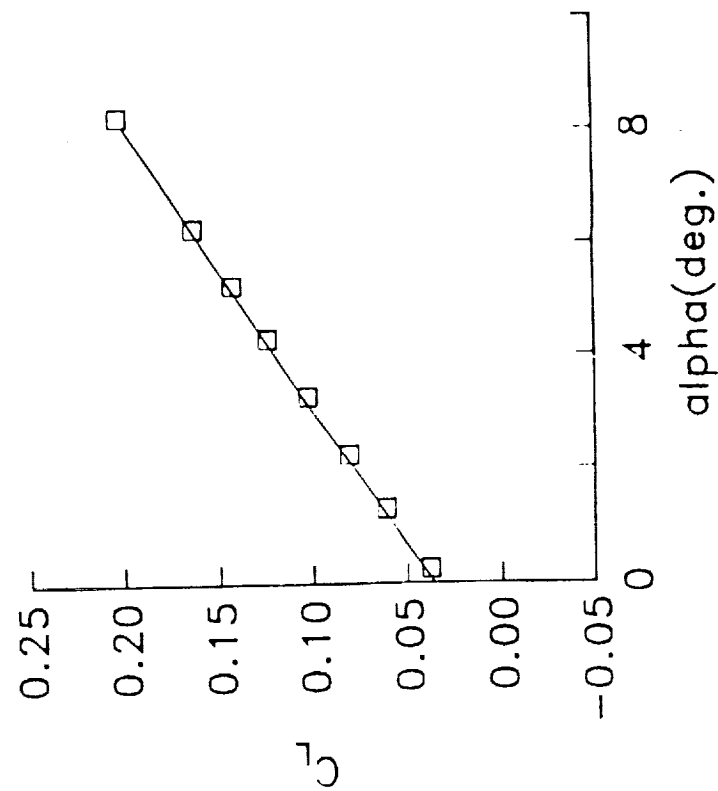


COMPARISON OF FORCE-COEFFICIENTS FOR HSCT

($M_\infty = 3.0$, $Re_l = 6.3 \times 10^6$)

(a) Lift coefficient (b) Drag coefficient

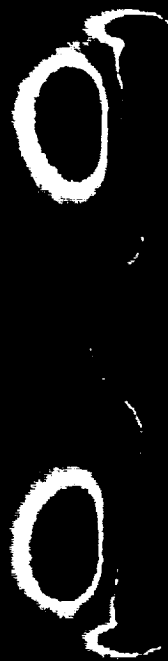
□ Experimental data — Present Results



HSC1 CONFIGURATION

Total Pressure

Mach = 3, alpha = 10 deg, Re = 4.4 million



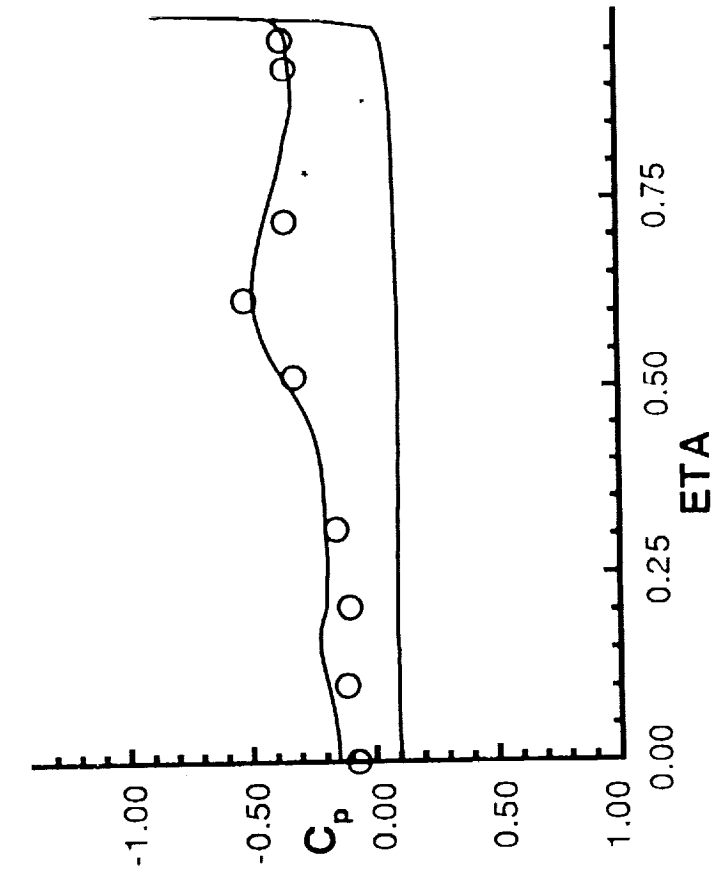
HSCT CONFIGURATION

Surface Pressure Distributions

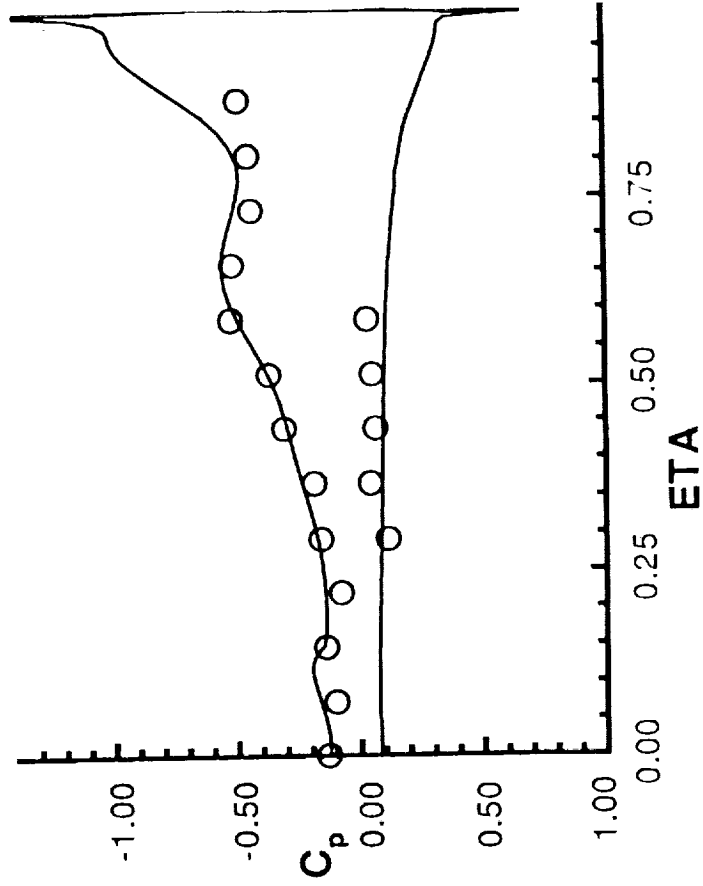
($M_\infty = 3$, $\alpha = 10.0^\circ$, $Re_L = 4.4 \times 10^6$)

○ Experimental

— CFL3D



$x = 129$



$x = 171$

NASA



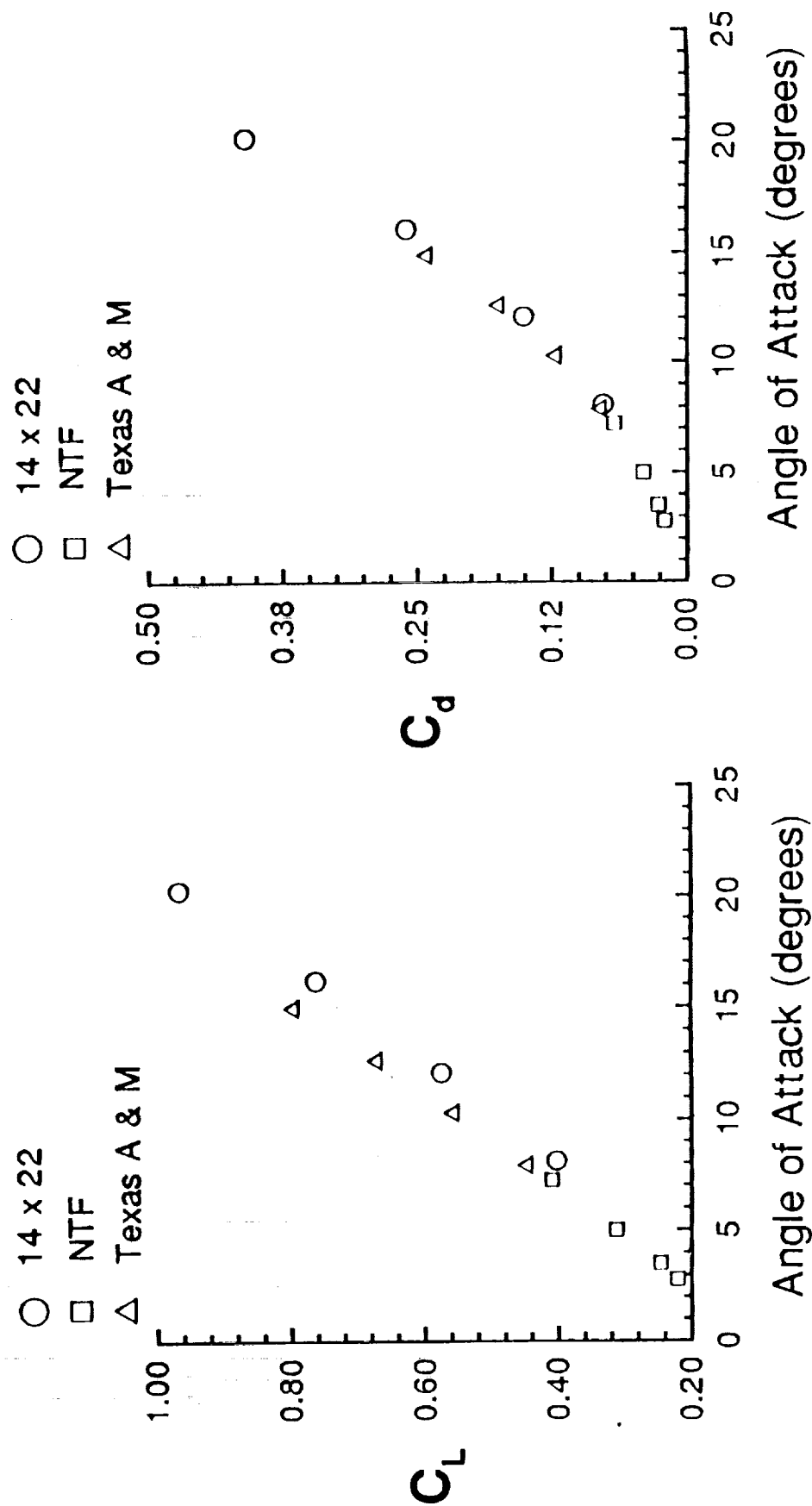
ORIGINAL PAGE IS
OF POOR QUALITY

1705

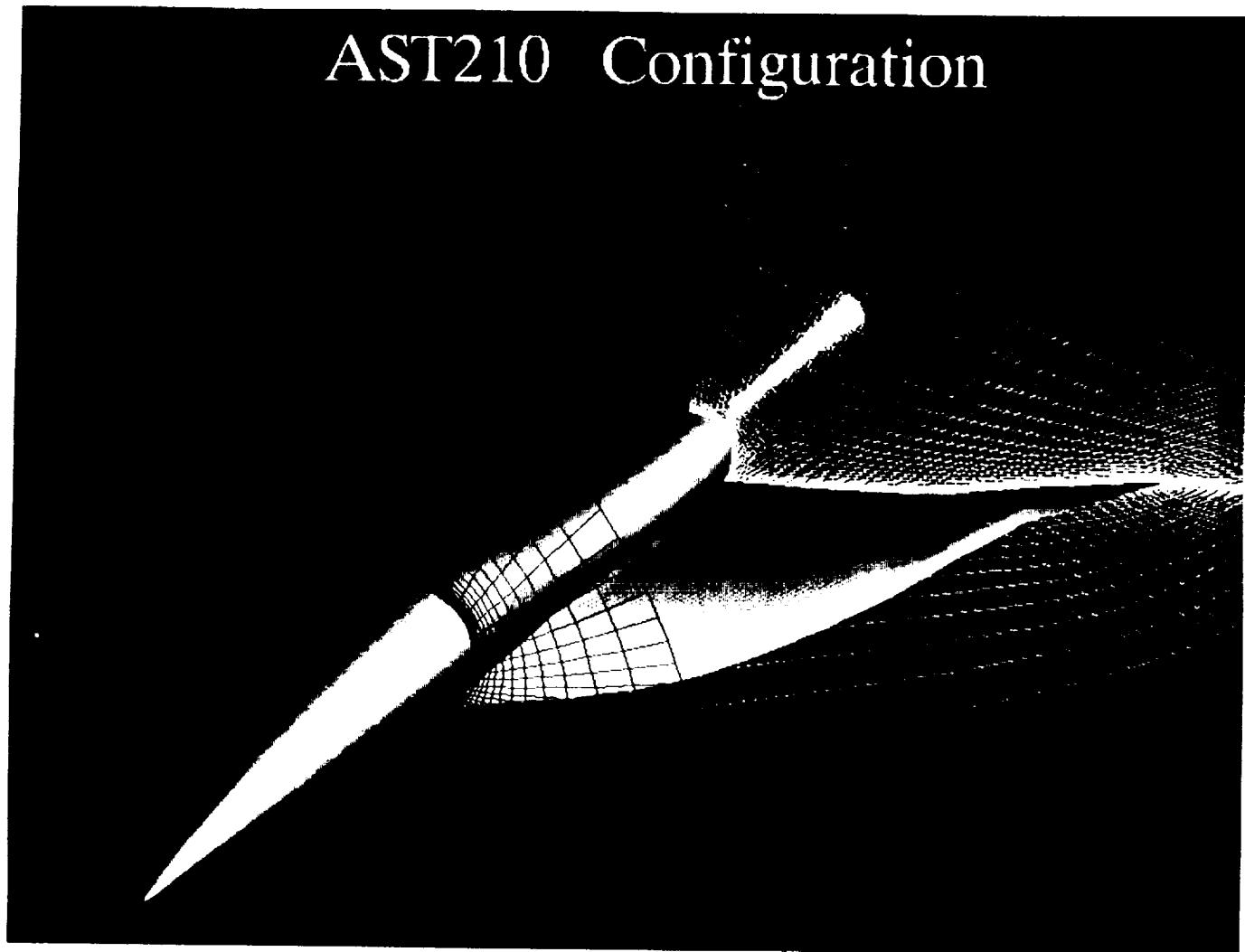
AST210 Configuration

Force Comparisons

Mach=.22



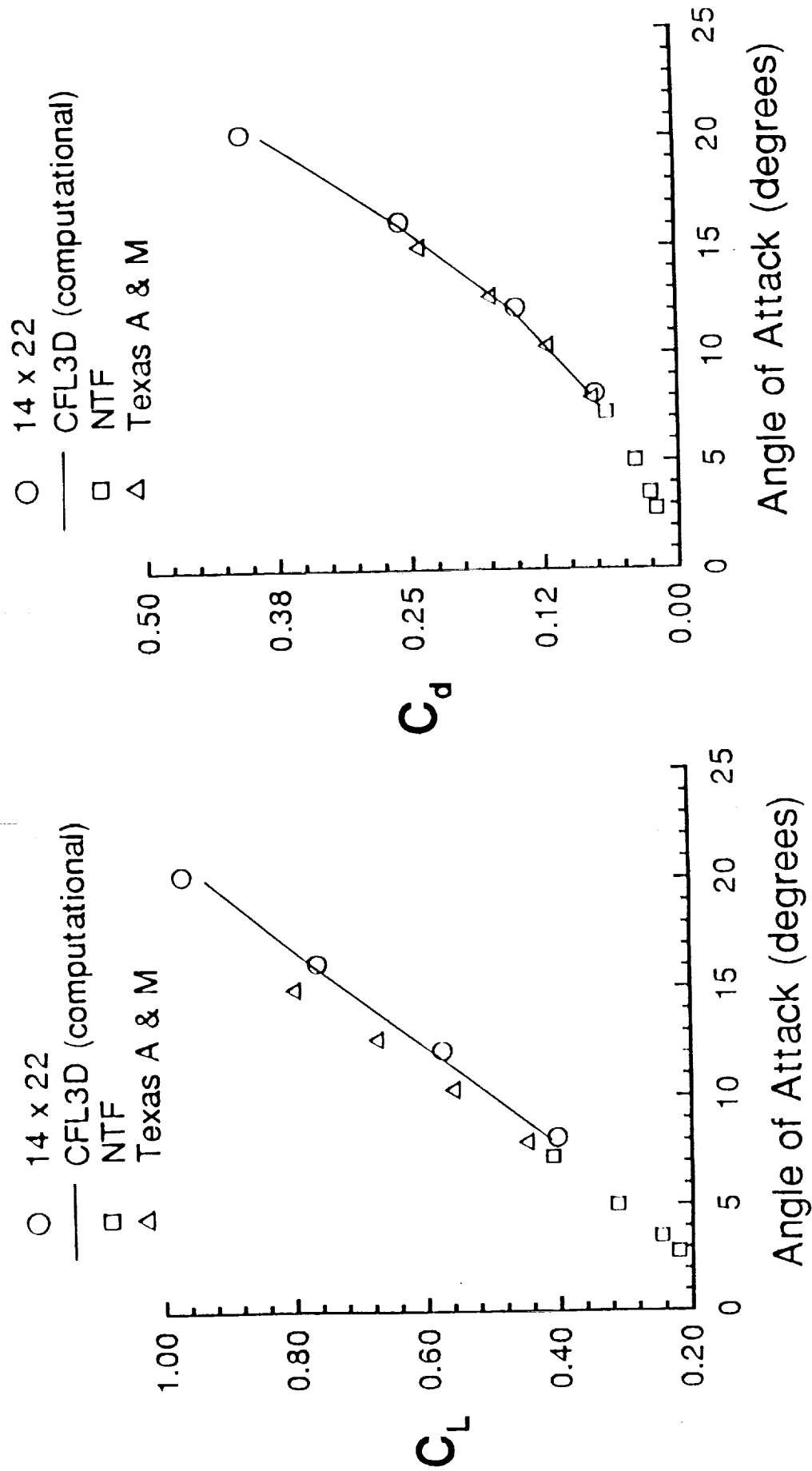
AST210 Configuration



AST210 Configuration

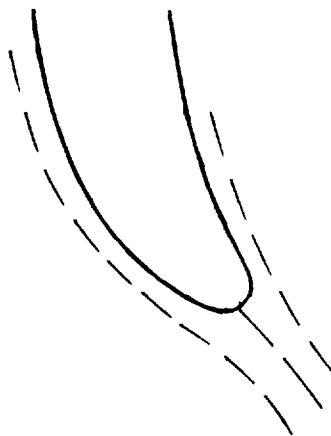
Force Comparisons

Mach=.22

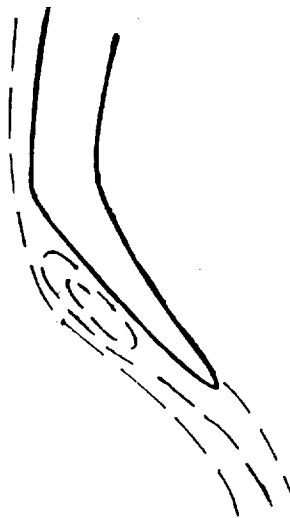


LEADING-EDGE FLAP DESIGN FOR HIGHLY-SWEPT, THIN WINGS

Vortex Suppression



Vortex Control



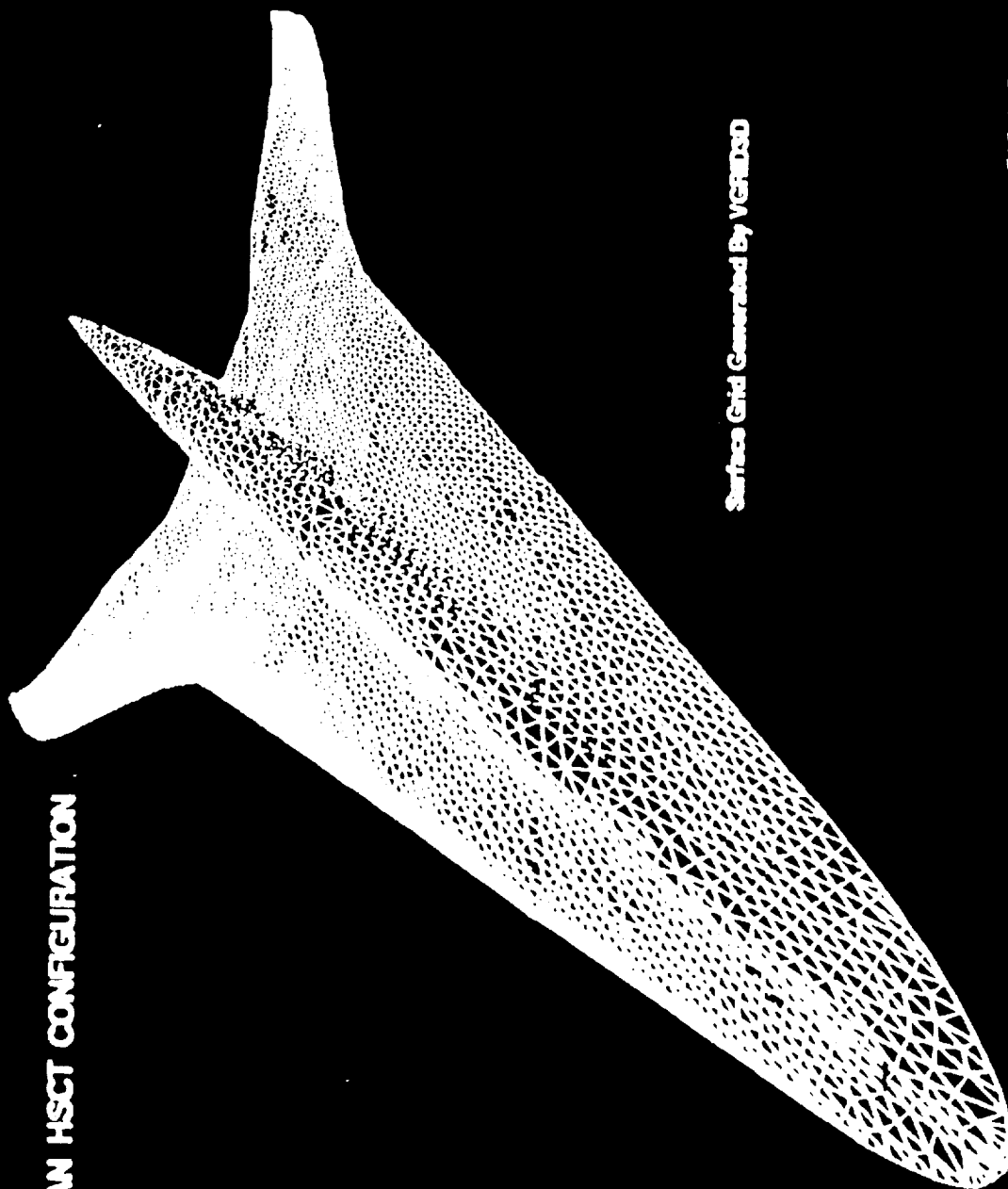
Attached Flow Flap

Vortex Flap

EMERGING GRID TECHNOLOGIES

- Chimera
- Unstructured
- Solution adapting

AN HSCT CONFIGURATION



Surface Grid Generated By VGRADSD

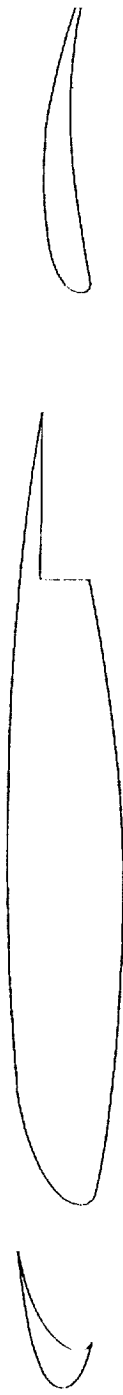
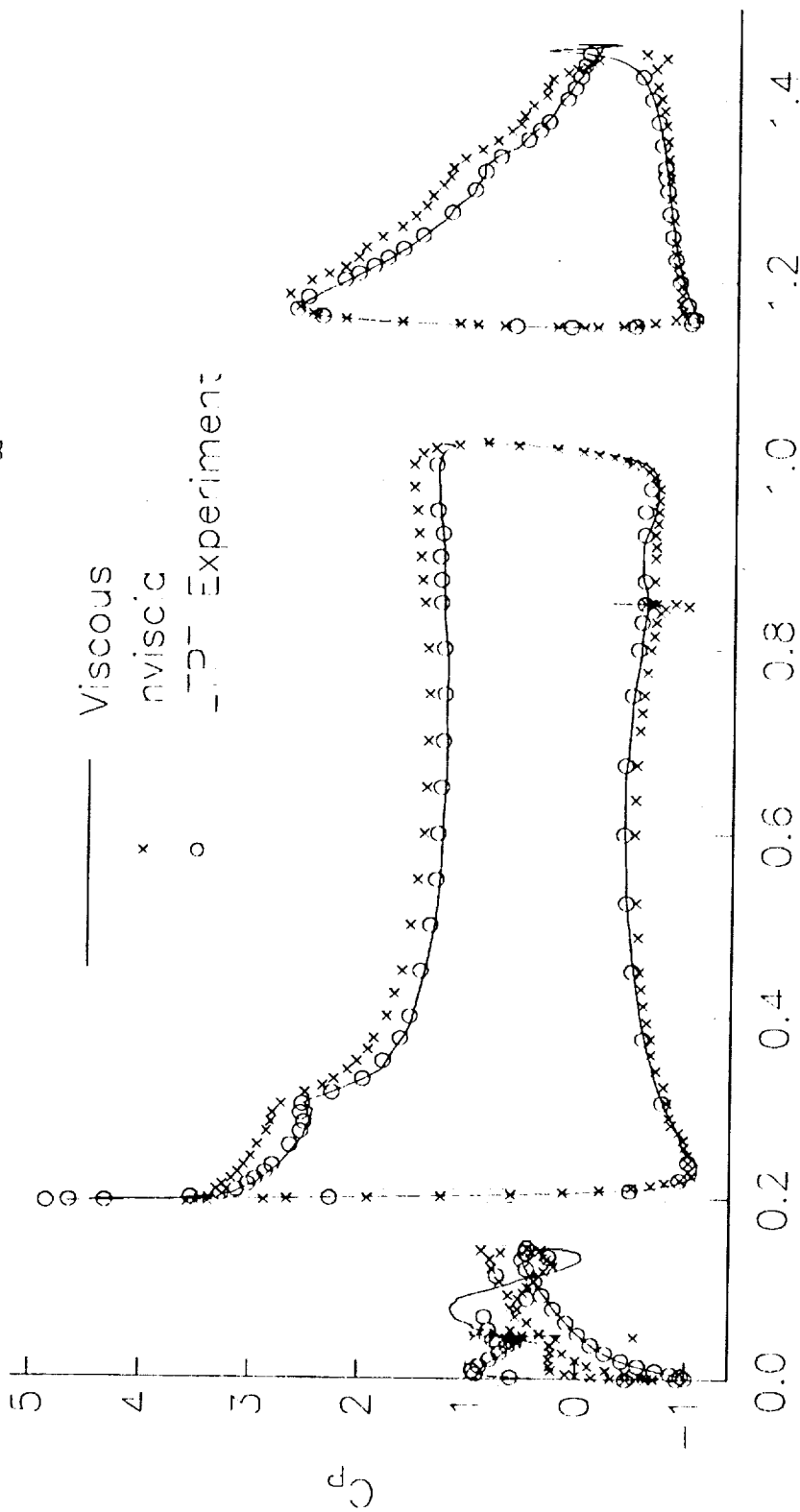
FIG. 4-10-1

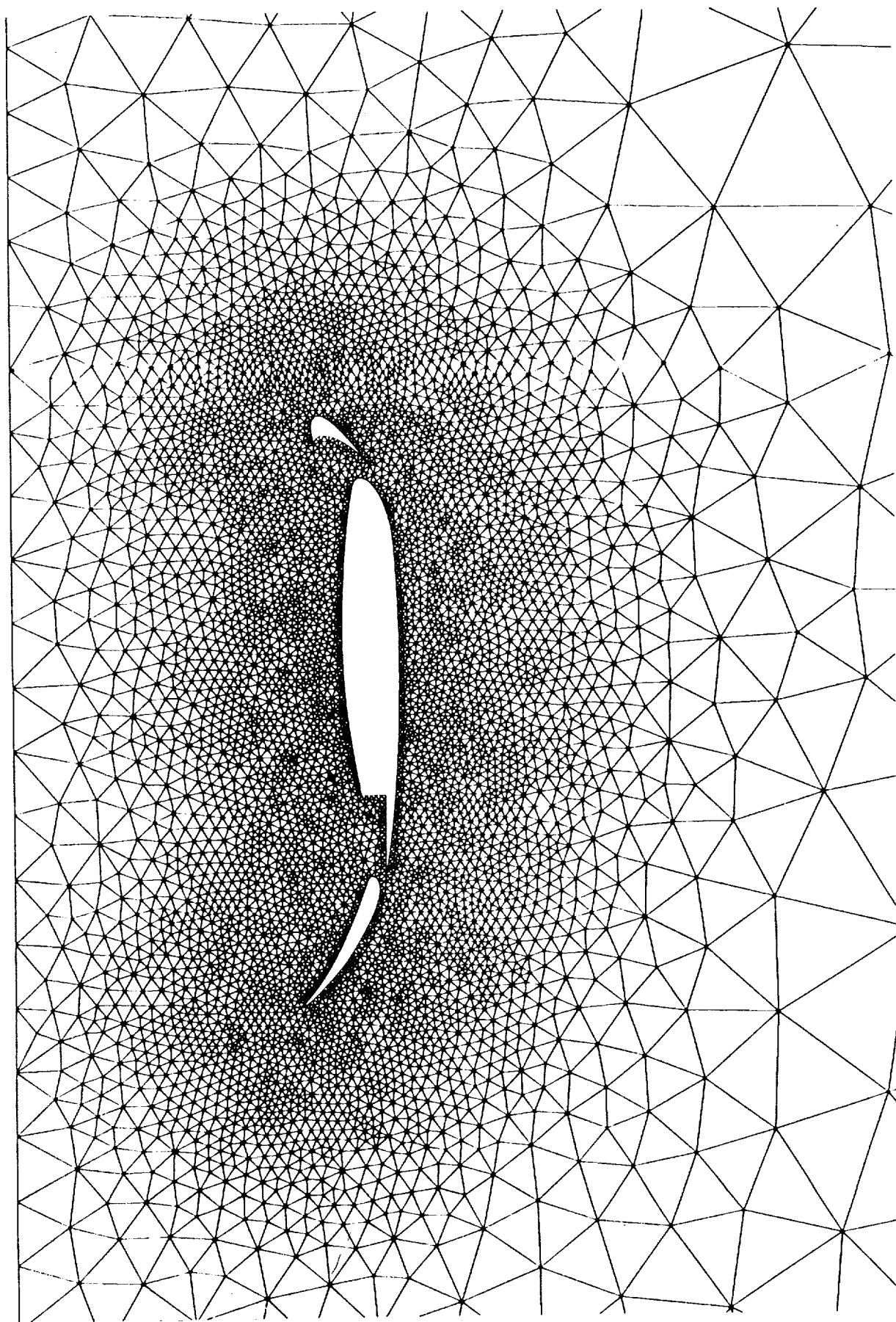
AN HSCT CONFIGURATION

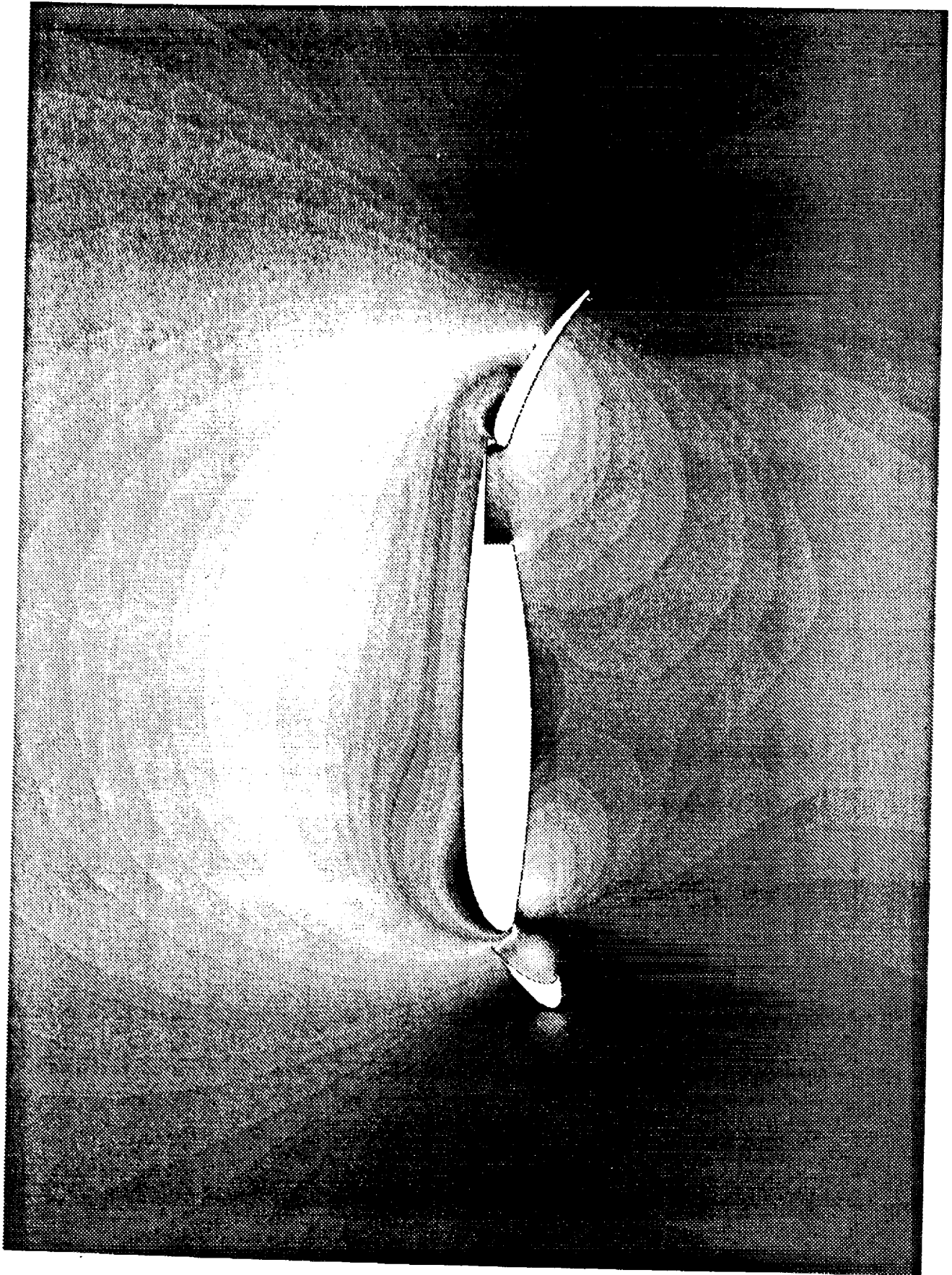
Mach = 8.98, Alpha = 6.47 Deg.

Enter Solution Using USRACD

$\alpha = 0.0^\circ$, $Re = 9 \text{ million}$, $M_\infty = 0.2$







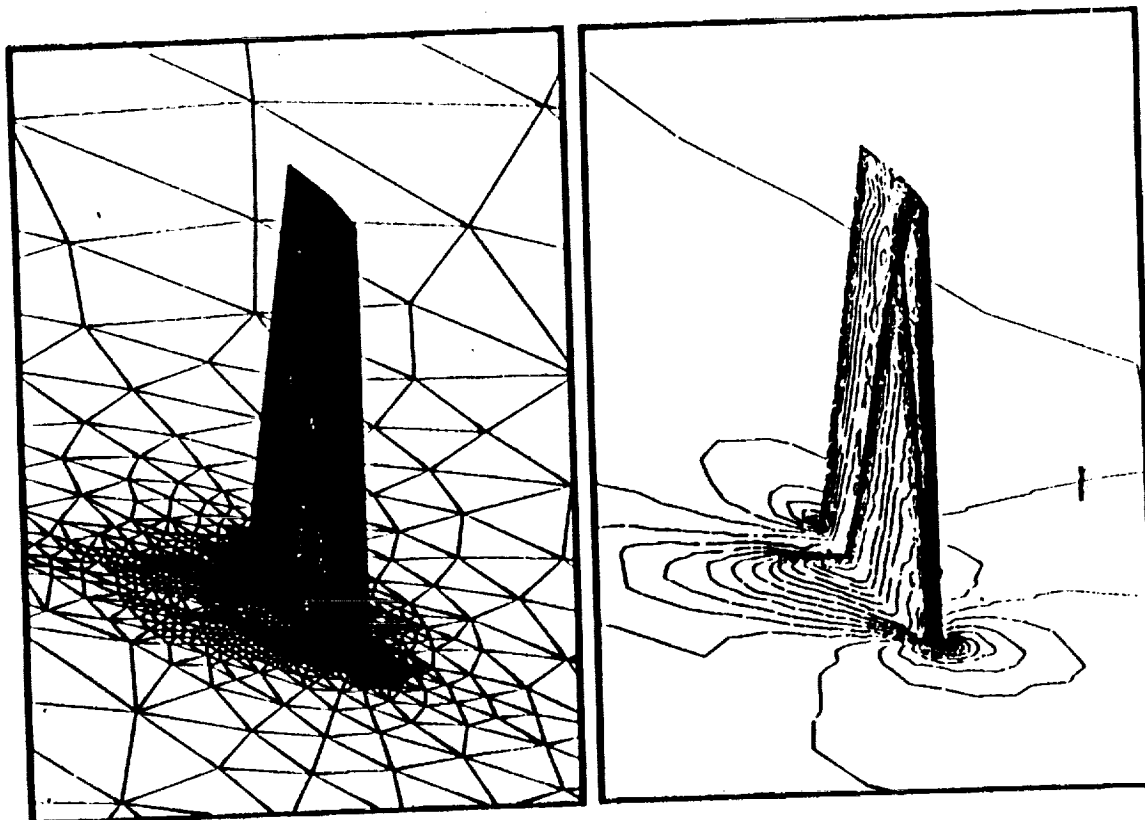


Figure 1: Adaptively Generated Mesh and Computed Mach Contours for Flow Over an ONERA M6 Wing
(Number of Grid Points $\approx 173,412$ Number of Tetrahedra $\approx 1,013,718$)
(Mach ≈ 0.84 , Incidence ≈ 3.06 degrees)

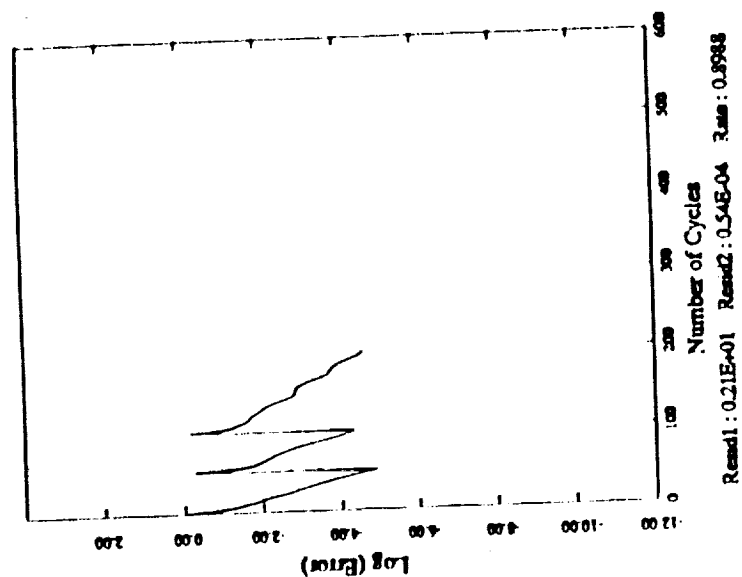


Figure 2: Multigrid Convergence History on the 3 Finest Grids of the Adaptively Generated Multigrid Sequence

CFD PLANS

- Develop unstructured-grid (USG) solver for Euler solutions for highly-swept wing with separated leading-edge flow (9/91)
- Develop capability to generate unstructured grids suitable for N-S calculations on HSCT high-lift systems (6/92)
- Develop USG solver for laminar/turbulent Navier-Stokes equations (9/92)
- Computational assessment of code high-lift predictive capability (9/93)
- Validation of enhanced computational methodology (9/94)
- Complete revisions of USG code as required by feedback from industry users (9/95)

THIS PAGE INTENTIONALLY BLANK

Session XII. High Lift

omit

HSR High Lift Research Program--Status and Plans
Jim Rose, NASA Ames Research Center

PRECEDING PAGE BLANK NOT FILMED

THIS PAGE INTENTIONALLY BLANK

54-02
11979

*HSR High Lift Research
Ames Research Center*

HSR High Lift Research Program

Status & Plans

*Jim Rose
Fixed Wing Aerodynamics Branch*

High Speed Research Workshop May 16, 1991

- Ames participants
- Objective and approach
- Current status
- Research plans

Ames Participants

- Fixed Wing Aerodynamics Branch (FFF)
 - NFAC
 - 7- x 10-Foot Wind Tunnel
 - Applied CFD
- Applied Aerodynamics Branch (RAA)
 - Applied CFD
 - 12 Foot Wind Tunnel
- Applied Computational Fluids Branch (RFA)
 - Computational tools
 - Applied CFD

Benefits of Improved High Lift Performance

- Reduced Noise
 - Increased rate of climb
 - Reduced thrust required
 - Increased utilization
(avoid curfew restraints)
- Reduced Weight
 - Shorter landing gear
 - Smaller/lighter wing
- Improved control/performance
 - Reduced horizontal tail size
 - Lower cruise drag
- Lower cost
 - Reduced complexity
 - Lower maintenance/down time

Objectives

- Evaluate & develop advanced concepts
- Validate design/analysis methods

High-lift systems that contribute to meeting
FAR Stage III noise abatement rules

Approach

CFD Techniques and Analysis:

- Potential flow
Concept development
- Euler
Design
Concept development
- Navier-Stokes
Analysis
Concept development
Rn effects

Wind Tunnel Experiments:

- 7x10 W.T.
Flow physics & understanding
- 40x80x120 W.T.
Concept evaluation & development
Scale effects
Integrated aerodynamics, acoustics,
& propulsion
High fidelity experiments
- 12 Foot High-Re W.T.
Rn effects
Mach number effects

Advanced High-Lift Concept

Trapped vortex to provide high lift at low α

Current Status

- Identified trapped vortex as promising technology
- Parametric studies using CFD tools
- Preliminary W.T studies with Boeing on simple systems
- Tests in preparation for 7 x 10 in summer '91
- Continuing CFD work to Euler & N-S computations of realistic configurations

High Speed Research Workshop May 16, 1991

Experimental Results to Date

- 2-D water channel experiments are encouraging
- Several 2-D wind tunnel experiments have shown similar results
- Tests of single fence configurations on Boeing low-speed model showed only small lift and pitching moment benefits

Two-fence configuration should increase performance

Tests Planned in FY '91

- Basic Research Test 7/91
 - Ames 7x10 W.T.
 - Examine effects of sweep and fence geometry
- Boeing HSCT test 8/91
 - Ames 7x10 W.T.
 - Two-fence configurations based on above results

High Speed Research Workshop May 16, 1991

Basic Research Test

7 x 10 Foot Wind Tunnel

sweep
angle

vortex fences

wing

false floor

strut fairing

wing mount

balance frame

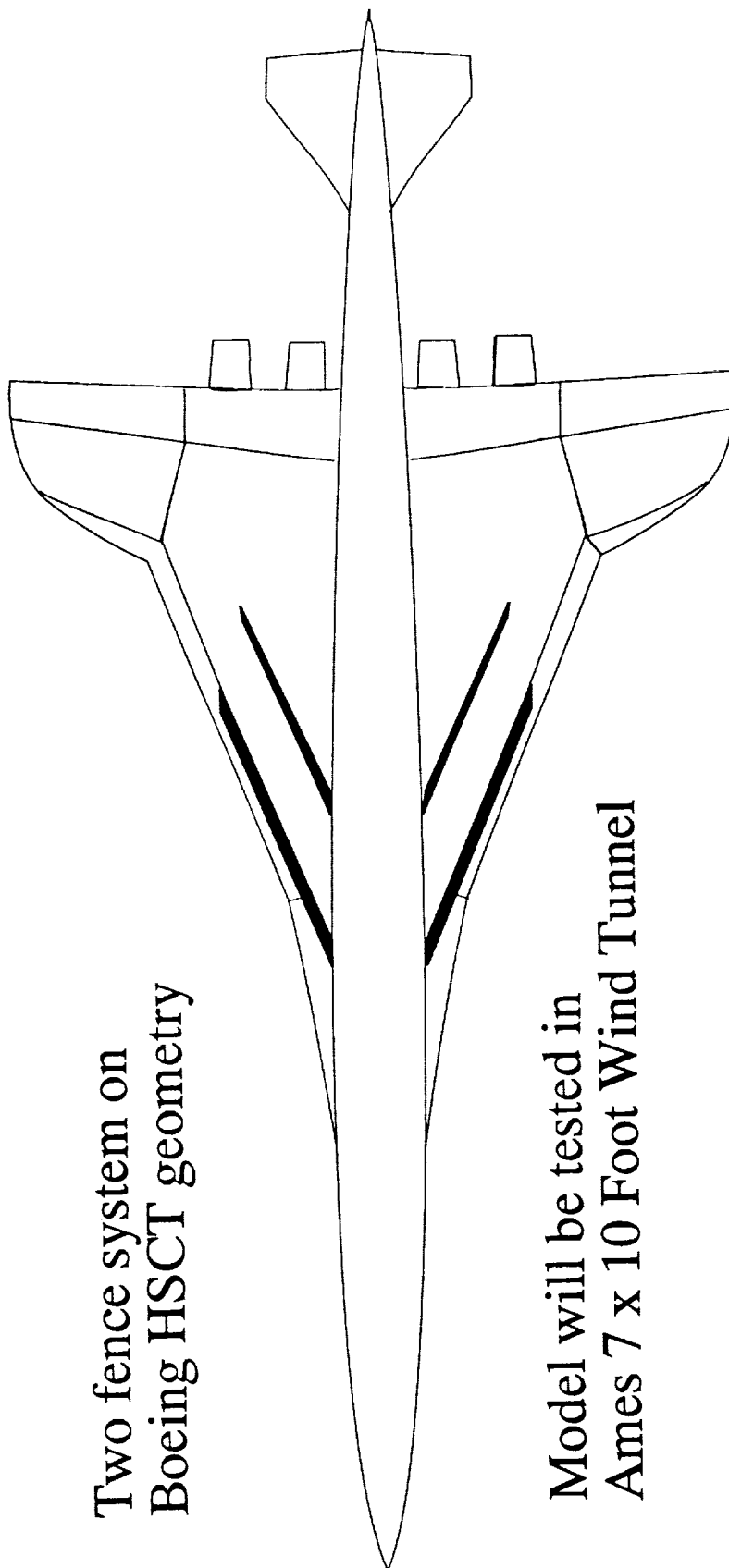
V

High Speed Research Workshop May 16, 1991

*HSR High Lift Research
Ames Research Center*

Application to HSCT Configuration

Two fence system on
Boeing HSCT geometry



Model will be tested in
Ames 7 x 10 Foot Wind Tunnel

High Speed Research Workshop May 16, 1991

Applied CFD

Objective:

To use and improve computational methods for evaluation and development of high-lift systems for HSCT configurations

Approach:

Use codes appropriate to level of development

- Potential flow
- Euler
- Navier-Stokes

Potential Flow Analysis

Trapped Vortex Stability Analyses

- Mapping technique
- Compute stable point for vortex
- Determine suction requirements
- Parametric fence geometry variations

~~8-2~~

Euler Method

- Unstructured Grid Code (TIGER)
 - Cell refinement capability
 - * Delta wing generic fighter (vortex tracking)
 - * ONERA M-6 wing (shock refinement)
 - Deflected flap analysis capability
 - * Straight wing with adjacent leading edge flaps
- Plans
 - Trapped vortex configurations (model small-scale tests)
 - SCAT-15 model

Navier-Stokes

- Incompressible N.S.
 - INS2D code validated for trapped vortex
 - * Backward facing step
 - * Single and double fence on plate
 - Initial 3-D results obtained for double fence case
- Plans
 - Examine R_n effects
 - Model small-scale experiments
 - Realistic HSCT wing geometry

Additional Research Opportunities

- Trapped vortex performance on SCAT-15 model (LaRC 14 x 22 test)
- Trapped vortex on E-7 model (40 x 80)
- Examine leading edge radius effects, drooped leading edge, & Krueger flap on E-7 model (cooperative studies with LaRC, Boeing and DAC in 40 x 80)
- LaRC vortex flap on E-7 model (40 x 80)

Summary

- Have identified trapped vortex as a candidate high-lift technology
- Preliminary analyses and experiments are promising
- Extension of analysis to 3-D is underway
- Two 3-D wind-tunnel experiments are in preparation and scheduled to begin in July

High Speed Research Workshop May 16, 1991

THIS PAGE INTENTIONALLY BLANK

omit

Session XII. High Lift

HSCT High Lift System Aerodynamic Requirements
John A. Paulson, Boeing Commercial Airplane Group

HSCT

HIGH LIFT SYSTEM AERODYNAMIC

REQUIREMENTS

55-02
11980

JOHN A. PAULSON
BOEING COMMERCIAL AIRPLANE GROUP
SEATTLE, WASHINGTON

HIGH SPEED RESEARCH WORKSHOP
LANGLEY RESEARCH CENTER

MAY 16, 1991

INTRODUCTION

Low speed aerodynamic performance has been identified as critical to the successful development of an HSCT. The airplane must takeoff and land at sufficient number of existing or projected airports to be economically viable. At the same time, community noise must be acceptable.

Improvements in cruise drag, engine fuel consumption, and structural weight tend to decrease the wing size and thrust required of engines. Decreasing wing size increases the requirements for effective and efficient low speed characteristics. Current design concepts have already been compromised away from better cruise wings, like arrow wings, for low speed performance. Flap systems have been added to achieve better lift-to-drag ratios for climb and approach and for lower pitch attitudes for liftoff and touchdown.

Research to achieve improvements in low speed aerodynamics needs to be focused on areas most likely and have the largest effect on the wing and engine sizing process. It would be desirable to provide enough lift to avoid sizing the airplane for field performance and to still meet the noise requirements. A more economically viable airplane would result if we can accomplish improvements in the high lift system. Some of the "compromises" to the cruise configuration could be returned. Some of the gain will require regulatory changes allowing innovative flaps and flap control systems.

Current design activities tend to be centered on double delta wings, trailing edge-mounted nacelles, and aft tail for trim and control. A "snap-shot" of the low speed strengths and weaknesses for this kind of a configuration will be examined. The airworthiness standards developed in 1971 for the USSST will be the basis for performance requirements for an airplane that will not be critical to the airplane wing and engine size.

Where should research for improved low speed performance be focused?

- A snap-shot for:
 - * One particular study airplane
 - * Wind tunnel characteristics for a similar configuration
 - * A proposed set of airworthiness standards
- A look at:
 - * Lift adequate for field performance and speed margins
 - * Drag required for climb gradient requirements
 - * Sensitivity of noise to drag improvements

SIZING FOR CRUISE PERFORMANCE

Ideally, an airplane's wing area and engine size is selected by cruise mission performance requirements without any penalties to give acceptable takeoff and landing performance. To find out what kind of lift and drag characteristics are required to do this, the climb, cruise, and descent performance is calculated for a range of wing areas and engine sizes similar to the illustration. Limitations due to fuel capacity for the class of wings and fuselages being studied can be indicated as limitations as can off-design performance requirements like a minimum rate of climb. The sized configuration would be the minimum wing area and engine size that satisfied all these conditions. Required low speed performance can be added next.

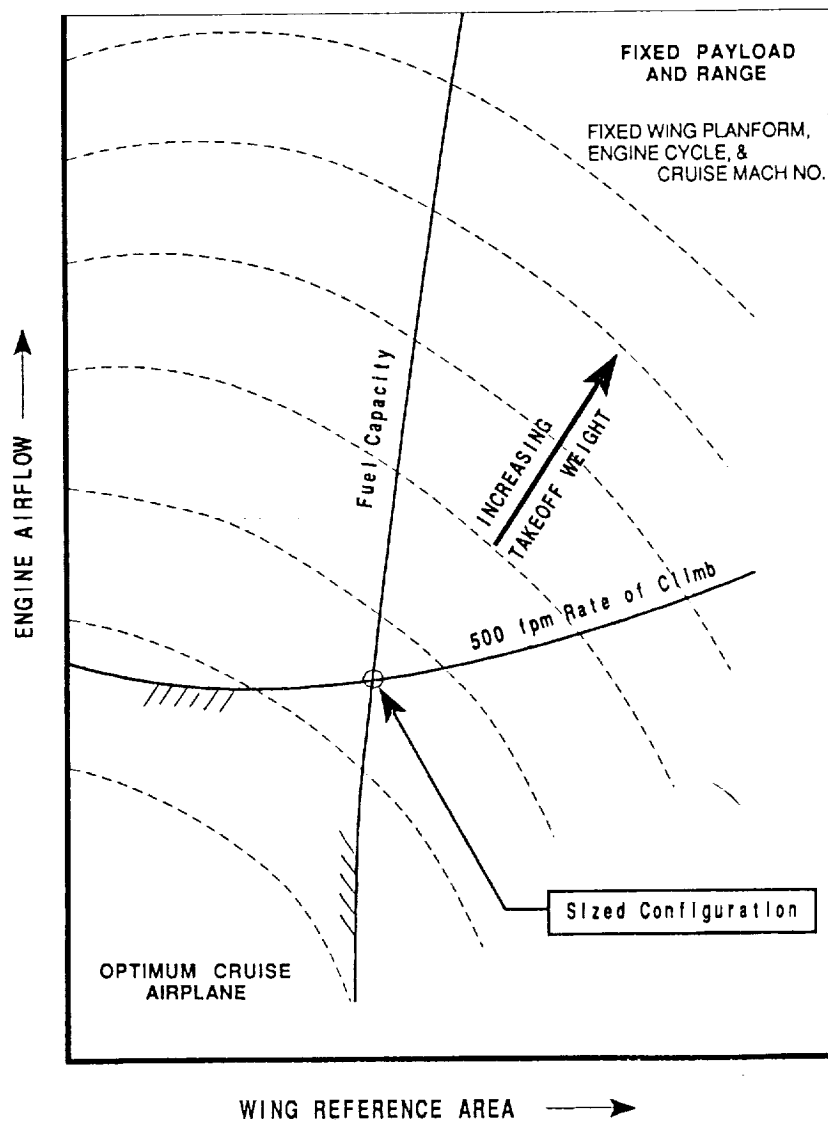


FIGURE 2

LOW SPEED LIFT REQUIRED

The limit of acceptable low speed performance is usually defined for the maximum take off gross weight and the maximum landing weight. The design takeoff field length is related to the airports that are expected to be used. The approach speed is the common parameter for landing and must be considered safe, acceptable to the flight crew, and not require excessive stopping distances even under adverse conditions. Current studies use 11,000 feet for the FAR takeoff field length and 155 knots for approach speed.

For the sized airplane wing area and engine thrust, liftoff and approach lift coefficients can then be calculated that give the design low speed performance. Locus of lines of constant field length and approach speed can then be calculated using these selected lift coefficients as shown for the cruise-defined thumbprint. The values of lift coefficient shown will next be used as starting points to describe related levels of lift that must also be achievable for satisfactory low speed performance.

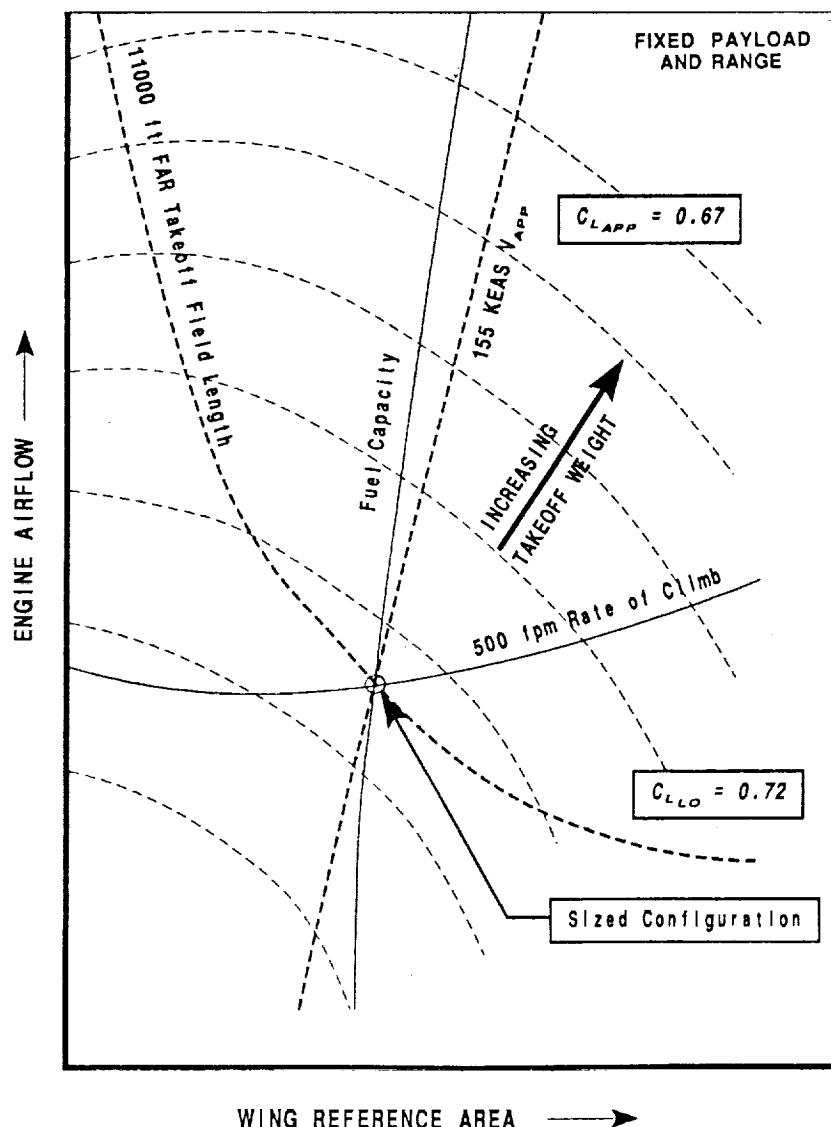


FIGURE 3

LOW SPEED MODEL

The lift and drag needed to give the required takeoff and landing performance will be compared against the characteristics of a low speed wind tunnel model typical of recent configuration studies. The high lift system consists of vortex flaps with vortex fences at the wing apex and unslotted trailing edge flaps. Suppression of leading edge separation was an objective for good climb and approach performance and vortex amplification was used for liftoff and touchdown configurations.

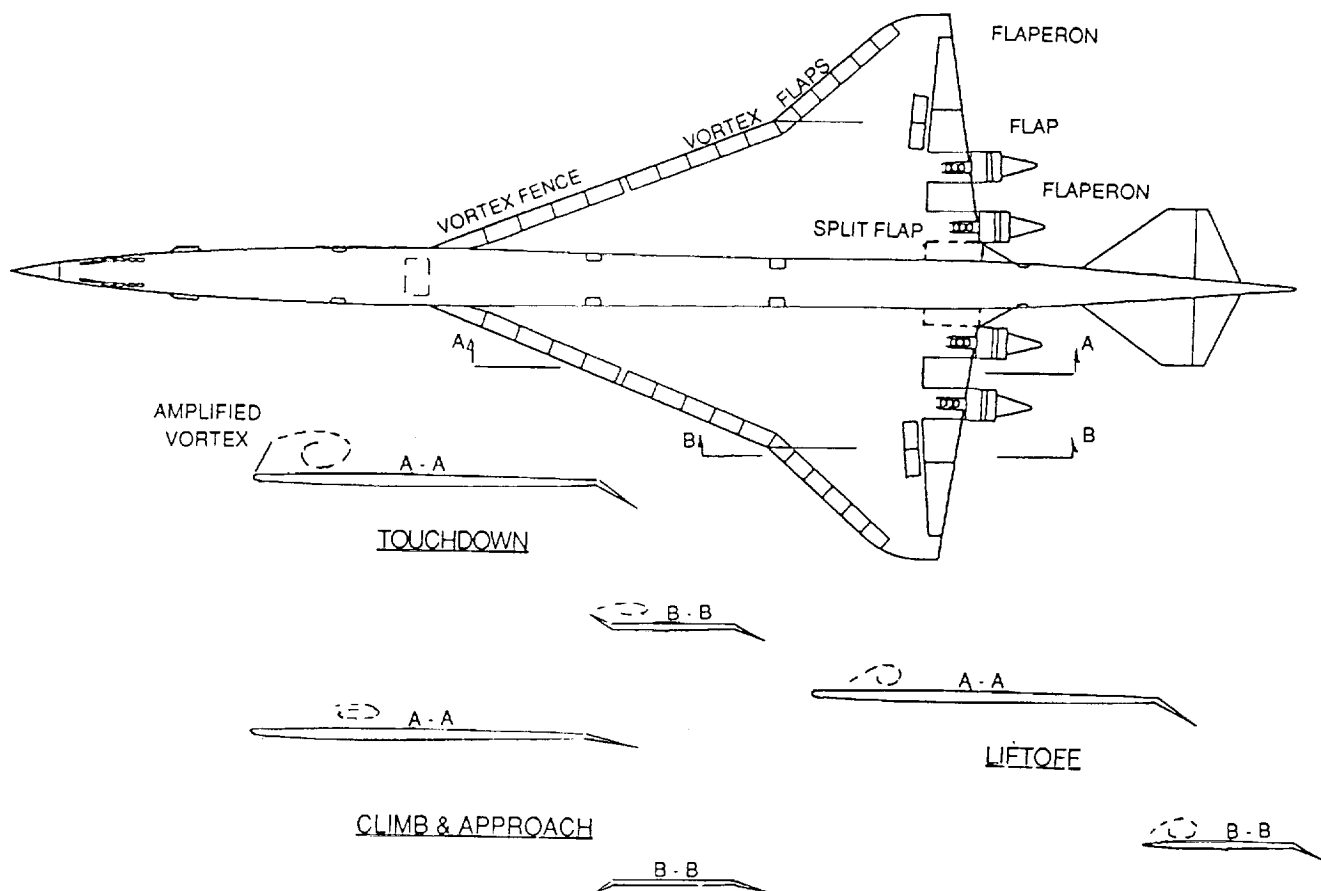


FIGURE 4

HIGH LIFT SYSTEM UTILIZATION

Currently certified airplanes maintain a fixed flap position through takeoff ground roll, liftoff, climb and acceleration until the landing gear is retracted. Similarly, the flap is fixed during landing final approach and is not changed until after touchdown. This convention in operating procedure is required by the Federal Air Regulations (FARs). Automatic procedures that move the flaps in ways that make changes in flap position "invisible" to the crew with equivalent safety need to be made acceptable to the rules when gains in performance can be made. Flaps that reposition themselves in response to angle of attack, speed, altitude, etc. are referred to as "programmed flaps". With them, liftoff and touchdown lift could be increased without necessarily reducing the lift-to-drag ratio during climb and approach. Better climb gradients and lower noise could then be achieved.

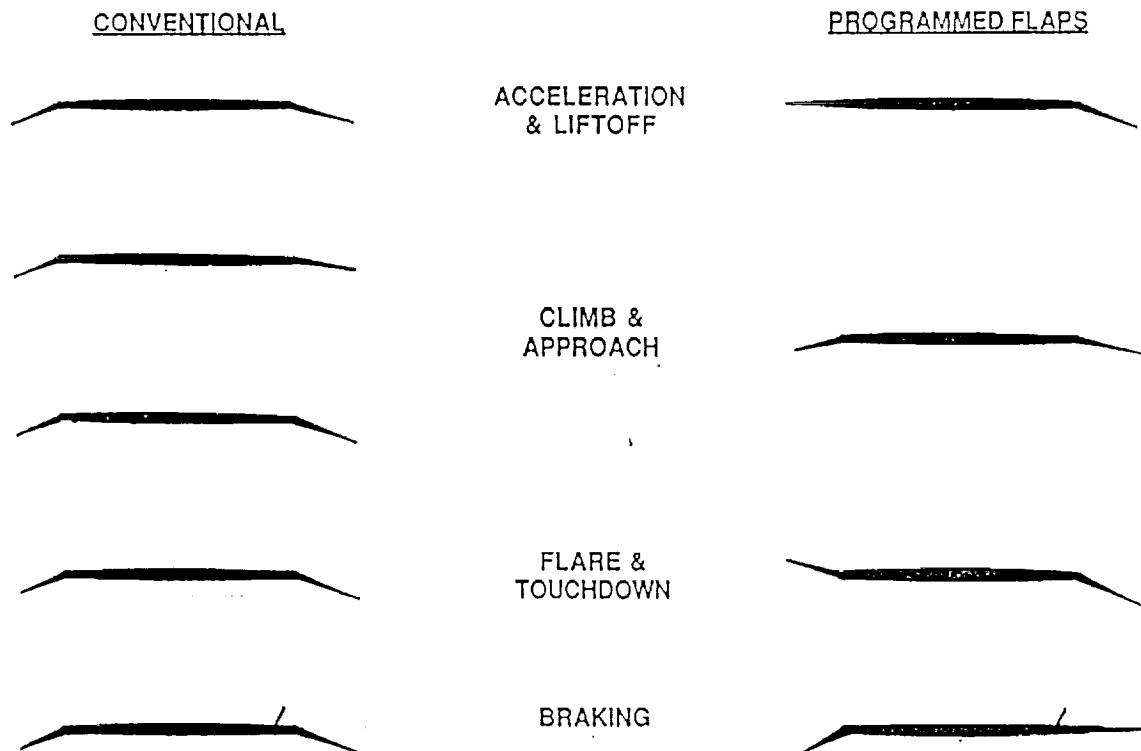


FIGURE 5

LIFT REQUIREMENTS

During the late 1960's and early '70's, a lot of effort was made to define the airworthiness standards for the USSST program prior to its cancelation. The results were the Tentative Airworthiness Standards for Supersonic Transport (1971). These proposed rules recognized, among other things, the significant differences in performance and handling characteristics expected with low aspect ratio wings and high thrust levels.

These proposed rules, along with the Concorde Special Conditions, will have to be reviewed by the industry and further developed to be consistent with projected new technology.

For this study, the TASST's as they existed in 1971 will be used to define and develop the required low speed performance criteria that would be needed in order to have no direct impact on the cruise-sized airplane.

TENTATIVE AIRWORTHINESS STANDARDS FOR SUPERSONIC TRANSPORT (TASST) (1971)

<u>CONDITION</u>	<u>SPEED</u>	<u>REQUIREMENT</u>
Liftoff	V_{lof}	FAR 25.104(b)must not require pitch or roll attitudes that may result in unwanted contact of the airplane with the ground. [V_{mu} requirements deleted but other abuse conditions added]
Touchdown	V_{td}	
Takeoff Climb	V_2	FAR 25.104(a)the selected speeds must provide adequate and defined margins above the minimum demonstrated speeds..... $V_2 > 1.15 V_{min}$ FAR 25.107(b)(1) $V_{app} > 1.23 V_{min}$ { no specific TASST requirement but this value was being used in 1971 }
Approach	V_{app}	
Zero Rate of Climb	V_{zrc}	FAR 25.107(b) ...Speed V_2 ...may not be less than: (3) $1.125 V_{zrc}$..
Minimum Performance Reference Speed	V_{min}	FAR 25.103(b)the applicant shall define, for each appropriate configuration, a minimum demonstrated flight speed V_{min}

FIGURE 6

TAKEOFF LIFT - ATTITUDE LIMITED

Assuming that the wind-tunnel data shown represents the study airplane's capability for lift, the pitch attitude margin to aft-body contact for the liftoff lift coefficient is shown. For maximum takeoff gross weight, a small acceleration occurs during climb to 35 feet (V_2). A feature of the assumed programmed flap system is that the angle of attack would have to be increased after liftoff to accommodate the flap that gives better L/D for climb.

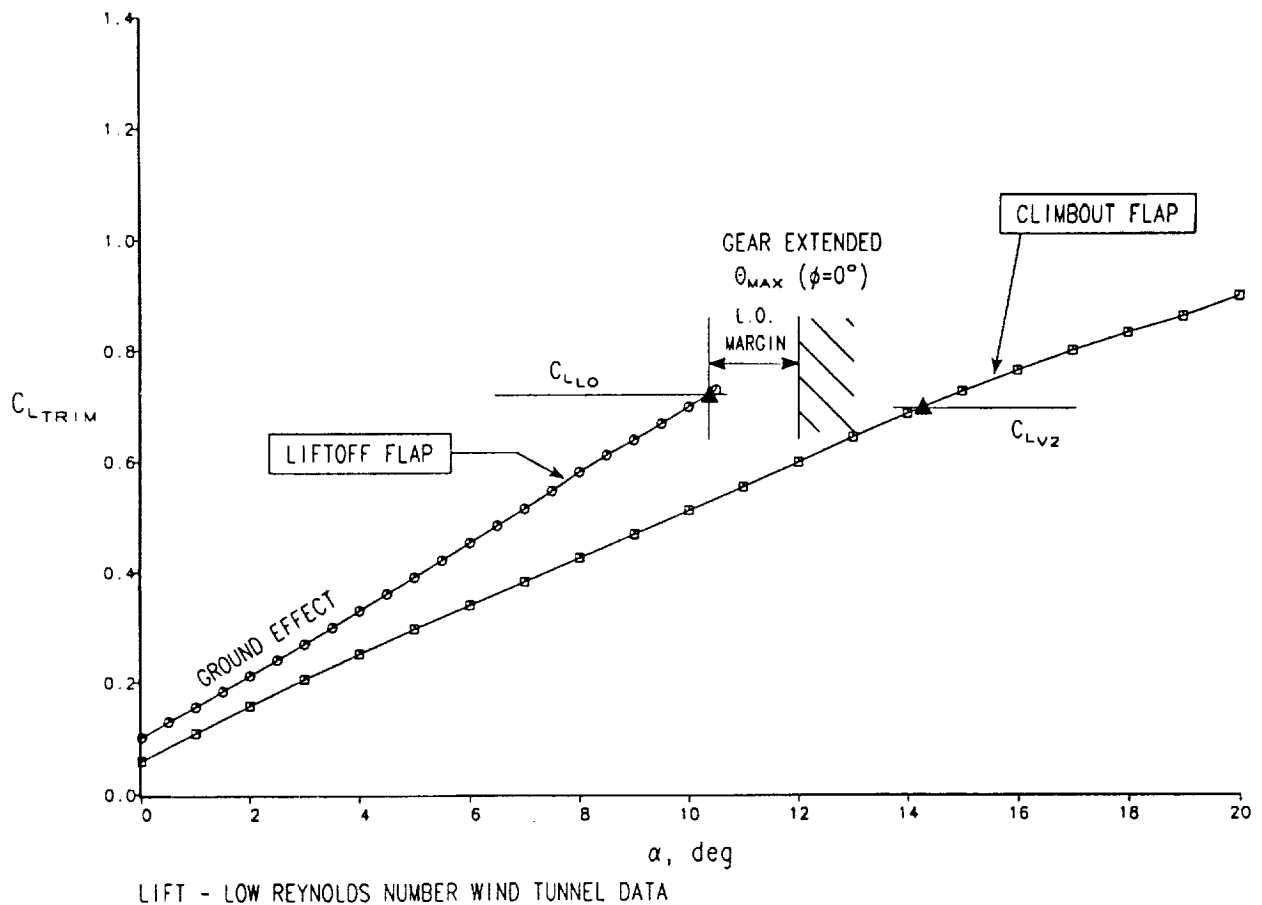


FIGURE 7

LANDING LIFT - ATTITUDE LIMITED

Approach lift coefficient would require a relatively high angle of attack for the programmed flap position that gives the best L/D. After passing the airport boundary, the programmed flaps would transition to the touchdown flap, speed would bleed off during flare, and touchdown would occur with some clearance margin to structural contact.

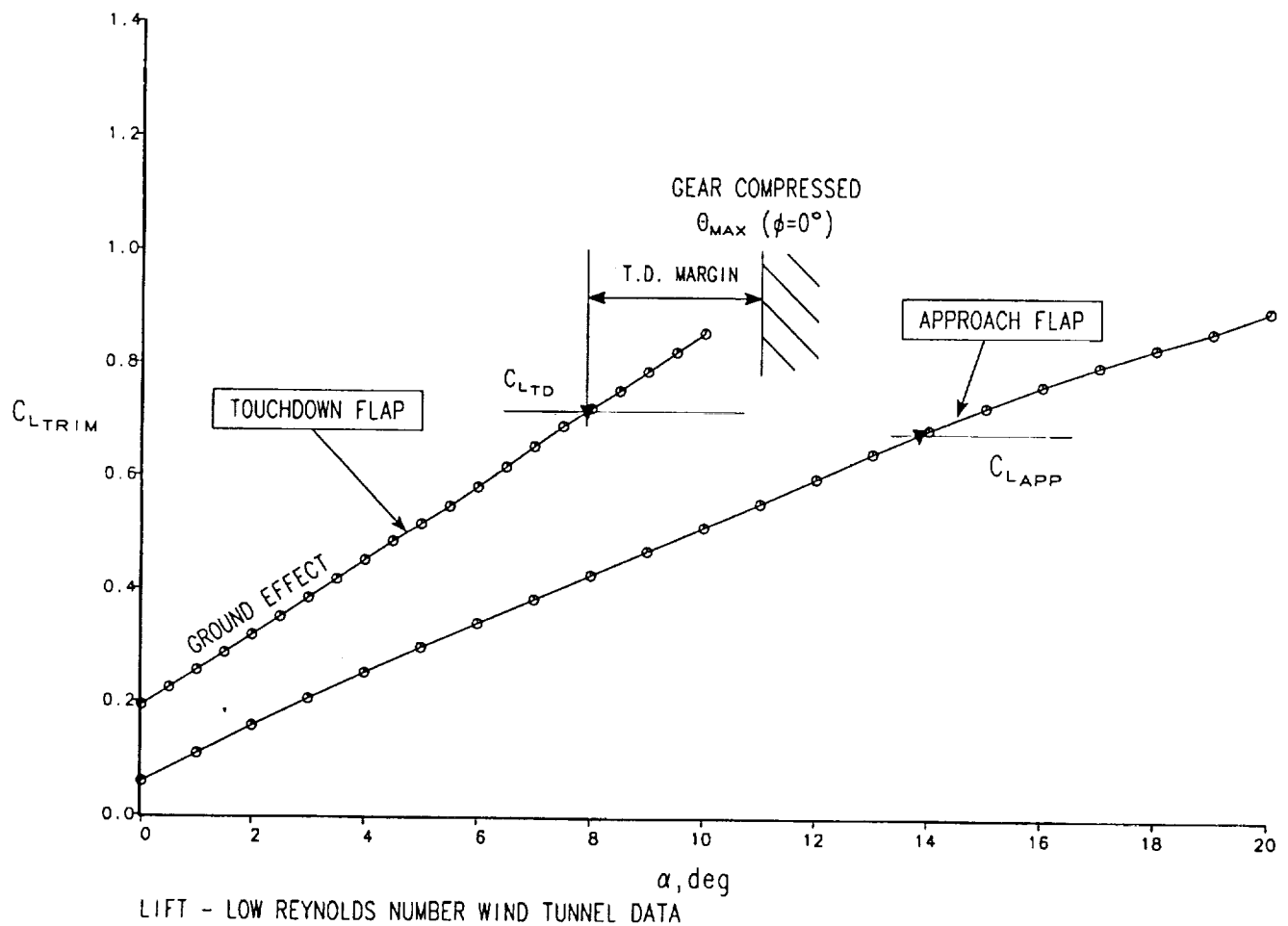


FIGURE 8

GROUND CLEARANCE MARGINS

Typical ground clearance margins for liftoff and touchdown are shown on a pitch-roll clearance plot. These margins must be adequate to give the clearances required to handle TASST abuse conditions and the real-life problems of cross-wind landings, gusts, etc. Clearance margins can be improved with longer landing gear, wing shear, etc., but at some cost in weight and complexity.

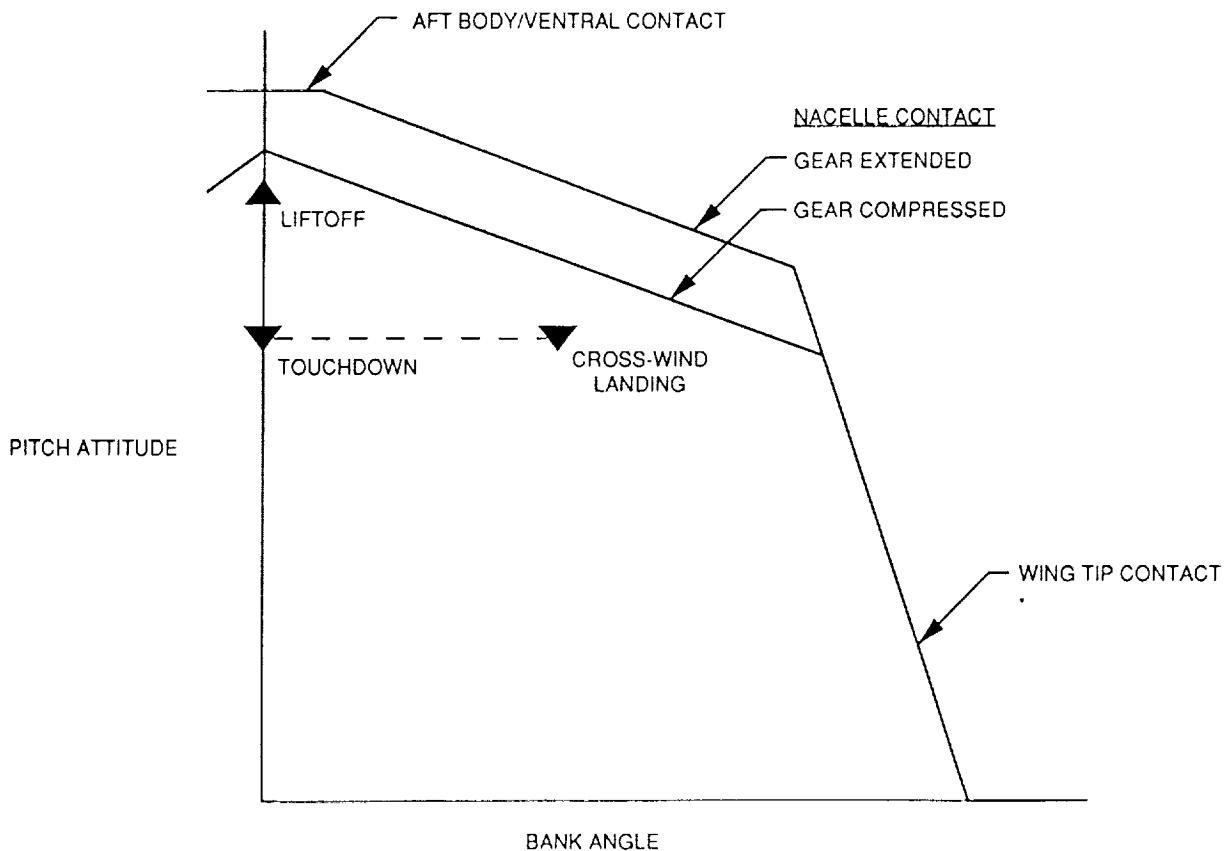


FIGURE 9

LIFT FOR MINIMUM DEMONSTRATED SPEEDS

A feature of the programmed flap system that could be included would be to adjust the flaps as angle of attack increases to give good characteristics for minimum speed demonstration and contribute to recovery if stall were to occur. The normal in-flight low speed configuration would be the flaps for maximum L/D at any angle of attack. This objective could be maintained as pitch attitude increased to the V_{min} demonstrated condition. If an attitude over-shoot occurred, the flap could further transition to a best recovery flap. The liftoff flap and the touchdown flap would also be included so that a single flap configuration would exist at excessive angles of attack.

Several segments of fixed flap data are shown below through which a line is drawn representing the programmed flap function. The lift coefficient for V_{min} required for the approach speed is more critical than for takeoff. It is still less than that available from the wind tunnel model, however.

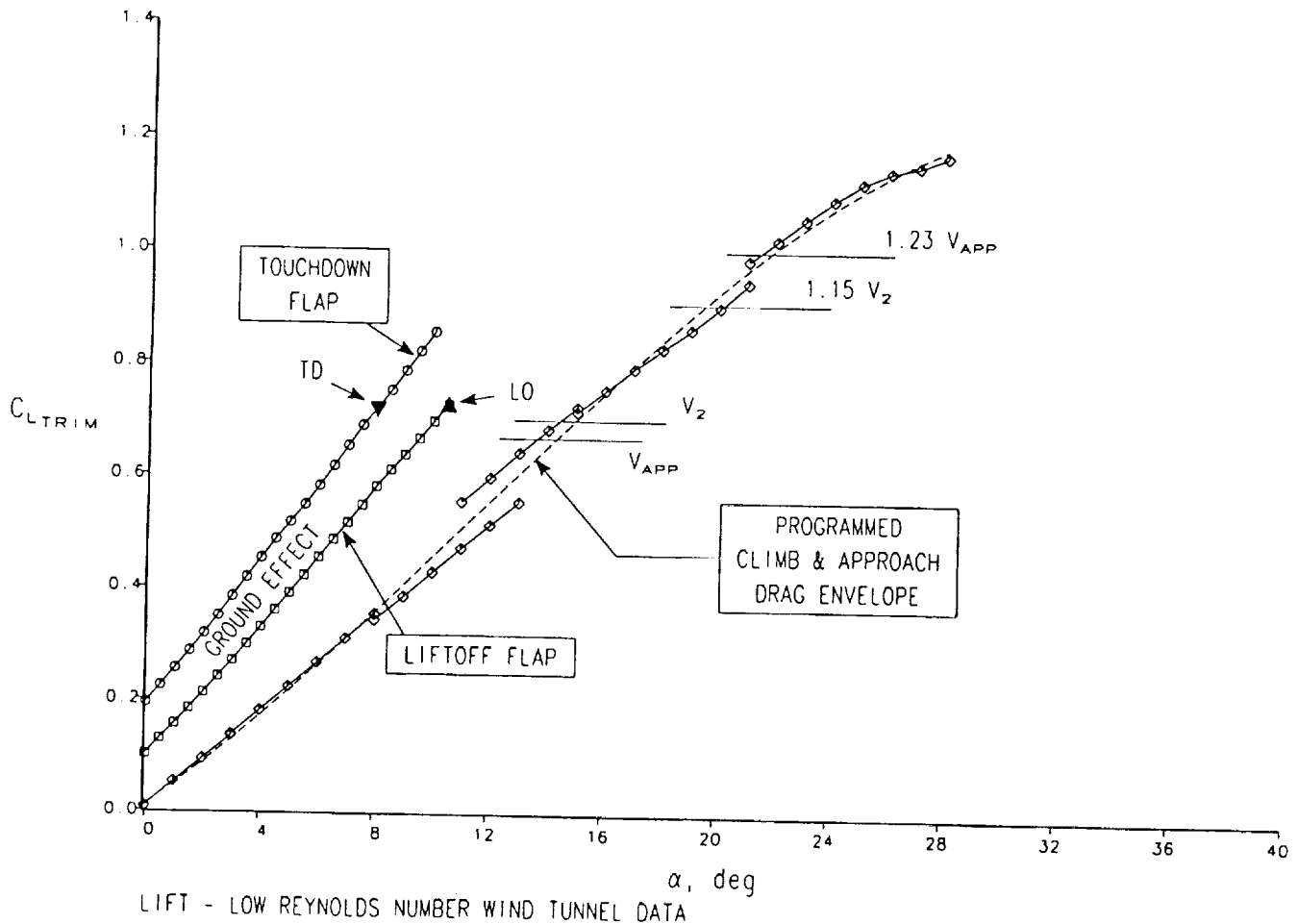
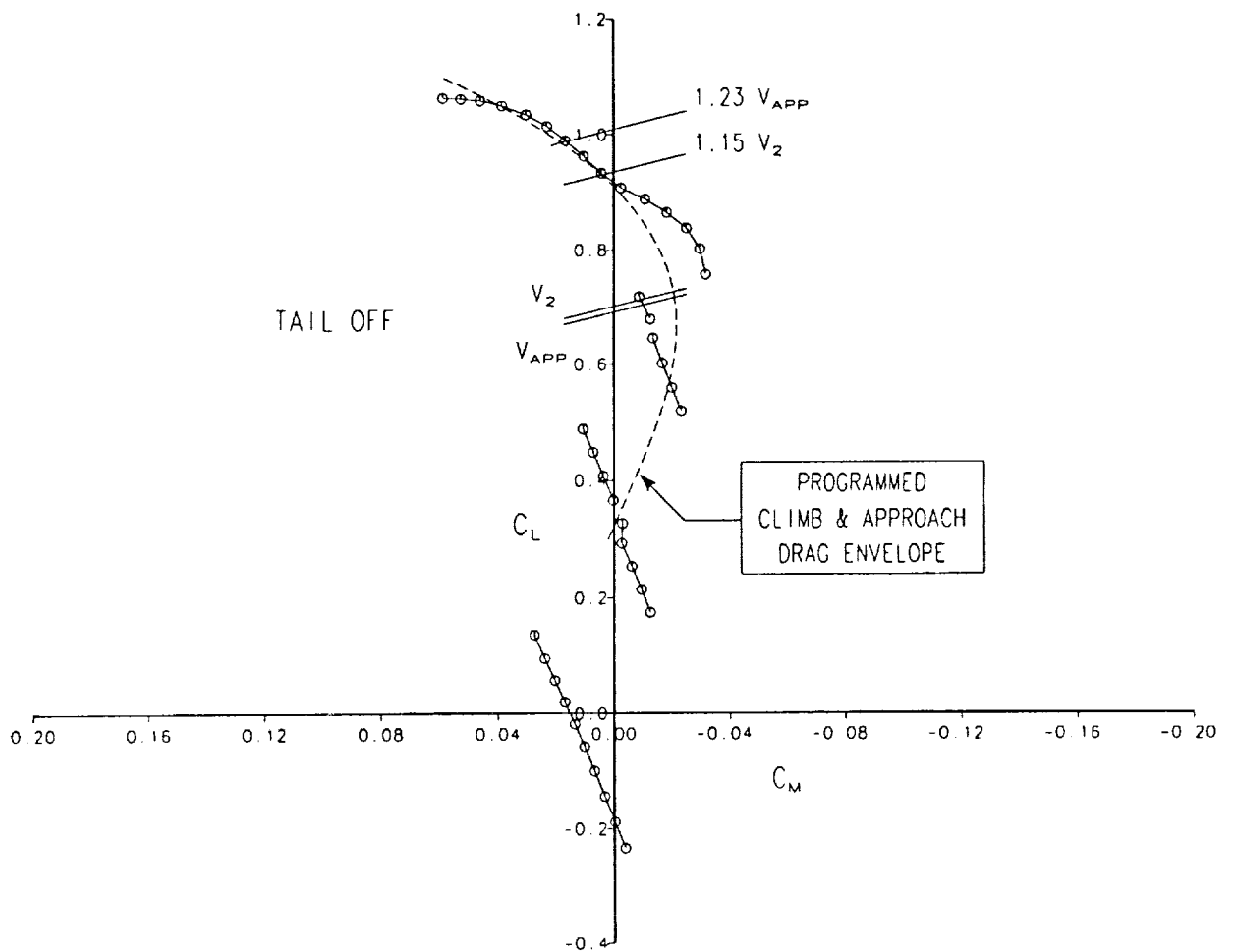


FIGURE 10

PITCHING MOMENT FOR MINIMUM DEMONSTRATED SPEEDS

Some tendency to pitch-up exists at high lift coefficient, but the airplane is nearly trimmed for the V_{min} conditions. Strong recovery capability from the horizontal tail is still possible.

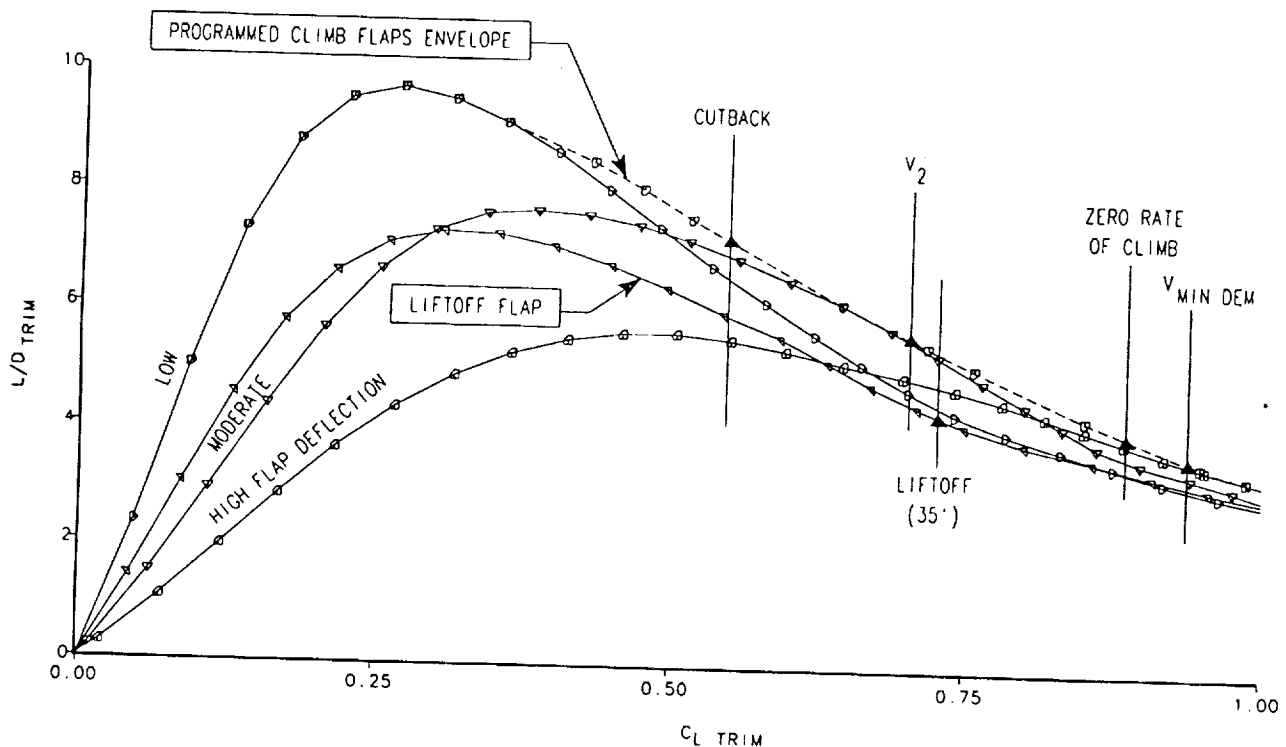


LIFT & MOMENT - LOW REYNOLDS NUMBER WIND TUNNEL DATA

DRAG WITH REQUIRED TAKEOFF LIFT

The drag characteristics with the selected takeoff flaps and speeds are shown below. The liftoff flap gives a lower L/D because higher lift coefficients are the objective. Beginning transition to the scheduled flaps for better L/D after reaching 35 feet gives noticeable improvement by the gear-up point (V_2). Further flap change and acceleration (lower lift coefficient) by the noise cutback point provides a significant improvement in L/D over that of the liftoff flap. If a fixed flap were required for takeoff, a compromised flap would have to be found, having less lift capability but better drag characteristics than the flap chosen for this study.

The zero-rate-of-climb condition and the minimum speed demonstration point are also on the best drag envelope.

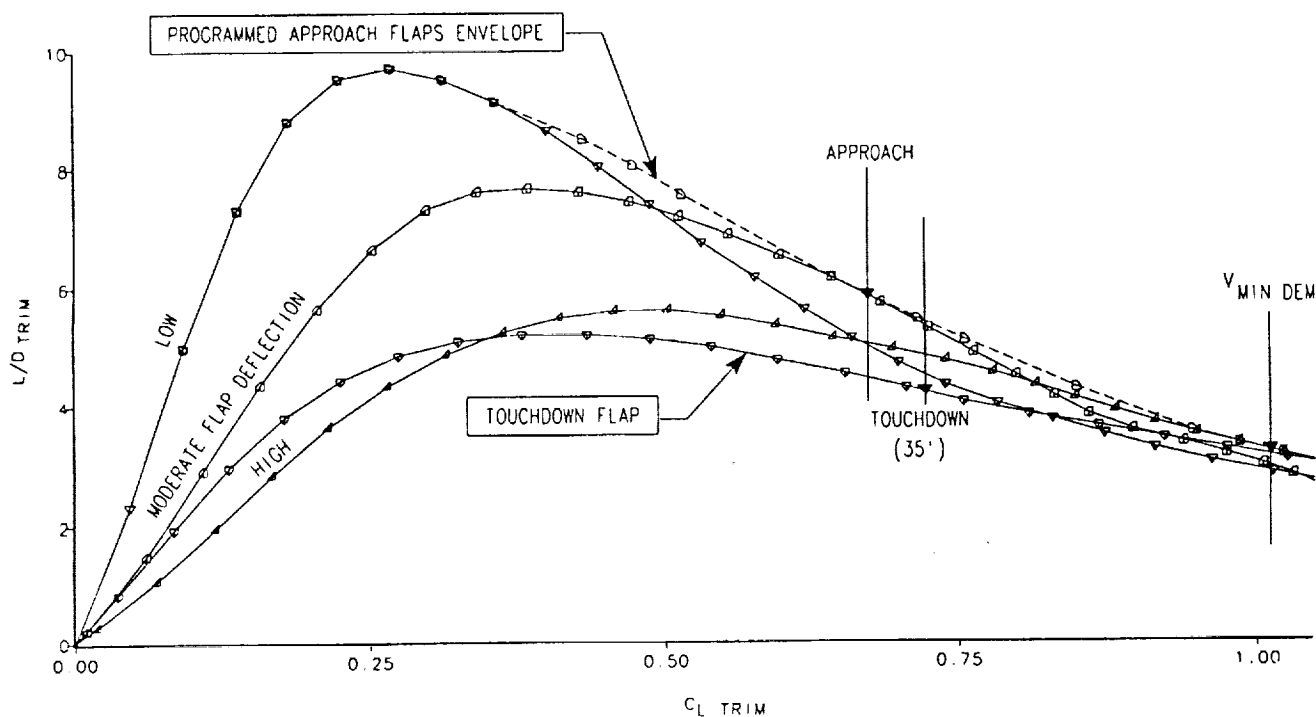


GEAR UP POLARS - LOW REYNOLDS NUMBER WIND TUNNEL TEST

FIGURE 12

DRAG WITH REQUIRED LANDING LIFT

the approach flight segment would be on the envelope for minimum drag. After passing over the airport boundary, the flaps would begin to transition to the touchdown flap. Since higher lift is desired to allow reduced touchdown attitudes, vortex lift from separated leading edges would be favored. The resulting drag increase would contribute to speed bleed-off. In order to maintain a fairly stable pitch attitude, the rate of flap extension may have to be coupled with automatic trim adjustments. Flare would occur with the increased lift due to ground effect.



GEAR UP POLARS - LOW REYNOLDS NUMBER WIND TUNNEL TEST

FIGURE 13

CLIMB GRADIENT REQUIREMENTS

The TASSTs expand on the climb requirements of the FARs by adding the Zero Rate of Climb and the Continued Approach conditions. In addition, four conditions must also be demonstrated maneuvering at 18 degrees of bank.




Zero rate of climb demonstration is part of the requirements for safe flight at high angles of attack, near the minimum demonstrated speed. Takeoff speeds would have a margin relative to V_{zrc} .

Continued Approach is a measure of the ability to safely continue approach following the loss of two engines.

Climb under maneuver conditions would account for the rapid drag build-up of low aspect ratio wings as lift is increased.

These gradient requirements can be used to calculate how low a drag level is required for the cruise-sized airplane to have adequate low speed performance.

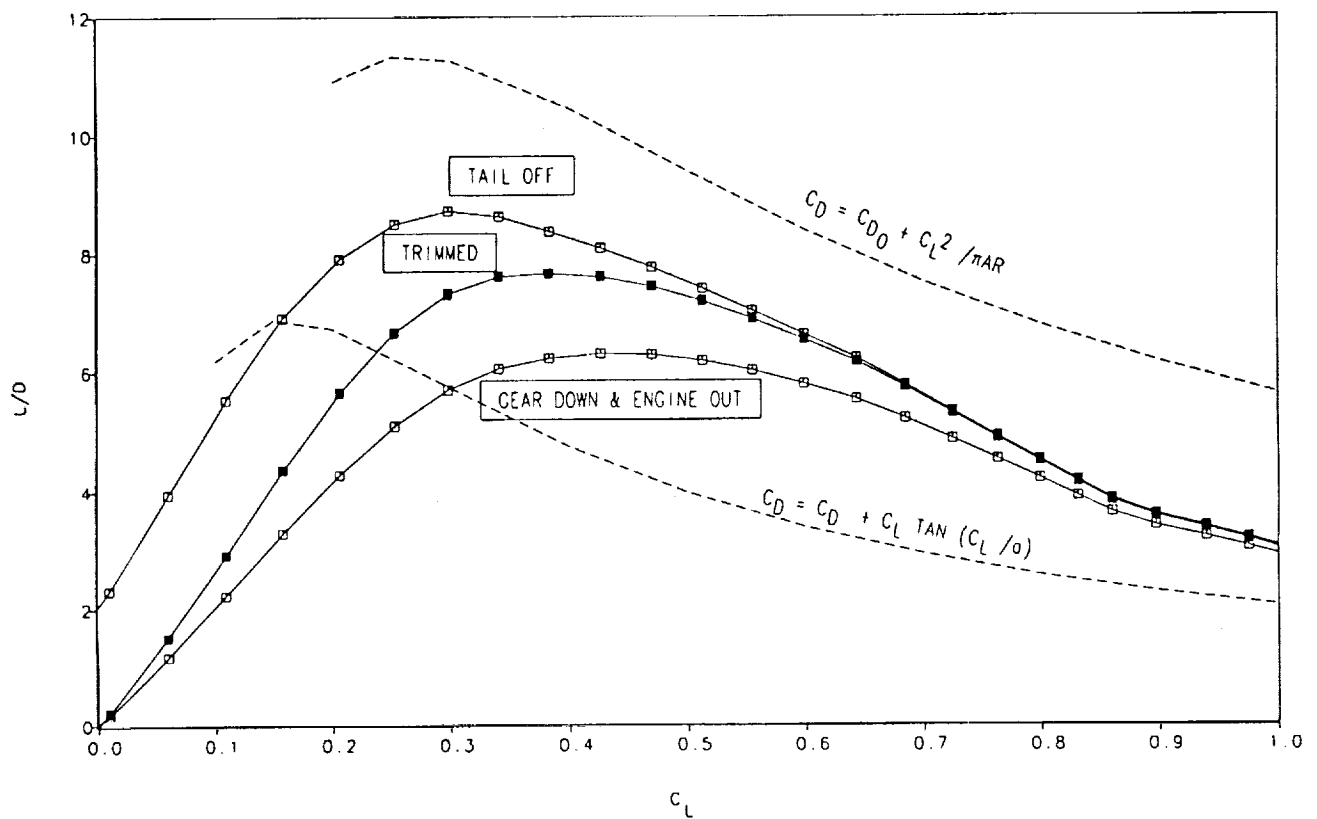
Tentative Airworthiness Standards For Supersonic Transport (TASST)
(1971)

Condition	Gradient Req'd		NO. ENG	GEAR	Specified Conditions		
	$\phi=0$	$\phi=18^\circ$			FLAP	THRUST	V
<u>Takeoff Climb</u>							
- First segment	.005	-	3	Down	Liftoff		V_{LOF}
- Sec Segment	.030	.020	3	Up	When Gear is Fully Retracted		V_2
- Zero R/C	0	-	3	Up	Takeoff Configuration	T.O.	$\leq V_2/1.125$
<u>Landing Climb</u>							
- Approach	.027	.017	3	Up	Approach	T.O.	V_{APP}
- Continued Approach	.024	.014	2	Up	8 sec 	8 sec	V_{APP}
- Landing	.032	.022	4	Down	Landing	8 sec	V_{APP}

- 1 Most Critical Propulsion Configuration to Gear Up.
 2 Most Critical Propulsion Configuration to 400 ft.
 3 Flaps or Thrust Available in 8 sec

INCREMENTS TO BASIC DRAG

The basic drag of a wing-body must be trimmed and landing gear and engine-out drag added before the climb gradients are determined. Results for one flap position and trim balance point is shown. Theoretical drag polars bracket the wind-tunnel results except at low lift levels where flap drag is excessive.



POLARS - LOW REYNOLDS NUMBER WIND TUNNEL DATA (ENGINE-OUT DRAG ESTIMATED)

L/D REQUIRED FOR CLIMB

When comparing the basic trimmed drag levels required to meet the various climb gradient requirements, it is necessary to account for landing gear drag and engine-out drag increments. Several gradient requirements can then be compared to wind-tunnel results for a symmetric model with gear off.

- Climb equation

$$\tan \gamma = T/W - [D/L + \Delta D/L_{eo} + \Delta D/L_{gear}]$$

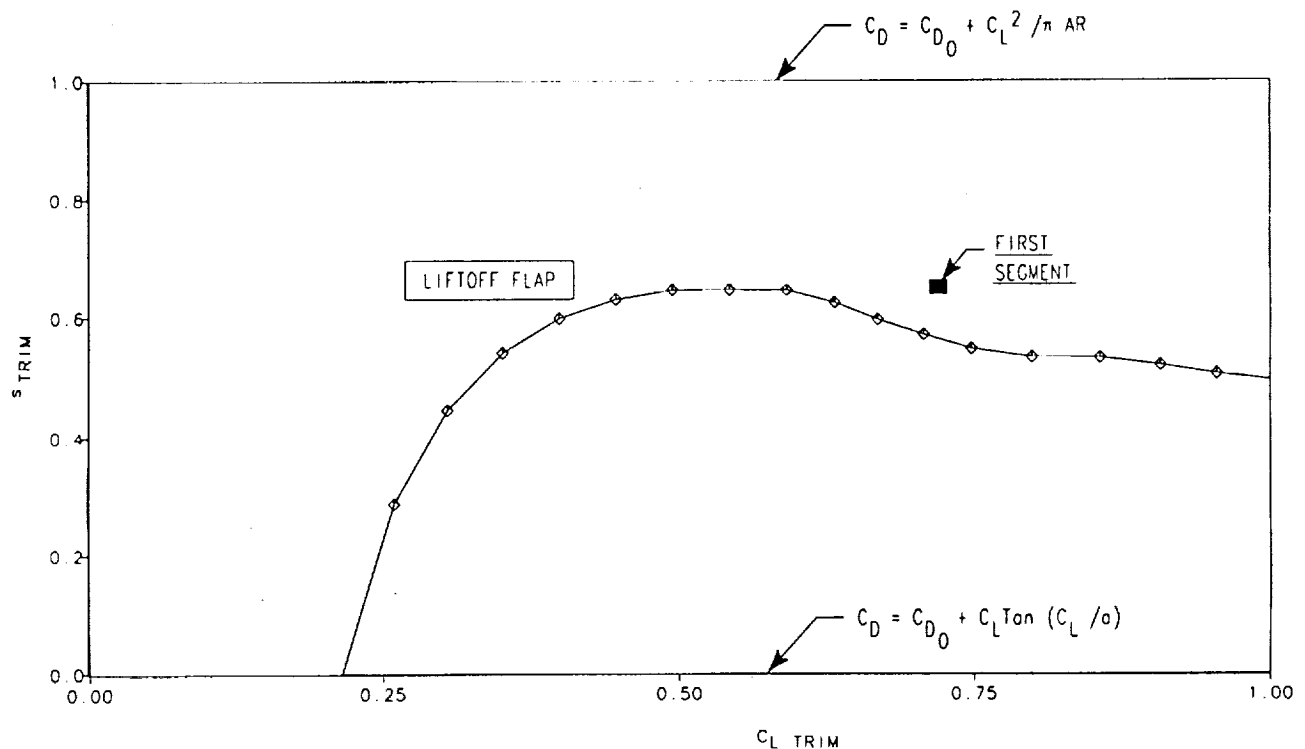
- L/D_{required} (symmetric thrust and gear up)

$$L/D_{req'd} = \frac{1}{[T/W_{avail.} - \Delta D/L_{eo} - \Delta D/L_{gear}] - \tan \gamma_{req'd}}$$

POLAR POINT REQUIRED FOR FIRST SEGMENT CLIMB

This and following charts are shown using the suction parameter, s , which is a measure of induced drag efficiency. Ideal polars consisting of skin friction and elliptic span loading induced drag define $s=1$, as low a drag level as possible. Completely separated flat plate induced drag plus skin friction define $s=0$. This parameter is a measure of drag efficiency and more independent of planform effects than is lift-to-drag ratio.

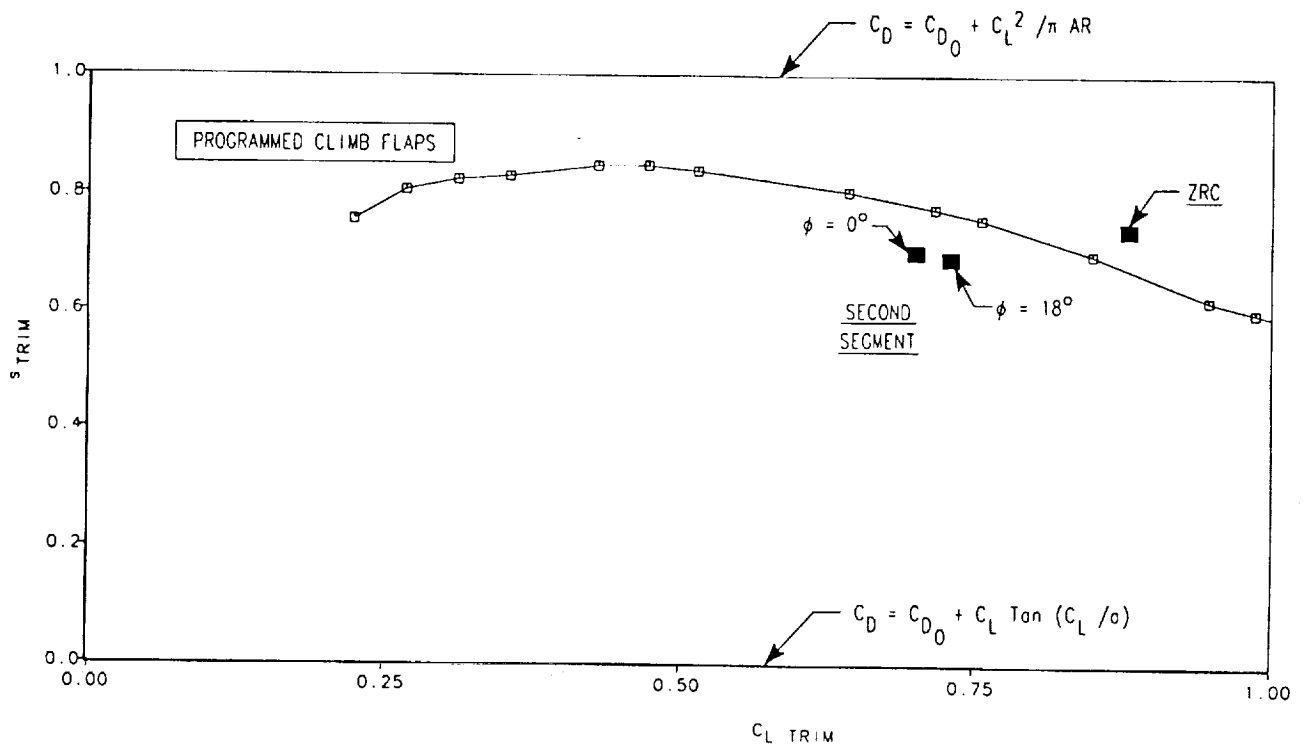
First Segment Climb is at 35 feet of altitude, the gear is still down and one engine is inoperative. The required drag level for First Segment Climb is less than the wind tunnel data used for the liftoff flap polar. A better liftoff L/D is needed, but the liftoff angle of attack might be compromised if adjustment in flap position, closer to the programmed flap envelope, is used.



ALL ENGINE/GEAR UP POLAR - LOW REYNOLDS NUMBER WIND TUNNEL DATA

POLAR POINTS REQUIRED FOR SECOND SEGMENT CLIMB AND ZERO RATE OF CLIMB

Second Segment Climb and Zero Rate of Climb requirements are with gear up and one engine inoperative. The wind tunnel polars being used for programmed climb flaps are better than the drag levels required to meet Second Segment gradients, even for the maneuver condition. The polars are deficient relative to the Zero Rate of Climb gradient drag, however.



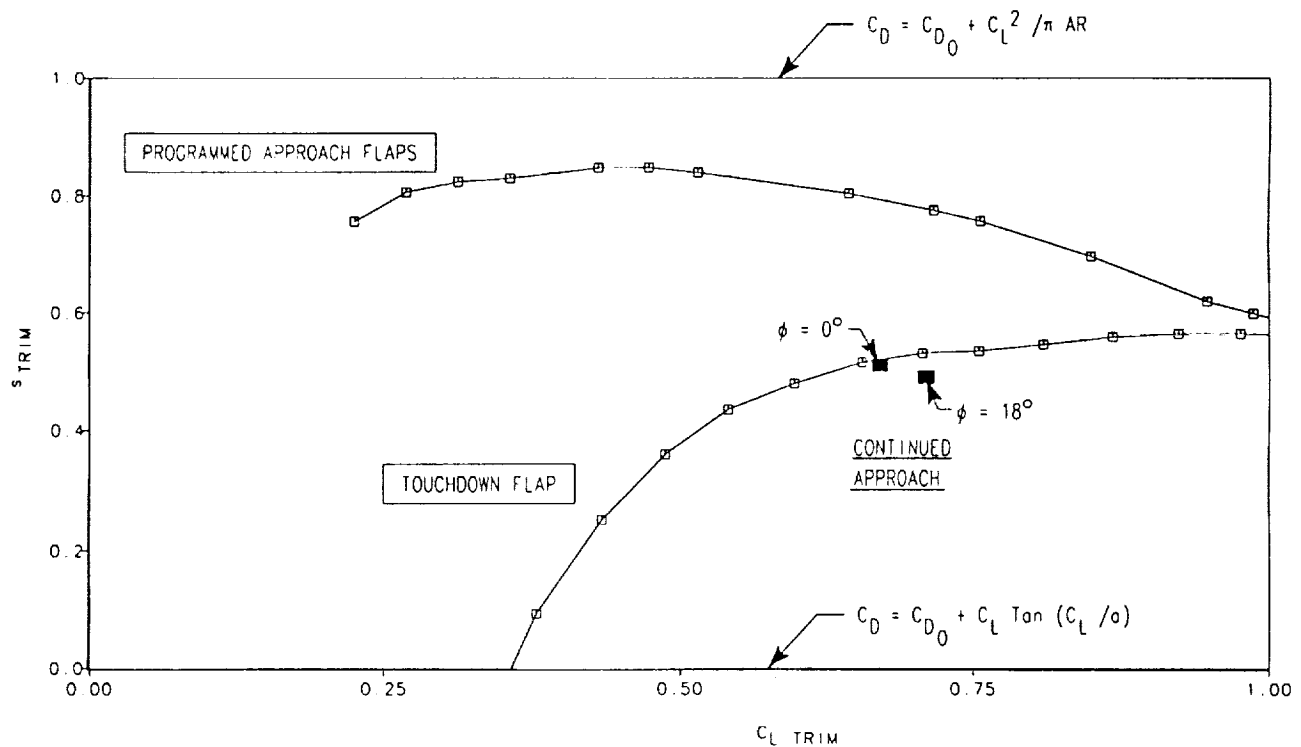
ALL ENGINE/GEAR UP POLAR - LOW REYNOLDS NUMBER WIND TUNNEL DATA

FIGURE 18

POLAR POINTS REQUIRED FOR CONTINUED APPROACH

Since maximum landing gross weight is much less than maximum takeoff weight, the thrust-to-weight ratio is higher. This makes it easier to meet the climb gradient requirements associated with landing.

On the figure below, only Continued Approach shows up, the required points for Approach and Landing Climb are below the $s=0$ line. Continued Approach requirements are with two engines inoperative but with gear up. Even so, the wind tunnel polars are better than required, even if the requirement had to be met with the higher drag touchdown flap.



ALL ENGINE/GEAR UP POLAR - LOW REYNOLDS NUMBER WIND TUNNEL DATA

DRAG EFFECTS ON NOISE

Community noise is a critical and designing constraint on the HSCT. Reducing drag to improve the noise characteristics is one of our principal goals. Reduced drag contributes in a number of ways but also has some limitations as noted below.

CLIMB

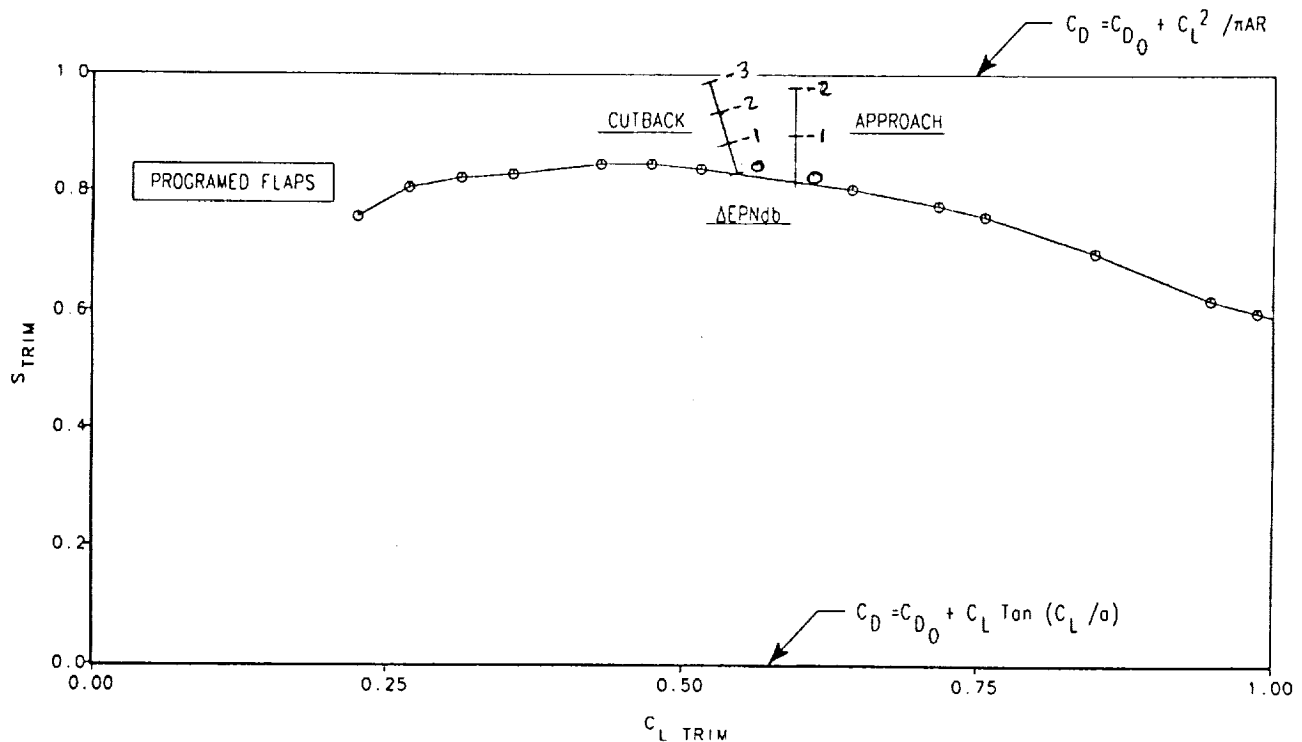
- Reduced climb drag has only a small effect on sideline noise
 - Need operational techniques - programmed lapse rate (PLR)
 - Need improved engine design and noise suppression
- Reduced drag improves the climb profile:
 - More height gained by cutback
 - More acceleration along the flight path
- Reduced drag allows a deeper cutback to lower thrust levels
 - Required climb gradient after spindown
 - 4% (all engine)
 - or, if more critical
 - 0% (engine-out)

APPROACH

- Reduced drag lowers engine thrust required
 - Inlet may unchoke
 - Idle thrust may become limiting
 - Airframe noise may become more important

NOISE SENSITIVITY AT CUTBACK AND APPROACH

Cutback and approach noise conditions require lift coefficients of 0.5 to 0.6 and are close to the maximum drag efficiency for the wind tunnel polars with flaps programmed for minimum drag. Cutback noise is 50% more sensitive to improvements in drag than is approach noise. Some potential for reducing drag still exists. One to two EPNdb reduction may be possible.



GEAR UP POLAR - LOW REYNOLDS NUMBER WIND TUNNEL DATA

FIGURE 21

CONCLUSIONS

This study had as its objective the identification of the lift and drag levels that were required to meet the performance requirements of tentative airworthiness standards established at the time of the USSST program in 1971 and that were important to community noise. Research to improve the low speed aerodynamic characteristics of the HSCT needs to be focused in the areas of performance deficiency and where noise can be reduced. Otherwise, the wing planform, engine cycle, or other parameters for a superior cruising airplane would have to be changed.

- Operating the flaps in the most effective way along the low speed flight profiles significantly improves low speed performance and noise.
- For this study configuration, relative to the tentative airworthiness standards being worked on in 1971:
 - Lift levels are achievable with programmed flaps
 - The critical drag conditions are first segment and zero rate of climb.
- For this study configuration:
 - Cutback noise is more sensitive to drag reduction than is approach noise.
 - The potential exists for one to two EPNdb from drag reduction.

THIS PAGE INTENTIONALLY BLANK

omit

Session XII. High Lift

HSCT High-Lift Technology Requirements
D. L. Antani and J. M. Morgenstern, Douglas Aircraft Company

PRECEDING PAGE BLANK NOT FILMED

THIS PAGE INTENTIONALLY BLANK

HSCT HIGH-LIFT TECHNOLOGY REQUIREMENTS

56-02
11981

D.L. Antani
J.M. Morgenstern
Douglas Aircraft Company
McDonnell Douglas Corporation
3855 Lakewood Blvd.
Long Beach, CA 90846

First Annual High-Speed Research Workshop
Williamsburg, Virginia
May 14-16, 1991

WARNING: INFORMATION SUBJECT TO EXPORT CONTROL LAWS This document may contain information subject to the International Traffic in Arms Regulation (ITAR) and/or the Export Administration Regulation (EAR) of 1979 which may not be exported, released, or disclosed to foreign nationals inside or outside the United States without first obtaining an export license. A violation of the ITAR or EAR may be subject to a penalty of up to 10 years imprisonment and a fine of \$100,000 under 22 U.S.C. 2778 or Section 2410 of the Export Administration Act of 1979. Include this notice with any reproduced portion of this document.

PRECEDING PAGE BLANK NOT FILMED

1767

AGENDA

The discussion topics are listed in this figure. The high-lift needs and related aerodynamic goals have been established in the recent system studies conducted for NASA. Next follows the status of the related high-lift database and available design and analysis methods. A summary of future high-lift technology requirements is presented followed by concluding remarks.

Agenda

- High-Lift Needs
- Status
- Technology Requirements
- Conclusions

Figure 1

MDC HSCT BASELINE DESIGN AND MISSION REQUIREMENTS

Current MDC HSCT baseline design and mission requirements are shown in this figure. There are 300 passengers in a three-class configuration, range is 5,500 nmi with 25-percent subsonic overland. The aircraft is to meet FAA Part 36 Stage 3 noise certification limits. The TOFL requirement is 11,000 ft. Note the significant portion of mission segments (indicated by a heavy line) where efficient low-speed, high-lift, and subsonic climb and subsonic cruise aerodynamics are required. Efficient subsonic characteristics are also required for all reserve segments to minimize reserve fuel requirements.

Douglas HSCT Baseline Design and Mission Requirements

NUMBER OF PASSENGERS = 300 (3-CLASS)
RANGE = 5,500 N Mi, TOFL = 11,000 FT (STD + 27F)
FAR PART 36 STAGE 3 NOISE CERTIFICATION LIMITS

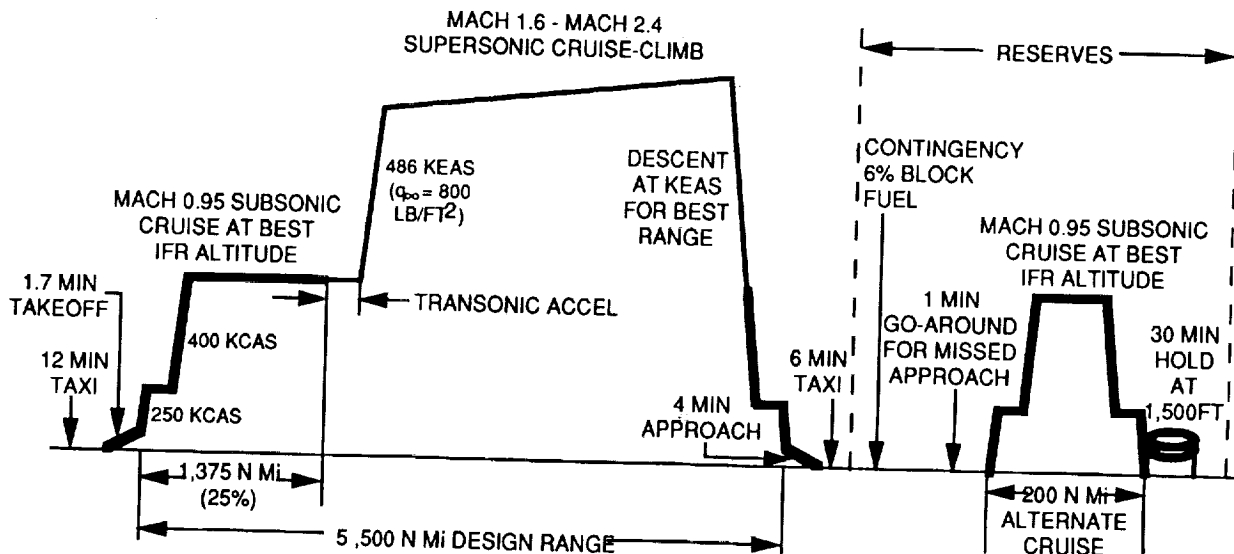


Figure 2

REFERENCE NOISE CERTIFICATION POINTS

Typical noise certification monitors at sideline, takeoff, and approach are shown in this figure. One of the objectives of the high-lift design is to improve aerodynamic efficiency so that the noise levels at these points are lowered. Results showing this effect are presented later.

Reference Noise Certification Points where Efficient High-Lift System is Required

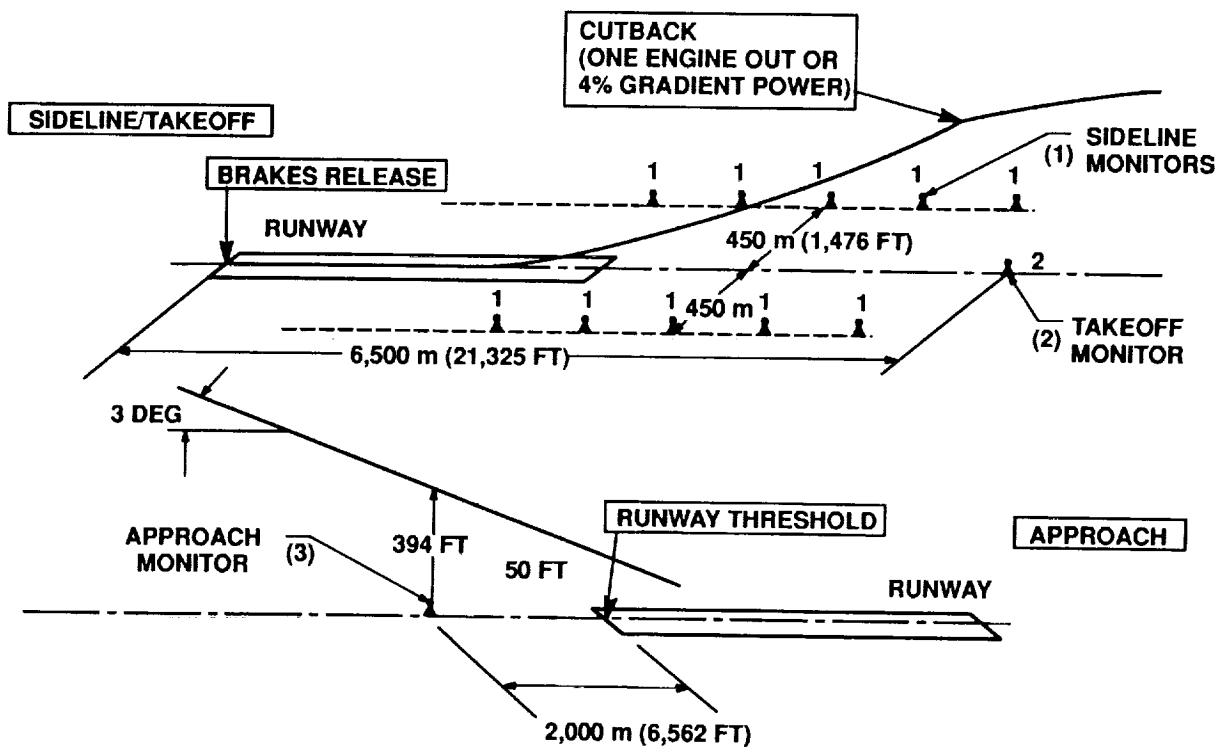


Figure 3

BALANCED AERODYNAMIC DESIGN

To make the HSCT economically viable and environmentally acceptable, the challenge is to design an HSCT wing that optimally balances low-speed, subsonic, and supersonic requirements. The figure shows that there are many low-speed takeoff and approach, and subsonic climb and cruise aerodynamic goals. These goals will have to be met by an optimum wing and high-lift system. The basic supersonic L/D requirements will also have to be met.

Balanced Aerodynamic Design is Required to Optimize Low-Speed, Subsonic, and Supersonic Performance

ECONOMIC VIABILITY AND ENVIRONMENTAL ACCEPTABILITY

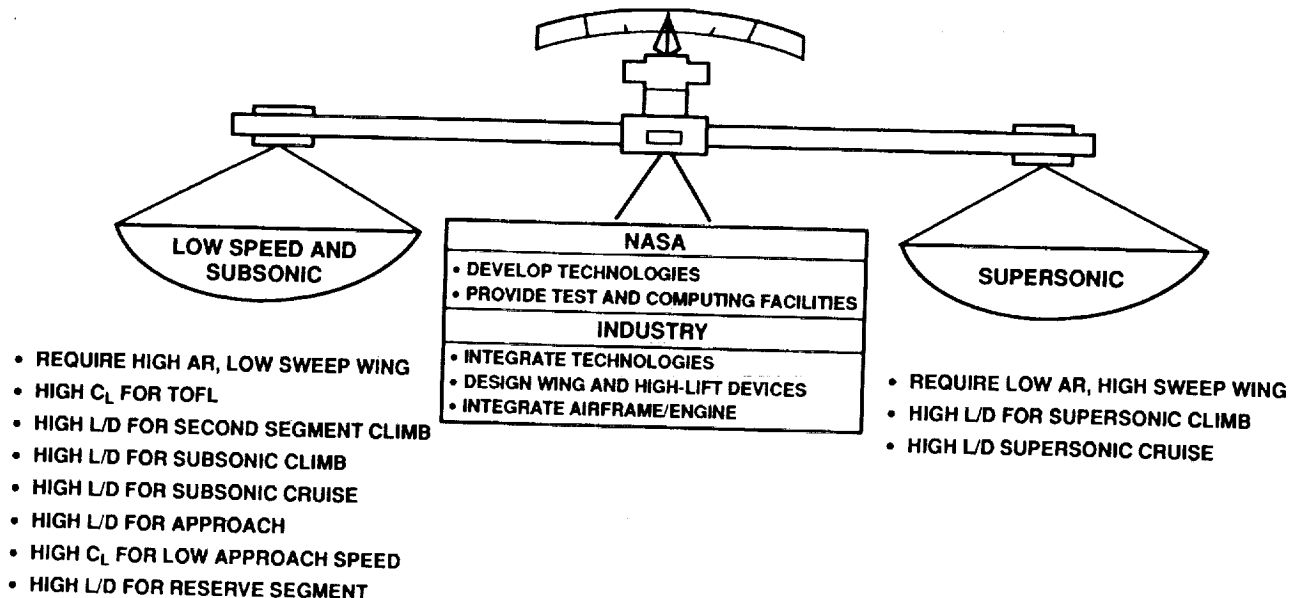


Figure 4

IMPACT OF HIGH-LIFT TECHNOLOGY

The impact of high-lift technology on performance, noise, and stability and control are highlighted in this figure. Note that the high-lift system will have to be integrated with other performance enhancing technologies, e.g., LFC and noise reduction devices (such as mixers/ejectors) as these technologies mature.

Impact of High-Lift Technology

Performance

- TOGW, engine size, TOFL, and approach speed are significantly affected by efficient high-lift capability.
- High subsonic L/D reduces fuel burn (\therefore weight) in the subsonic climb and cruise mode.

Noise

- L/D improvements reduce takeoff, community, and climb-to-cruise noise levels.

Stability and Control

- Leading-edge devices have a positive effect on longitudinal stability and lateral control effectiveness.

Integration

- Must be integrated with LFC and advanced engine nozzles.

EFFECT OF HIGH-LIFT ON TOGW AND ENGINE THRUST

The figure shows results of recent system studies indicating a significant increase in L/D (at appropriate takeoff conditions) due to optimum leading edge deflections. This increase in aerodynamic efficiency will provide corresponding reductions in takeoff thrust and TOGW. Note that for the tailed configuration that was analyzed, best trailing-edge deflections were about 10 to 15 degrees in the trimmed mode.

Effect of High-Lift Settings at Takeoff

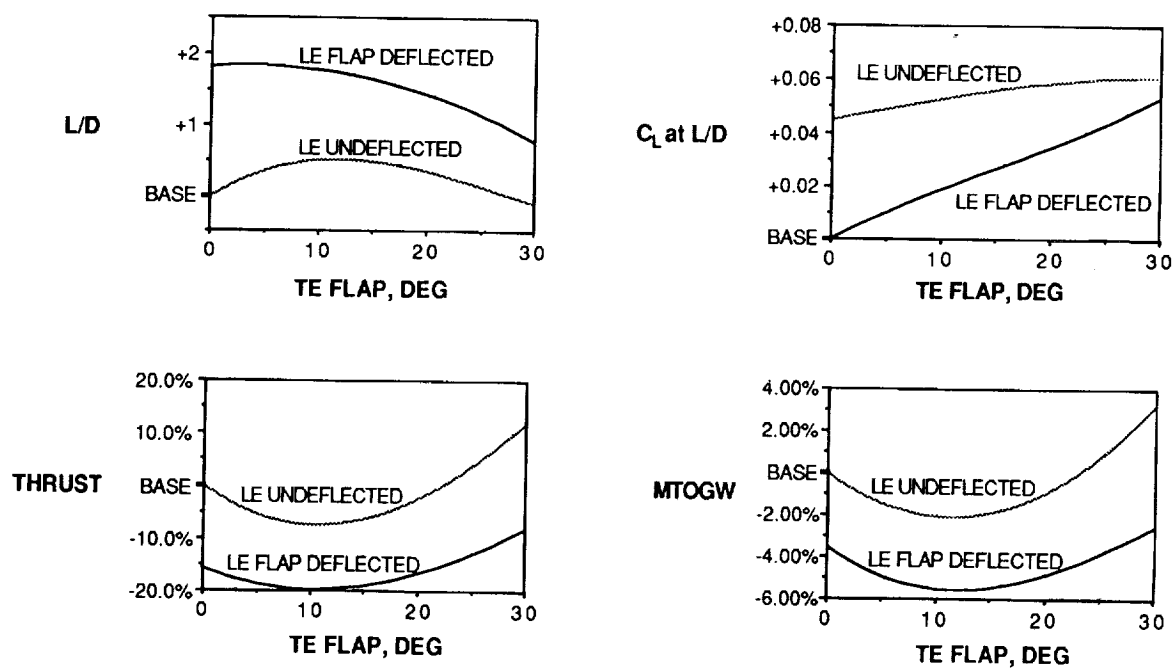


Figure 6

EFFECT OF L/D ON SIDELINE, TAKEOFF, AND APPROACH JET NOISE

The figure shows that for a given configuration, the L/D improvements can reduce the takeoff and approach noise levels. However, no significant reduction of sideline noise was obtained with the L/D increase.

Effect of L/D on Sideline, Takeoff, and Approach Jet Noise

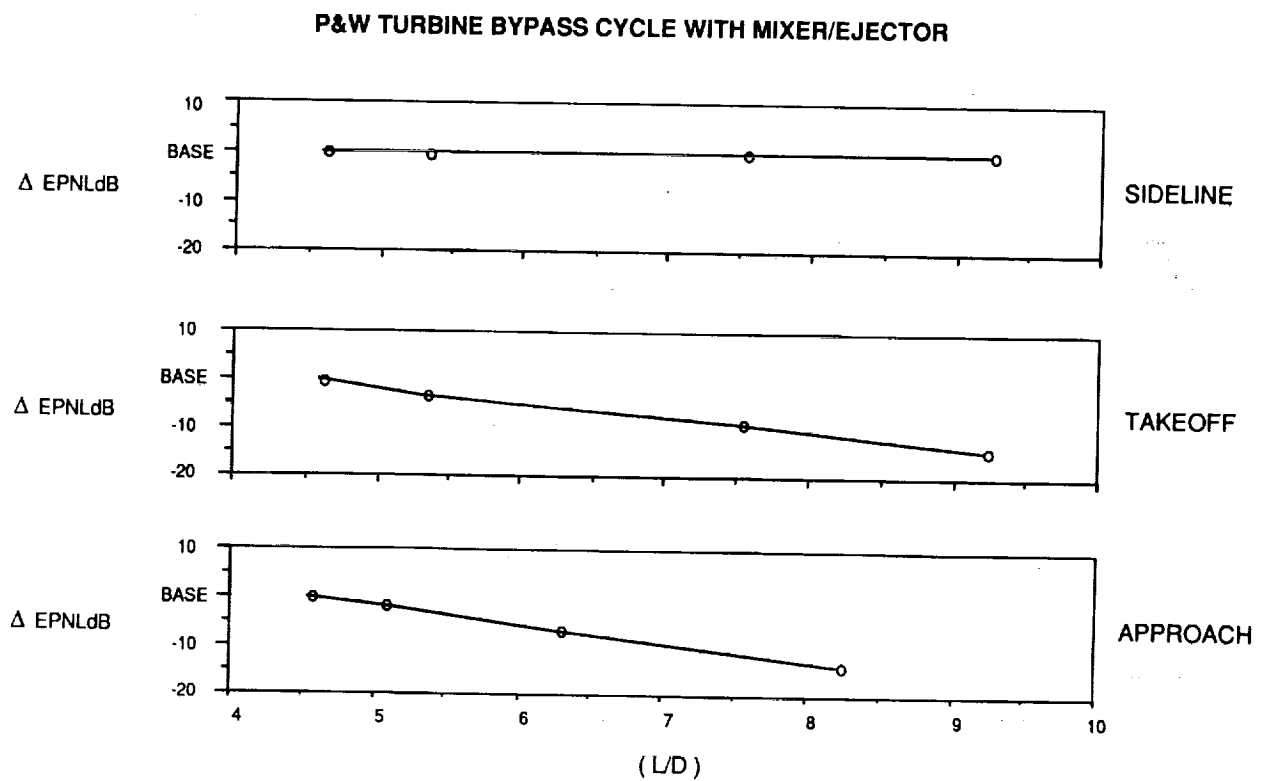


Figure 7

SUBSONIC CLIMB AND CRUISE PERFORMANCE REQUIREMENTS

As indicated earlier, there is a large segment of the mission where an improvement in subsonic aerodynamic efficiency is needed because 25-percent of the range is being flown at subsonic conditions. The figure shows that a significant increase in L/D could be obtained with optimum leading-edge deflections at subsonic speeds. There is also a beneficial increase in C_L at which L/D maximizes when flaps are deployed. This means that the flap systems required for the low-speed, high-lift segment will also have to be deployed in the subsonic mode. We should include this requirement as part of the high-lift technology development.

Subsonic Climb and Cruise Performance Requirements

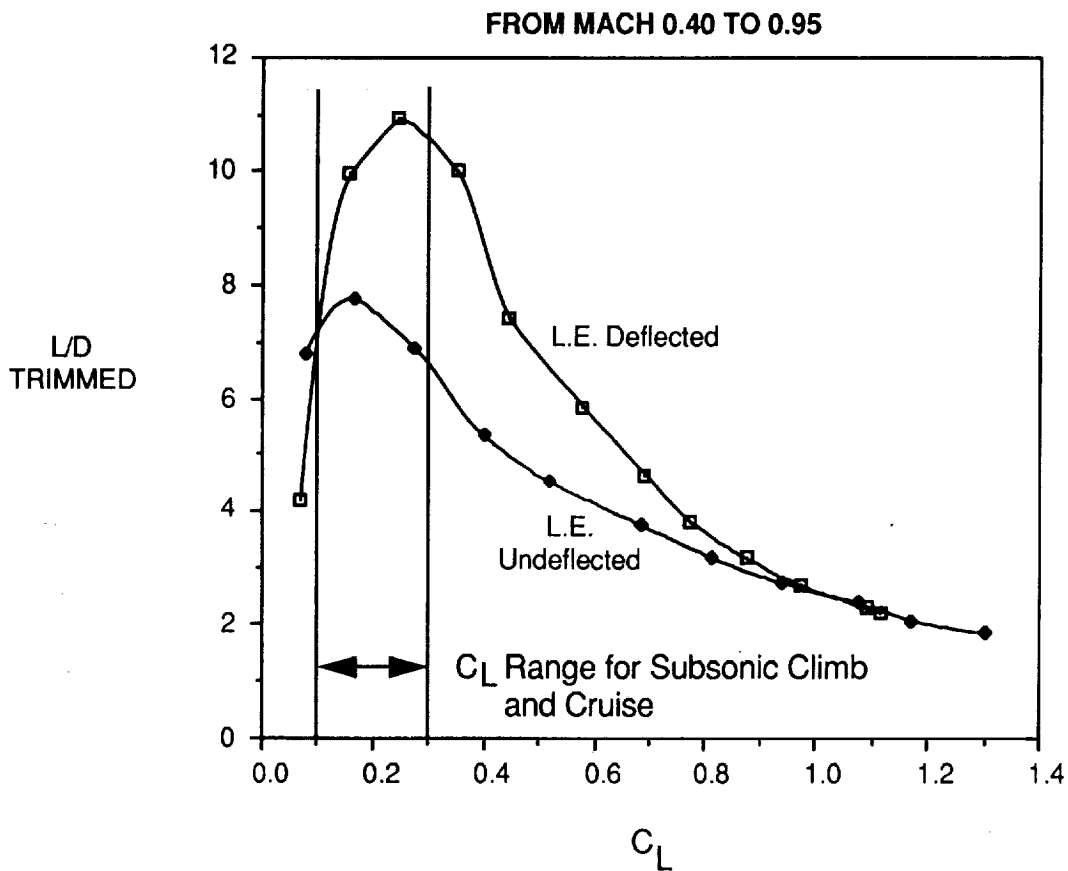


Figure 8

HSCT HIGH-LIFT AERODYNAMIC GOALS

We have established aerodynamic goals for a desirable high-lift system based on recent system studies. The goals are presented for the takeoff, approach, and subsonic climb and cruise modes. It is believed that these goals are attainable within the expected 1998 technology availability date. An important aspect here is that if the wing and its high-lift system has to perform significantly better than certain minimum requirements, the wing planform may be compromised which may lead to a large penalty on the supersonic aerodynamic efficiency, this in turn will cause large weight and economic penalties.

HSCT High-Lift Aerodynamics Goals (Trimmed Conditions)

Takeoff

C_L Ground Angle Limit	>	0.75
(L/D) Second Segment Climb	>	8.0
LE Suction Factor Second Segment Climb	\geq	0.8

Approach

(L/D) Approach	>	7.5
LE Suction Factor Approach	\geq	0.8

Climb

$(L/D)_{M = 0.5 \text{ to } 0.95}$	>	14
------------------------------------	---	----

HSCT HIGH-LIFT TECHNOLOGY STATUS

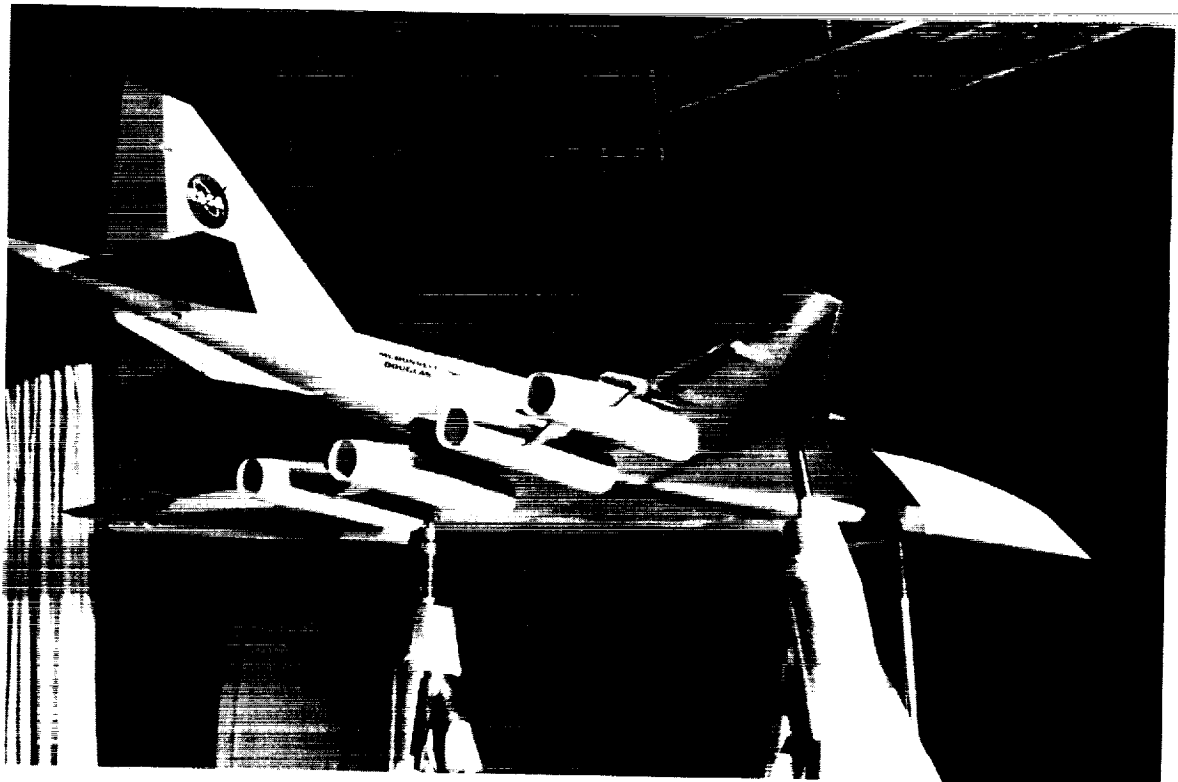
There is a good set of high-lift wind tunnel databases available for the past supersonic transport configurations. These data were mainly obtained at conventional wind tunnel Reynolds numbers. The flap design methodologies developed by Carlson, Frink, etc., at NASA Langley are quite useful to aerodynamic designers for guiding them toward optimum flap designs. The CFD codes will have to be calibrated for application to flowfields associated with HSCT wings and flaps.

HSCT High-Lift Technology Status

- Extensive SST, SCAR, SCR, and AST databases are available.
- Flap design methodologies (by Carlson, Frink, etc.) based on linear subsonic flows and L E suction/vortex lift corrections are available.
- Navier-Stokes codes are available. However, the codes and their turbulence models need to be calibrated and verified for their application to highly 3-D, vortex-dominated, separated flowfields.

NASA 0.1-SCALE LOW-SPEED MODEL OF DOUGLAS AST CONFIGURATION

An example of an available model for high-lift testing is shown here. This particular 0.1-scale model is for the NASA/Douglas Mach 2.2 Advanced Supersonic Transport configuration, with the aspect ratio 1.84, leading-edge sweep 71/57-degree wing planform. The model has been tested in the Langley 30-by 60-foot tunnel with a full wing/high-lift-system/tail/nacelle configuration. A plan for testing this model with new flaps is being formulated.



ORIGINAL PAGE
BLACK AND WHITE PHOTOGRAPH

Figure 11

EXAMPLE OF NAVIER-STOKES/EULER CODES APPLICATION

An example of MDC application of the CFL3D code in the Euler and Navier-Stokes modes for a delta wing is shown here. A good comparison of the predicted vortex location using the code with the test data is shown. Further work is being done for the application of this and similar codes to the HSCT type planforms with flaps.

Example of Navier-Stokes/Euler Codes Application

Ref. MCAIR 90 - 021

Medium Mesh, $M_\infty = 0.30$, $Re_c = 1 \times 10^6$, $\alpha = 20^\circ$

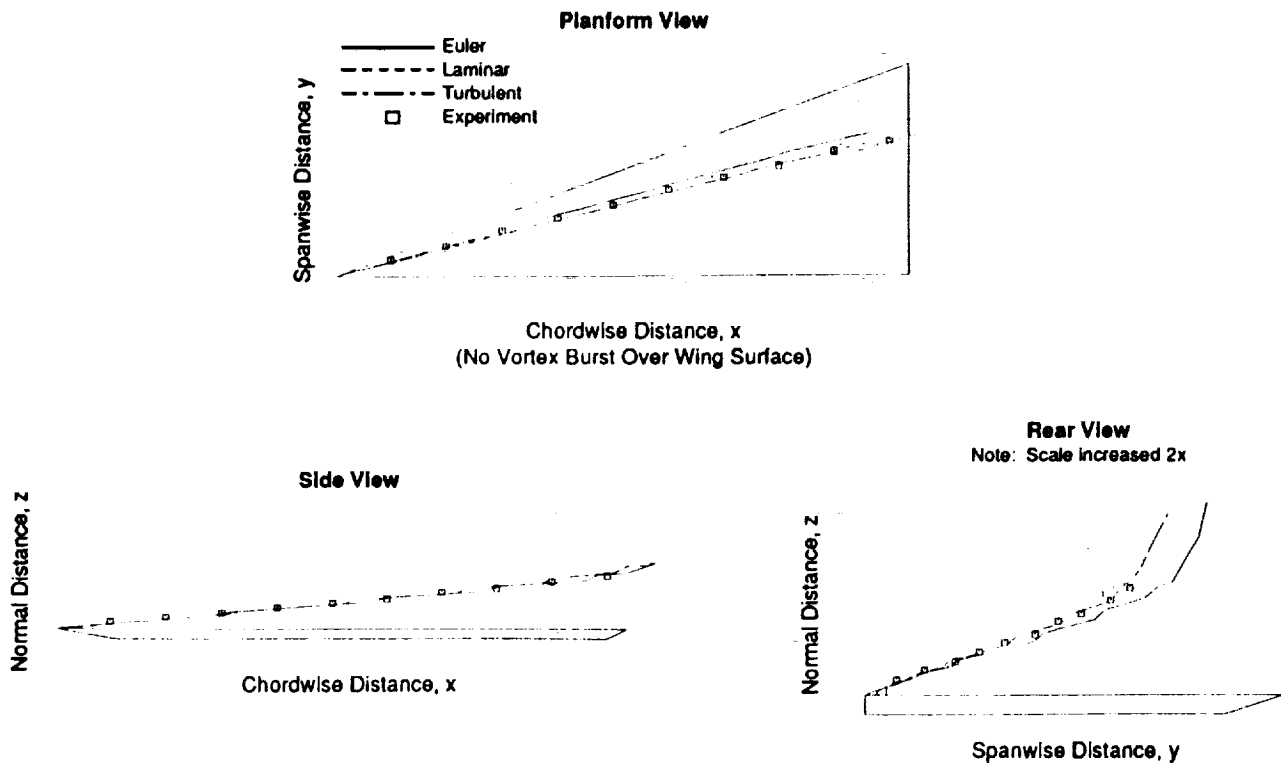


Figure 12

HSCT HIGH-LIFT RESEARCH AND TECHNOLOGY AREAS

Various high-lift research and technology areas for future work are listed in this figure. Each topic is discussed on the following pages.

HSCT High-Lift Research and Technology Areas

- Innovative Concepts Verification.
- Flap Design Methodology Application and Verification.
- CFD Calibration and Application.
- High Reynolds Number Testing.
- Subsonic/Transonic Flap Optimization.
- Flight Testing.

SOME CANDIDATE INNOVATIVE HIGH-LIFT CONCEPTS

Some of the candidate innovative concepts are shown here. The vortex flap concept, apex fence, deployable canards/strakes, apex blowing, etc., have a potential for improving L/D , C_L , and trim control to varying degrees. Some of these concepts have been tested by NASA in the past. Further work is required for a full assessment of the benefits and risks of each concept.

Some Candidate Innovative High-Lift Concepts

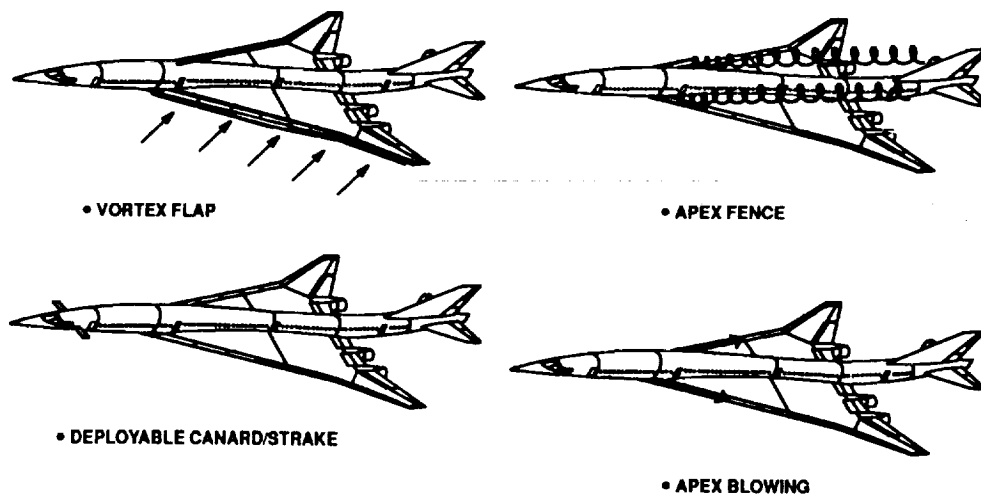
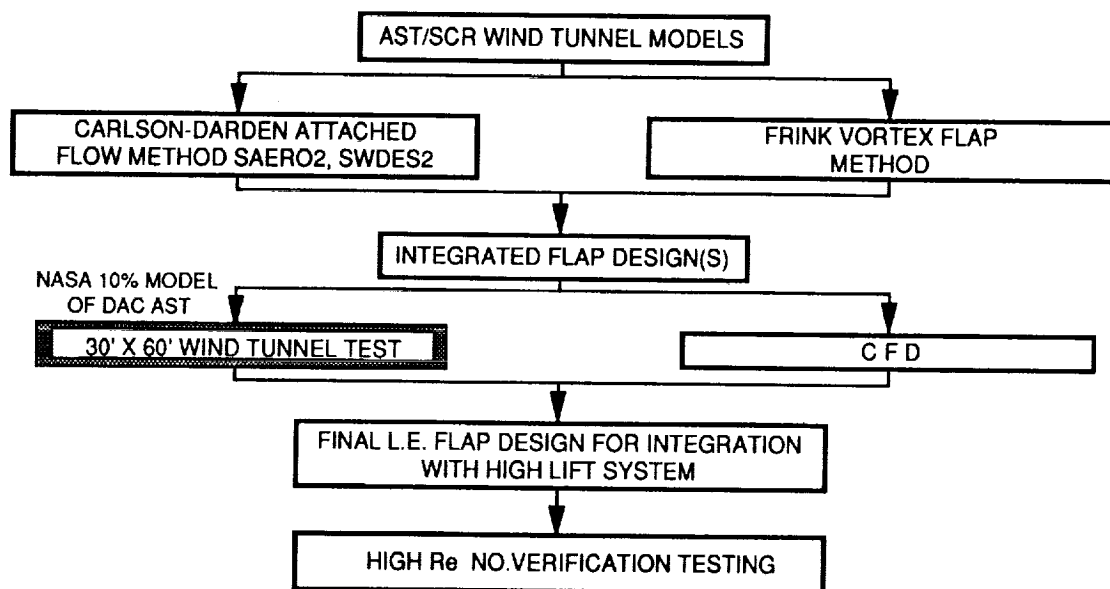


Figure 14

APPLICATION AND VERIFICATION OF CURRENT L.E. FLAP DESIGN METHODOLOGIES

The important area of applied methods development and verification is discussed in this figure. Douglas is currently applying the Carlson-Darden flap design and analysis codes and Frink vortex flap design code to the HSCT high-lift problem. The near-term objective is to select flap configurations for verification in the NASA Langley 30- by 60-foot tunnel with the NASA 0.1 model of the Douglas AST configuration. A parallel CFD application to the flap design process is also planned before final flap configurations are selected for advanced testing, e.g., high-Re testing.

Application and Verification of Current L.E. Flap Design Methodologies



CFD CALIBRATION AND APPLICATION NEEDS

CFD calibration and application needs are listed in this figure. The codes and their turbulence models will have to be verified for their application to the complex 3-D viscous, vortex-dominated, separated flowfields. We need to aggressively pursue this area so that the codes can be made available for the flap design process. The goal is also to be able to analyze full wing/body/tail/nacelle configurations by the 1995-1998 timeframe. These codes will also allow us to predict aerodynamic loads with vortex effects - a very important input to the structural design process.

CFD Calibration and Application Needs

- Understand complex 3-D viscous flowfield around low AR, high sweep wings with and without flaps.
- Understand L E vortex development and breakdown.
- Guide flap design process.
- Study high Reynolds number effects.
- Analyze full trimmed configurations (body, tail, and nacelle effects).
- Predict aerodynamic loads.

HIGH REYNOLDS NUMBER RESEARCH AND TECHNOLOGY

Areas of high Reynolds number research and technology development are shown in this figure. The HSCT full-scale Reynolds number in the takeoff and approach modes is typically on the order of 100-150 million based on a wing mean aerodynamic chord. Most of the test data are available at a conventional Re of about 4 million. The effect of higher Re will have to be simulated in the NTF, 12 foot, or 40- by 80-foot tunnels. These results will help in selecting candidate concepts for flight testing.

High Reynolds Number Research and Technology Areas

- Understand dependency of vortex formation and leading-edge suction on wing leading-edge radius and Reynolds number (Re).
- Study effectiveness of flaps (L E and T E), strakes, and fences at high Re .
- Study tail effectiveness at high Re .
- Generate data for CFD code validation.
- Select final flight test configurations through parametric testing at high Re .

SUBSONIC CLIMB/CRUISE FLAP OPTIMIZATION TECHNOLOGY

As stated earlier, flap settings must be optimized and verified for subsonic climb and cruise to enhance performance. CFD and high-Re technology development activities should reflect this need.

Subsonic Climb/Cruise Flap Optimization Technology Areas

- Determine and validate optimum flap settings for subsonic climb and cruise.
- Apply CFD codes to the design process.
- Verify designs through high Re testing.

ROLE OF FLIGHT TESTING IN THE HSCT HIGH-LIFT RESEARCH
AND
TECHNOLOGY DEVELOPMENT

This figure addresses the role of flight testing in the high-lift research and technology areas. For many purposes, a high Reynolds number wind tunnel test may be quite sufficient. However, a cost-effective flight test could provide additional data beyond the wind tunnel testing. The flight testing could be the most appropriate means of simulating interactions between high-lift devices and an actual engine noise-reduction system.

**Role of Flight Testing in the High-Lift Research
and Technology Development**

- High-Re wind-tunnel testing (in, e.g., NTF, 12', 40' x 80') can be utilized for:
 - Understanding basic high Re effects.
 - Sorting out configurations.
 - Generating large controlled databases for pressures and forces and moments.
- Flight testing of aircraft with appropriate AR and sweep can be suitable for:
 - Observing flow phenomena not simulated in the tunnels.
 - Generating clean data without wall, ground, and support system interference.
 - Validating final high-lift concepts.
 - Simulating interactions between high-lift devices and engine noise reduction systems (suppressors, ejectors, mixers, etc.).
- Cost effectiveness of either approach can be a major decision factor in scoping various technology development plans.

HSCT HIGH-LIFT TECHNOLOGY DEVELOPMENT NEAR-TERM PLAN

An HSCT high-lift technology development near-term plan is shown in this figure. B1 and B2 represent updated 1991 and 1992 baselines with their respective optimized wing planforms and engine cycles. In addition to the innovative high-lift concepts verification, the Carlson's and Frink's linear methods will be applied for flap designs in the near term. The long-term plan is to apply CFD to the wing (W) and its flaps by 1992, followed by its application to the wing-body (WB) and a full B2 baseline configuration. Most of the wind tunnel test verification may be required for the B2 configuration. However, there may be a need for an interim small-scale testing of the B1 configuration. The final configuration validation testing may involve some flight-testing and/or 40- by 80- foot wind tunnel testing.

HSCT HIGH-LIFT TECHNOLOGY DEVELOPMENT NEAR-TERM PLAN

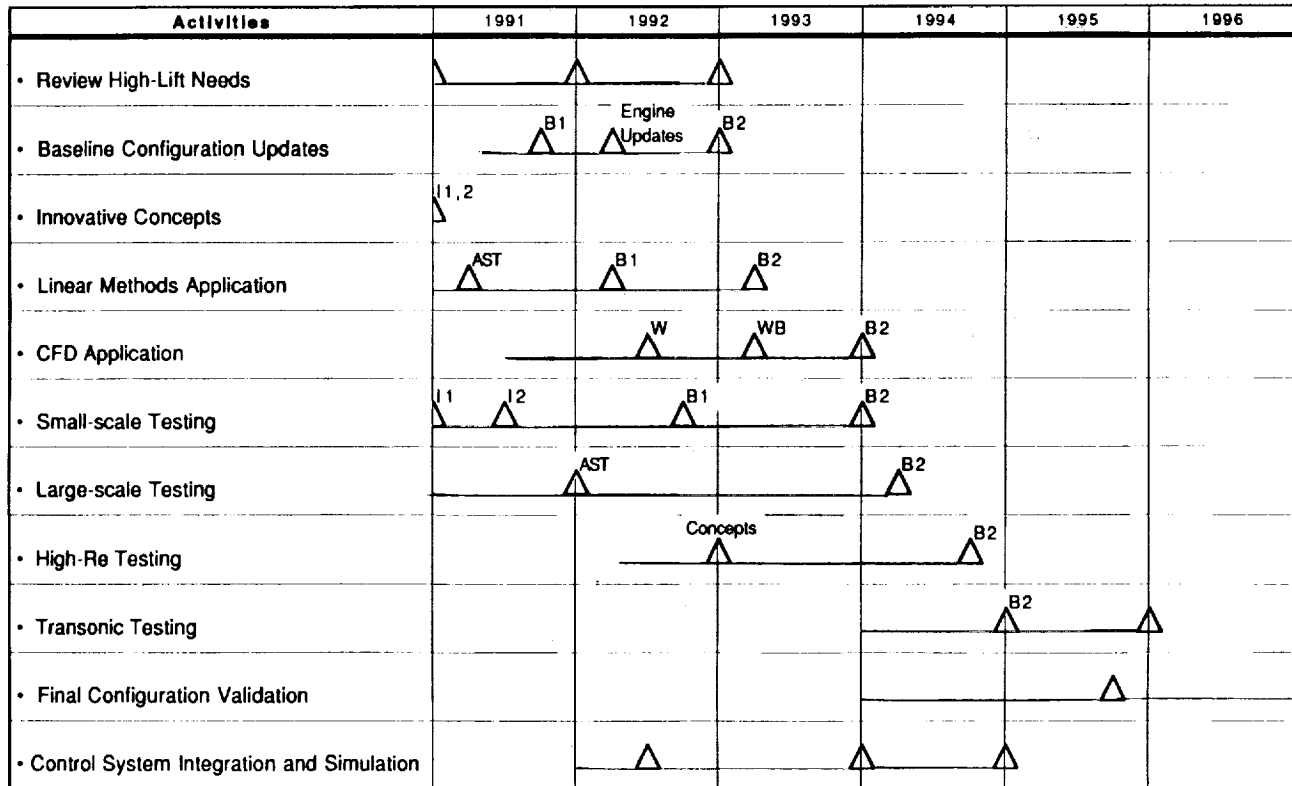


Figure 20

CONCLUSIONS

Some general concluding remarks are made in this figure. It is believed that with an aggressive technology development effort, the high-lift aerodynamic goals can be met.

Conclusions

- Efficient high-lift, high L/D system for HSCT is required to minimize TOGW, improve economics, and help meet noise goals.
- Optimum flap settings will be required to operate at max L/D in the subsonic climb and cruise segments. There is a scarcity of database in this area.
- Future enabling technology/research needs include verification of new high-lift designs, aggressive CFD application, flight test verifications, and high Reynolds number testing.

Session XII. High Lift

omit

Lift Enhancement by Trapped Vortex
Vernon J. Rossow, NASA Ames Research Center

THIS PAGE INTENTIONALLY BLANK

LIFT ENHANCEMENT BY TRAPPED VORTEX

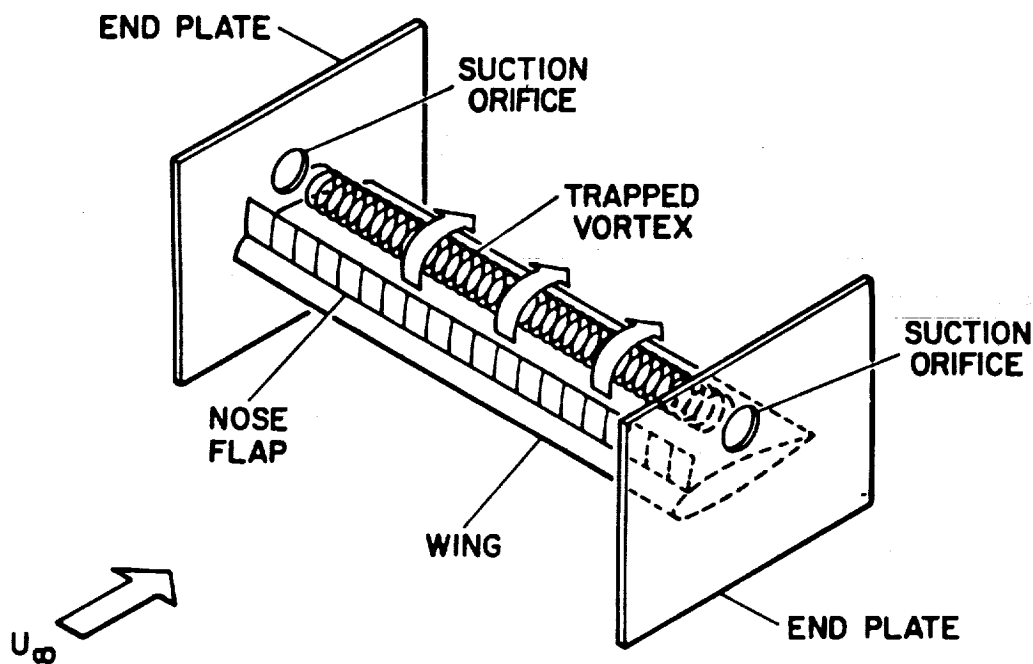
Vernon J. Rossow
NASA AMES RESEARCH CENTER
MOFFETT FIELD, CA 94035-1000

FIRST ANNUAL HIGH-SPEED RESEARCH WORKSHOP
WILLIAMSBURG, VA MAY 14-16, 1991

57-02
11982

Efforts are continuously being made to find simple ways to convert wings of aircraft from an efficient cruise configuration to one that develops the high lift needed during landing and takeoff. The high-lift configurations studied here consist of conventional airfoils with a trapped vortex over the upper surface. The vortex is trapped by one or two vertical fences that serve as barriers to the oncoming stream and as reflection planes for the vortex and the sink that form a separation bubble on top of the airfoil. Since the full three-dimensional unsteady flow problem over the wing of an aircraft is so complicated that it is hard to get an understanding of the principles that govern the vortex trapping process, the analysis is restricted here to the flow field illustrated in the first slide. It is assumed that the flow field between the two end plates approximates a streamwise strip of the flow over a wing. The flow between the endplates and about the airfoil consists of a spanwise vortex located between the suction orifices in the end plates. The spanwise fence or spoiler located near the nose of the airfoil serves to form a separated flow region and a shear layer. The vorticity in the shear layer is concentrated into the vortex by withdrawal of fluid at the suction orifices. As the strength of the vortex increases with time, it eventually dominates the flow in the separated region so that a shear or vortical layer is no longer shed from the tip of the fence. At that point, the vortex strength is fixed and its location is such that all of the velocity contributions at its center sum to zero thereby making it an equilibrium point for the vortex. This presentation describes the results of a theoretical analysis of such an idealized flow field.

WING WITH TRAPPED VORTEX



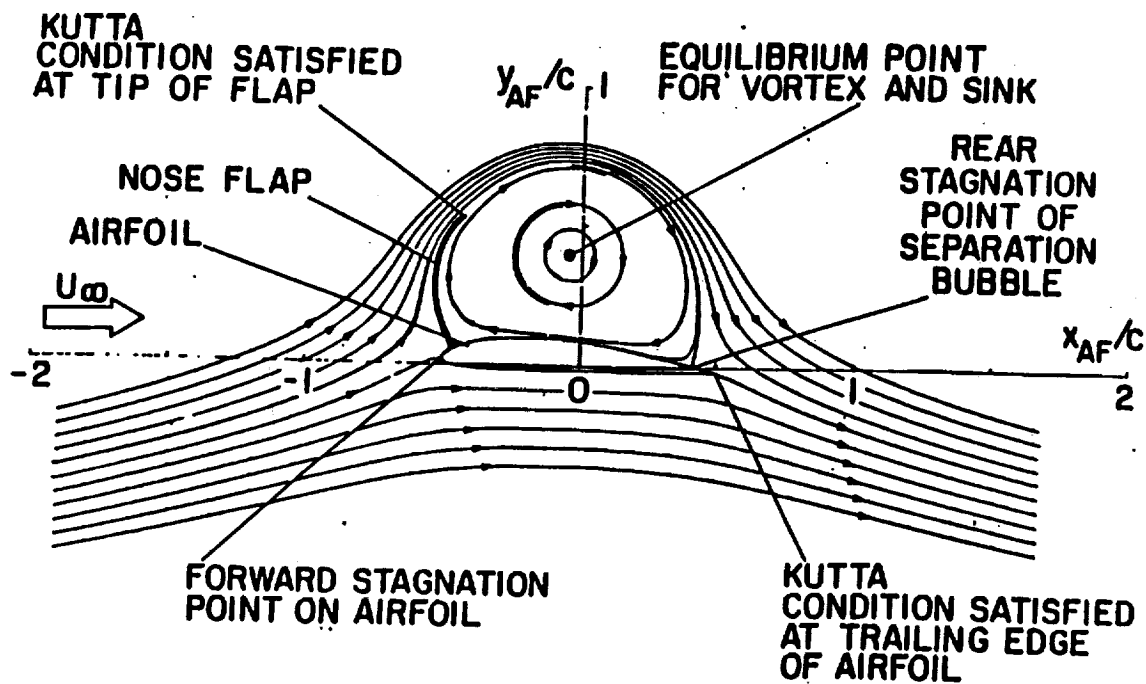
This slide presents a two-dimensional idealization of the experimental configuration presented in the previous slide that will be used in the theoretical analysis. A large trapped-vortex bubble is shown over the airfoil to emphasize the fact that the analysis is most interested in those configurations wherein the vortex bubble covers a large fraction of the upper surface of the airfoil. If such a flow field can be established, the lift enhancement by the trapped vortex is substantial enough to yield lift coefficients that are in the range of the value, $C_L = 6$, shown in the slide. The two-dimensional flow field is assumed to be inviscid and incompressible so that it can be represented by potential flow theory. Conformal mapping techniques can then be used to develop the desired flow-field configuration from the flow about a circular cylinder. A substantial advantage of the conformal mapping technique is that it yields directly the location of the equilibrium point for the center of the vortex/source combination, the circulation, Γ , of the vortex, and the source strength, \dot{m} . Knowledge of Γ and \dot{m} then yield the lift due to the trapped vortex and the drag attributed directly to the trapping process which is designated by C_d . As indicated in the slide, the flow is assumed to depart smoothly from the tip of the fence and from the trailing edge of the airfoil in order to satisfy the Kutta condition at those locations.

The single fence case was first studied, Ref. 1, in order to gain an understanding of the nature of the flow field and to obtain an estimate of the magnitude of lift enhancement that can be achieved by means of a trapped vortex.

Ref. 1: Rossow, Vernon J., "Lift Enhancement by an Externally Trapped Vortex", AIAA Journal of Aircraft, Vol. 15, No. 9, Sept. 1978, pp.618-625.

TWO-DIMENSIONAL FLOW FIELD MODEL

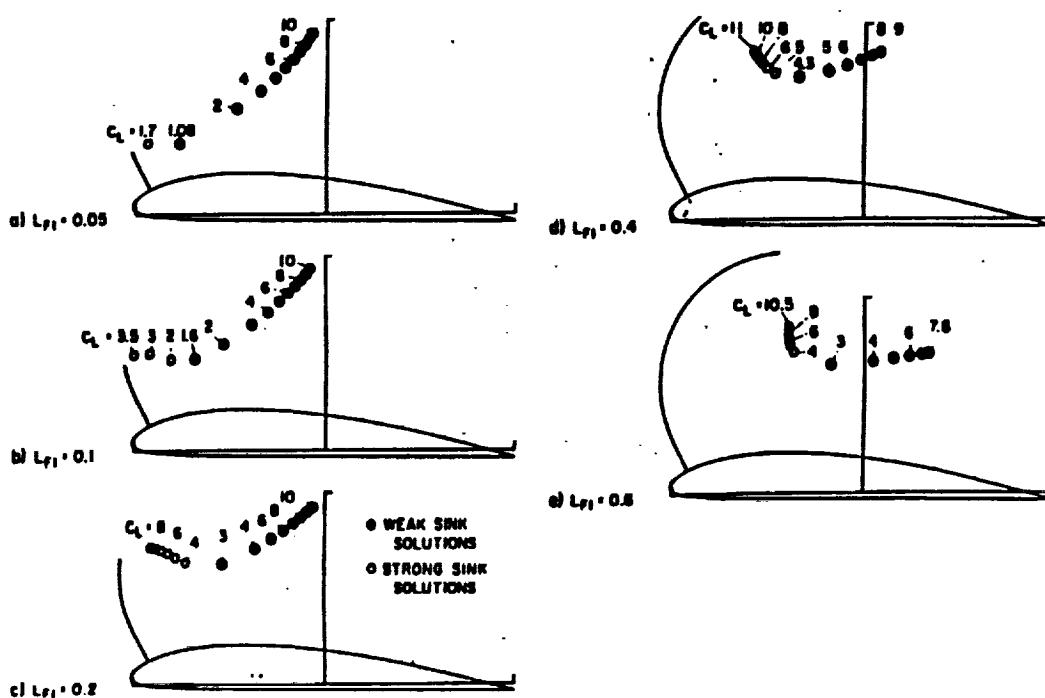
$$C_L = 6, C_D = 0.16$$



The results presented here for the single fence case illustrate the location of the equilibrium point for the vortex/source combinations for several different fence lengths and lift coefficients. It is to be noted that the lift coefficient has been specified but the downstream extent of the vortex bubble has not been fixed. It was assumed that the length of the fence and location of the equilibrium point would be enough to fix the size of the vortex bubble. However, when experiments were conducted in a water channel, it was found that a trapped vortex could be formed in some cases but that a large amount of fluid had to be withdrawn from the center of the vortex to not only form the vortex but also to sustain it. This result was predicted by the theory through the magnitude of the sink required to achieved an equilibrium condition at the center of the vortex. Not immediately apparent is the fact that the sink flow also represents a drag that is attributable to the vortex trapping process. It was then reasoned that not only is the drag undesirable, but a large amount of fluid moving along the vortex core can disrupt the vortex formation and, if large enough, can actually occupy the entire trapped vortex region at spanwise stations near the wingtip where the core flow spills into the free stream. Research was then started on finding ways by which the mass flow at the source/vortex location could be made to vanish.

LOCATIONS OF EQUILIBRIUM POINTS IN AIRFOIL PLANE

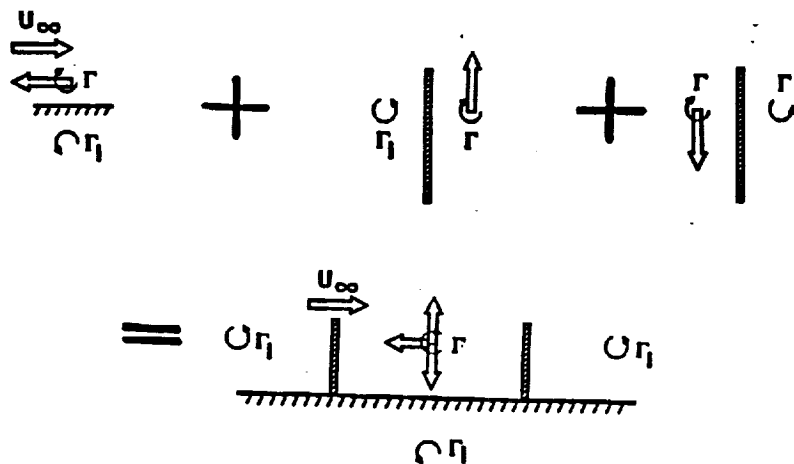
$$\beta_{rh} = -0.75 \text{ rad}, x_{f1} = 0.05c, \alpha = 0.1 \text{ rad}$$



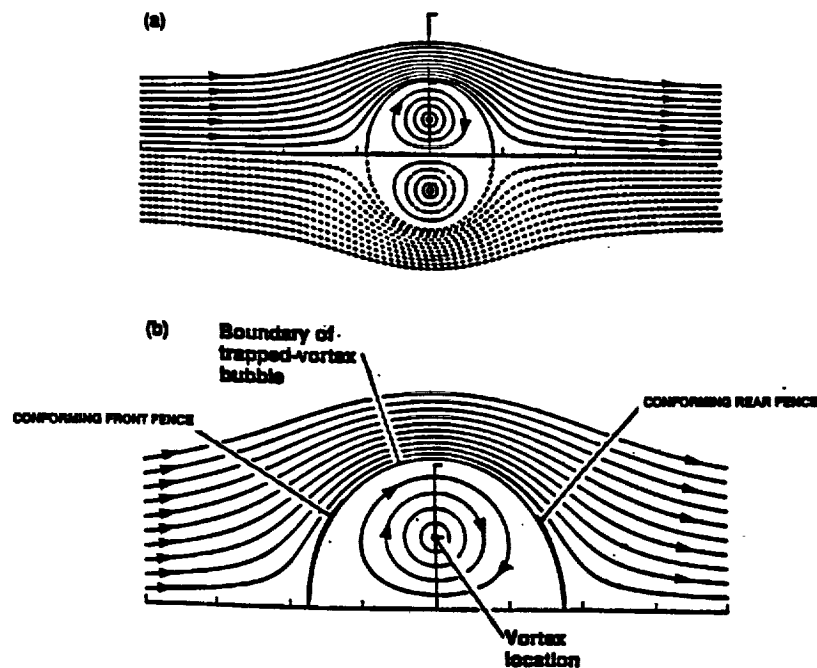
A mechanism whereby the source flow can be made to vanish and still have an equilibrium point for the vortex is illustrated here. The two-fence trapped-vortex configuration in the lower part of the figure is divided into three separate flat-plate boundaries. In the first, the horizontal flat plate serves as a reflection plane with an image vortex below the surface which induces an upstream velocity on the vortex that is exactly equal to the oncoming free-stream velocity. This configuration yields an equilibrium point without a source but requires a fence of some sort to promote the formation of the vortex. A fence upstream of the vortex provides the shear layer mentioned previously that builds the circulation in the vortex. The vertical boundary also induces an upward velocity through the influence of the image vortex needed to make the surface a streamline. The upward velocity due to the front fence needs to be offset by a sink located beneath the horizontal plane if some other artifice is not used to bring about an equilibrium condition. Such an artifice is available as a fence downstream of the vortex. As indicated in the figure, the image vortex for the rear fence induces a downward velocity on the vortex. Therefore, if the vortex to be trapped is midway between two vertical surfaces of about the same size, an equilibrium condition is achieved for the vortex without the presence of a source or sink.

The two-fence concept does several things for the flow field. First, it makes it possible to trap a vortex at its equilibrium location without the use of a source or sink. The front fence serves as an upstream limit on the trapped-vortex flow field and as a means for generating a shear layer that supplies vorticity to the vortex. The second fence serves as a downstream limit on the size of the vortex bubble and as a reflection plane for the vortex so that trapping can be achieved without the need for a source or sink. Since a source or sink is not required for the establishment of an equilibrium point, the drag due to vortex trapping is negligible which means that efficient lift enhancement has been achieved. Another big advantage is that the flow along the core of the vortex is also negligible making it much easier to establish and maintain the vortex flow field. Mass removal from the core is then only necessary to establish the vortex and to remove low energy fluid generated by viscous losses.

TWO-FENCE CONCEPT



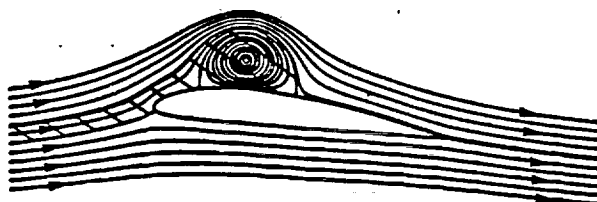
Before proceeding to airfoil-type trapped-vortex configurations, consider the simple case wherein a vortex is trapped over an infinite plane. As mentioned previously, a source is not needed in order to achieve an equilibrium condition. In practice however, fences are needed to fix the upstream and downstream extents of the vortex bubble and to provide a separated flow region with a shear layer to supply the vorticity that builds into the circulation for the vortex. Fences can be added to the flow field without disturbing the equilibrium condition or the streamline pattern if the fences are placed upstream and downstream of the vortex on the surface of the vortex bubble as shown in the lower part of the figure. If the fences are thin and fit, or conform to, the surface of the vortex bubble, the flow field characteristics are unchanged by addition of the fences. A number of the solutions to be presented will be noted to have only one fence that is flat and that is needed to make $m = 0$. The other fence is assumed to be of the conforming type that fits the vortex bubble so closely that no appreciable change in the flow field is brought about.



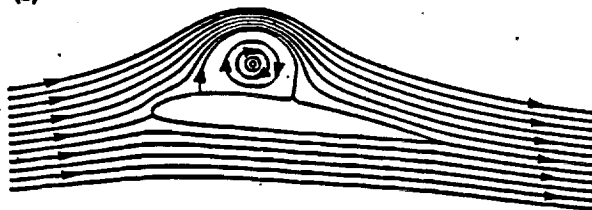
a. Image and physical streamlines for trapped vortex flow field.
b. Fences fore and aft that conform to shape of vortex separation bubble.

The procedure that was used to calculate the trapped-vortex flow field over an airfoil wherein a source or sink is not needed is illustrated in the figure below. The first step in the procedure is to calculate the flow field when only the front and rear stagnation points of the vortex bubble are specified. In such a case, the vortex bubble is assumed to have conforming fences that do not interfere with the equilibrium condition. Under those conditions, if a sink is required in order to achieve an equilibrium condition for a source/vortex combination as shown in the upper figure, the height of the rear fence (which is approximately flat) is increased in steps until the sink flow is negligibly small. The sink flow is highlighted in the upper figure by cross-hatching the streamtubes entering the sink. When the proper height of the flat plate rear fence has been found by such an iterative process, it is retained as the most efficient, or $\dot{m} = 0$, solution for a vortex bubble of a specified size and location on an airfoil at a given angle of attack. Conversely, if the flow field solution for the conforming-fence geometry had required a source rather than a sink, the height of a flat front fence would have been increased until $\dot{m} = 0$. The foregoing procedure was used to obtain all of the $\dot{m} = 0$ trapped-vortex solutions presented here.

(a) CONFORMING FENCES ONLY



(b) CONFORMING FRONT FENCE



a. No fences; $h_1/c = 0, h_2/c = 0$; $x_{ps} = -0.197, y_{ps} = +0.216, \Gamma/cU_\infty = -1.749, \Gamma_o/cU_\infty = +0.869, \dot{m}/cU_\infty = -0.034; C_L = 1.761, C_D = 0.108$.

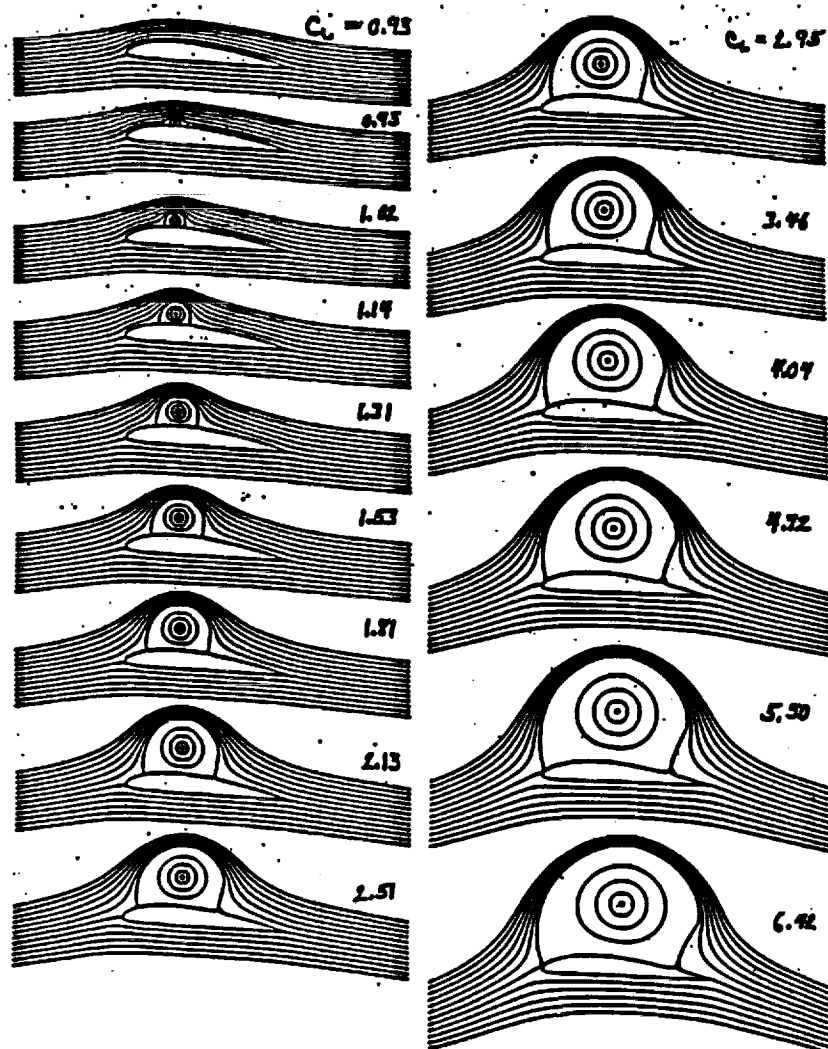
b. Rear fence just large enough to reduce \dot{m} to zero. $h_1/c = 0, h_2/c = 0.114; x_{ps} = -0.165, y_{ps} = +0.332, \Gamma/cU_\infty = -1.886, \Gamma_o/cU_\infty = +0.998, \dot{m}/cU_\infty = 0.0; C_L = 1.777, C_D = 0.0$.

Vortex trapped on Clark Y airfoil (NACA 4412); $\alpha = 0.1$.

In order to obtain a data set of solutions that can be used to study the characteristics of airfoils with trapped vortices, a sequence of $m = 0$ cases were calculated for the flow over an NACA 4412 (or Clark Y) airfoil at angles of attack from $\alpha = -4^\circ$ through $\alpha = +12^\circ$ in increments of 2° . Since the streamlines for the various solutions do not change very much, only the solutions for $\alpha = +4^\circ$ are presented on this slide. The various solutions differ from one another in that the size of the trapped-vortex bubble increases gradually from zero to a size that nearly covers the entire upper surface of the airfoil. It could be imagined that the sequence of figures represents a streamwise cross-section of the flow field as the wing is changed from its cruise configuration (i.e., no vortex) to the vortex-bubble size (and lift) needed for landing. Conversely, when the aircraft takes off, the fences are first deployed so as to develop the size of trapped-vortex needed for high lift. As the aircraft becomes airborne and increases its flight velocity, the fences are changed so that the vortex bubble shrinks in size progressively until the cruise configuration is achieved.

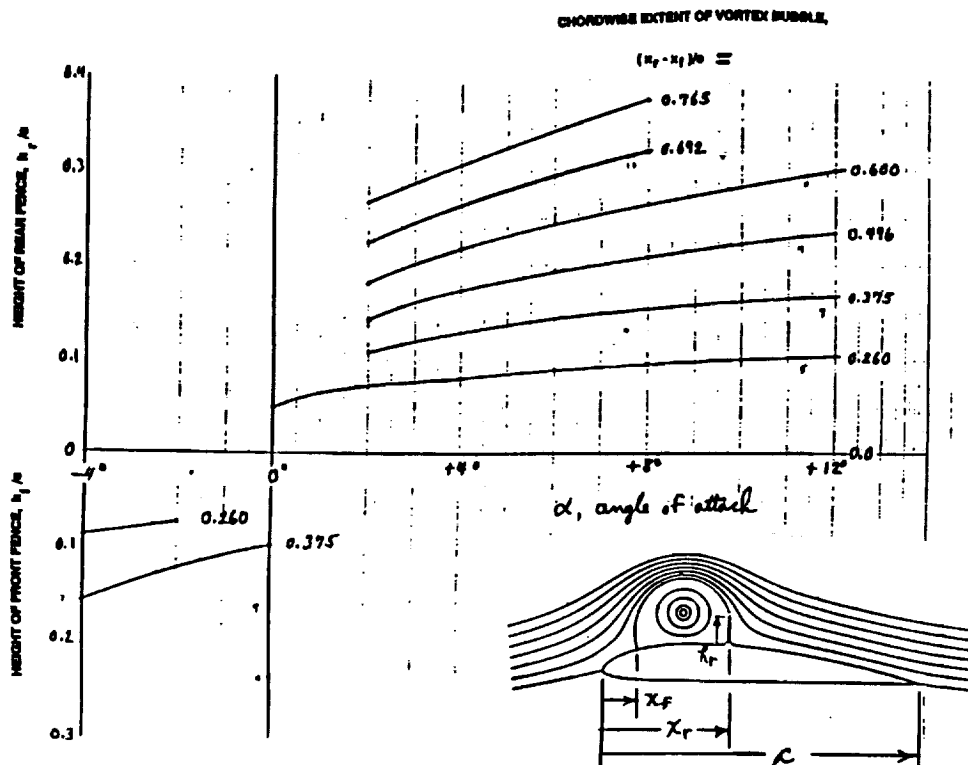
STREAMLINE PLOTS FOR RANGE OF VORTEX BUBBLE SIZES

$$\alpha = 4^\circ$$



The various characteristics of the trapped-vortex airfoils are now presented. The first parameter illustrated is the height of the flat fences used to bring about the $\dot{m} = 0$ condition. The parameters that are used to define the chordwise extent of the vortex bubble are shown in the inset figure. The chordwise beginning or front of the bubble, x_f , is taken as the intersection of the bubble or fence surface with the upper surface of the airfoil. Similarly, the rear or downstream end of the vortex bubble, x_r , is defined as the point where the bubble surface intersects the surface of the airfoil. It is noted that a flat fence length of about $0.1c$ is required in order to obtain a vortex bubble that covers 26% of the airfoil. A flat fence length of about $0.2c$ produces a vortex bubble that covers about half of the airfoil surface. This figure and the previous one clearly show that the size of the vortex bubble is largely controlled by the spacing between the front and rear fences. The height of the fences that are flat and do not conform to the shape of the vortex bubble govern the magnitude of the source or sink needed for equilibrium and are used to make $\dot{m} = 0$. Conforming fence portions of a certain length will likely also be necessary in practice to produce the shear layer needed for the development of the vortex and to control the physical limits of the vortex bubble. The present study does not include a study of the size of conforming fences that are needed.

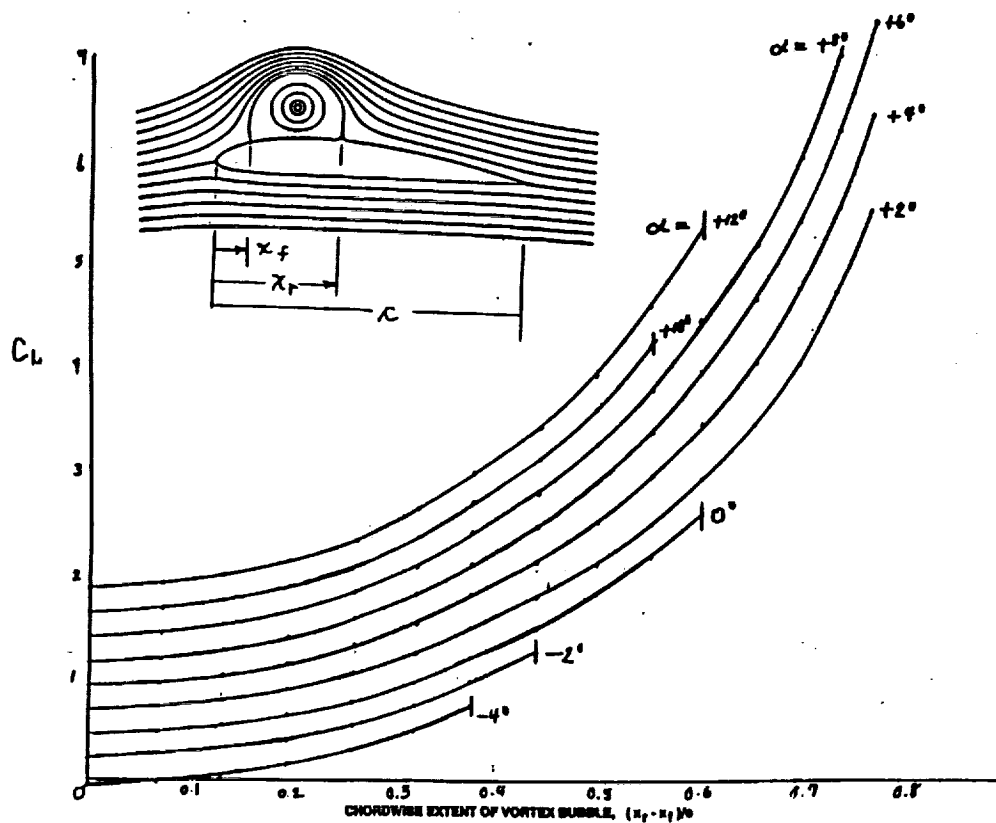
LENGTH OF FENCES REQUIRED FOR ZERO SOURCE STRENGTH



The lift coefficient developed by the various trapped- vortex configurations is presented on this slide for the range of vortex bubble sizes that were studied. It is noted that the lift increases slowly at first as the size of the vortex bubble increases from zero. At the larger vortex sizes, the lift changes rapidly with the size of the vortex bubble. Also to be noted is that not all of the curves end at the large vortex bubble sizes. The computations indicate that it is not possible to find an equilibrium point for $m = 0$ in certain cases. Although a physical reason for the solution failure was not found, it seems reasonable that fence heights above certain values should not be possible solutions because the fences begin to interfere with the vortical flow field and cause it to become too distended in the vertical direction. An explanation or criterion for the fence lengths above which solutions can no longer be found was not found.

Even a casual look at the curves of lift as a function of bubble size suggests that the curves are about of the same shape and that they might possibly collapse to a single curve if the lift increment due to the trapped vortex is plotted as a function of the size of the vortex bubble, $(x_r - x_f)/c$. Those results are presented on the next slide.

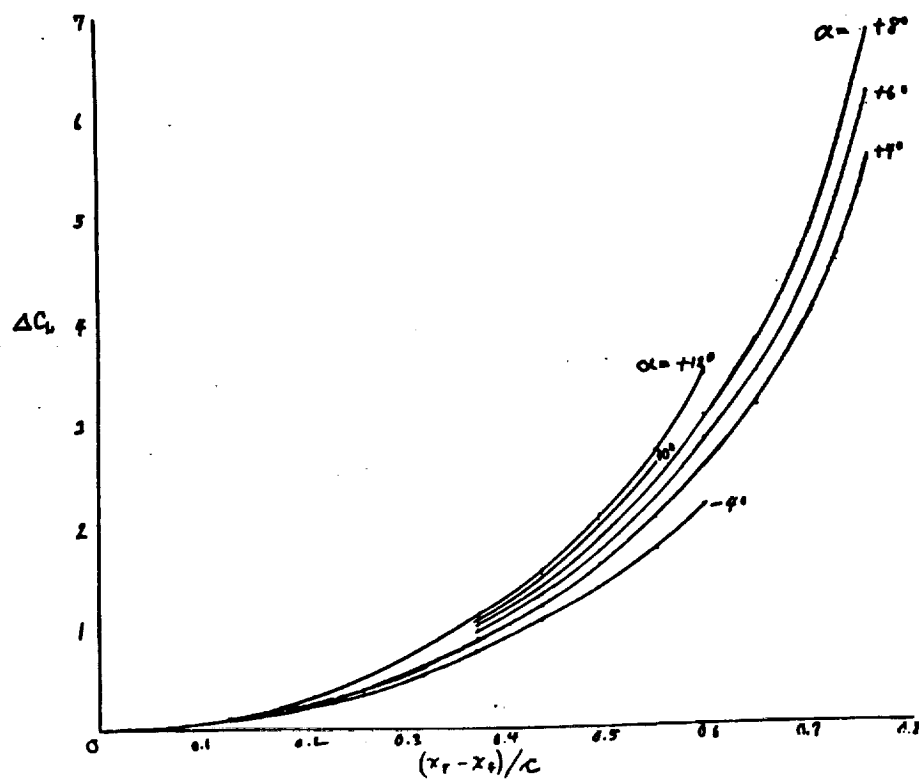
LIFT COEFFICIENT AS A FUNCTION OF VORTEX BUBBLE SIZE



7-25-91

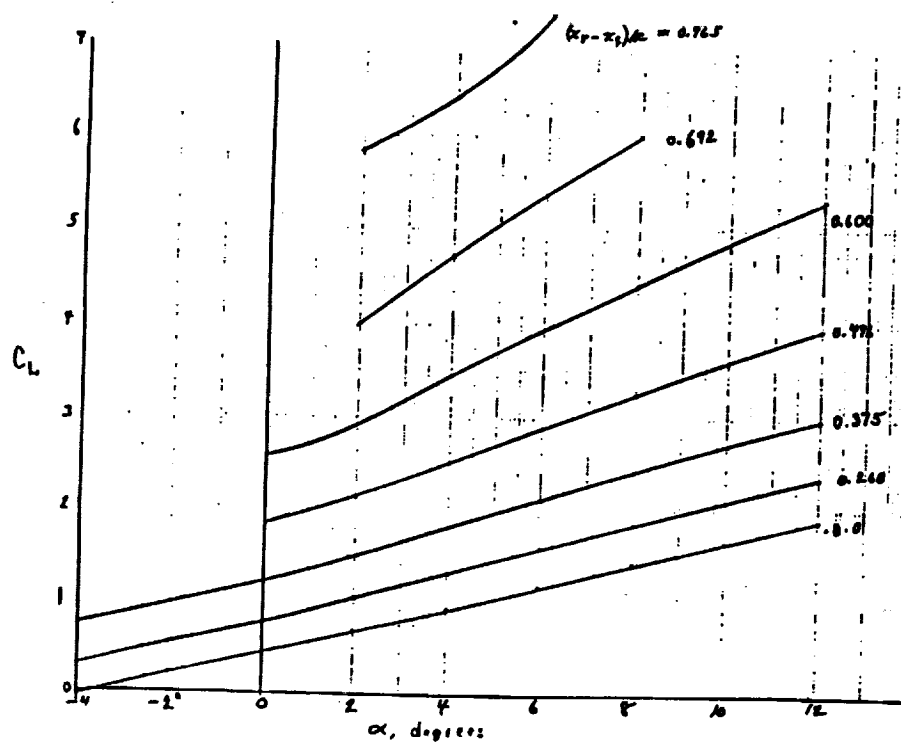
The data on the previous slide collapses to a single curve only for the smaller values of $(x_r - x_f)/c$. As the vortex bubble size increases the differences between the curves increases, even though the curves all have about the same shape. Manipulation of the various parameters might provide a better correlation of the data but was not tried.

INCREMENT IN LIFT COEFFICIENT DUE TO TRAPPED VORTEX



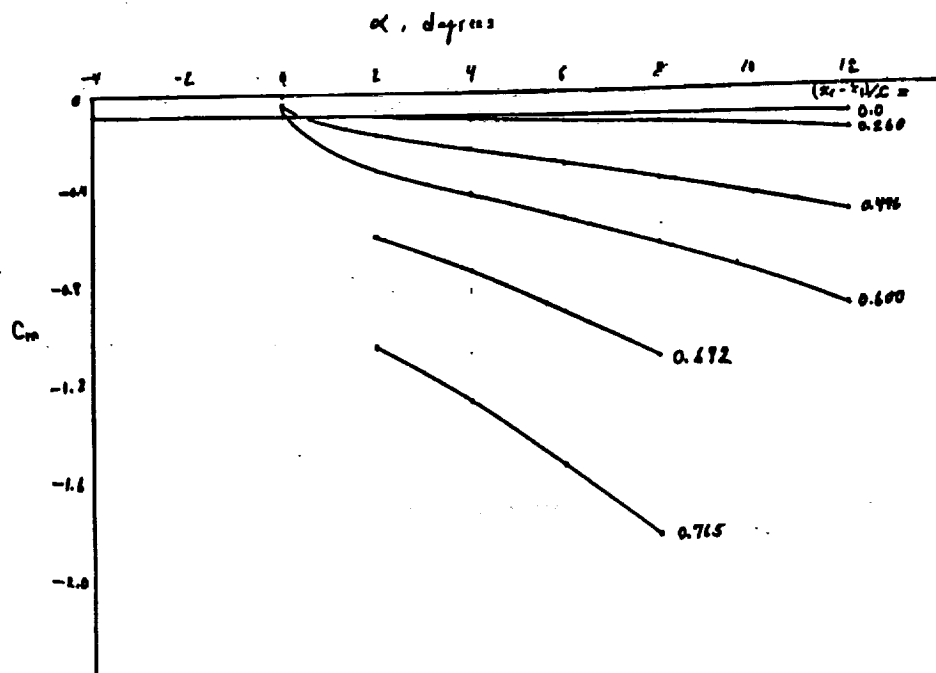
In order to demonstrate that the lift responds in the conventional way to angle of attack, this slide presents the lift produced as a function of angle of attack for various sizes of the trapped-vortex bubble. It is noted that the variation of lift with angle of attack for bubble sizes that are 60% or less of the chord are approximately linear with angle of attack. The slope of the lift curves increases with increasing size of the vortex bubble but not dramatically. These results indicate that trapped-vortex airfoils have a conventional response to angle of attack. The figure also provides an estimate of the reduction in angle of attack that can be achieved by adding a trapped vortex to the flow field over the airfoil. For example, addition of a trapped vortex that covers 26% of the airfoil, permits about a 4° reduction in angle of attack for a given section lift coefficient.

LIFT COEFFICIENT AS A FUNCTION OF ANGLE OF ATTACK



The pitching moment about the quarter-chord location is expected to vary greatly when the vortex bubble is large and moves aft. Even though an attempt was made to keep the center of the vortex bubble at about the same chordwise station, the pitching moment is seen to become quite large. Latitude is available, however, for placing the vortex bubble fore or aft on the airfoil to influence the pitching moment—see next slide.

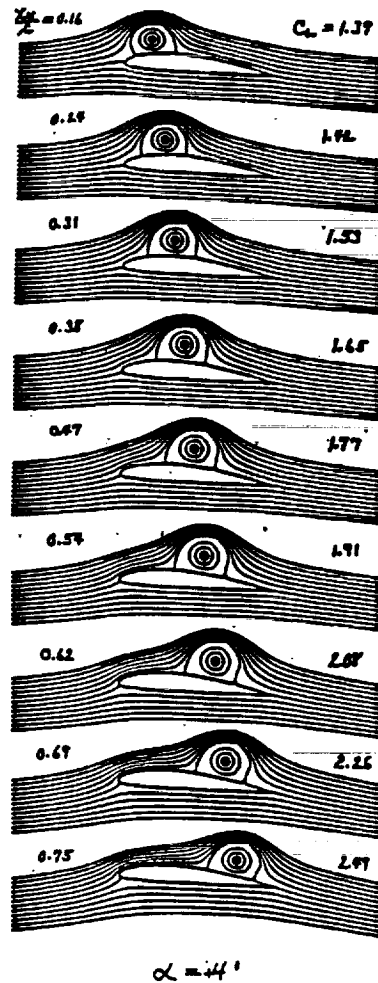
PITCHING MOMENT COEFFICIENT VS. ANGLE OF ATTACK



9-24 71

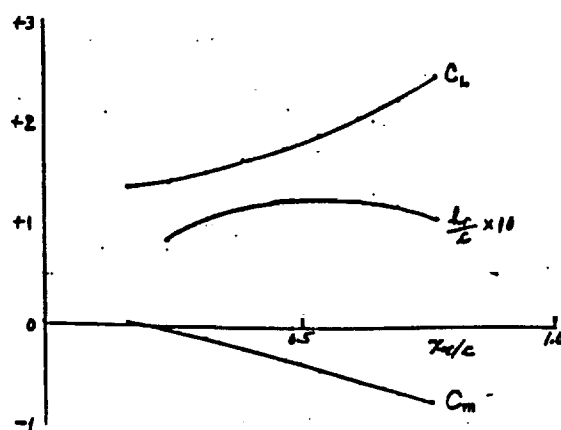
In this particular sequence of trapped-vortex cases, the size of the trapped-vortex bubble is held approximately constant as the chordwise location of the bubble is move aft in a series of steps from a very forward location. The cases presented illustrate some of the latitude that is available for manipulating the characteristics of the airfoil.

STREAMLINE PLOTS FOR RANGE OF CHORDWISE LOCATIONS OF VORTEX BUBBLE



The characteristics of the trapped-vortex cases presented on the previous slide are summarized here. As expected, the pitching moment can be made as small as desired by moving the vortex bubble forward. The lift generated by the trapped vortex does decrease with the more forward location but not disastrously. The minimum height or length of the flat fences also changes a bit with the location of the trapped vortex but not by a large amount.

AIRFOIL CHARACTERISTICS FOR RANGE OF CHORDWISE LOCATIONS OF VORTEX BUBBLE



The foregoing slides provide an overview of the characteristics of one airfoil shape which has its lift enhanced by a trapped vortex flow field. Results for other airfoil shapes will differ in detail but will generally have much the same character. This information provides the beginning steps in the fulfillment of the objective of the research which is to find the necessary and sufficient conditions for vortex trapping. Not only should the vortex trapping be efficient and effective for two-dimensional (or airfoil) situations but also in the three-dimensional or wing situations. Furthermore, the trapped-vortex configurations should be efficient, easy to produce and maintain and not too onerous to implement on actual aircraft. With these guidelines for the research program, it is concluded from the investigation presented here that vortex trapping in two-dimensions is reaching a point of good understanding. More detailed studies not only with conformal mapping methods but also with other methods need to be carried out to fill out the characteristics of trapped-vortex airfoils. As noted in the items listed below, the most pertinent contributions of the present study to date include the introduction of a second fence to help control the characteristics of the trapped-vortex flow field. In particular, the use of fence curvature and height to bring about the equilibrium or zero velocity condition at the center of the vortex with negligible mass removal from the vortex core makes the trapped-vortex high-lift concept an efficient one. In this way the two-fence concept provides the necessary tools in two-dimensions at least for producing efficient easily formable high lift airfoils. The other conclusions listed below are essentially self explanatory. It should be remarked, however, that the steps from two- to three-dimensions will require some good ideas if the trapped-vortex flow fields are to be realized on real wings wherein only the local flow fields are used as the suction needed for evacuating the vortex core. The special suction orifices used in two dimensions will not then be needed. Encouragement is provided however, by the success achieved with the two-dimensional results and it is believed that comparable success can be achieved with three-dimensional configurations.

CONCLUSIONS

- 1. TWO DIMENSIONAL RESULTS INDICATE THAT TRAPPED VORTICES CAN PROVIDE LARGE AMOUNTS OF LIFT ENHANCEMENT.**
- 2. AN UPSTREAM AND A DOWNSTREAM FENCE APPEAR TO BE NECESSARY PARTS OF THE TWO-DIMENSIONAL TRAPPING PROCESS.**
- 3. FENCE HEIGHTS MUST BE ADJUSTED SO THAT SOURCE STRENGTH IS ZERO IN ORDER TO PROMOTE VORTEX FORMATION AND TO REDUCE DRAG.**
- 4. ADDITIONAL DESIGN GUIDELINES WILL NO DOUBT BE NEEDED FOR VORTEX TRAPPING ON WINGS IN THE FULL THREE-DIMENSIONAL ENVIRONMENT.**

Session XIII. Supersonic Laminar Flow Control

THIS PAGE INTENTIONALLY BLANK

Session XIII. Supersonic Laminar Flow Control

omit

NASA F-16XL Supersonic Laminar Flow Control Program Overview
Dr. Michael C. Fischer, NASA Langley Research Center

PRECEDING PAGE BLANK NOT FILMED



THIS PAGE INTENTIONALLY BLANK

**NASA F-16XL SUPERSONIC LAMINAR FLOW CONTROL
PROGRAM OVERVIEW**

Michael C. Fischer

NASA, Langley Research Center
Hampton, Virginia

HIGH SPEED RESEARCH WORKSHOP

Williamsburg, Virginia
May 14-16, 1991

PRECEDING PAGE BLANK NOT FILMED

OBJECTIVES OF THE F-16XL SUPERSONIC LAMINAR FLOW CONTROL EXPERIMENT

Successful application of laminar flow control to a High Speed Civil Transport (HSCT) offers significant benefits in reductions of take-off gross weight, mission fuel burn, cruise drag, structural temperatures, engine size, emissions and sonic boom (refs. 1-3). The ultimate economic success of the proposed HSCT may depend on the successful adaption of laminar flow control, which offers the single most significant potential improvement in L/D of all the aerodynamic technologies under consideration. The F-16XL Supersonic Laminar Flow Control (SLFC) Experiment was conceived based on the encouraging results of in-house and NASA supported industry studies (refs. 1-3) to determine if laminar flow control is feasible for the HSCT. The primary objective, as illustrated in figure 1, is to achieve extensive laminar flow (50-60 percent chord) on a highly swept supersonic wing. Data obtained from the flight test will be used to validate existing Euler and Navier Stokes aerodynamic codes and transition prediction boundary layer stability codes. These validated codes and developed design methodology will be delivered to industry for their use in designing supersonic laminar flow control wings. Results from this experiment will establish preliminary suction system design criteria enabling industry to better size the suction system and develop improved estimates of system weight, fuel volume loss due to wing ducting, turbocompressor power requirements, etc. so that benefits and penalties can be more accurately assessed.

F-16XL SHIP 2 SUPERSONIC LAMINAR FLOW CONTROL EXPERIMENT

OBJECTIVES

- **Achieve 50-60% chord laminar flow on a highly swept wing at supersonic speeds**
- **Deliver validated CFD codes and design methodology to industry for designing supersonic laminar flow wings**
- **Establish initial LFC suction system design criteria to allow industry to more accurately integrate concept into HSCT and determine benefits**

F-16XL SUPERSONIC LAMINAR FLOW CONTROL FLIGHT TESTING

There are two F-16XL aircraft involved in supersonic laminar flow flight testing. The F-16XL was chosen for the experiment because it has a highly swept cranked wing planform that closely resembles the HSCT configurations proposed by industry. The inboard section of the wing is swept 70 degrees, while the outboard section is swept 50 degrees. The F-16XL Ship 1 has a single place cockpit (see figure 2) and is currently being utilized in a cooperative laminar flow control flight test program involving North American Rockwell International and NASA. The objectives of the Rockwell/NASA program are to develop and validate CFD methodology and demonstrate that laminar flow is achievable to a limited chord extent on a highly swept wing at supersonic speeds. The laminar flow control test article on Ship 1 is considerably smaller in span and chord extent as compared to the planned NASA experiment on Ship 2, thus extensive laminar flow will not be demonstrated on Ship 1. Also, the airfoil section and pressure distribution on the Ship 1 test article is different than that planned for the NASA experiment on Ship 2. Flight testing began on Ship 1 in May, 1990. Flight data obtained from Ship 1 has proven to be very informative and useful in reducing the risk for the NASA Ship 2 experiment. Ship 1 flight data is being utilized to calibrate Euler and Navier Stokes codes and boundary layer stability codes. F-16XL Ship 2, which has a two place cockpit, as shown in figure 2, arrived at DFRF in February, 1991 and is being instrumented for flight testing.

SUPERSONIC LAMINAR FLOW CONTROL FLIGHT TESTING

F-16XL Ship 1
Rockwell/NASA Test

Test Article

- Single Place Cockpit
- F100-PW-200 Engine

Objectives:

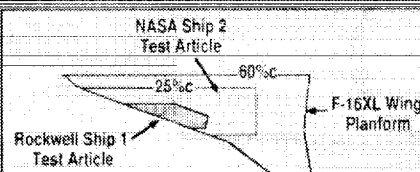
- Develop and Validate CFD Methodology
- Demonstrate Laminar Flow Achievable on a Highly Swept Wing at Supersonic Speeds

F-16XL Ship 2 NASA Experiment
High Speed Research Program

- Dual Place Cockpit
- F110-GE-129 Engine

Objectives:

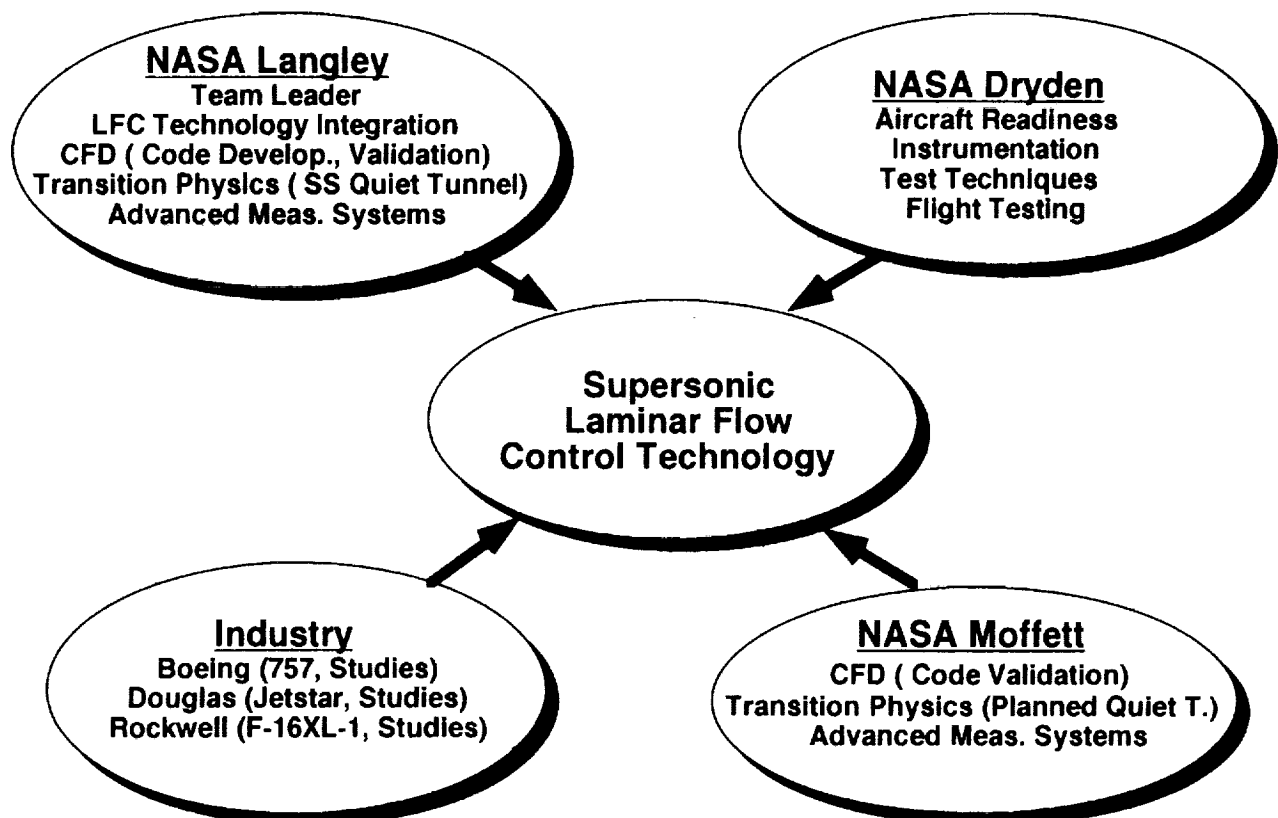
- Achieve 50-60% Chord Laminar Flow on a Highly Swept Wing at Supersonic Speeds
- Deliver Validated CFD Codes and Design Methodology to Industry for Designing Supersonic Laminar Flow Wings
- Establish Initial LFC Suction System Design Criteria



NASA / INDUSTRY TEAM APPROACH ON THE F-16XL SLFC EXPERIMENT

To carry out the F-16XL experiment, NASA has structured a combined NASA / Industry team approach to take advantage of the broad LFC experience base within Industry and NASA (see figure 3). NASA Langley has overall responsibility for management of the program, based on its proven LFC technology expertise and integration capabilities established over numerous successful laminar flow flight programs. Langley is also responsible for Navier Stokes and Euler code validation, transition prediction methodology through both boundary layer stability code development and validation and transition experiments with swept model tests in the Supersonic Low-Disturbance Pilot Tunnel, and advanced measurement systems. NASA Dryden is responsible for aircraft readiness, instrumentation, test techniques and flight testing. NASA Moffett is responsible for Navier Stokes and boundary layer stability code validation, transition experiments in a planned low disturbance supersonic wind tunnel, and advanced measurement systems. The industry team which has laminar flow control flight experience consists of Boeing, Douglas and Rockwell. These three companies are also participating in LFC technology studies for NASA. Industry involvement is essential to ensure practical, relevant LFC technology is developed and validated and to ensure rapid transfer of the technology to application. A contractor to be chosen in a competitive procurement will be responsible for the design, fabrication and installation of flight test hardware and associated systems on the F-16XL Ship 2.

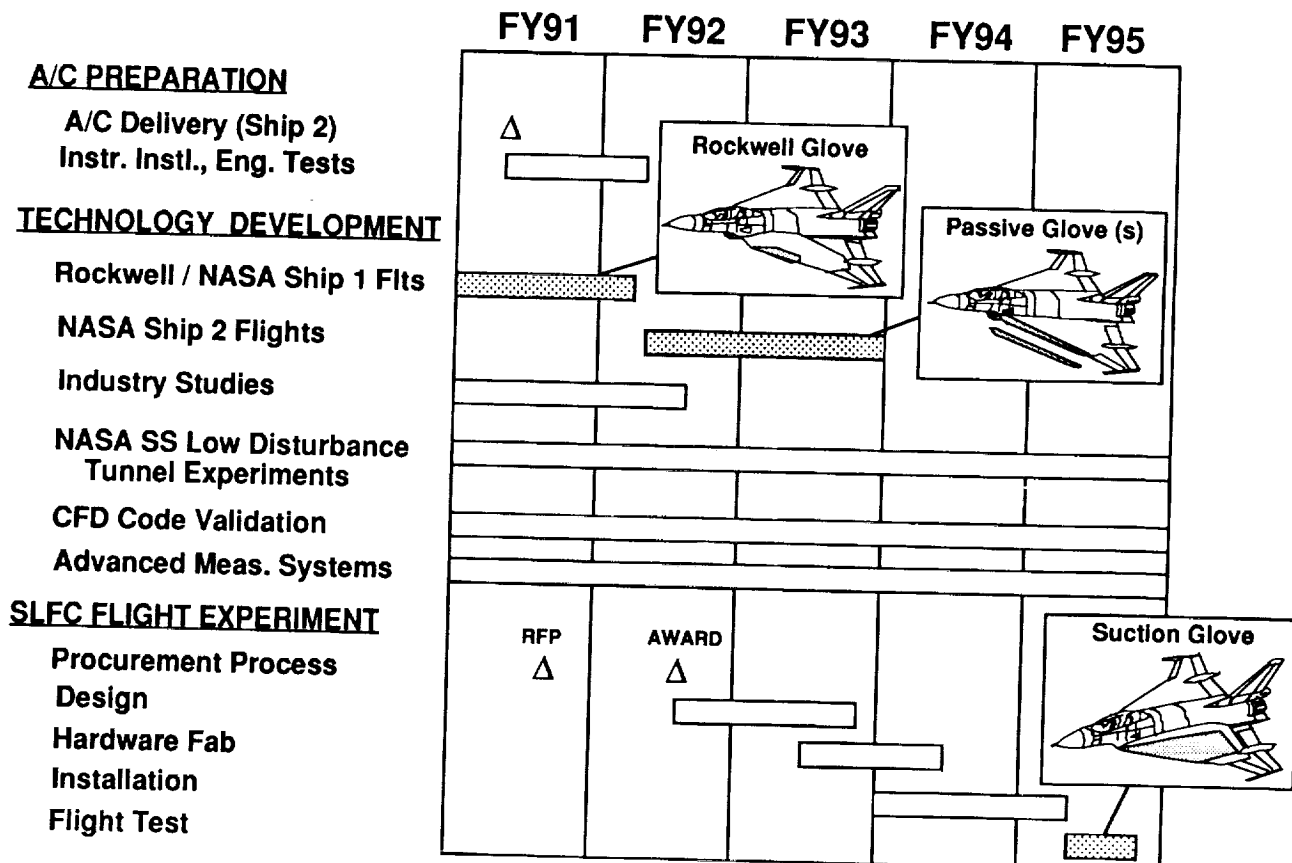
NASA / INDUSTRY TEAM APPROACH ON F-16XL SLFC EXPERIMENT



SCHEDULE FOR THE F-16XL SUPERSONIC LAMINAR FLOW CONTROL EXPERIMENT

The activities leading to the eventual flight experiment on the F-16XL-2 are shown in figure 4. F-16XL-2 arrived at DFRF in February, 1991 and is currently being instrumented for flight testing. Prior to the actual Ship 2 suction panel laminar flow control experiment, there is a need to reduce the risk to the experiment by developing key technologies through industry studies, obtaining flight and supersonic wind tunnel data for design criteria and code calibration, and evaluating advanced instrumentation. The initial series of Rockwell/NASA Ship 1 flight tests will be completed and followed by proposed NASA tests to determine suction level-laminar flow sensitivities and obtain other useful data. Leading-edge passive gloves will be flight tested on Ship 2 to obtain attachment-line design criteria and surface pressure and transition location data for code calibration. Swept wing suction and non-suction models will be tested in supersonic low disturbance tunnels to obtain attachment line and crossflow stability data for comparison with flight data and establishment of design guidelines. The CFD code validation effort will be a continuing refinement process as flight and wind tunnel data become available. The request for procurement (RFP) package will be released in June 1991 with award expected in April 1992. The contractor chosen will be responsible for designing, fabricating and installing the test hardware and related suction system. Flight testing to demonstrate achievement of extensive laminar flow is scheduled to conclude in late FY95.

F-16XL SLFC EXPERIMENT SCHEDULE



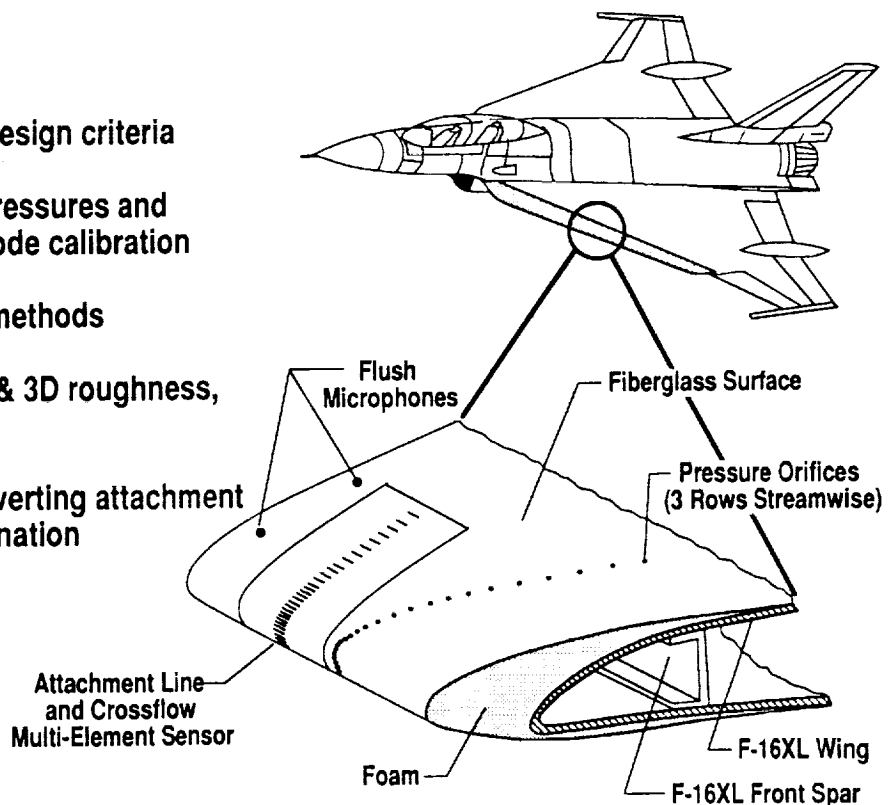
F-16XL-2 LEADING EDGE PASSIVE GLOVE(S)

Proper design of the leading-edge region is crucial to ensure control of spanwise leading-edge turbulence contamination, and to prevent unacceptable growth of both attachment line boundary layer disturbances and crossflow disturbances. This design process will involve careful tailoring of the leading edge radius and local suction level. There is limited leading-edge transition data available at supersonic conditions, so a non-suction leading-edge passive glove will be designed and flight tested on Ship 2 to provide needed design criteria and reduce the risk for the NASA experiment (see figure 5). Momentum thickness Reynolds number (R_{θ}) limits for transition of the attachment line with no suction will be obtained and compared with theoretical calculations. Transition on the upper surface due to crossflow will also be determined for a range of leading-edge surface pressure accelerations. The transition and surface pressure data will be used to calibrate stability and CFD codes and improve existing transition prediction methods. The passive glove tests will also provide the opportunity to evaluate advanced measurement methods, such as multi-element sensors, improved anemometers and flow visualization techniques. Both 2D steps and 3D roughness effects on leading-edge laminar flow will be explored to provide design criteria for suction panel joints and acceptable insect accretion height. It may be possible to provide the needed flight data with one passive glove operating at both design and off-design conditions, however, if required and the schedule permits, a second glove could be evaluated.

F-16XL LEADING-EDGE PASSIVE GLOVE(S)

Objectives:

- Obtain attachment line design criteria
- Measure leading-edge pressures and transition location for code calibration
- Evaluate measurement methods
- Determine effects of 2D & 3D roughness, steps, on laminar flow
- Evaluate methods for diverting attachment line turbulence contamination



F-16XL-2 SUPERSONIC LAMINAR FLOW CONTROL EXPERIMENT

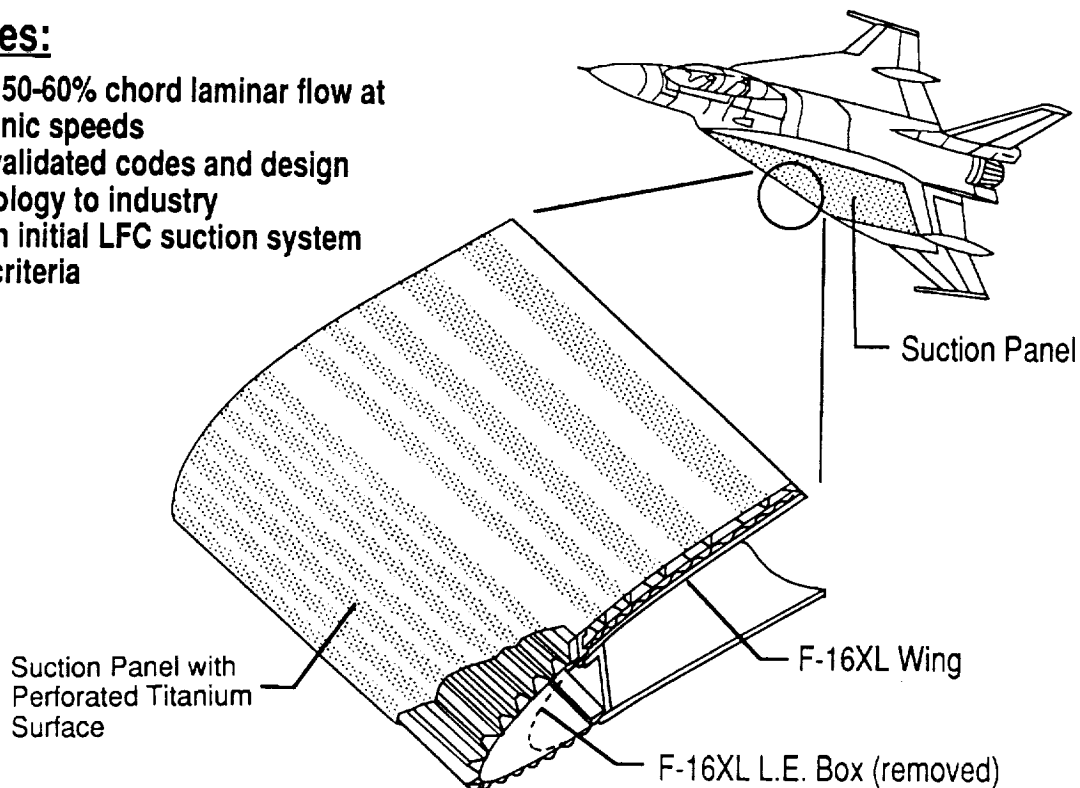
The NASA experiment will involve flight testing an active suction panel(s) to achieve laminar flow to 50-60 percent chord, as illustrated in figure 6. The test article will be designed to achieve laminar flow over a range of Mach numbers and altitudes to provide laminar flow data for a wide variation in pressure distributions, unit Reynolds number, and attachment line conditions. Suction flow rate level and distribution will be varied in flight to determine the sensitivity of laminar flow extent to changes in suction flow, pressure distributions and Reynolds numbers. These flight data will be extremely valuable in validating the Euler and Navier Stokes codes and the boundary layer stability codes. These validated codes will enable the establishment of a design methodology for designing supersonic laminar flow control wings which will be delivered to industry for their use. Data from the experiment should also provide preliminary estimates for LFC system sizing to allow Industry to more accurately determine the benefits and penalties of LFC.

It is important to recognize that the F-16XL SLFC Experiment is an aerodynamic feasibility experiment and not a technology demonstration program. Before industry will implement laminar flow control on a HSCT, a high confidence level in such areas as performance, cost, reliability, maintainability, safety, system and structural integration, etc. must be demonstrated. To achieve these goals, a parallel NASA / Industry program must be developed and initiated in the near future to address those critical technologies not being pursued in the F-16XL SLFC Experiment.

F-16XL-2 SUPERSONIC LAMINAR FLOW CONTROL EXPERIMENT

Objectives:

- Achieve 50-60% chord laminar flow at supersonic speeds
- Deliver validated codes and design methodology to industry
- Establish initial LFC suction system design criteria



ACCOMPLISHMENTS

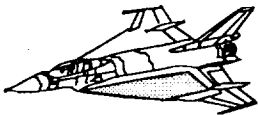
In the past year, there have been many significant accomplishments in the program, as shown in figure 7. Flight data on the F-16XL-1 has been obtained and is being used to calibrate Navier Stokes and boundary layer stability codes. Navier Stokes solutions of the complete F-16XL configuration have been obtained with several codes. A re-start of testing on the F-16XL-1 is planned in the near future to map out the transition front across the test article for a range of flight conditions. Planning for NASA follow on F-16XL-1 tests is underway also. The F-16XL-2 vehicle arrived at DFRF in February and is now being instrumented for flight testing. A NASA sponsored study performed by DAC indicated the feasibility of achieving 60 percent chord laminar flow on F-16XL-2. A leading-edge passive glove design for the F-16XL-2 is underway and is scheduled for testing in early calendar year 1992. Blockage models were successfully tested in the LaRC Supersonic Low-Disturbance Tunnel and a non-suction thin-skin instrumented model is being fabricated for testing in July, 1991. Thin-film micro-element sensors were further developed, tested in several wind tunnels and designed/fabricated for the F-16XL leading-edge. The F-16XL RFP procurement package was prepared with release scheduled for June 1991. Industry technology study tasks have been identified and are being implemented to address "technology holes".

ACCOMPLISHMENTS

- Rockwell / NASA F-16XL-1 flight data obtained, tests nearing re-start
- Plans for follow-on F-16XL-1 tests being finalized
- Navier Stokes F-16XL-1 solutions obtained, codes being calibrated with flight data
- F-16XL-2 arrived February, 1991 at DFRF, instrumentation being installed
- DAC study indicated feasibility of achieving 60% c laminar flow on F-16XL-2
- Passive glove design for F-16XL-2 tests underway
- Non-suction model for LaRC SS Low-Disturbance Tunnel being fabricated, testing begins July 1991
- Micro-element sensors developed and tested in wind tunnels, designed and fabricated for F-16XL
- F-16XL-2 RFP procurement package being prepared, release scheduled for June 1991
- Industry technology study tasks being initiated to address "technology holes"

SUMMARY

NASA has carefully tailored the program to achieve a balance of both NASA and industry participants to take advantage of the laminar flow control expertise available. There is also a proper mix of computational effort, ground facility experiments, and flight testing. Flight tests with the Rockwell laminar flow control test article on F-16XL-1 is providing useful data that will reduce the risk for the F-16XL-2 experiment. Leading-edge passive glove tests on F-16XL-2 will provide attachment line design criteria and code calibration data that will add confidence to the design process for the suction panels. The RFP for the design, fabrication and installation of suction panel(s) and associated suction system hardware is scheduled for release to industry in June 1991 and award in April 1992. Flight testing of the active suction panel(s) will be conducted in 1995.



SUMMARY

- Program has a balance of participants and technologies
 - NASA- industry roles
 - CFD, wind tunnel tests, flight tests
- Flights with F-16XL-1 have been, and continue to be, informative & will reduce risk for F-16XL-2 experiment
- Passive glove testing on F-16XL-2 will provide attachment line criteria and code calibration data
- Plan to issue RFP to industry for design, fabrication and installation of suction panel(s) and associated suction hardware in June 1991
- Flight test active suction panel(s) in 1995

REFERENCES

1. Powell, A. G.; Agrawal, S.; and Lacey, T. R.: Feasibility and Benefits of Laminar Flow Control on Supersonic Cruise Airplanes. NASA CR 181817, July 1989.
2. Boeing Commercial Airplane Staff: Application of Laminar Flow Control to Supersonic Transport Configurations. NASA CR 181917, July 1990.
3. Pfenninger, W.; and Vemuru, C.S.: Design Aspects of Long Range Supersonic LFC Airplanes Especially With Highly Swept Wings. SAE Paper No. 881397, 1988

Session XIII. Supersonic Laminar Flow Control

Supersonic Laminar Flow Control - Challenges and Opportunities
Arthur G. Powell, Douglas Aircraft Company

THIS PAGE INTENTIONALLY BLANK

SUPERSONIC LFC -
CHALLENGES AND OPPORTUNITIES

59-02
11984

A.G. Powell

Douglas Aircraft Company
McDonnell Douglas Corporation
Long Beach, California
Ca. 90846

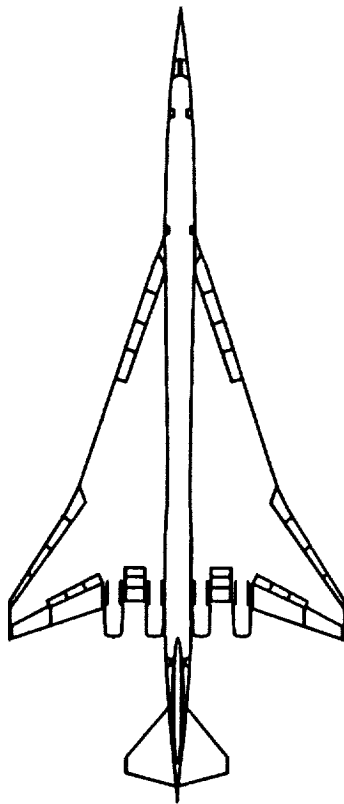
FIRST ANNUAL
HIGH SPEED RESEARCH WORKSHOP
Williamsburg, Virginia
May 14-16, 1991

WARNING: INFORMATION SUBJECT TO EXPORT CONTROL LAWS This document may contain information subject to the International Traffic in Arms Regulation (ITAR) and/or the Export Administration Regulation (EAR) of 1979 which may not be exported, released, or disclosed to foreign nationals inside or outside the United States without first obtaining an export license. A violation of the ITAR or EAR may be subject to a penalty of up to 10 years imprisonment and a fine of \$100,000 under 22 U.S.C. 2778 or Section 2410 of the Export Administration Act of 1979. Include this notice with any reproduced portion of this document.

INTRODUCTION

The high fuel fractions required for long range supersonic airplanes give significant leverage to technologies for cruise drag reduction such as Laminar Flow Control (LFC). Fuel burn benefits are further enhanced when sizing effects are considered. These effects may even be powerful enough to reduce airplane production cost over a turbulent baseline. This is an important goal for LFC technology development.

The intent of this paper is to present the results of recent aerodynamics studies on the application of Laminar Flow Control (LFC) technology to the highly swept wings of supersonic airplanes. Important questions of applicability, realistic benefit, and critical application issues were addressed in a NASA-sponsored study conducted by MDC in 1987-88 (ref. 1). Figure 1 outlines the major thrusts of that study, the centerpiece of which was the Mach 2.2, 308 passenger airplane shown. More recent efforts, aimed at establishing the feasibility of demonstrating extensive Laminarization on the F-16XL-2 airplane, are also summarized in this paper.



Feasibility

Realistic Benefit

Critical Application Issues

How to Best Address Issues

Recommendations

Figure 1. Objectives of 1987-88 Supersonic LFC Study

LFC BENEFIT POTENTIAL

The 1987-88 study indicated LFC to be feasible for the Mach 2.2 configuration. The boundary layer instabilities requiring the largest suction flow to subdue were those associated with the highly swept attachment line and leading edge acceleration region. The original wing design featured a gradual acceleration on both upper and lower wing surfaces. An LFC-modified wing, having a steeper acceleration in the leading edge region, showed improvements in drag due-to-lift in addition to reduced suction flow requirements. The drag due-to-lift improvement was not considered fundamental to LFC and was not counted as a benefit.

With both surfaces of the wing and tail laminarized to the flap hinges, a 15% improvement in lift/drag ratio was realized, resulting in a resized fuel burn reduction of 17% and an empty weight reduction of 1.3% relative to a turbulent baseline. This analysis accounted for laminar area lost to bodyside turbulent wedges (ref. 2), the aerodynamic effects of LFC suction, and the weight of the suction system. The wing was assumed to be sized by initial cruise conditions.

Figure 2 shows the sensitivity of LFC benefits to system weight. Empty weight is included since this relates directly to production cost. Note the large payoff for minimizing suction system weight.

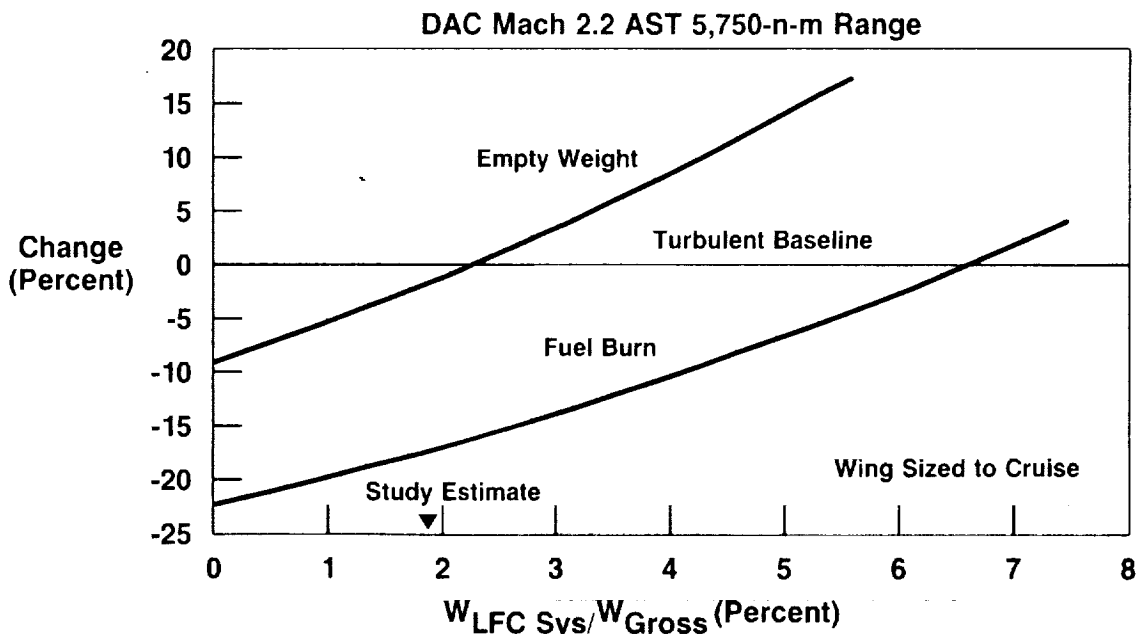


Figure 2. LFC Benefits VS. System Weight

SOME TECHNICAL RESULTS

The 1987-88 study gave several interesting results, summarized in Figure 3 below. In the subsonic case, the upper-surface drag reduction potential for laminarization is roughly twice that of the lower surface. For the Mach 2.2 case roughly 4/7 of the total drag reduction comes from the lower surface, making both surface laminarization more attractive. This is partially due to the lack of a pressure drag benefit due to reduced displacement thickness in the aft region of the wing. No such benefit exists in the supersonic case, where there is essentially no aft recovery. However, this presents an opportunity to laminarize a larger wing area fraction, and to reduce pressure and viscous drag by exhausting the suction air at low speed in a region of closure, thickening the trailing-edge boundary layer. The large chords and high sweeps of typical supersonic wings rule out the use of pressure gradients for stabilization, invalidating the HLFC concept.

The Tollmien-Schlichting mechanism of laminar boundary layer instability is known to be significantly weakened at supersonic speeds (ref. 3), while the attachment line and crossflow mechanisms are strengthened by the high leading edge sweep. These latter mechanisms were found to dominate, accounting for nearly all of the suction required. With careful aerodynamic design, particularly in the leading edge region of the wing upper surface, suction flows much lower than those of the study are possible. On the wing lower surface, careful aerodynamic design can allow wall cooling using fuel to partially supplant suction for boundary layer stabilization. Maximum LFC benefit requires suction minimization through aerodynamic design.

Both-Surface Active Stabilization Is Required

Attachment Line and Crossflow Effects Dominate

Sensitivities:

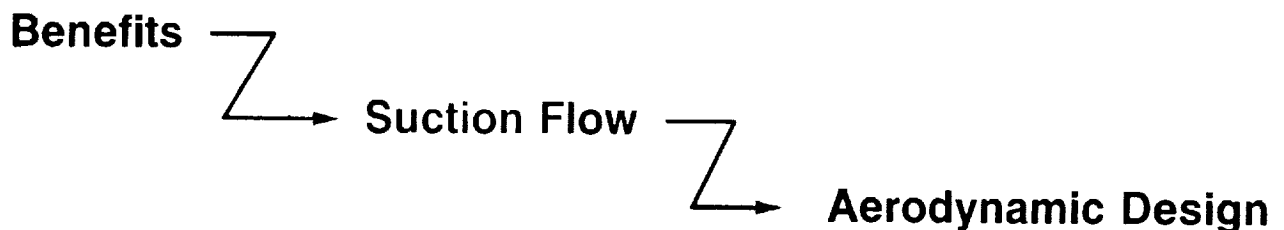


Figure 3. 1987-88 Supersonic LFC Study Technical Findings

CRITICAL APPLICATION ISSUES

As part of the 1987-88 study, a prioritized list of technical issues for supersonic LFC application was formulated. This list is shown in Figure 4 below. Heading the list is contamination protection, which is more difficult for cases where lower-surface laminarization is required, since the Kreuger-shield cannot be used. If liquids are to be used, their distribution over the wing is critical, and must match accretion patterns.

Attachment line criteria, well developed for the subsonic case (ref. 4) need to be extended into the supersonic regime. This impacts leading edge radius and suction. Step and gap criteria, also developed for the subsonic case (ref. 5,6), need extension to higher Mach numbers. This is important in integrating LFC and high lift systems. The supersonic excrescence criterion relates to environmental contamination, especially insect remains, the majority of which are supercritical subsonically. A supersonic transition database, taken in the actual flight environment, will be useful in the further development and calibration of transition prediction methods. Other potential issues exist, but are considered to have lesser impact or to be better understood.

Contamination Protection

Attachment Line Criteria

Step, Gap, and Excrescence Criteria

Supersonic Transition Database

Others

Figure 4. Technical Issues - 1987-88 Supersonic LFC Study

F-16XL-2 TEST ARTICLE

The 1987-88 study identified the F-16XL-2 as the best available testbed for supersonic LFC flight research. NASA LFC program personnel have reached the same conclusion independently. Both prototype F-16XL aircraft have been acquired for this and other HSR-related testing purposes. The LFC test program will be directed by the LFC Program Office at Langley Research Center, with the flight testing done at the Dryden Flight Research Facility.

Douglas Aircraft has been asked by the NASA LFC Program Office to help determine the feasibility of conducting meaningful supersonic LFC testing on the F-16XL-2 airplane. Part of the intent of this study was to uncover specific technical issues peculiar to using this vehicle for this type of testing. A possible LFC test article configuration is shown below in Figure 5. The left wing is gloved from the bodyside to the leading edge sweep break. The glove extends from forward of the original leading edge aft to the elevon hingeline. The crosshatched area is the laminar test region. This layout makes possible a laminar run of 21 feet. LFC suction air would pass through ducts imbedded in the external glove to an engine-bleed driven turbocompressor located in the gun bay area. The selection of a suitable turbocompressor unit will depend critically on the suction airflow, collection conditions, projected ducting and mixing losses, and local static pressure at exhaust.

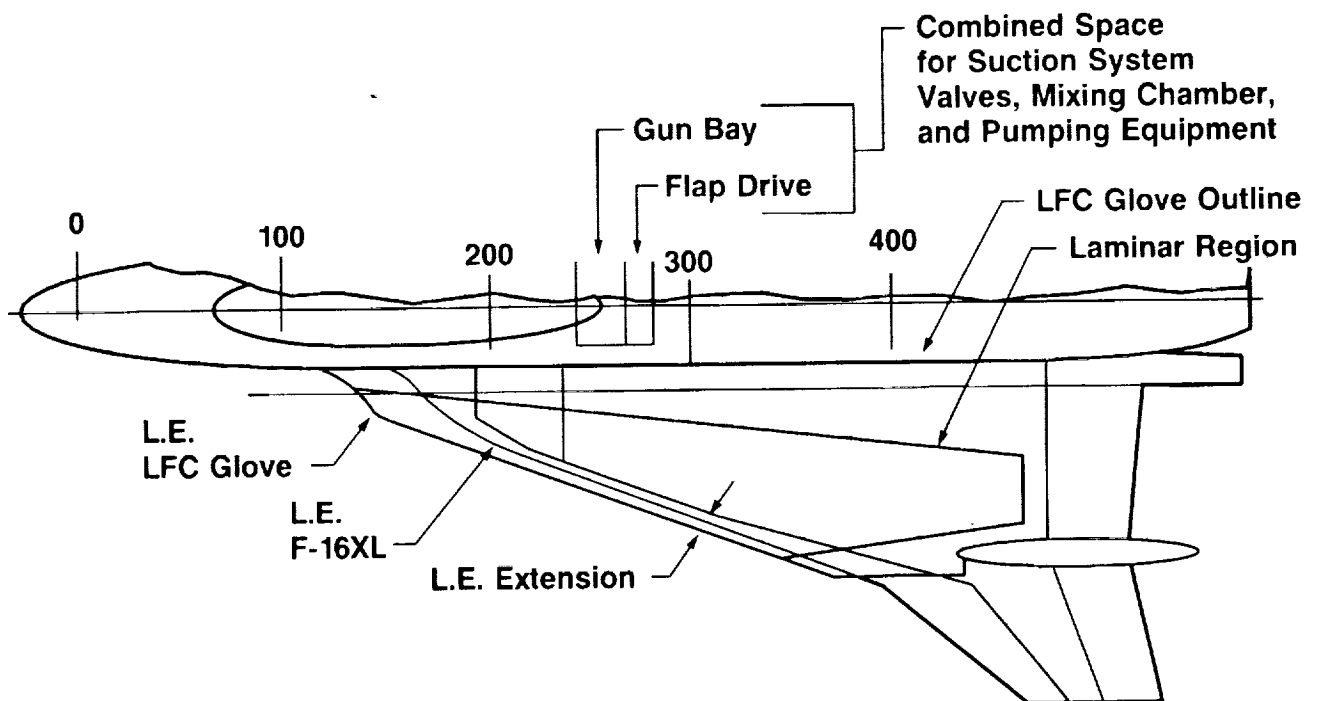


Figure 5. F-16XL-2 Study LFC Glove Planform

ESTIMATED TEST ENVELOPE

Figure 6 shows an estimated supersonic test envelope for the clean F-16XL-2 with an F110-GE-129 engine. Dashed lines of constant unit Reynolds number are shown. A study design point was selected at 1.90 Mach and 44 kft. The tropopause is indicated at 36,089 feet. In the stratosphere, where the ambient temperature is invariant with altitude, the additional pressure drag of the test article can be compensated for by taking data in descending flight without spurious thermal effects. This allows the potential of realizing the full envelope. In the troposphere, where the temperature lapse rate is nonzero, all data must be taken in level flight. Test article drag will likely limit maximum Mach numbers to something inside the envelope. The additional test article drag is not fundamental to design for LFC; it stems from large differences in design objectives between the original wing and the glove, and the necessity of providing room inside the glove for ducting.

Note the extremely wide range of unit Reynolds number available with this fighter airplane. The test article design should reflect this capability in terms of aerodynamics, temperature capability, and structural strength and stiffness in order to maximize its experimental value. Properly designed, a test article on this airplane could demonstrate laminar runs in excess of 120 million.

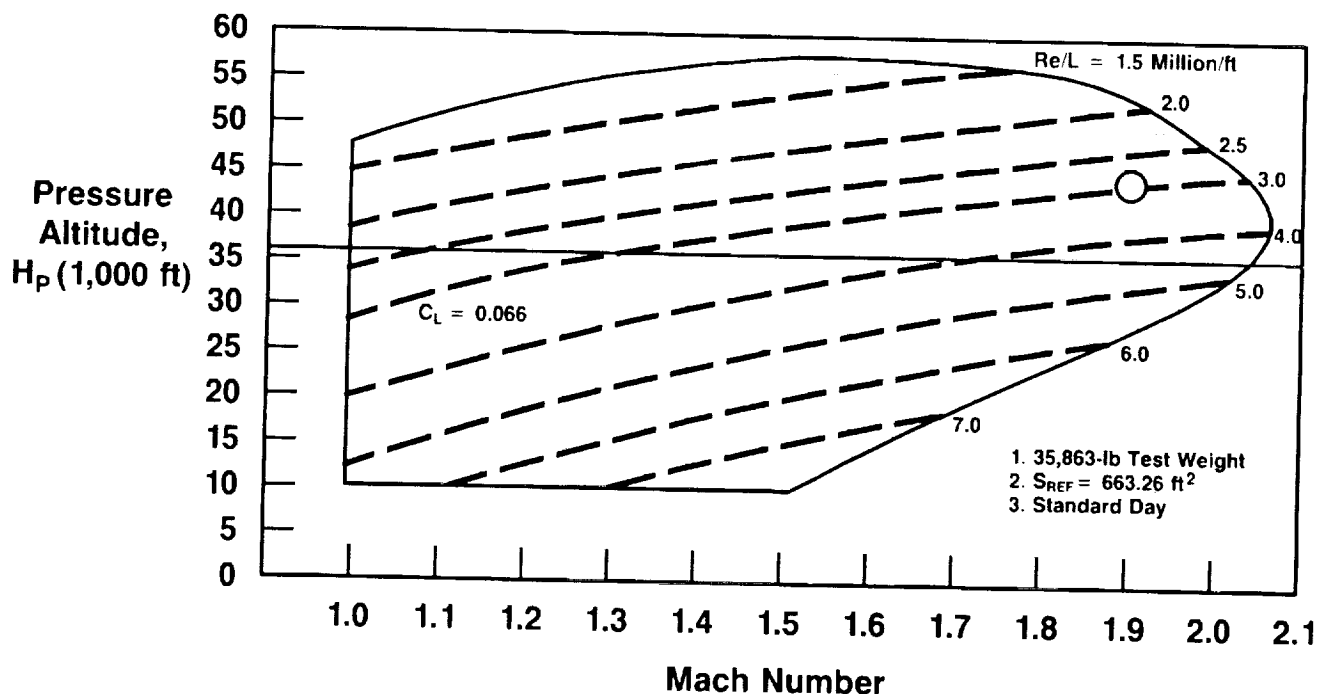


Figure 6. F-16XL-2 Estimated Supersonic Envelope

CRITICAL EXCRESCENCE HEIGHT

Figure 7 is an estimate of the effect of Mach number on critical excrescence height along a 70 degree attachment line, such as that of the F-16XL-2. Calculations were done for two values of laminar attachment line momentum-thickness Reynolds number, 100 and 240. This Reynolds number is based on attachment line external velocity and temperature. These two values have significance in the case of the incompressible, laminar attachment line. Below 100 a turbulent attachment line will relaminarize downstream. Above 240 a laminar attachment line will spontaneously transition to turbulence, due to amplification of Tollmien-Schlichting waves.

Also shown are sonic height limits: a shock will be created by any particle taller than the limit, presumably causing transition. Little relief is seen as Mach number is increased. The insect on the plot is indicative of the average height of insects deliberately collected on the JetStar Leading Edge Test Article during one flight (ref. 7). Subsonic and supersonic transports typically fly at unit Reynolds numbers between 1.5 to 2.0 million/foot, so insect impingement still must be protected against.

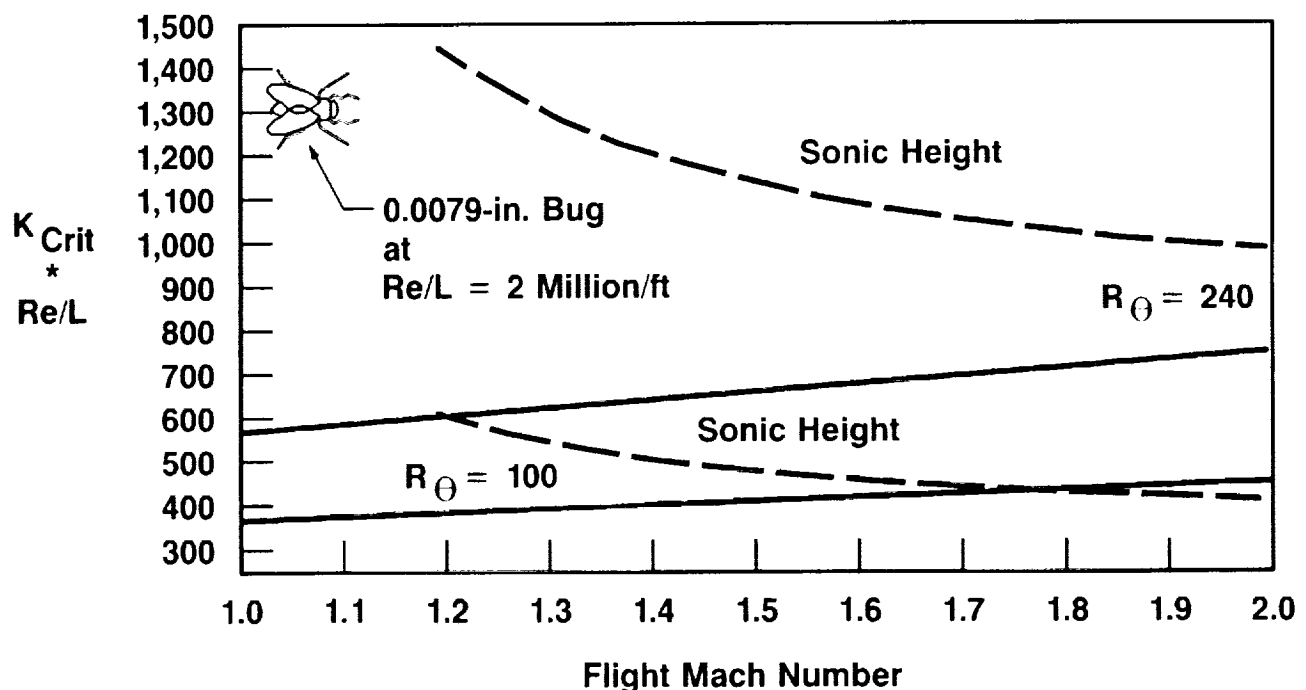


Figure 7. Estimated Critical Excrescence Height on 70 Degree Swept Attachment line

STEPS AND GAPS

Figure 8, below, is an estimate of the beneficial effect of compressibility on laminarization criteria for steps and gaps. The incompressible values were taken from the final X-21 report (ref. 5). These types of disturbances do not project upward into the boundary layer, but affect the boundary layer at the wall. The higher temperatures and viscosities at the wall create increased damping of disturbances as Mach number is increased. A single curve represents this estimated benefit. Sweeping steps and gaps beyond the local Mach angle avoids shock waves, the effect of which on transition is not known a priori. The improvement with Mach number is important if the supersonic airplane is to have leading-edge high lift devices.

Verification testing is needed. It would be valuable to know the effect of supersonic flow normal to a step or gap. The correct noise and freestream disturbance environment is critical in developing an experimental database for step and gap laminarization criteria; meaningful testing can only be done in flight. Data control calculations prior to testing are very important, so that expensive test time and fuel are not wasted.

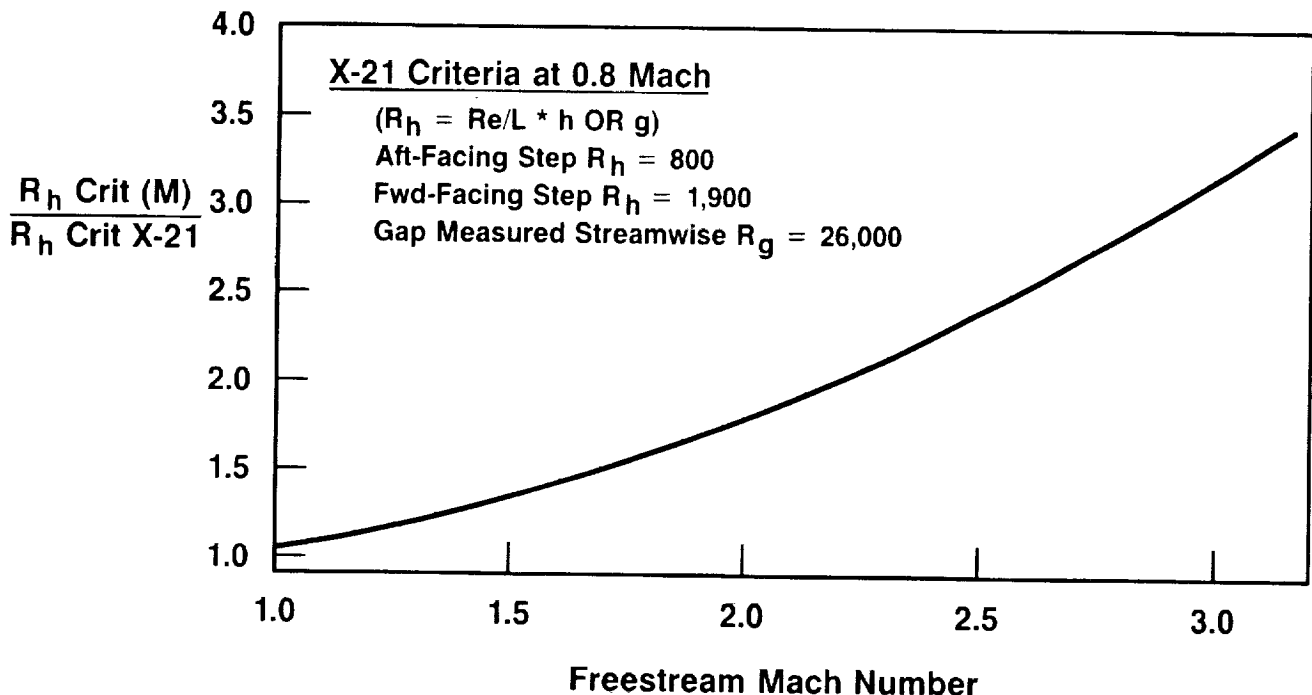


Figure 8. Estimated Mach Number Effect on Criteria for Steps and Gaps Swept Beyond Local Mach Angle

SUCTION AND HOLE SIZE LIMITS

As Mach number is increased, the increase in skin temperature causes a lowering of density and an increase of viscosity for the air entering the suction holes. Since the flow through the suction holes is laminar, these effects tend to reduce the per-hole massflux at any given pressure drop. This can be countered by reducing hole spacing and/or increasing hole size. The latter is advantageous as it also increases the hole Reynolds number, allowing more massflux through the hole. However there exists a criterion for maximum hole flow, beyond which the boundary layer is tripped (ref. 8).

A study was conducted to determine if, under likely test conditions, there would be a problem getting sufficient suction flow through the skin at the attachment line without tripping the boundary layer. The results are shown in Figure 9. For a given hole pitch-to-diameter ratio, the limiting hole diameter and corresponding largest suction coefficient was found. A large amount of latitude clearly exists. This is important since careful suction surface design will be necessary in order to allow testing at high unit Reynolds numbers.

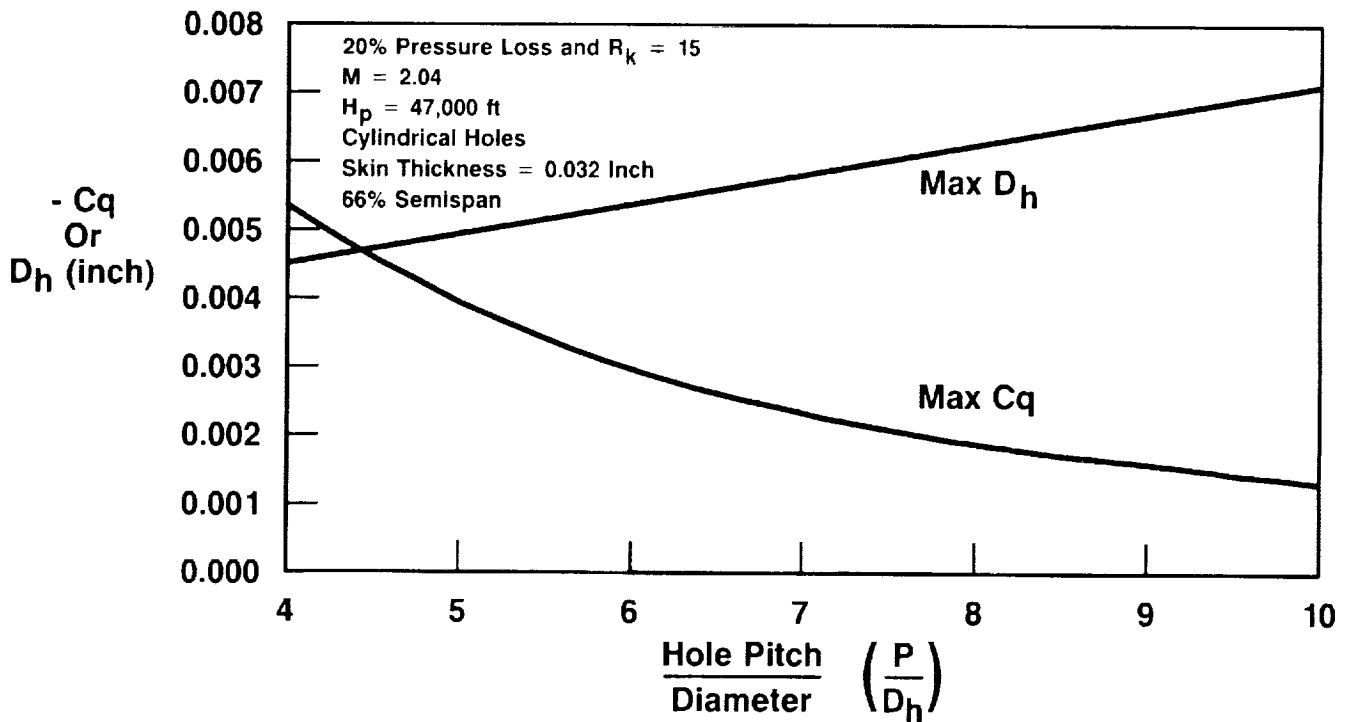


Figure 9. Estimated Maximum Suction and Perforation Size, 70 Degree Swept Leading Edge

LEADING EDGE RADIUS

The selection of leading edge radius for the test article is strongly driven by attachment line and suction criteria, and attachment line travel under off-design conditions. Laminarization considerations will set leading-edge radius and shape on a laminar flow supersonic transport as well. At the present time, attachment line criteria are only known for the subsonic case: essentially zero attachment line tangential Mach number (ref. 4). Indications are that these may not vary too much with Mach number, but sufficient experimental latitude must be allowed for in the design of the test article. Computational work at NASA Langley is underway to estimate attachment line laminarization criteria under conditions typical of the F-16XL-2 test.

Figure 10 shows the effect of suction coefficient on the leading-edge radius required to maintain attachment-line momentum-thickness Reynolds number at 100 and 240, respectively, at the study design point of 1.90 Mach, 44 kft. The compressible curves were computed using the formulation of Poll (ref. 9). A normal leading-edge radius of 0.800 inch was selected for the study.

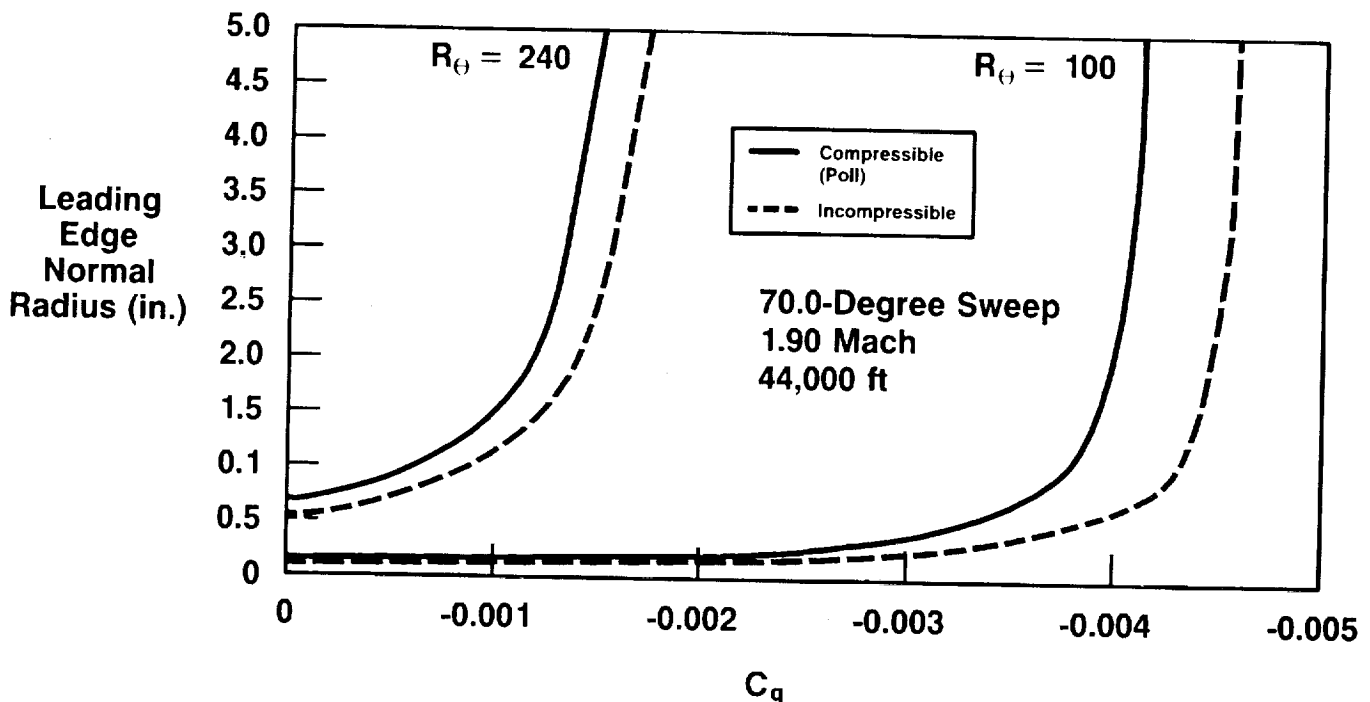


Figure 10. Attachment Line Normal Radius VS. Suction for Given R_{θ} , F-16XL-2 LFC Glove

STUDY GLOVE GEOMETRY

Figure 11 shows a candidate geometry for an LFC test article on the F-16XL-2. The glove extends forward of the original leading edge a nominal 4.00 inches in the normal direction, and has a minimum vertical clearance of 1.00 inches. The leading edge sweep of 70 degrees is retained. In order to create the kind of pressure distribution required for suction flow minimization at the design point it was necessary to extend the glove inboard to the bodyside, especially in the leading edge region. In the bodyside region the glove leading edge sweep is decreased to 30 degrees and the radius decreased to near zero to act as a turbulence diverter. This inboard part of the glove nullifies geometrical features of the original wing which were found to contribute substantially to the extended region of favorable gradient found in the leading edge region. The glove extends aft to the elevon hingeline. The convex region leading to glove aft termination causes an accelerating pressure field in this area, but this was intentionally located underneath the canopy closure shock at the design point, so its effect is minimized. At lower Mach numbers the canopy closure shock unsweeps, moving forward and potentially limiting achievable laminar run. A fuselage fairing designed to remove or block the canopy closure shock would be useful in allowing a wider range of useful test conditions. Lower Mach numbers are important since high unit Reynolds number conditions are only achievable at lower altitudes, where maximum speeds are lower.

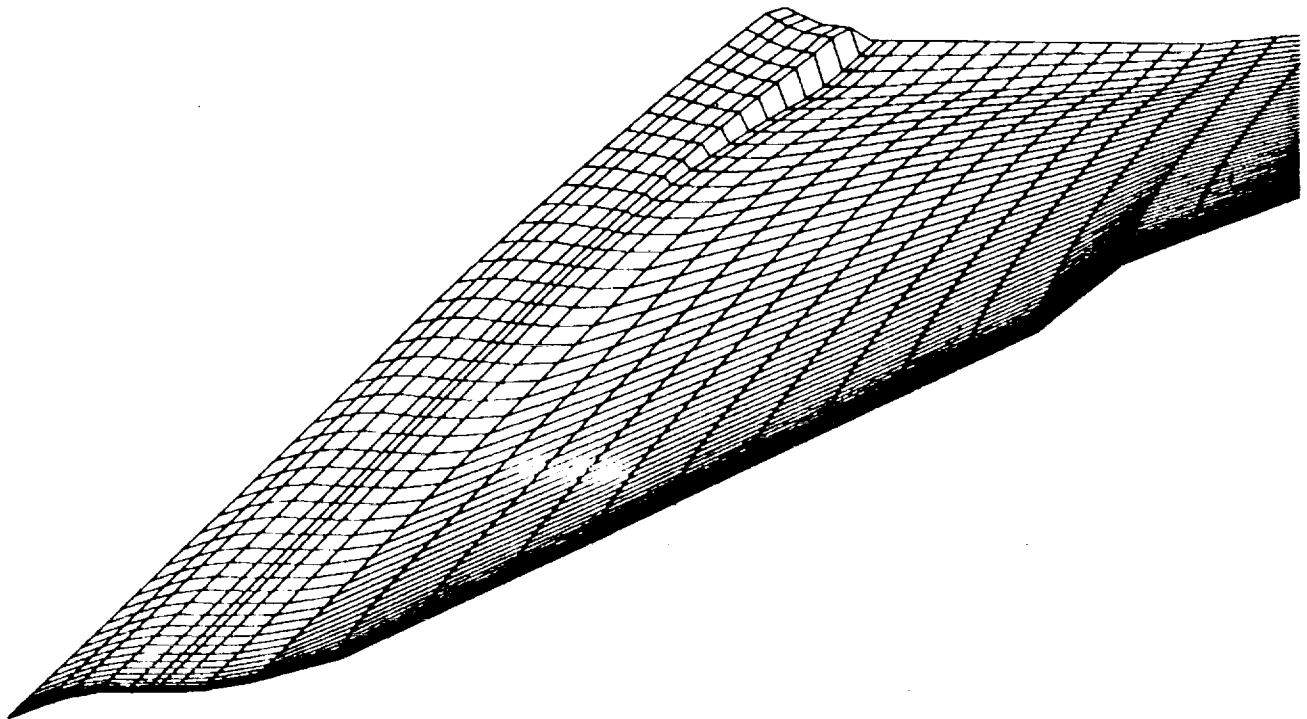


Figure 11. F-16XL-2 Study LFC Suction Test Article

COMPUTED PRESSURE DISTRIBUTION

Figure 12 compares FLO-58 - computed pressure distributions of the original wing and the study glove at the study design point of 1.90 Mach, 44 kft. The values of C_p are much smaller than one is accustomed to seeing transonically. Note the extensive region of accelerating pressure gradient on the original wing. This is very unfavorable for laminar flow, since the resulting cross-stream pressure gradients give rise to crossflow instability, which takes considerable suction to suppress. Note the considerable improvement achieved by the glove. Further improvements are possible through design refinement. The canopy closure shock is visible as a region of compression in the original pressure distribution. Although the shock is relatively weak, its static pressure rise is of the same order of the wing upper surface C_p . This is due to the low lift coefficient at the glove design point. The degree to which it is spread out chordwise in the Euler solution is probably a creature of the grid density, which is locally low so that computational points could be bunched in the leading edge region. Eliminating the shock or moving it aft via a fuselage fairing would enable demonstration of very high Reynolds number laminar runs at the lower Mach, high unit Reynolds number test points.

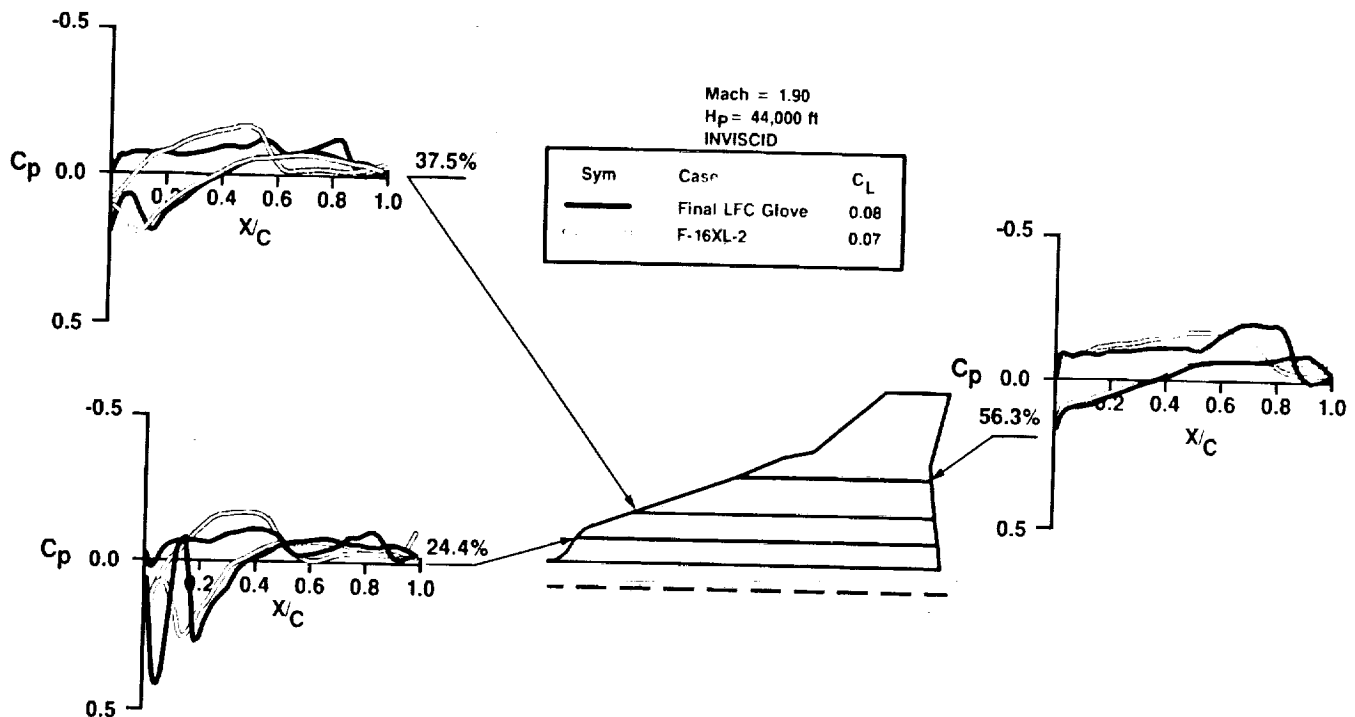


Figure 12. FLO-58 - Computed LFC Glove Chordwise C_p Distributions in Fuselage Presence

STATIONARY CROSSFLOW

A cursory analysis of stationary crossflow stability was conducted at the design point using the MARIA code (ref. 10). This code computes and integrates the growth of stationary crossflow vortices only, utilizing an approximate method involving table lookups. Experience has shown this code to be conservative in supersonic cases, but does a good job of identifying the wavelengths of the most amplified waves and giving trends. One question of interest in the design of the test article is whether or not it will be possible to distinguish between attachment line and crossflow effects. Figure 13 indicates that even with no suction, transition by crossflow is not predicted until 2 percent chord or later on the study glove. This strongly suggests that the effects will be separable experimentally if transition instrumentation is properly located.

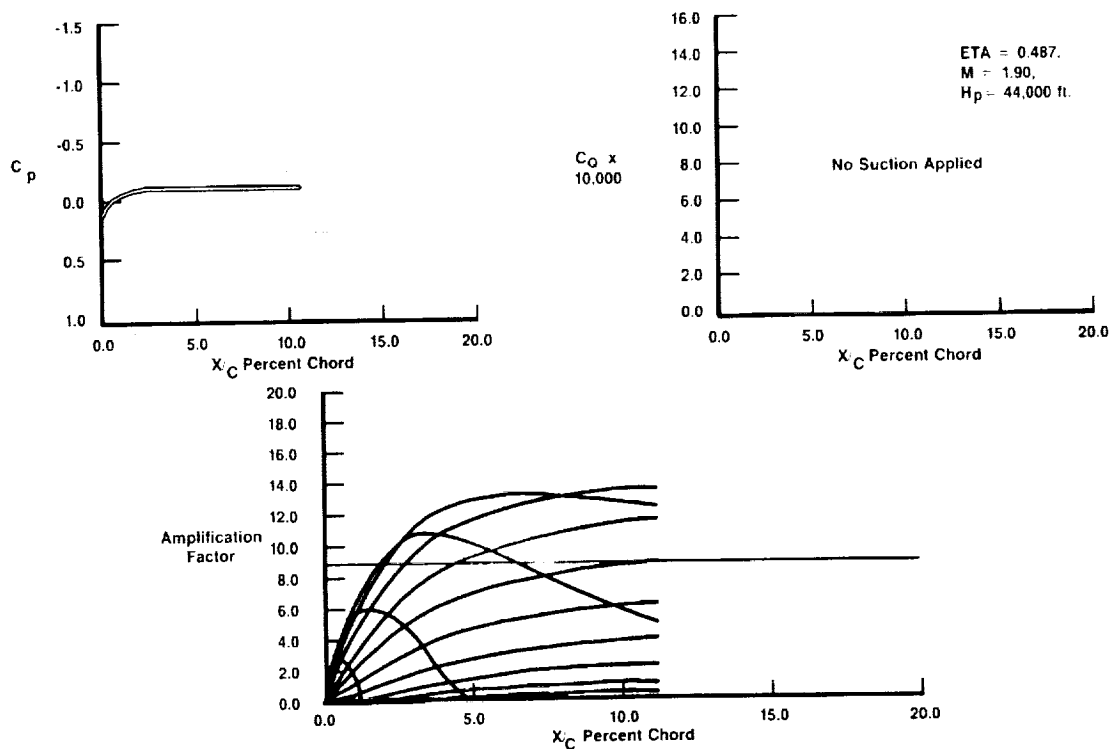


Figure 13. Stationary Crossflow Stability Analysis
F-16XL-2 Study Glove

CONCLUSIONS

Figure 14 presents the major conclusions of the F-16XL-2 LFC Test Article Study. The study has identified no major roadblocks to a successful experimental program. A carefully designed test article, used in a well designed test program keyed to agreed upon major experimental objectives could provide a wealth of information directly applicable to HSCT laminarization at overall minimum program cost. It is important that the test article design reflect technological as well as demonstration goals.

Analysis Indicates Feasibility

Very Large Re/L Range Possible

**Attachment Line and Crossflow Effects
Are Separable**

**Meaningful Test Program Will Require
Careful Design**

- **Glove Shape**
- **Perforated Surface**
- **Structure**
- **Flying Qualities**
- **Instrumentation**
- **Test Program**

Figure 14. F-16XL-2 LFC Study Conclusions

TECHNOLOGY INTEGRATION

In order for LFC technology to earn its way onto the HSCT, it must be demonstrated to be feasible, to reliably produce the expected benefit, and integrate well with other technologies, a list of which is given in Figure 15, below. The F-16XL-2 Flight Test program is expected to establish feasibility and demonstrate the low suction levels required. Follow-on activities should focus on technology integration issues. Attention should be paid to technology combinations having possible synergisms. For example, incorporation of nonlinear effects into the aerodynamic design process is expected to result in optimized wings having lower sweep, blunter leading edges, and upper-surface pressure distributions essentially compatible with LFC requirements (ref. 12). Consistent with this design direction, alternative approaches to achieving high levels of leading-edge thrust at low speeds have been demonstrated which do not require a movable leading edge, and do not rely on suction for boundary layer separation control (ref. 13).

The contamination avoidance issue must be given serious attention. Although it is always possible in principle to design a liquid system that will work, various alternatives (ref. 14) should be investigated. The F-16XL-2 flight test should be used to document accretion patterns for future studies.

After design studies and testing have defined the best integration of technologies, bringing technical risk to acceptable levels may require in-flight demonstration.

Laminar Flow Control

Contamination Avoidance

Nonlinear High-Speed Design

Low-Speed System

Structures and Materials

Sonic Boom

Figure 15. HSCT Wing Technologies

REFERENCES

1. Powell, A.G., Agrawal, S., and Lacey, T.R.: "Feasibility and Benefits of Laminar Flow Control on Supersonic Cruise Airplanes", NASA CR-181817, July 1989.
2. Fischer, M.C.: "Spreading of a Turbulent Disturbance", AIAA Journal, Vol. 10, No. 7, pp. 957-959, July 1972.
3. Lekoudis, S.G.: "Stability of Three-Dimensional Compressible Boundary Layers Over Wings With Suction", AIAA paper No. 79-0265, January 1979.
4. Bacon, J.W. Jr. and Pfenninger, W.: "Transition Experiments at the Front Attachment Line of a 45-degree Swept Wing with a Blunt Leading Edge", Technical Report AFFDL-TR-67-33, June 1967.
5. Northrop Corp., Norair Division: "Final Report on LFC Aircraft Design Data - Laminar Flow Control Demonstration Program", Report NOR-67-136, August 1967.
6. Holmes, B.J., Obara, C.J., Martin, G.L., and Domack, C.S.: "Manufacturing Tolerances for Natural Laminar Flow Airframe Surfaces", SAE Paper 850863, April 1985.
7. Maddalon, D.V., Fisher, D.F., Jennett, L.A., and Fischer, M.C.: "Simulated Airline Service Experience with Laminar-Flow Control Leading-edge Systems", NASA CP-2487, Part 1, pp. 195-218, March 1987.
8. Goldsmith, J: "Critical Laminar Suction Into an Isolated Hole or a Single Row of Holes", Northrop Report NAI-57-529, February 1957.
9. Poll, D.I.A.: "Leading Edge Transition on Swept Wings", AGARD-CP-224, pp. 21-1 through 21-11, May 1977.
10. Dagenhart, J.R.: "Amplified Crossflow Disturbances in the Laminar Boundary Layer with Suction", NASA TP-1902, November 1981.
11. Collier, F.S. Jr.: "Curvature Effects on the Stability of Three-Dimensional Laminar Boundary Layers", Ph.D. dissertation, Virginia Polytechnic Institute and State University, May 1988.
12. Mason, W.H. and DaForno, G.: "Opportunities for Supersonic Performance Gains Through Non-Linear Aerodynamics", AIAA Paper 79-1527, July 1979.

13. Rao, D.M. and Johnson, T.D.: "Investigation of Delta Wing Leading-Edge Devices", AIAA J. Aircraft, Vol. 18, No. 3, pp. 161-167, March 1981.
14. Croom, C.C. and Holmes, B.J.: "Flight Evaluation of an Insect Contamination Protection System for Laminar Flow Wings", SAE Paper 850860, April 1985.

Session XIII. Supersonic Laminar Flow Control

omit

Status of the F-16XL Supersonic Laminar Flow Control Numerical Design Validation

Mike George, Rockwell International; and Marta Bohn-Meyer and Bianca Anderson, NASA Ames-Dryden Flight Research Facility

THIS PAGE INTENTIONALLY BLANK

Status of F16XL SSLFC Numerical Design Validation

Mike George
Rockwell International

Marta Bohn-Meyer
Dryden Flight Research Center

Bianca Anderson
Dryden Research Center



N94- 33527

510-02
11985

High-Speed Research Workshop
May 14-16, 1991
Williamsburg, Virginia

MGE-910506-5675

ORIGINAL PAGE IS
OF POOR QUALITY

PRECEDING PAGE BLANK NOT FILMED

The F-16XL SSLFC Program is a joint ongoing effort involving Rockwell's North American Aircraft Division, NASA Ames-Dryden Flight Research Facility, and NASA Langley Research Center. The objectives of the program are to demonstrate that laminar flow can be obtained on a highly swept wing at supersonic speeds, validate the capabilities of a numerical methodology designed to predict boundary layer transition and validate the capabilities of the methodology in the design of active and passive LFC concepts.

The F-16XL SSLFC Program consists of the design, fabrication, installation, and flight test of an active laminar flow control glove for the F-16XL. The glove design emphasized the active (suction) control of attachment line and crossflow boundary condition instabilities. The glove design envelop was constrained by the existing geometry, safety of flight considerations, and space requirements for the suction mechanism. The leading edge extension of the glove was limited to 10 inches for consideration of asymmetric flying qualities and the glove height above the existing surface restricted to two inches. The active (suction) portion of the wing extends to nominally 25% chord. The glove was constructed of a micro-perforated titanium sheet (hole diameter = .025 inches, spacing ratio = 1/8, sheet thickness = .0025 inches). The glove design includes 22 separate chambers to allow suction variation in the chordwise direction. The F-16XL SSLFC program is currently in the flight test phase.

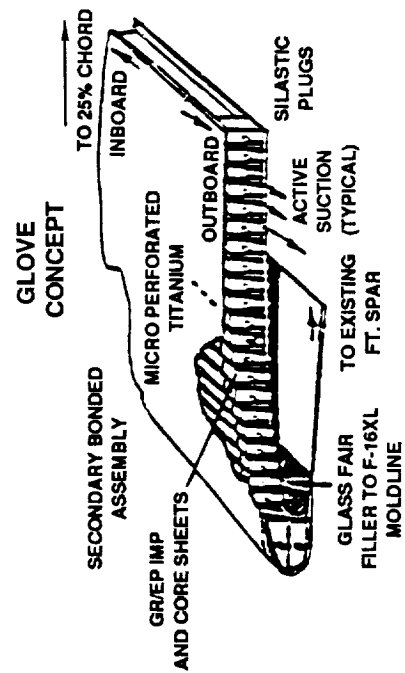
SUPERSONIC LAMINAR FLOW CONTROL EXPERIMENT

- Objective

- Demonstrate supersonic laminar flow for highly swept planforms

- Approach

- Validate design methodology through flight demonstration of an F-16XL at $M = 1.6$, 44K feet



COOPERATIVE EFFORT

- Rockwell International North American Aircraft
- NASA Ames-Dryden Flight Research Facility
- NASA Langley Research Center

MGE-910501-5663

The presentation will briefly address the design of the active glove and the glove fabrication and will emphasize the Computational Fluid Dynamics (CFD) methodology, ongoing flight test program, and tentative future plans for the program.

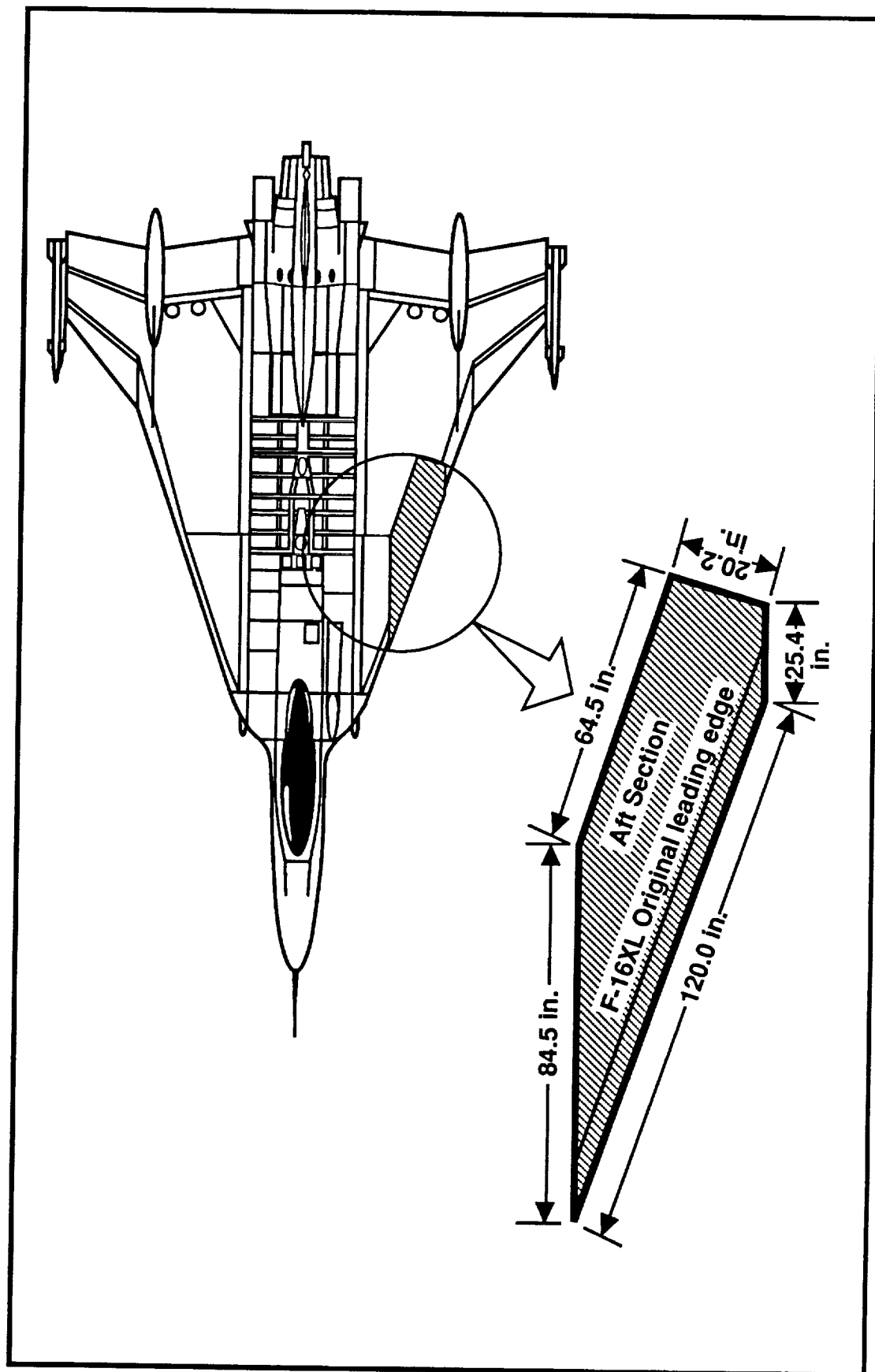
PRESENTATION OUTLINE

- LFC design for the F-16XL
- F-16XL glove fabrication and installation
- CFD approach
- Flight test results
- Future plans

The active glove was mounted on the inboard of the left wing of the F-16XL vehicle where the leading-edge sweep is 700 (the sweep of the outboard portion of the wing is 500). The active glove begins just aft of the leading edge on the lower surface, wraps around the leading edge and continues to nominally 25 % chord of the original wing. The flight design condition for the F-16XL SSLFC program was Mach number = 1.6, angle-of-attack = 20, and an altitude of 44,000 feet.

F-16XL SSLFC GLOVE

DESIGN CONDITION: MACH = 1.6, ALPHA = 2 DEG., ALT = 44K FT



MGE-910502-5680

The glove was designed with emphasis in avoiding attachment line transition and cross-flow transition. To achieve laminar flow at the design condition a smooth favorable pressure gradient augmented by suction was designed.

The design criterion for avoiding leading edge attachment line contamination was to keep the compressible momentum thickness Reynolds number at the attachment line below a value of 114. Based on empirical data the attachment line momentum thickness Reynolds number below which disturbances decay, was taken to be 114* and at values of 265* natural transition was assumed to occur. Between these limits the boundary layer state is affected by propagation of turbulence from the fuselage and inboard wing and the critical Reynolds number is configuration specific.

The criterion for control of crossflow instabilities was to keep the amplification factor below 6. An amplification factor of 6 is a conservative value (10 is commonly used). The amplification factor is a measure of the relative growth in amplitude of a disturbance seeded in the boundary layer.

Another consideration in the design was to minimize the suction hole velocity to avoid any disturbances due to the suction.

A series of codes including two-dimensional and three-dimensional Euler codes, boundary layer programs, and stability codes were used in an iterative design procedure to arrive at the final glove shape and suction distribution.

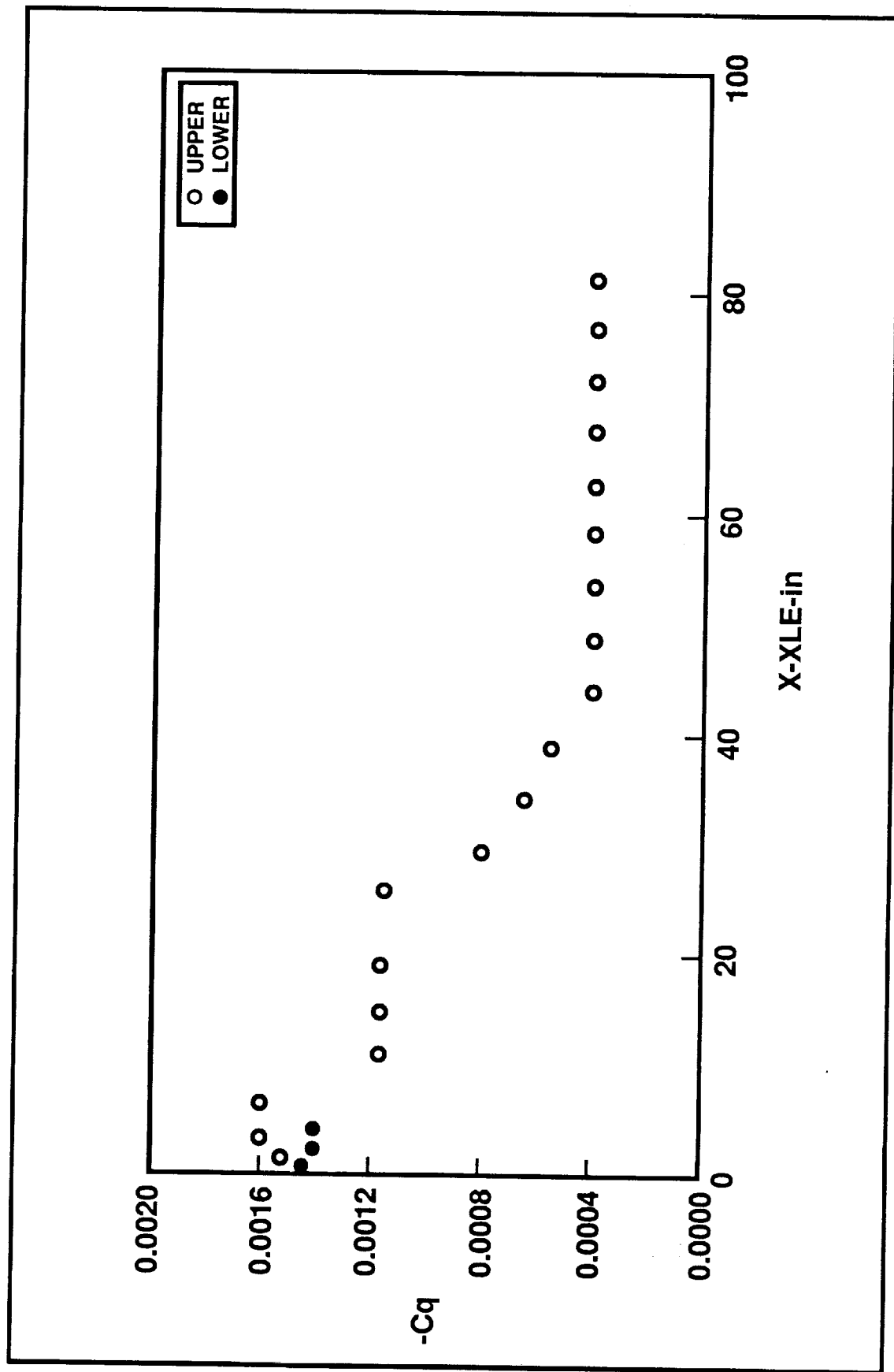
*Poll, D. I. A., "Transition Description and Prediction in Three-Dimensional Flows," AGARD Report R-709, Paper 5 March 1984.

GLOVE DESIGN

- Design Criteria
 - Attachment line
 - Compressible $Re_{\theta} < 114$
 - Crossflow instabilities
 - Amplification factor $N < 6$
 - Minimize suction hole velocity
- Methodology
 - 2D Euler (yawed wing)
 - 3D Euler (space marching)
 - Boundary layer programs
 - Stability analysis

Restrictions on the minimum allowable bending radius (.25 inches) of the titanium sheet required suction coefficients of between -.001 and -.002 in the leading edge region to meet the momentum thickness Reynolds number criteria. The suction strength in the chordwise direction decreased meeting requirements of amplification factors less than 6 for crossflow instabilities. The variation in chordwise suction distributions was achieved through the twenty-two chordwise suction flutes.

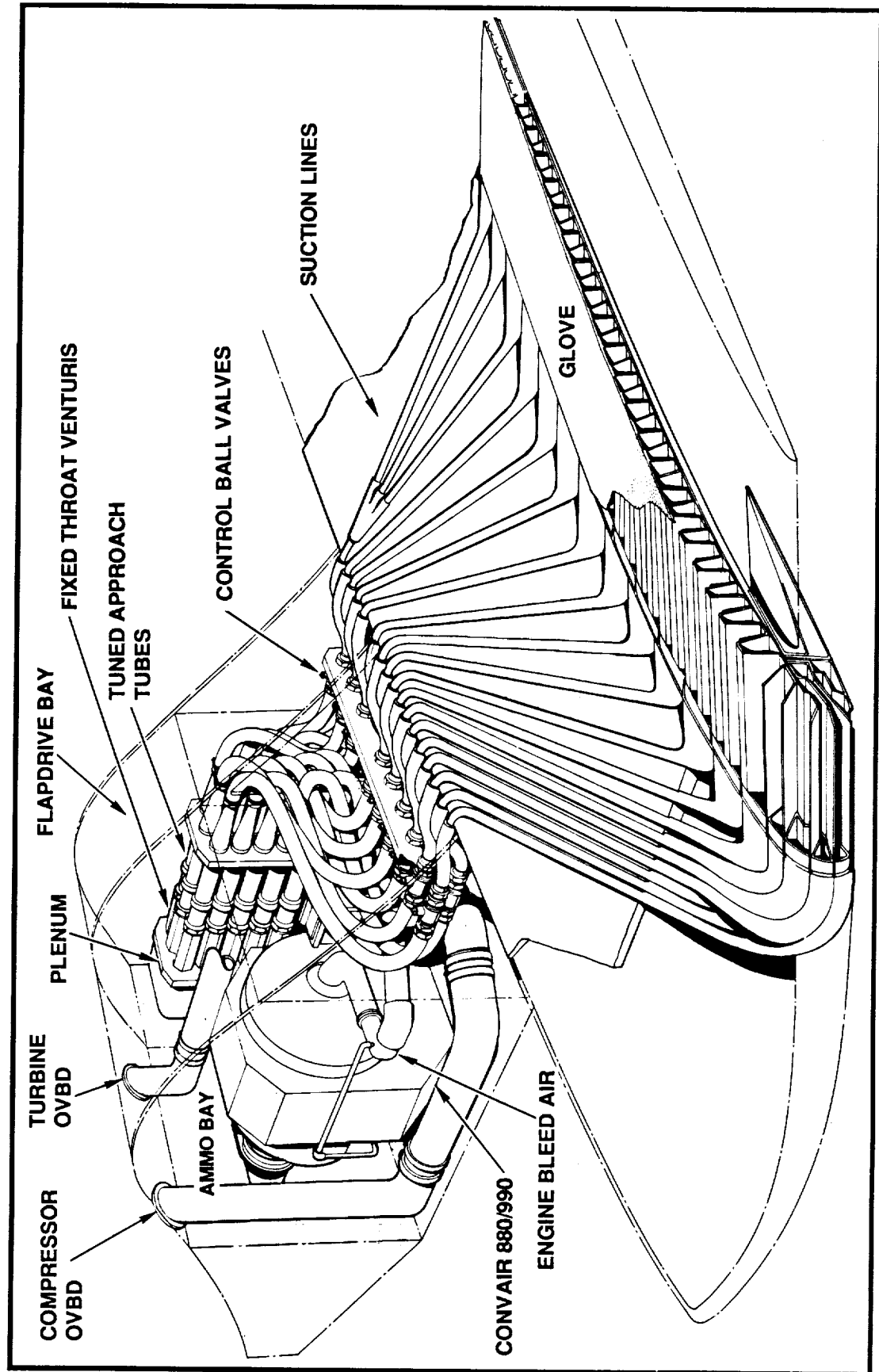
SUCTION DISTRIBUTION AT MIDSPAN



MGE-910502-5670

The suction subsystem was designed around a Convair 880 Auxiliary Power Unit (APU) compressor that was used as the suction pump. The pump was mounted in the ammunition bay behind the canopy. 17 fixed throat venturils were connected between the pump and the chordwise flutes in the active glove. The venturils were designed to achieve the design suction distribution in a choked mode.

SUCTION SUBSYSTEM DESIGN



DS-91-5660

The numerical approach developed and currently being validated as part of the ongoing F-16XL SSLFC program was based on the coupling of a Navier-Stokes code and a linear compressible boundary-layer stability method.

The Navier-Stokes method used was the Unified Solution Algorithm (USA) code developed by Rockwell's Science Center*. The USA code is based on a finite-volume implementation of an upwind Total Variation Diminishing (TVD) formulation embedded in a multi-block structured-grid bookkeeping framework.

The Compressible Stability Analysis (COSAL) code developed by Malik** was used for temporal theory applications to calculate an amplification factor. The application of the stability theory to transition prediction consists of the computation of laminar profiles with superimposed small perturbations and the resultant integration of the disturbance amplitude growth rates. Transition occurs when the amplification factor reaches a prescribed value N. Stability theory does not provide the absolute amplification level, so the N-factor is extracted from experimental correlation.

The USA and COSAL codes were coupled in such a way to enable stability calculations to be made for arbitrary three-dimensional flows. The COSAL interface was modified to replace the essentially two-dimensional profile definition with a general three-dimensional search and interpolation procedure. The analysis follows the streamline if no instability exists and the direction of the group velocity vector if an unstable mode is encountered.

The development of the computational methodology and its application to the F-16XL SSLFC program is discussed in detail in AIAA Paper 91-0188***.

* Chakravarthy, S. R., Szema, K. Y., and Haney, J. W., "Unified 'Nose-to-Tail' Computational Method for Hypersonic Vehicle Applications," AIAA Paper 88-2564, June 6-8, 1988.

** Malik, M. R., "COSAL - A Black-Box Compressible Stability Analysis code for Transition Prediction in Three-Dimensional Boundary Layers," NASA CR 165925, May 1982.

*** Woan, C. J., George, M. W., "CFD Validation of a Supersonic Laminar Flow Control Concept," AIAA Paper 91-0188, January 7-10, 1991.

COMPUTATIONAL METHODOLOGY

CFD ANALYSIS (USA)

- Navier-Stokes equations
- Finite volume formulation
- 3rd order accurate TVD scheme
- Roe's flux-difference splitting

Stability Analysis (COSAL)

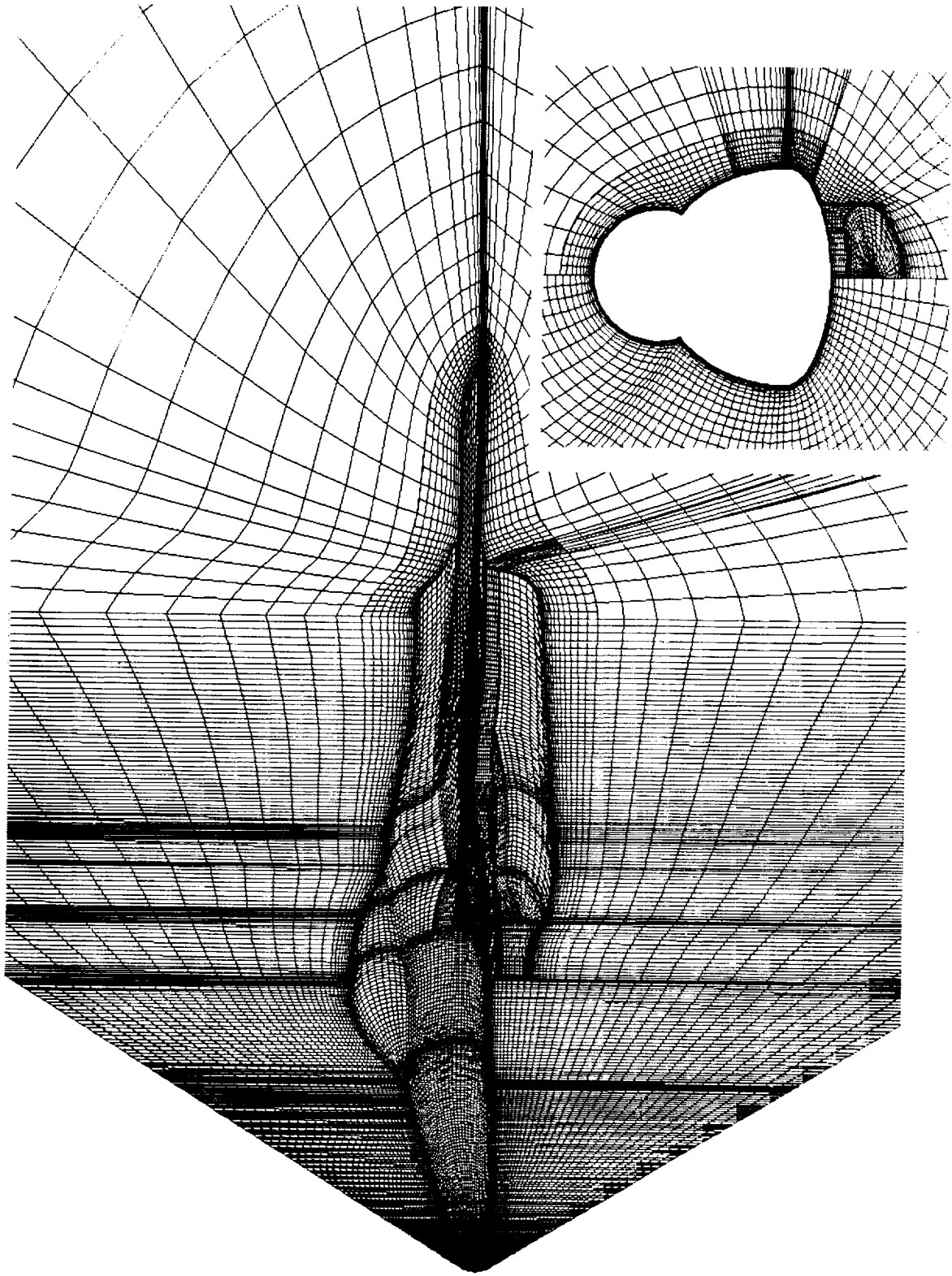
- 3D linear compressible BL stability theory
- Temporal theory
- Computation of amplification factor N
- Design for swept tapered wing

USA/COSAL Coupling

- Generalize 3D input BL profiles
 - Along the external streamline if no instability exists
 - Along the group velocity vector direction if unstable mode is encountered

The grid topology used to numerically represent the F-16XL SSLFC consisted of four major blocks in the streamwise direction. Each major streamwise block was further divided into sub-blocks resulting in 21 blocks with approximately one million grid points. To capture the complexity of the geometry, a non-aligned block grid approach was used and applied at the interface of blocks 3 and 4. The non-aligned block interface was located upstream of the inlet plane to avoid strong gradients.

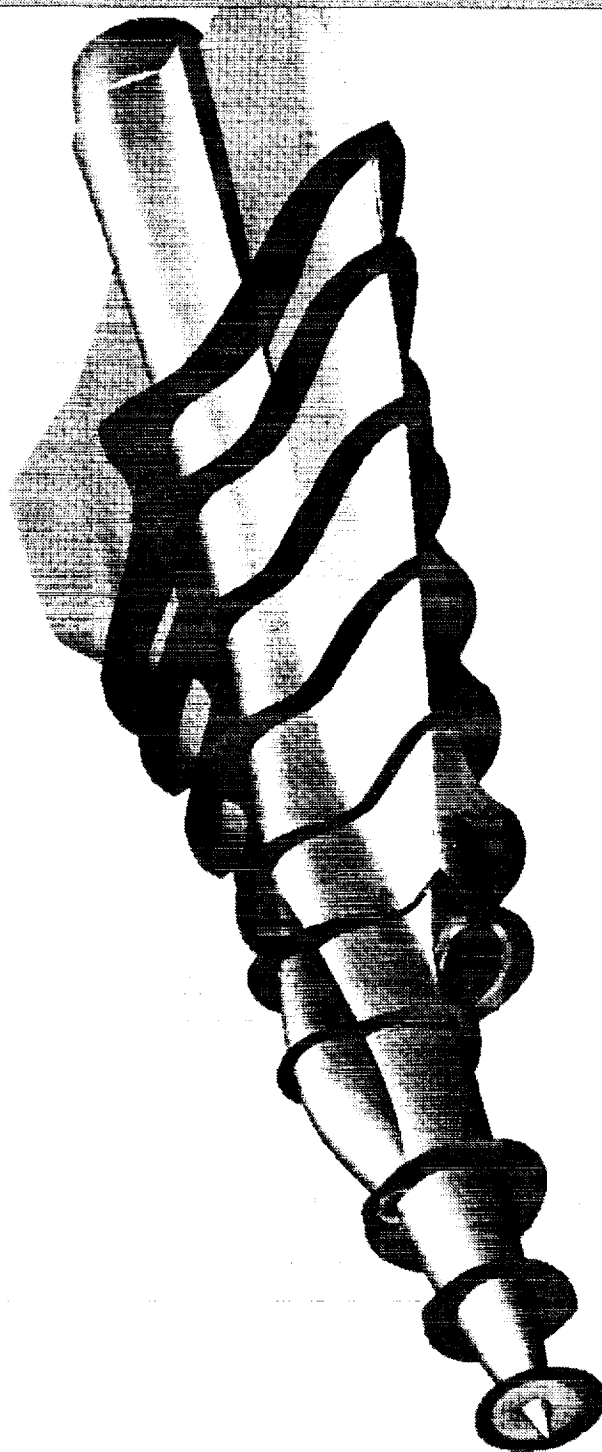
F-16XL SSLFC GRID TOPOLOGY



For the LFC calculations it was important to capture the effects of the wing, body, canopy, inlet, diverter, and environmental control inlet (ECI). Of specific concern were the shock systems emanating from the fore and aft regions of the canopy and from the main and ECS inlets. To study the effect of grid density two grids were utilized, with approximately 750,000 and 1,000,000 grid points. The larger grid had ten additional nodes in the boundary layer.

F-16XL Navier Stokes Cp Contours

At Mach = 1.6 and Alpha = 2 deg.

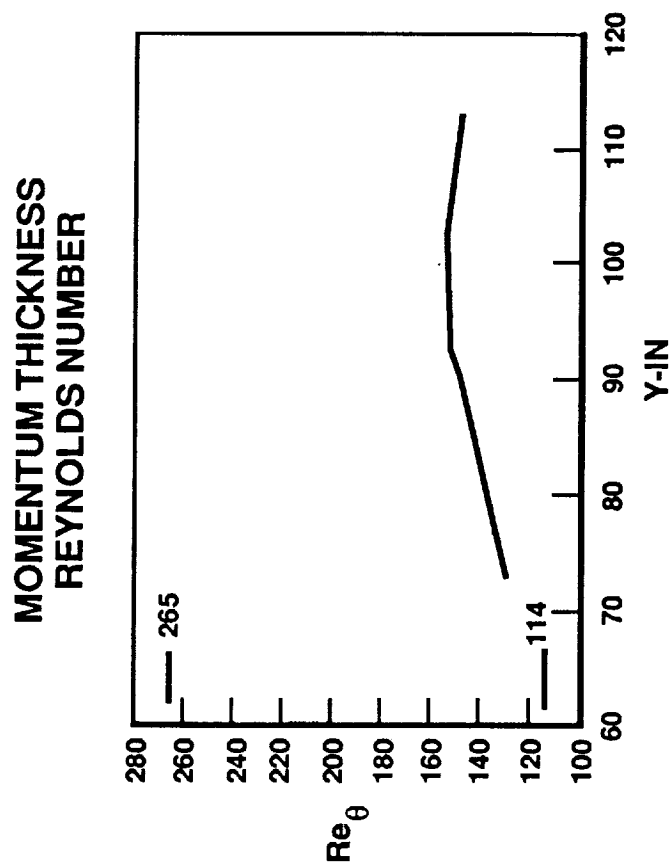


Results of the Navier-Stokes code indicated that the attachment line location and momentum thickness Reynolds number at the attachment line deviated from the design goals. The desired location for the attachment line was the nose of the wing sections. The nose is the location of maximum curvature resulting in minimum momentum thickness Reynolds number. The attachment line at the inboard of the active glove was located on the nose and proceeded to move onto the lower surface as a function of spanwise direction and then back onto the upper surface at the outboard wing section of the active glove. The deviation of the attachment line from the nose of the wing sections resulted in an increasing momentum thickness Reynolds number in the spanwise direction. The resultant values of the momentum thickness Reynolds number are slightly over the design goal of 114 but are well below the natural transition value of 265.

265 is the value of Reynolds number above which transition occurs due to freestream turbulence levels and 114 is the value below which turbulence or disturbances emanating from the wing-body junction would decay along the attachment line. The values of 265 and 114 are arrived from experiment and represent the limits of the band of scattered experimental data.

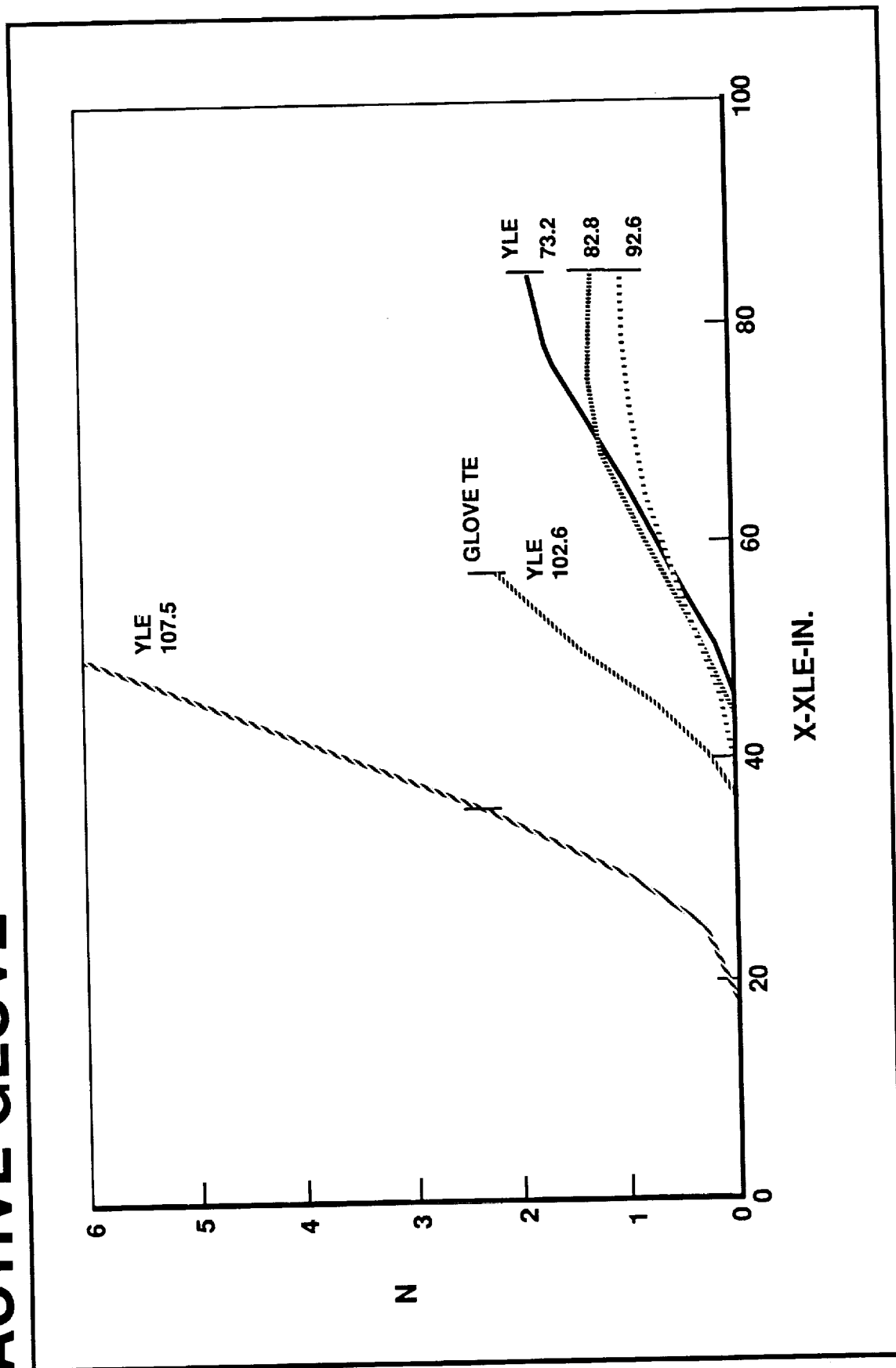
In between the values of 114 and 265, whether transition occurs or not at the attachment line will depend on the upstream disturbance levels.

ATTACHMENT LINE CHARACTERISTICS



The stability predictions resulting from the coupling of the Navier-Stokes code and the stability analysis code indicated that laminar flow would be obtained over the entire glove. The maximum amplification factor N reached on the glove was less than 3.

STABILITY PREDICTION OVER ACTIVE GLOVE



MGE-910501-5661

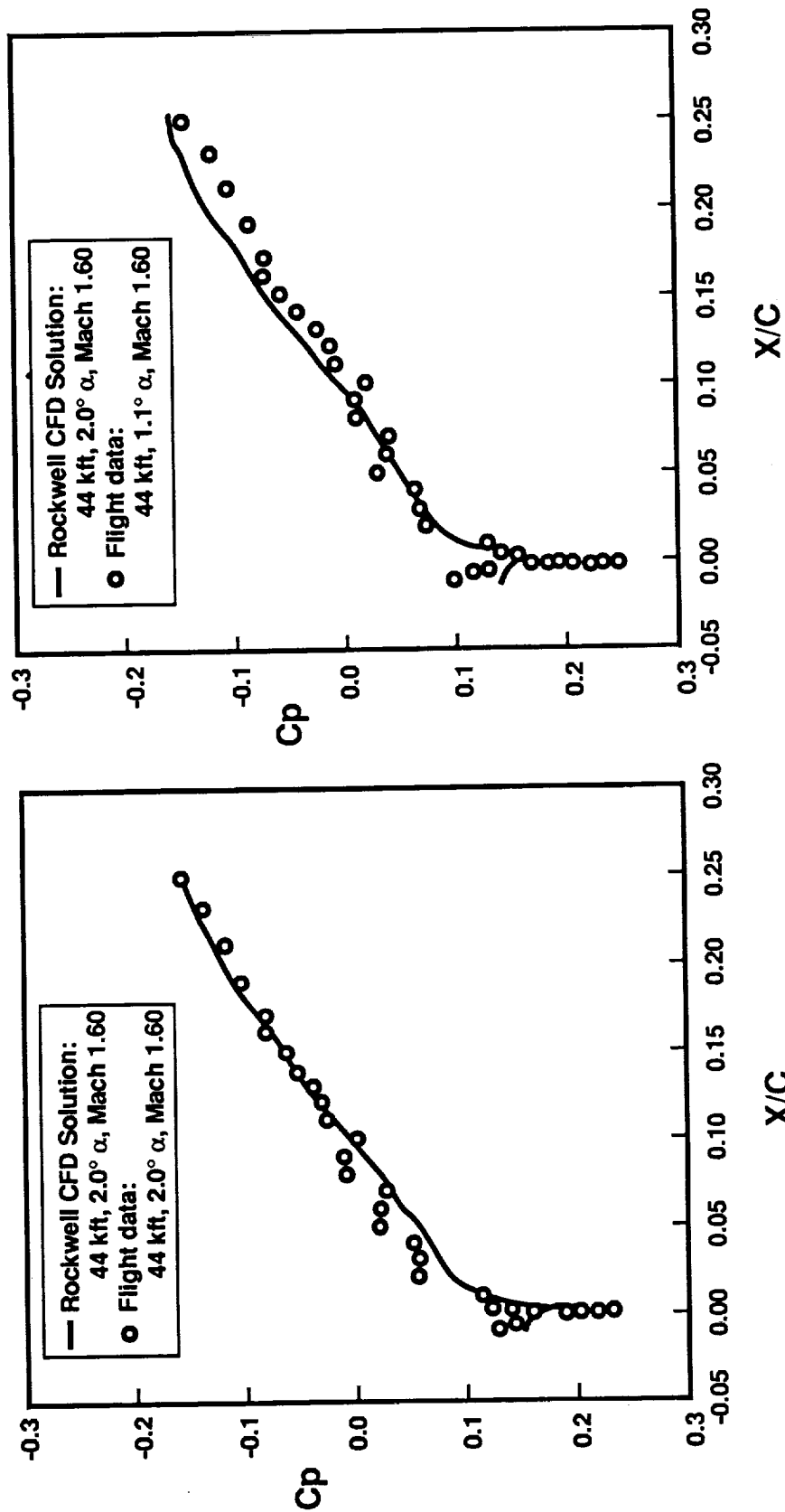
Two rows of pressure taps were placed on the F-16XL SSLFC vehicle. The rows were located at the inboard and outboard edges of the active suction glove.

The comparison of the Navier-Stokes pressure results with the flight test results indicate relatively good agreement at the inboard station. The flight test pressure results contained a series of chordwise oscillations that have not been explained to date.

SLK-DSK114-91 0430 26
Revised 05-07-91

F-16XL-SSLF EXPERIMENT CFD TO FLIGHT DATA COMPARISON

INBOARD ORIFICE ROW



MGE-910502-5659

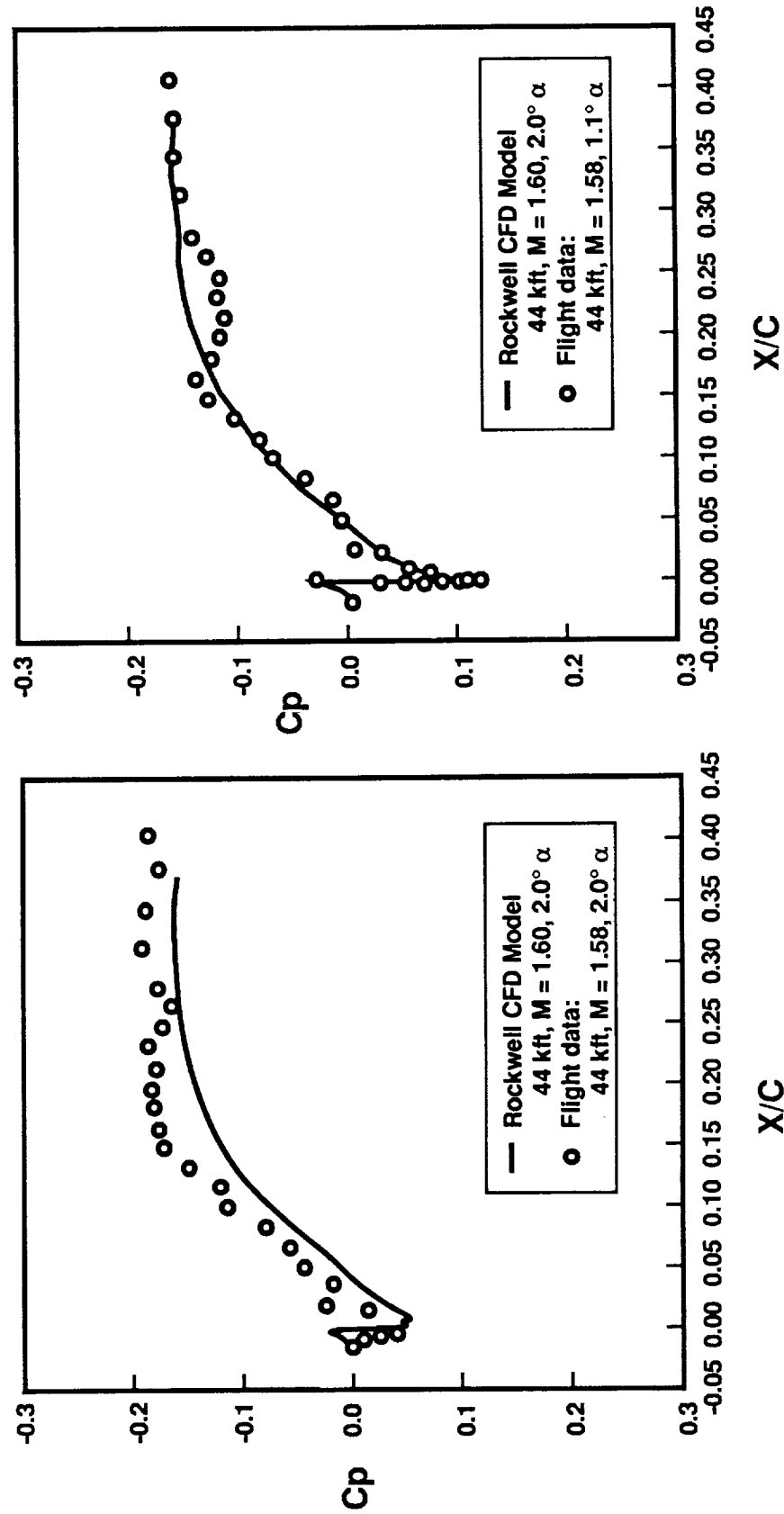
The comparison of the Navier-Stokes pressure results with the flight test results for the outboard pressure row were not as good as the inboard comparisons. The comparisons indicate a possible twist difference of approximately one degree between the numerical model and flight vehicle.

SLK-DSK114-91 0430 28
Revised 05-07-91

F-16XL-SSLF EXPERIMENT CFD TO FLIGHT

DATA COMPARISON

OUTBOARD ORIFICE ROW

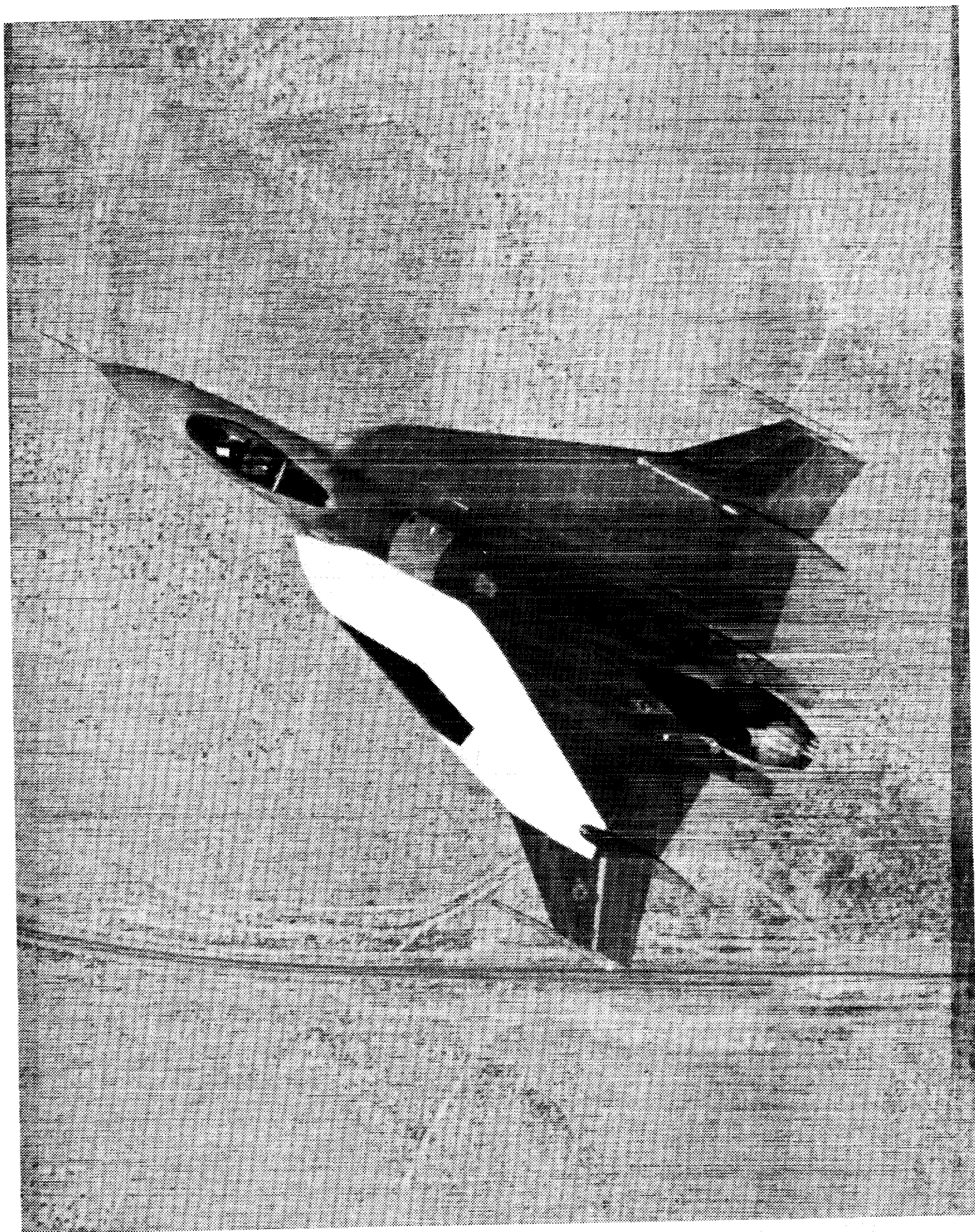


F-16XL SSLF INSTRUMENTATION LAYOUT

The left wing of F-16XL Ship 1 has been modified with a Supersonic Laminar Flow Control Glove (dark section). The edges of the active glove have been instrumented to measure surface static pressures for pressure distribution documentation. Using relocatable hot-film sensors, researchers can detect the character (laminar or turbulent) of the flow anywhere on the gloved wing surface in flight.

For initial flight tests, as many as 18 hot-film sensors were located as shown. By locating sensors along the outboard and trailing edges of the glove, researchers can determine if the entire glove is laminar at design condition. By locating sensors on the passive glove immediately inboard of the active glove, and on the active glove inboard edge, researchers can determine if the small step between the passive and active gloves has a significant effect on the amount of laminar flow detected.

The unusual angle of alignment for the hot-film sensors (approximately 30 degrees to the streamline) was determined to be necessary to prevent disturbances shedding from a forward sensor, from affecting the measurements of the sensors behind it.



ORIGINAL PAGE
BLACK AND WHITE PHOTOGRAPH

1871

THIS PAGE INTENTIONALLY BLANK

TEST MATRIX

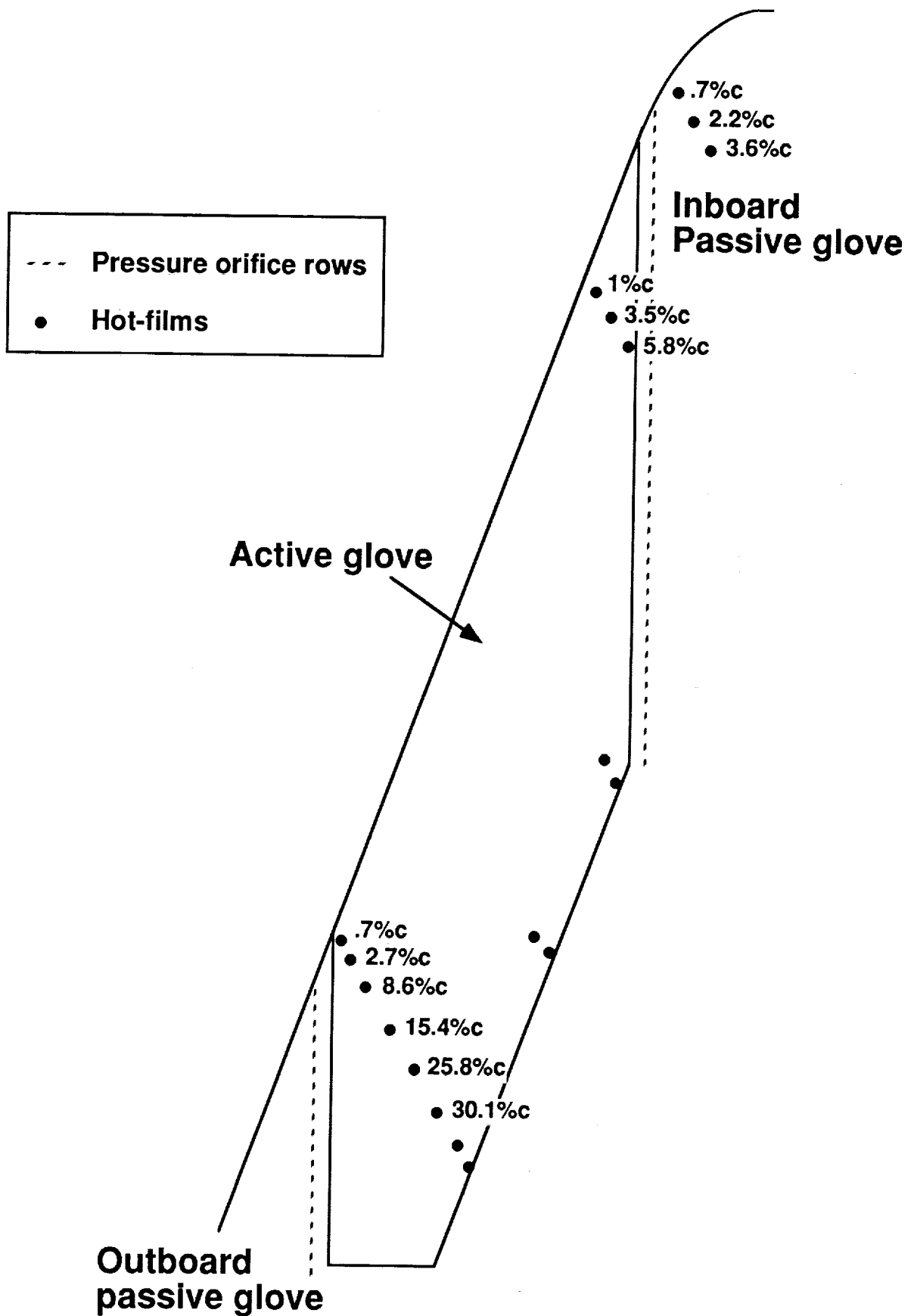
Completed Test Points

Shown is the limited flight envelope of the F-16XL Ship 1 with the completed test points. Flight data for various Mach numbers, altitudes, and angles of attack from these test points were used to determine the character of the attachment line (with no active suction), the location of transition (with and without suction), and the pressure distributions at 2 span stations (inboard and outboard of the active glove).

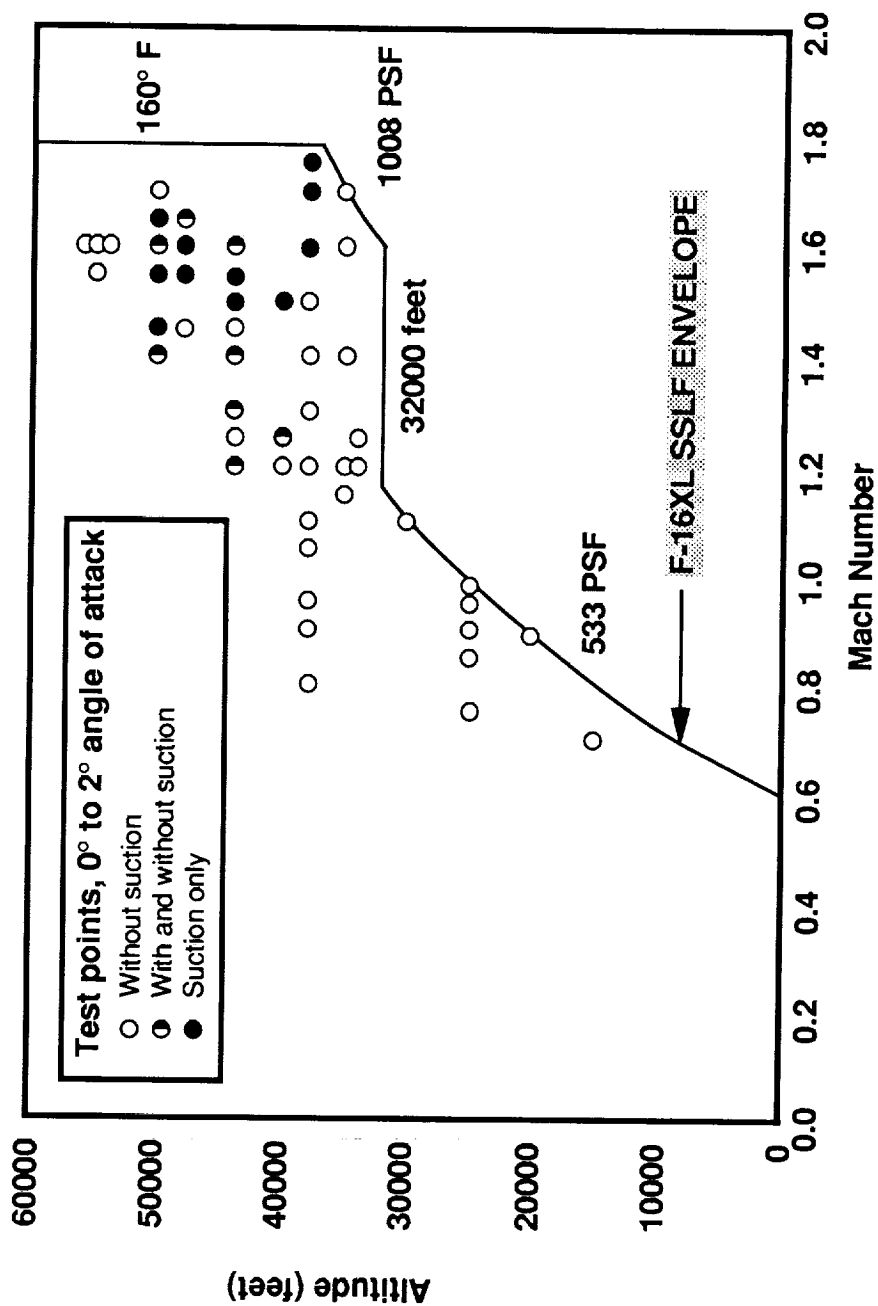
The solid circles are test points completed with active suction. (The suction pump was installed and operating.) The open circles are test points completed without active suction. (The suction pump was removed from the aircraft, however, some air may have been passing through the porous skin.) The half-solid circles are test points completed once with active suction and repeated after the suction pump was removed.

Some of the results from these flight tests are shown in the succeeding charts.

INSTRUMENTATION LAYOUT



Phase I Test Matrix - Completed Test Points



FLIGHT CONDITIONS FOR A LAMINAR ATTACHMENT LINE Passive Glove - Inboard

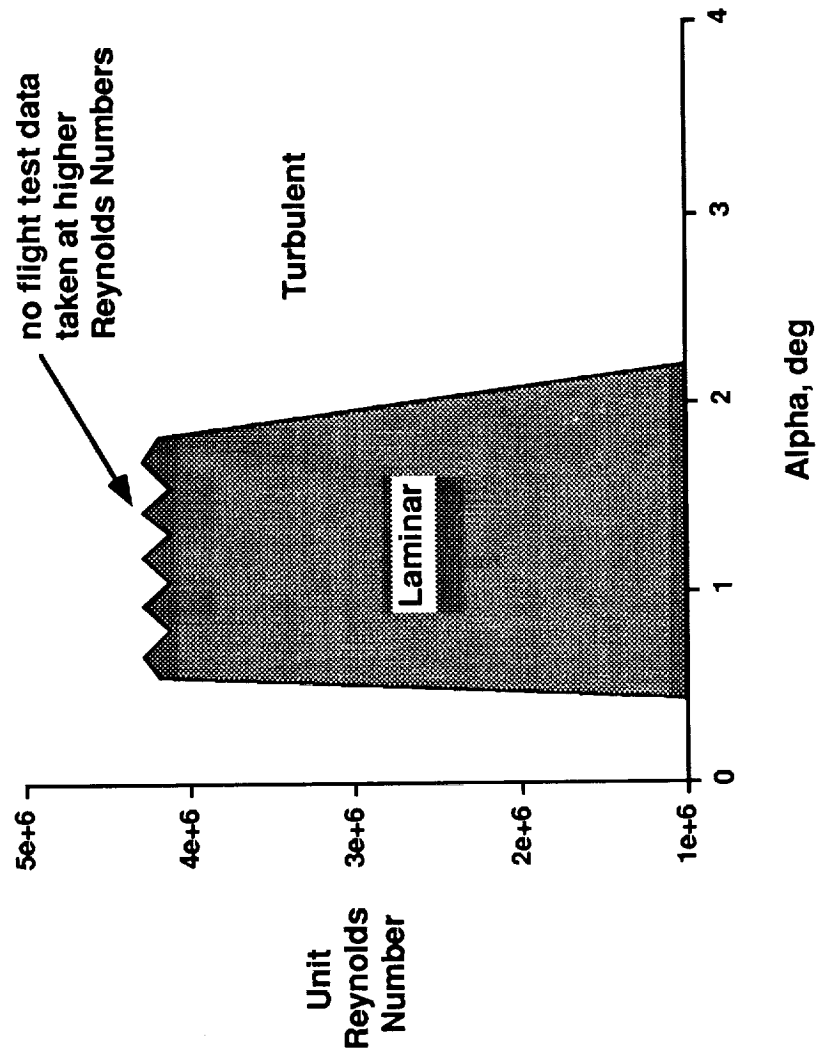
The unit Reynolds Number, as a function of angle of attack (α), at which transition occurs on the inboard passive glove, is shown.

Within the boundaries of the shaded region, a laminar attachment line exists on the inboard passive glove to .7% chord. The passive glove attachment line was found to be laminar to a unit Reynolds number of at least 4 million. The 'jagged' top of the shaded region is intended to indicate that although no flight data has been obtained at higher unit Reynolds numbers, there is a possibility that a laminar attachment line exists beyond a 4 million unit Reynolds number.

It is interesting to note that a laminar attachment line exists for an α range from about $1/2$ to $2\ 1/4$ degrees. Beyond the α boundaries a turbulent attachment line exists. This wide angle of attack envelope of laminar attachment on the inboard passive glove was not expected, due to the relatively small leading edge radius of the glove. These data indicate that maintaining a laminar attachment line for a small leading edge may be easier than predicted by stability codes.

Flight Conditions for a Laminar Attachment Line

Passive Glove - Inboard



FLIGHT CONDITIONS FOR A LAMINAR ATTACHMENT LINE

Active Glove - Typical (without active suction)

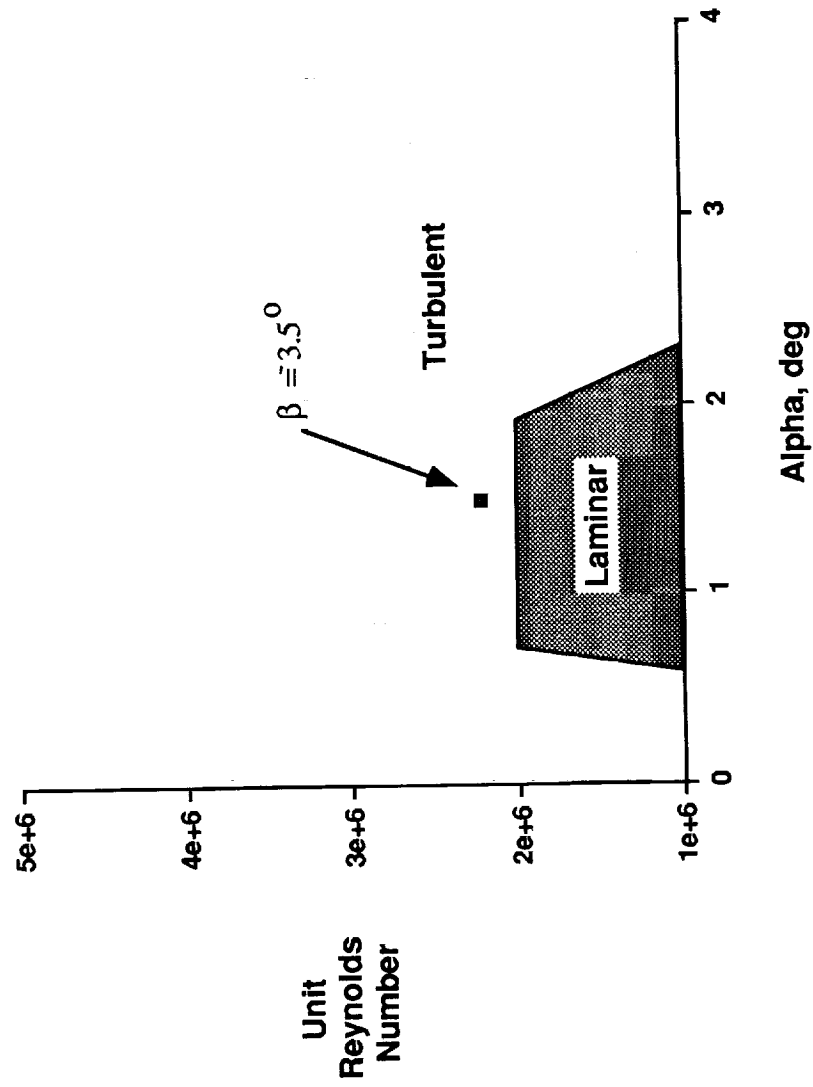
The unit Reynolds number, as a function of angle of attack (α), at which transition occurs on the 'typical' active glove section (inboard or outboard), is shown. All test points were flown without active suction.

Within the boundaries of the shaded region, a laminar attachment line exists on the active glove inboard and outboard to 1 and to .7% chord respectively. The unit Reynolds number limits shown represent the maximum unit Reynolds numbers for a laminar attachment line. The flat top of this region is indicative of the finding that for this typical active glove section the attachment line is not laminar beyond a Reynolds Number of approximately 2 million.

One series of test points were flown with -3.5 degrees side slip, effectively unsweeping the left wing from 70 degrees sweep to 66.5 degrees sweep. This reduction in sweep increased the unit Reynolds number, for a laminar attachment line, to approximately 2.2 million.

Flight Condition for Laminar Attachment Line

Active Glove - Typical (without active suction)



PRELIMINARY TRANSITION DATA Outboard Active Glove, 1.4 M

Glove transition results are based entirely on interpretation of hot-film signals, which is discussed in detail in NASA TM 100444 "Techniques Used in the Variable Sweep Transition Flight Experiment" (Anderson et al, 1988)

The transition location at the outboard active glove station, as a function of α , for Mach 1.4, 50,000 ft (1.7 million unit Reynolds number) is shown for a limited suction and a no active suction case. The term, 'limited suction' is used in lieu of 'maximum suction' to indicate the case when the suction pump was operating, but was providing only a small percentage of the maximum suction. (Actual mass flow and C_q is not available.)

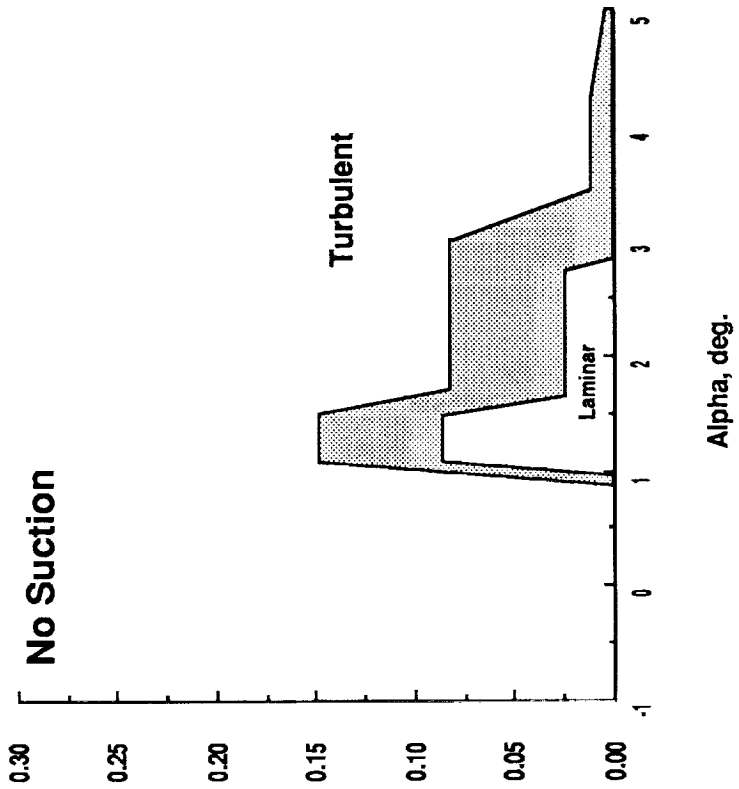
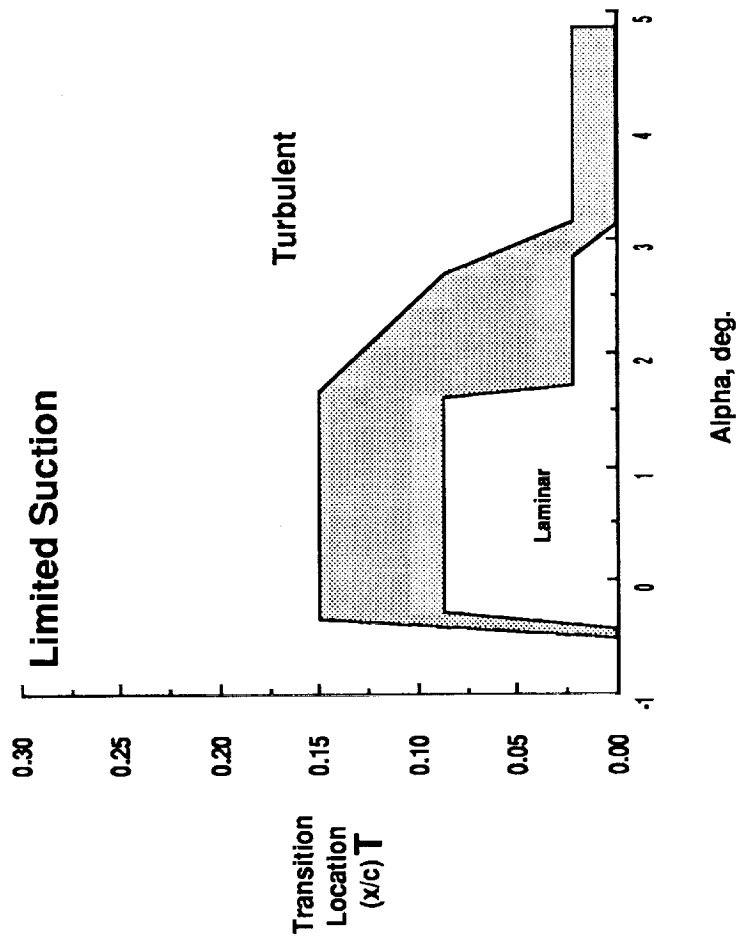
The shaded region represents the zone in which transition occurs. Because of size and space limitations on the active glove, the hot film sensor array used provided transition information for specific locations only. Thus, the shaded region indicates that transition occurred somewhere between 8.6 and 15.4 % chord. (The signal was laminar at 8.6% chord, but turbulent at 15.4% chord.) Beyond the α boundaries, a turbulent attachment line exists.

In a comparison of the limited suction and no suction case, one effect of suction can clearly be seen in this chart. By adding some suction, the maximum extent of laminar flow did not increase, however, the angle of attack range increased significantly.

Preliminary Transition Data

Outboard Active Glove

Mach = 1.4
Alt = 50,000 ft
Re/ft = 1.7 million



PRELIMINARY TRANSITION DATA Outboard Active Glove, 1.6 M

Outboard active glove station transition location for Mach 1.6, 50,000 ft (1.9 million Reynolds number) is shown for maximum and no suction condition. 'Maximum' suction indicates that the suction pump was operating normally. (Actual mass flow and C_q is not available.)

Like the Mach 1.4 case, the shaded region represents the zone in which transition occurs.

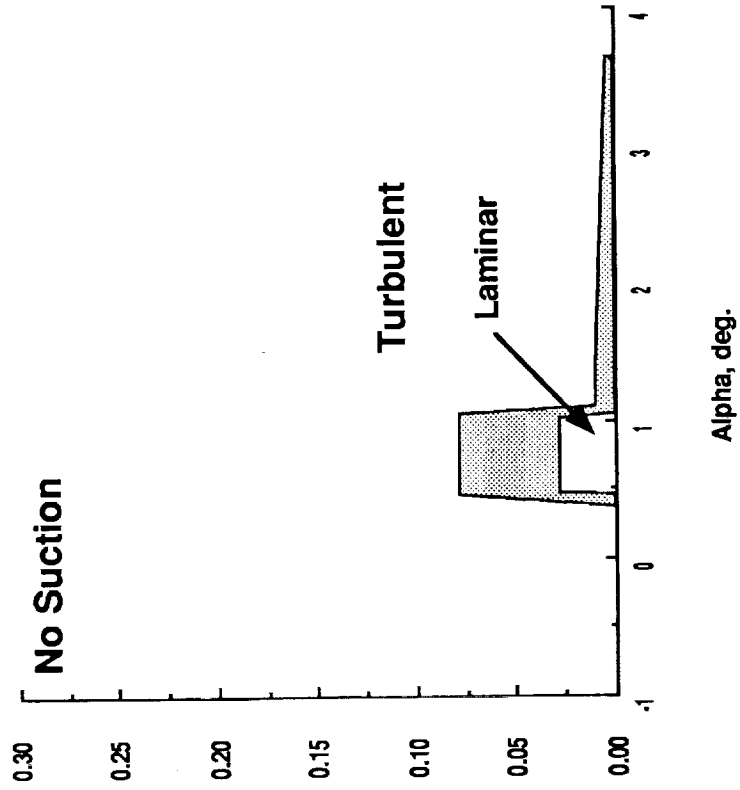
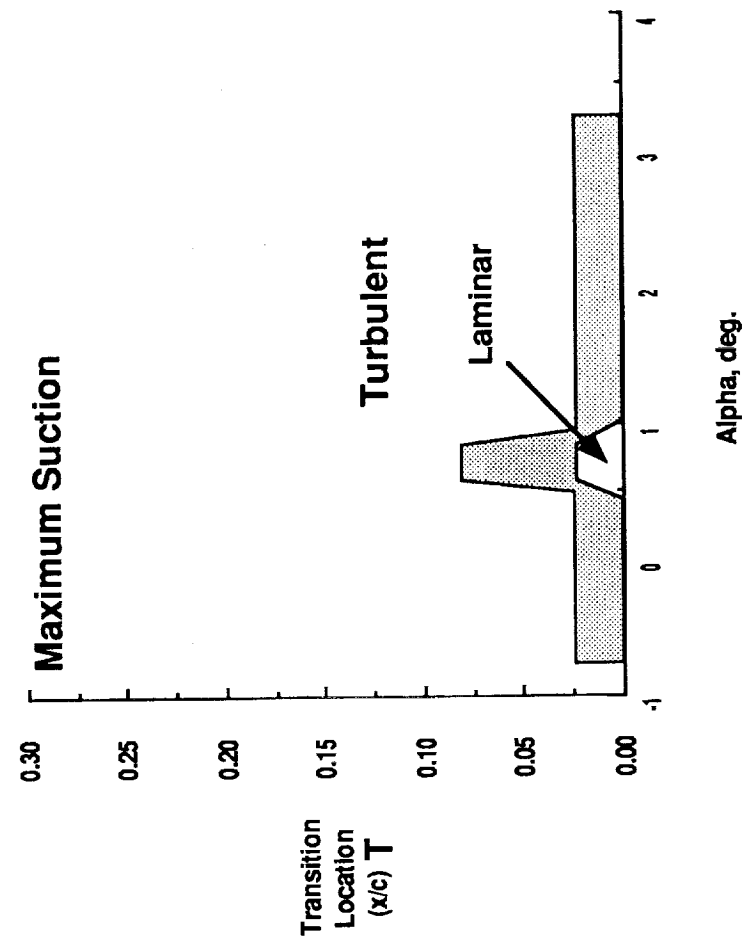
A comparison of the maximum suction and no suction results indicates that the extent of the laminar region does not change significantly with or without suction. It appears, in fact, that the maximum extent of laminar is slightly greater without suction. Since only one data point was available for this comparison, further flight testing is required.

The apparent difference in the transition region (shaded region) for the two cases may be related to instrumentation layout differences. That is, for the maximum suction case, the first hot-film sensor was at 2.7% chord, whereas, for the no suction case, the first hot-film was at .7% chord. Transition may occur further forward in the maximum suction case. Further flight testing is required to determine the actual transition location for the maximum suction case.

Preliminary Transition Data

Outboard Active Glove

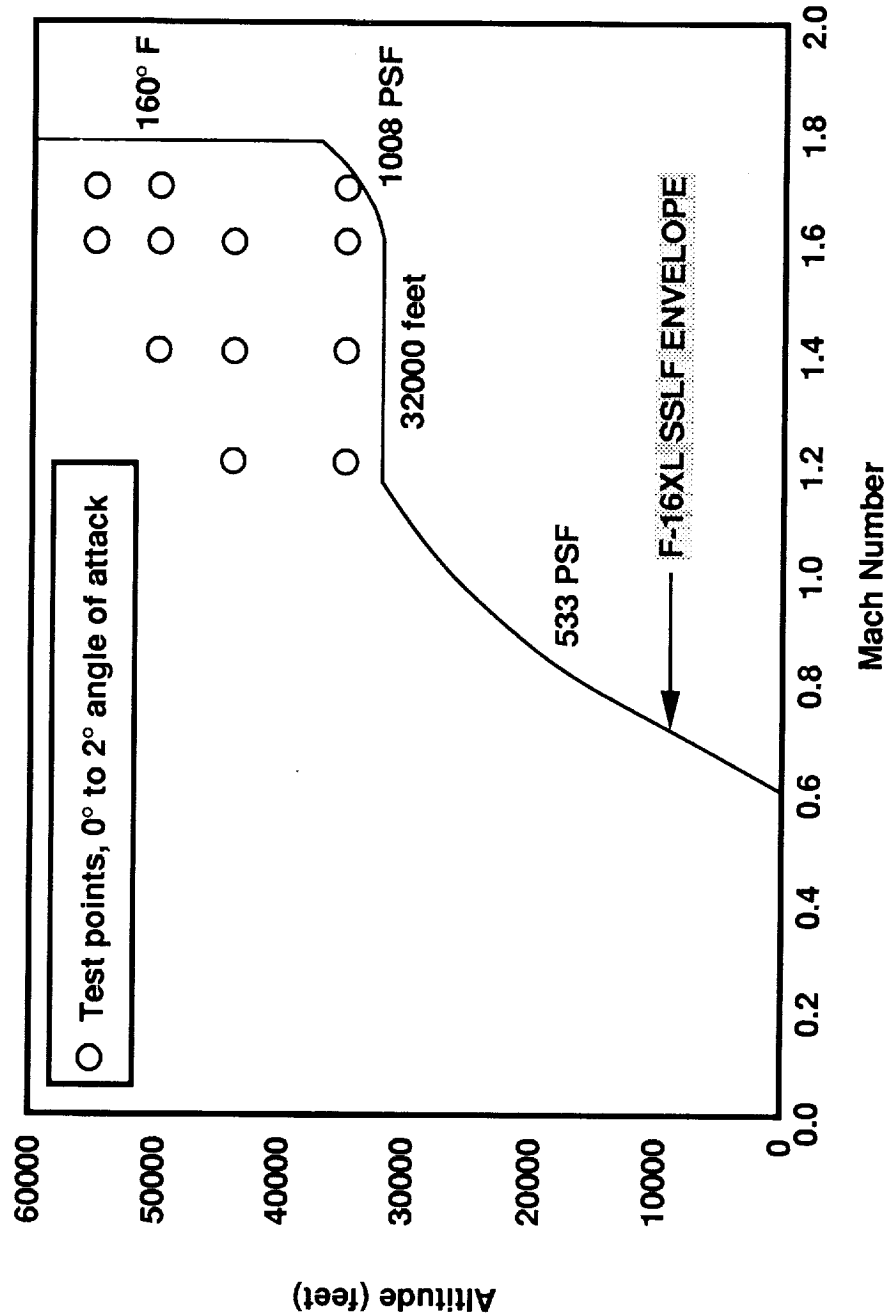
Mach = 1.6
Alt = 50,000 ft
Re/ft = 1.9 million



TEST MATRIX Remaining Test Points

Continued flight evaluation of this glove with and without suction is required. Shown is the flight envelope of the F-16XL Ship 1 with the planned test points. For each test point shown, various angles of attack will be examined with the suction pump providing maximum and no suction. The hot-film sensor array will be changed as necessary to document transition location both span and chordwise. In addition, the α boundaries for attachment line transition will be documented. It is expected that this evaluation will require 10-12 research flights.

Phase I Test Matrix - Remaining Test Points



F-16XL SSLF Proposed Follow-On Activities

A number of objectives for follow-on research are shown. The accomplishment of these follow-on activities will provide researchers with additional information on suction effects, as well as additional data for code validation.

Currently, NASA Ames-Dryden and NASA Langley are developing the procedures and plans to accomplish the six stated objectives by January 1992. Specific details on how these objectives will be achieved are not available at this time.

F-16XL SSLF Proposed Follow-on Activities

Objectives

- **Conduct suction distribution studies for code validation**
- **Evaluate techniques for controlling attachment line turbulence**
- **Evaluate effects of 2-D and 3-D roughness on transition**
- **Evaluate flow visualization techniques to detect transition and cross flow disturbances**
- **Assess effects of advanced sensors on transition**
- **Evaluate noise levels in laminar and turbulent boundary layers**

SUMMARY OF RESULTS TO DATE

The flight evaluations to date have resulted in several findings. Those findings are summarized in this chart.

Summary of Results to Date

- Laminar flow was achieved supersonically.
- A laminar attachment line was maintained over a wider range of alphas than anticipated.
- The attachment line remains laminar on the passive glove to a higher unit Reynolds number than on the active glove.
- Reducing sweep increased the unit Reynolds number for a laminar attachment line on the active glove.
- The effect of suction is inconsistent and not quantified. Further flight testing is necessary.
- Planned follow-on activities will provide additional information on suction effects as well as code validation data.

THIS PAGE INTENTIONALLY BLANK

Session XIII. Supersonic Laminar Flow Control

omit

Code Validation for the Simulation of Supersonic Viscous Flow About the F-16XL
Jolen Flores, Eugene Tu and Lyndell King NASA Ames Research Center

THIS PAGE INTENTIONALLY BLANK

**CODE VALIDATION FOR THE SIMULATION OF SUPERSONIC
VISCOUS FLOW ABOUT THE F-16XL**

*511-02
11986*

**Jolen Flores, Eugene Tu and Lyndell King
Applied Computational Fluids Branch
Fluid Mechanics Laboratory
NASA Ames Research Center
Moffett Field, California 94035**

**Presentation at the 1st HSRP Workshop
May 14-16, 1991
Williamsburg, VA**

INTRODUCTION

Because of the large potential gains related to laminar flow on the swept wings of supersonic aircraft, recent interest in the application of laminar flow control (LFC) techniques in the supersonic regime has increased. A supersonic laminar flow control (SLFC) technology program is currently underway within NASA. The objective of this program is to develop the data base and design methods that are critical to the development of laminar flow control technology for application to supersonic transport aircraft design. Towards this end, the program integrates computational investigations currently underway at NASA Ames-Moffett and NASA Langley with flight-test investigations being conducted on the F-16XL at the NASA Ames-Dryden Research Facility in cooperation with Rockwell International.

The computational goal at NASA Ames-Moffett is to integrate a thin-layer Reynolds averaged Navier-Stokes flow solver with a stability analysis code.¹ The flow solver would provide boundary-layer profiles to the stability analysis code which in turn would predict transition on the F-16XL wing. To utilize the stability analysis codes, reliable boundary-layer data is necessary at off-design cases. Previously, much of the prediction of boundary-layer transition has been accomplished through the coupling of boundary-layer codes with stability theory.^{2,3} However, boundary-layer codes may have difficulties at high Reynolds numbers, of the order of 100 million, and with the current complex geometry in question. Therefore, a reliable code which solves the thin-layer Reynolds averaged Navier-Stokes equations is needed.

The objective of the current research is two-fold. The first objective is method verification, via comparisons of computations with experiment, of the reliability and robustness of the code. To successfully implement LFC techniques to the F-16XL wing, the flow about the leading edge must be maintained as laminar flow. Therefore, the second objective is to focus on a series of numerical simulations with different values of α and Reynolds numbers. The purpose of the simulations is to study their effects on the two main factors which precipitate transition to turbulence at leading edges of highly swept wings (e.g. "spanwise contamination" and "crossflow instability"). The bulk of this presentation will focus on the first stated objective.

CNS BACKGROUND

The Compressible Navier-Stokes (CNS) code is utilized in this research. The CNS code is a time-dependent Navier-Stokes solver implemented in a zonal methodology. The zonal approach allows grids for complex configurations to be generated in topologically simple pieces and patched together to form the global mesh. In addition to simplifying the grid generation process, the zonal approach enhances computational efficiency by allowing zones to involve different physical models so that only the complexity necessary for the local flow field is assumed. The zonal method also gives the user flexibility in allowing different convergence strategies to be used in different zones.

Characteristics of the integration scheme ARC3D are given. The algorithm uses central-differencing in all three directions. Second and fourth order artificial dissipation is added both explicitly and implicitly for stability considerations. The inversion process involves inverting only scalar penta-diagonals. The Baldwin-Lomax model is used to model turbulence viscosity in the thin-layer Reynolds-averaged Navier-Stokes equations.⁴

CNS CODE CHARACTERISTICS

ZONAL SCHEME

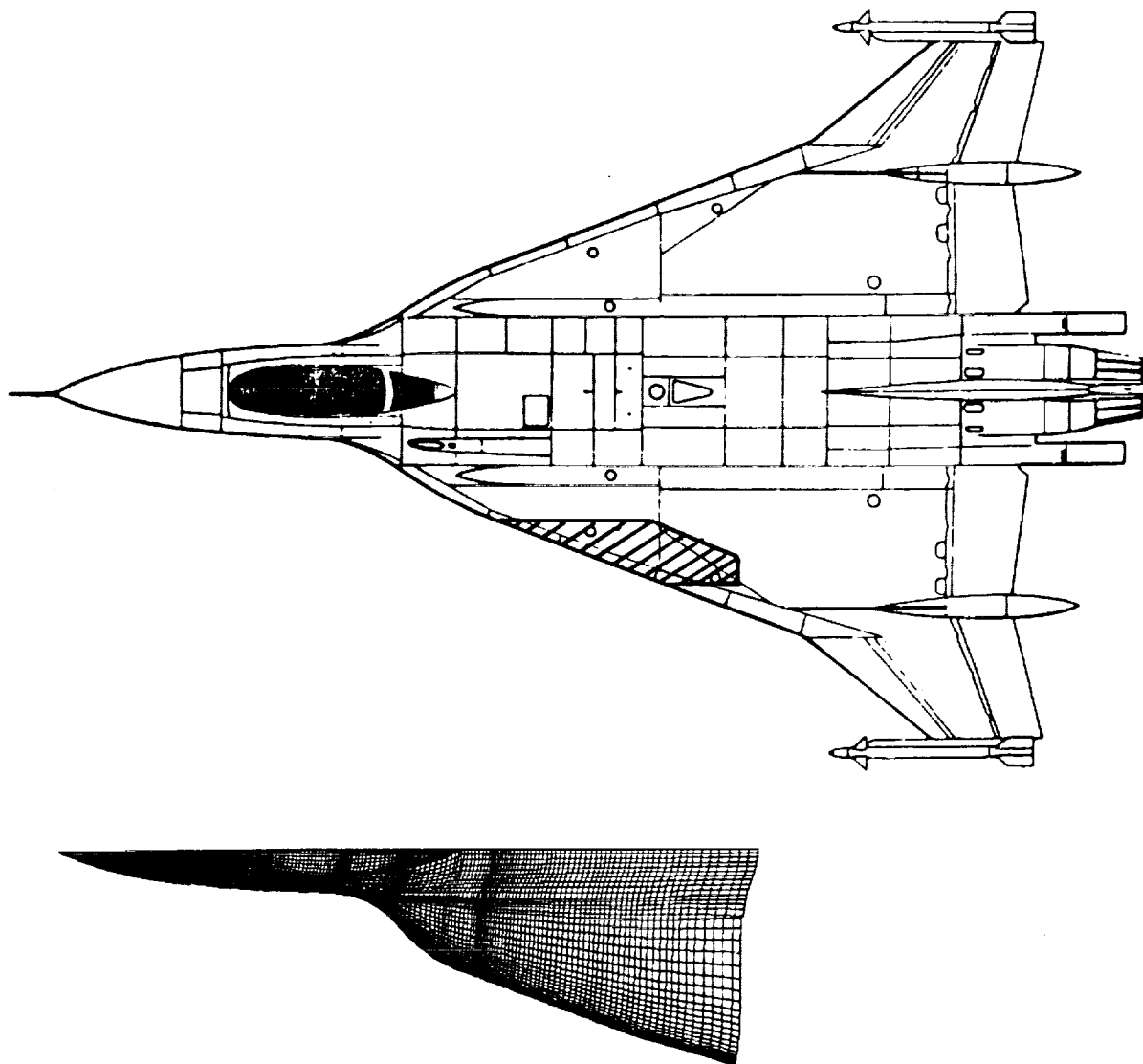
- SIMPLIFY GRID GENERATION FOR COMPLEX GEOMETRIES
- COMPUTATIONAL FLEXIBILITY AND EFFICIENCY

ARC3D ALGORITHM

- CENTRAL-DIFFERENCED SCHEME IN ALL THREE DIRECTIONS
- 2ND AND 4TH ORDER EXPLICIT AND IMPLICIT DISSIPATION
- BALDWIN-LOMAX TURBULENCE MODEL

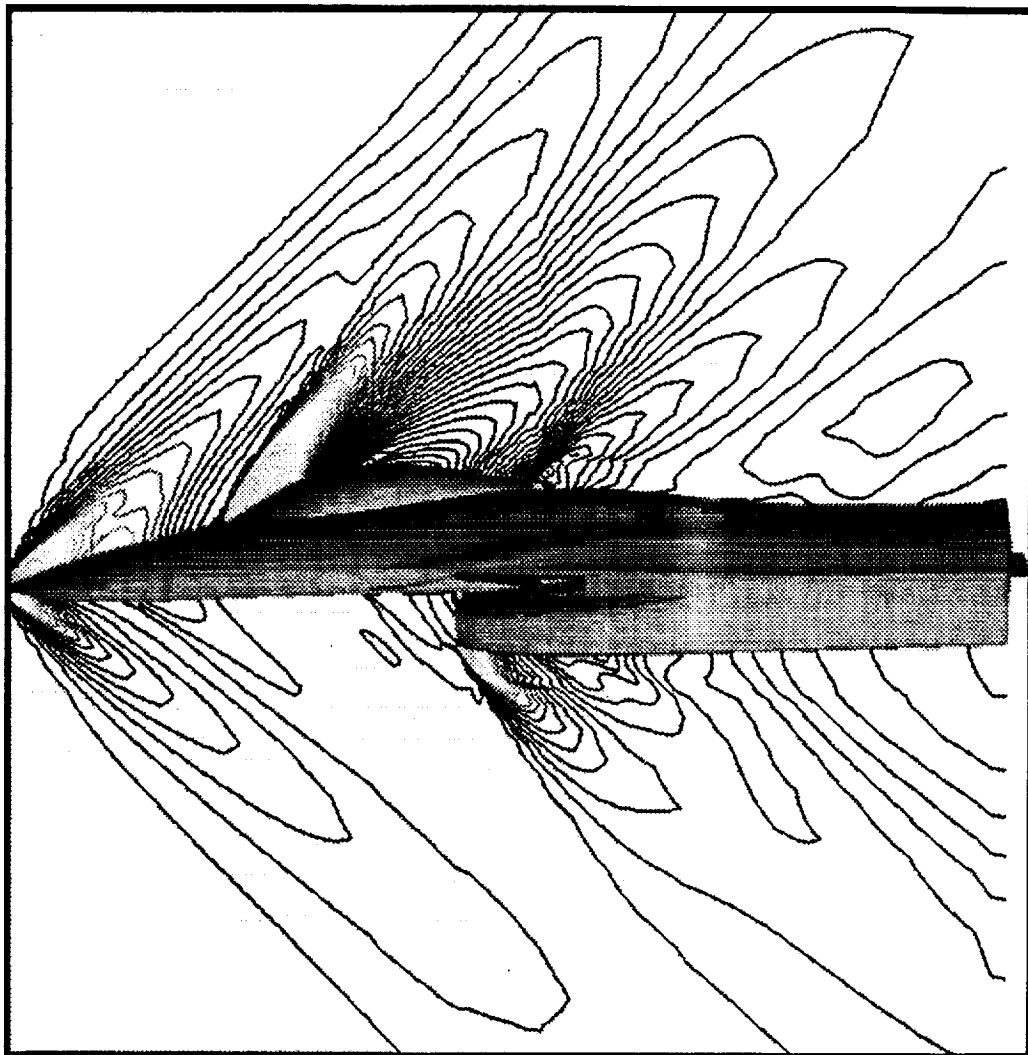
GEOMETRY AND GRID

The geometry used for the SLFC program is the F-16XL configuration. It is basically an F-16A with the original wing replaced with a double delta-wing having a sweep angle of 70° , forward of the wing-break. The figure shows a planform view of the surface grid used in the computations. The surface and flow field grids were graciously provided by Dr. C. J. Woan of Rockwell International. Not shown, but modeled, are the inlet, diverter, and environmental control system on the underside of the geometry. Instrumented on the actual flight configuration is a fitted glove on the upper surface of the wing. The glove surface contains tiny holes, created by laser beams to provide suction as a means of maintaining laminar flow. The approximate location of the glove geometry is shown in the figure.



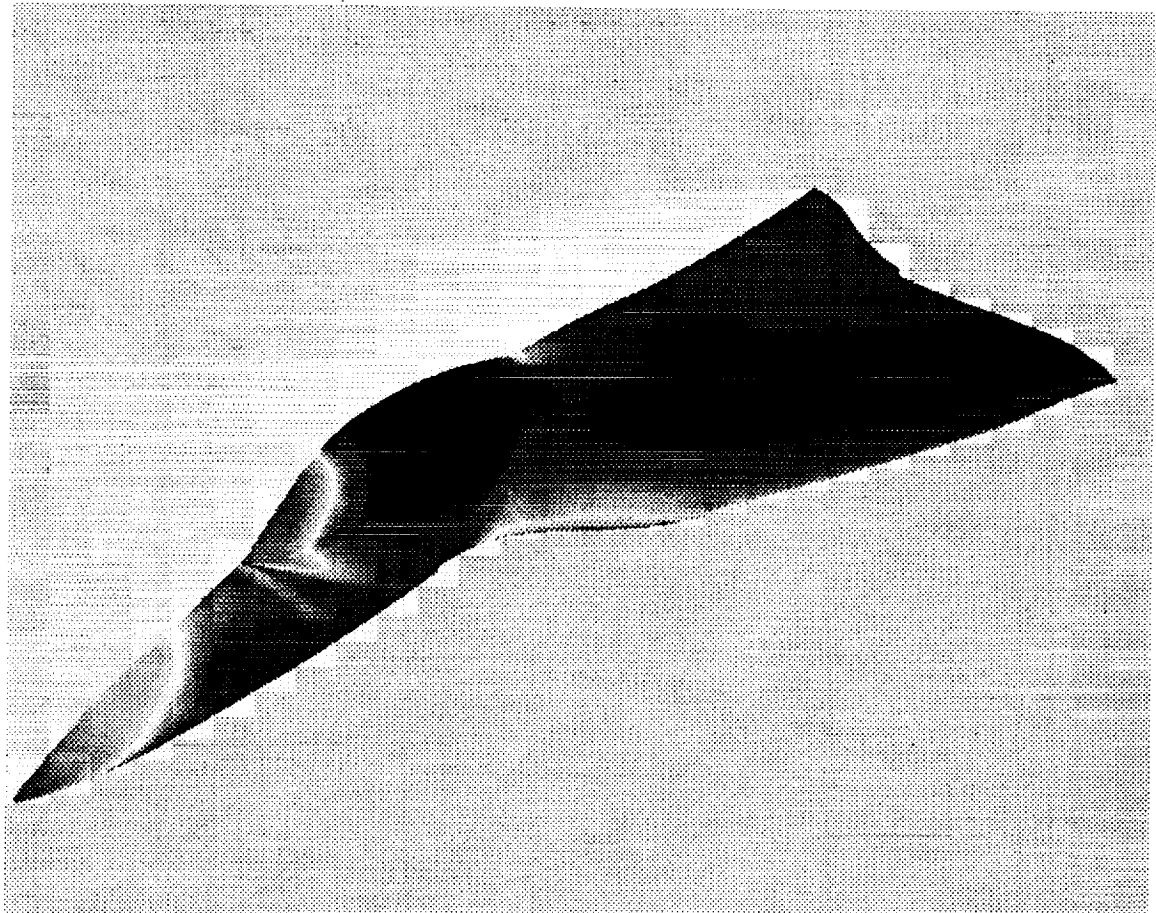
SYMMETRY PLANE PRESSURE CONTOURS

The numerical simulation was conducted with flow conditions approximately matching flight conditions at $M_\infty = 1.6$, $\alpha = 2.0^\circ$ and $Re_L = 116$ million. The Reynolds number is based on the fuselage length, which is approximately 550 inches. Nineteen zones were used for the computation with a total of one million grid points. The computation required approximately 2500 iterations to drop the initial L2-norm in each zone by three orders of magnitude. On the NASA supercomputer, this required approximately 13 hours of cpu time. The figure illustrates the pressure contours on the symmetry planes. Shocks can be seen at the nose, canopy and lip of the inlet on the geometry. What can also be noted is the smoothness of the contours, even though they are traversing different zones. An expansion wave at the top of the canopy, as well as a recompression shock at the back of the canopy, can also be seen. These regions cause adverse pressure gradients which can cause the flow to separate.



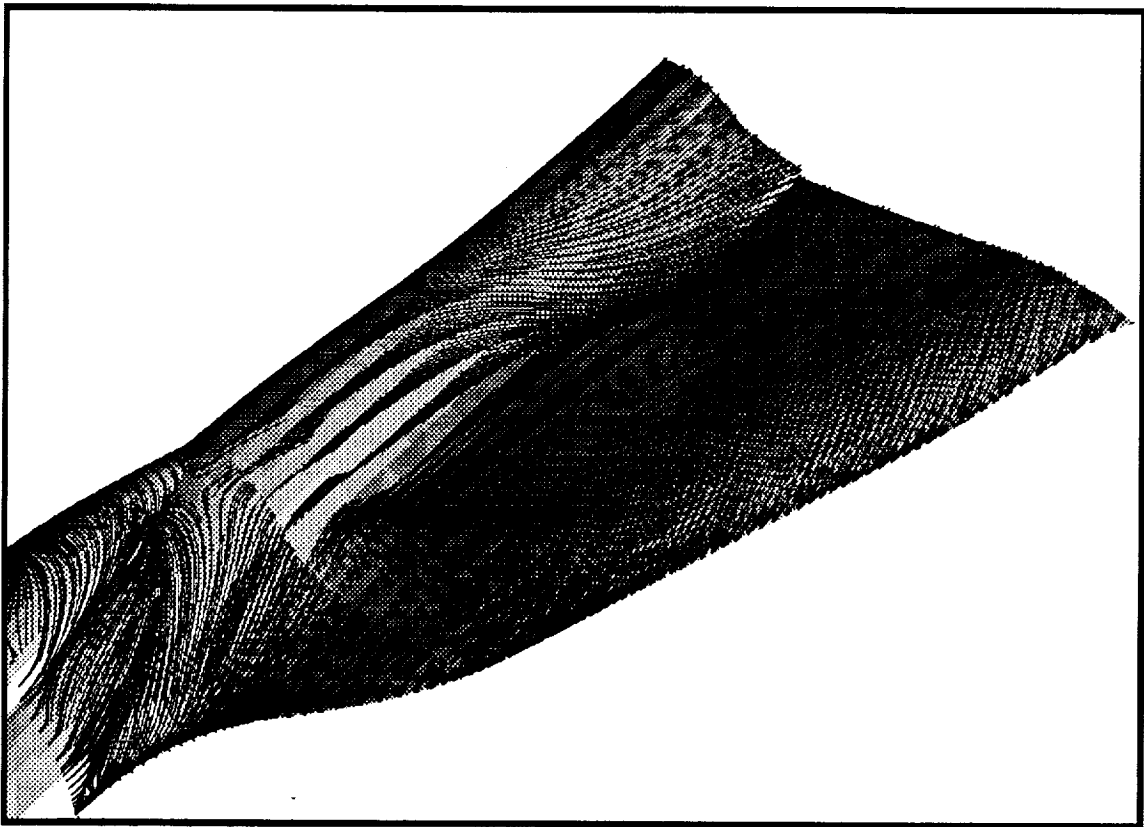
SURFACE PRESSURE MAP

The surface pressure map is illustrated in this figure. Again, the "hot spots" (light shaded regions) at the nose and front of the canopy are noted. The low pressure region (dark shaded regions) at the top of the canopy is also seen and is due to the expansion of the flow about the canopy. A large low pressure region is also seen on the wing of the geometry. It will be shown that this region will have a large influence on the flow pattern in this area.



SIMULATED OIL FLOW PATTERN

Oil flow patterns on the geometry are simulated by releasing and restricting particles to one grid point off the surface and tracking their subsequent journey downstream. As can be seen, a separation region occurs due to the recompression shock at the back of the canopy, however it quickly reattaches downstream. The low pressure region at the top of the canopy causes an upwash of the flow about the fuselage-strake region. Also the flow just off the symmetry plane near the back of the fuselage is seen to be pulled down onto the wing due to the aforementioned low pressure on the wing. This same low pressure also causes the flow coming from the leading edge to head slightly inboard before proceeding downstream.

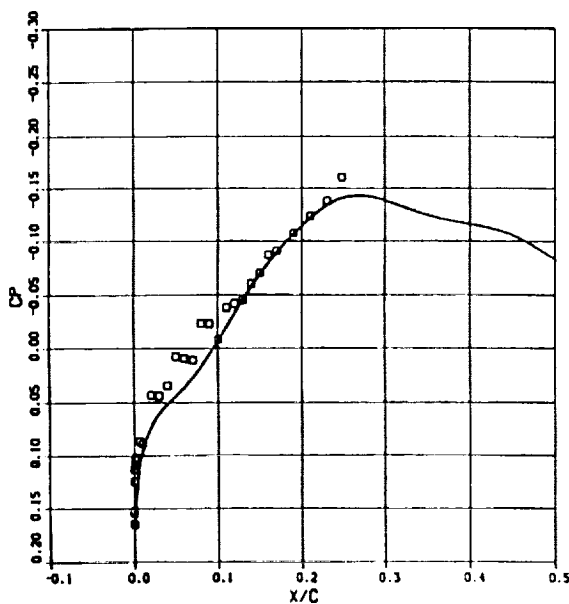


PRESSURE COEFFICIENT COMPARISONS

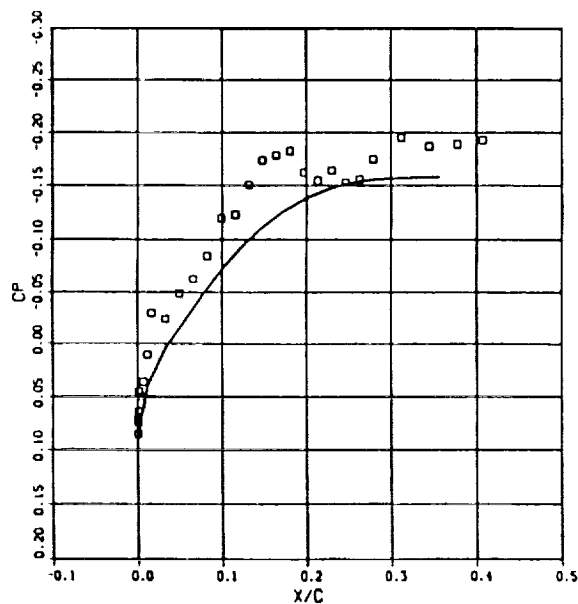
Computed pressure coefficients are compared to inflight data obtained from NASA Ames-Dryden. These are given at two span stations. The inboard span station (72 inches from the symmetry plane) corresponds to the location just inboard of the laminar flow control glove. Since the computational grid lines did not correspond to constant span stations, cubic spline interpolation was necessary to compute the flow variables at the appropriate span stations. The solid lines indicate the computations and the rectangles indicate experiment. For the inboard station, pressure taps were instrumented up to 25 percent of local chord, while outboard taps were instrumented up to 40 percent of local chord. The computations at the inboard station compare fairly well with the experimental data, with a slight underprediction. The slight underprediction occurs at 2-9 percent of chord. The computations are in excellent agreement with experiment from 10 percent of chord onward, and compare fairly well at the leading edge. At the outboard station, the computations consistently underpredict the experiment over the entire chord. However, there may be twist at this span station in the actual geometry which has not been accounted for in the computational model.

$$M = 1.6, \alpha = 2.0^\circ, Re_L = 116 \text{ million}$$

— COMPUTATIONS
□ TEST DATA (DRYDEN)



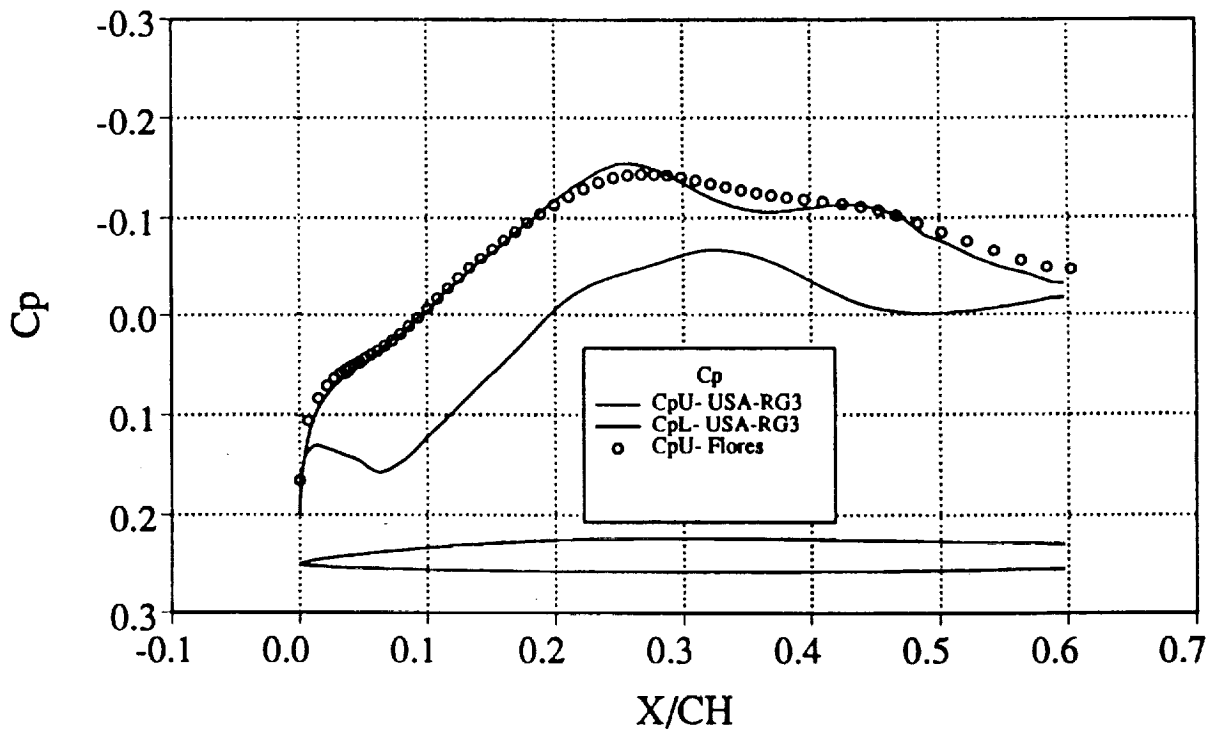
INBOARD STATION (72")



OUTBOARD STATION (114")

COMPUTATIONAL COMPARISONS OF PRESSURE COEFFICIENT

In the previous result, the computations underpredict the experimental pressure coefficients, especially between 2-9 percent of local chord at the inboard station. A comparison of the numerical results obtained by the CNS code and that due to a completely different code, called the USA-RG3 code⁵ developed by Rockwell International, was conducted using the same grid. As can be noted, there is very good agreement between the two numerical results at the inboard station. In particular, where the CNS results were quite different from experiment in the 2-9 percent local chord region, there is excellent agreement obtained there between the two different codes.



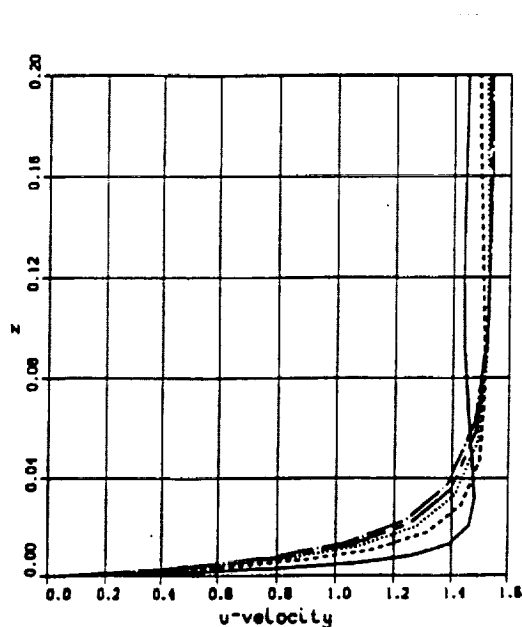
VELOCITY PROFILES AT THE INBOARD STATION

An examination of the velocity profiles is conducted along the inboard station at different chordwise locations. The y-axis is the vertical height, in inches, above the geometry. The streamwise component of velocity is discussed first. The boundary layers all exhibit the standard expected profile. The boundary layer near the leading edge is very thin relative to the downstream profiles. At $x/c = 3.2$ percent the boundary-layer maintains a fairly constant thickness downstream to about $x/c = 4.7$ percent. The boundary-layer thickness near the leading edge is approximately .015 inches.

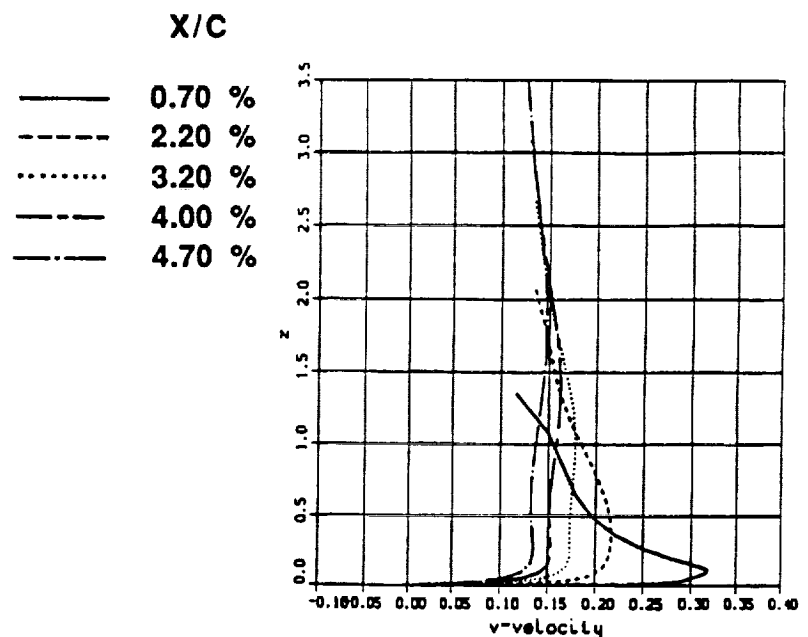
From examining the crossflow component it can be noted that the maximum crossflow occurs near the leading edge ($x/c = .7$ percent). At $x/c = 2.2$ percent, and downstream, the crossflow velocity has decreased dramatically. From $x/c = 3.2$ percent, and downstream, the crossflow velocity decreases continually, but not significantly. The inflection point of the crossflow velocity profile increases in height for the first three chordwise locations and then appears to decrease.

$$M = 1.6, \alpha = 2.0^\circ$$

$$Re_L = 100 \text{ million}$$



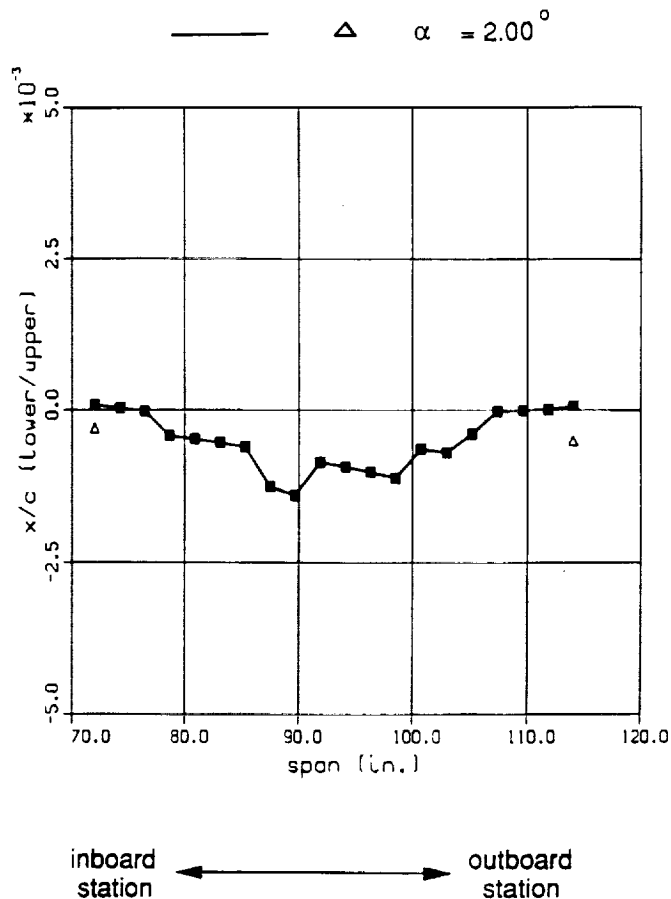
STREAMWISE VELOCITY



CROSSFLOW VELOCITY

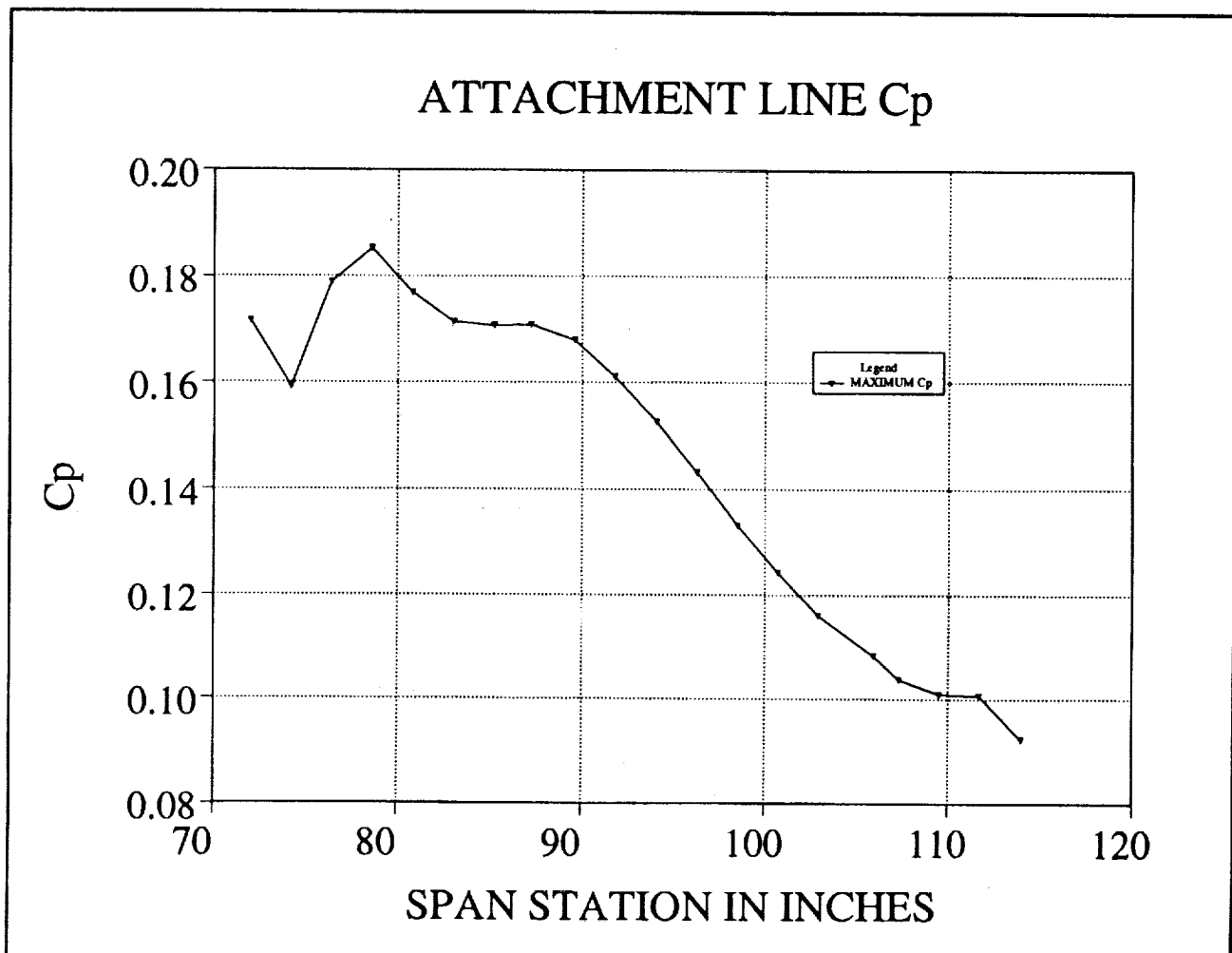
ATTACHMENT LINE LOCATIONS

The following results map the movement of the attachment line location from the inboard location of the wing to the outboard location. The experimental data points exist only at the inboard and outboard portion of the glove. The vertical axis indicates the position of the attachment point, either on the upper surface, (positive x/c) or on the lower surface (negative x/c). The leading edge itself is at $x/c = 0.0$. There are twenty equally-spaced interpolated span stations between the inboard and outboard stations. The stagnation point, at each span station, was determined by finding the grid point corresponding to the maximum pressure coefficient and is consistent with the experimental determination of the stagnation point. The procedure accounts for the discontinuities in the plot. The computations seem to indicate that the stagnation point is right on the leading edge of the inboard station, then goes below the leading edge at 75 inches and stays on the lower portion of the wing. At about 110 inches, the stagnation point returns to the leading edge of the wing. The experimental data points indicate the stagnation points slightly below the leading edge at both inboard and outboard stations. Other computational results⁵ indicate the same trend as the current computational results.



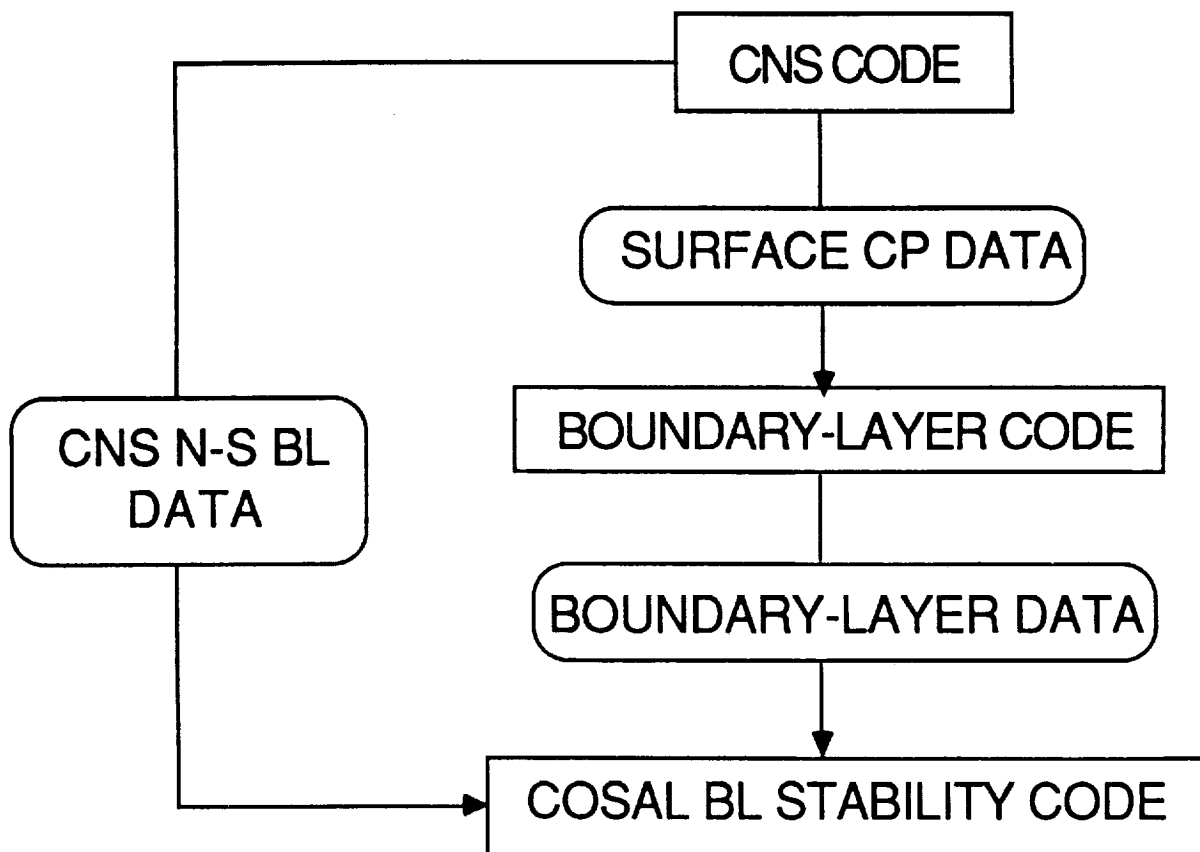
PRESSURE COEFFICIENT ALONG ATTACHMENT LINE

The following results reflect the pressure coefficient at the stagnation point from the inboard to outboard station. There is a dip in the pressure coefficient at a span station of about 74 inches. This location is about two inches away from where the inboard portion of the glove begins. The pressure coefficient then shows a favorable pressure gradient along the attachment line and levels off at a span station of about 110 inches. The last data point indicates that the pressure coefficient may take another dip here, which interestingly occurs close to the location where the glove ends. This result indicates that there may be some effect of how the glove is faired into the original wing.



FLOW SOLVER - STABILITY CODE COUPLING

The Navier-Stokes code is currently coupled to the stability code in the following manner. The pressure distribution at various span stations from inboard to outboard is read into the boundary-layer code. The boundary-layer code uses a conical flow assumption in computing its boundary-layer data based on the given pressure distributions. This boundary-layer data is then read into the stability code. Depending on the N-factor value prescribed for the determination of transition, the stability code will determine the x/c location of transition for each span station. Future work will be performed to couple the Navier-Stokes solution from the CNS code directly into the stability code.



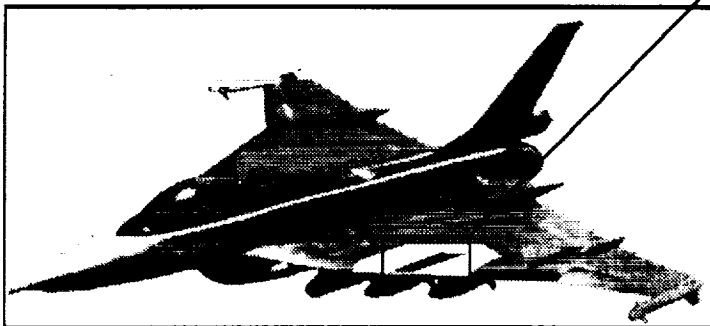
HSRP CODE VALIDATION

A composite result is displayed which illustrates the end product of the transition predicted by the CNS - COSAL code coupling. An N-factor equal to 10 was used in the COSAL code. The white area on the F-16XL wing designates the glove location. The box illustrates an expanded view of a small section of the glove. At a span station of 89 inches, transition occurs at about 1.7 inches (.6 percent of x/c) from the leading edge. Slightly outboard of that transition occurs at about 2.2 inches (.9 percent of x/c). It can be noted that for this case, transition occurs very close to the leading edge which is consistent with experimental findings. The corresponding C_p for the outboard location is also illustrated. The leading edge geometry of the wing is also indicated below the C_p graphic.

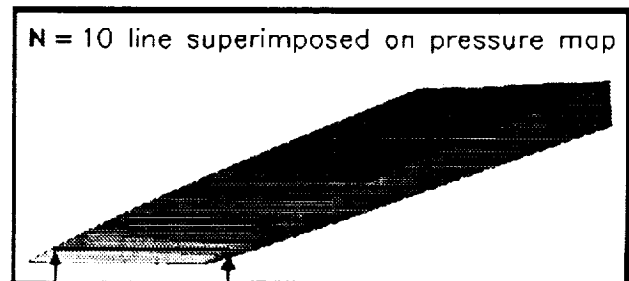
HSRP Code Validation

Ames Fluid Mechanics Laboratory
Ames Applied Computational Fluids Branch

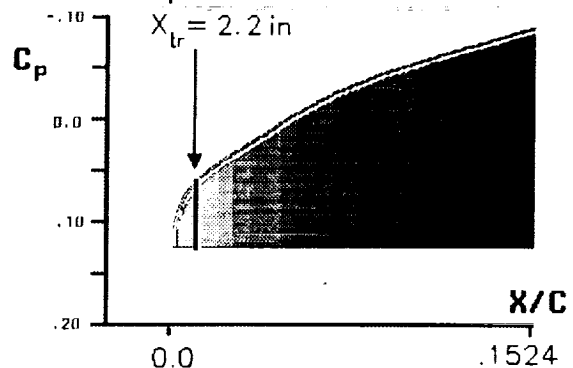
- N-S Code for basic flow
- COSAL code for transition (N=10)
- Passive Glove



F16XL



$X_{tr} = 1.7$ in



SUMMARY AND FUTURE DIRECTIONS

In summary, the CNS code has been used to predict the flow about the F-16XL in supersonic flight. Comparisons were made between the numerical and experimental pressure coefficients with good agreement between the two. Further numerical comparisons were conducted with the results from another Navier-Stokes code. Velocity profiles, for both streamwise and crossflow components, were analyzed at the inboard station for various x/c values. A mapping of the attachment line from the inboard to the outboard area of the glove was conducted. Finally, the numerical results from the CNS code were used in the COSAL code to predict transition.

SUMMARY

COMPUTED NUMERICAL SOLUTION OF THE FLOW FIELD ABOUT THE F-16XL IN SUPERSONIC FLIGHT

- COMPARISONS OF THE NUMERICAL SOLUTION WITH IN-FLIGHT EXPERIMENTAL DATA WAS CONDUCTED
- VELOCITY PROFILES FOR INBOARD STATION ANALYZED
- MAPPING OF ATTACHMENT LINE LOCATION WAS CONDUCTED

CNS CODE COUPLED TO COSAL CODE

- TRANSITION PREDICTED ON THE GLOVE PORTION OF THE WING

FUTURE DIRECTIONS

CNS CODE

- CONTINUE VALIDATION OF THE CODE
- IMPLEMENT SUCTION BOUNDARY CONDITIONS

CNS/COSAL CODE

- MAP TRANSITION LINE AND VALIDATE WITH IN-FLIGHT DATA
- ADD CAPABILITY TO UTILIZE NAVIER-STOKES SOLUTION DIRECTLY

REFERENCES

1. Malik, M.R., "COSAL - A Black Box Compressible Stability Analysis Code for Transition Prediction in Three-Dimensional Boundary-Layers," NASA CR-165925, 1982.
2. Mack, L.M., "On The Stability of the Boundary Layer on a Transonic Swept Wing," AIAA Paper No. 79-0264.
3. Mack, L.M., "Transition Prediction And Linear Stability Theory in Laminar-Turbulent Transition," AGARD Conference Proceedings No. 224, pp. 1-1 to 1-22, 1977.
4. Flores, J. and Chaderjian, N.M., "Zonal Navier-Stokes Methodology for Flow Simulation About A Complete Aircraft," Journal of Aircraft, Vol. 27, No.7, July 1990, pp. 583-590.
5. Woan, C.J., Gingrich, P.B., and George, M.W., "CFD Validation of a Supersonic Laminar Flow Control Concept," AIAA Paper No. 91-0188.

Session XIII. Supersonic Laminar Flow Control

omit

Inviscid and Viscous Flow Calculations for the F-16XL Configuration
Dr. Vinket Iyer, Vigyan, Inc.

THIS PAGE INTENTIONALLY BLANK

512-02

11987

**INVISCID AND VISCOUS FLOW CALCULATIONS
FOR THE F16XL CONFIGURATION**

Venkit Iyer

Vigyan Inc.

(Theor. Flow Physics Br., NASA LaRC)

First Annual High-Speed Research Workshop

May 14-16, 1991, Williamsburg, VA

THIS PAGE INTENTIONALLY BLANK

This presentation is a report on the ongoing activity at NASA LaRC in support of Supersonic Laminar Flow Control (SLFC) research. Details of the computation involved in obtaining the meanflow around bodies in high-speed flow and interfacing the results to a stability analysis will be presented. Particular attention is given to the F16XL configuration, which is the test-bed for the supersonic LFC experiment.

Meanflow solution for two geometries will be discussed. The first one is for the F16XL wing, with emphasis on the flow near the attachment line and the upper surface. Calculations have been done with and without suction. The results have been processed using an interface program and fed into a stability analysis program.

The second geometry is a scale model of a swept wing leading edge at $M=3.5$. Experimental measurements on transition on this model are planned at NASA LaRC. The computations are in support of this effort.

Computational Study of LFC

for Supersonic Fuselages and Swept Wings

Cases Under Study:

(1) F16XL Wing LFC Experiment

$M=1.6-2.0$, $\alpha=0-2$ deg., $\Lambda=70$ deg, Suction On/Off

(2) Supersonic Swept Leading Edge

Closer Study of L.E. region B-L stability

$M=3.5$, $\Lambda=77.1$ deg., α , Re variable

A number of programs, all developed at NASA LaRC have been used to address the problem of supersonic boundary-layer stability. The codes CFL3D and GASP are upwind-differenced, finite volume N-S solvers that have been applied to a wide variety of flows. For simpler geometries, 3D boundary-layer solvers can be applied, which uses the boundary layer-edge pressure boundary condition from an Euler calculation. Two such programs, one implicit and the other explicit are available.

The boundary layer stability program COSAL has been modified to interface with any of the above programs.

COMPUTATIONAL TOOLS

MEAN-FLOW

N-S/EULER SOLVERS

CFL3D (TLNS)
GASP (PNS)

3-D B-L SOLVERS

$O(\Delta Z^2)$ and $O(\Delta Z^4)$ Programs

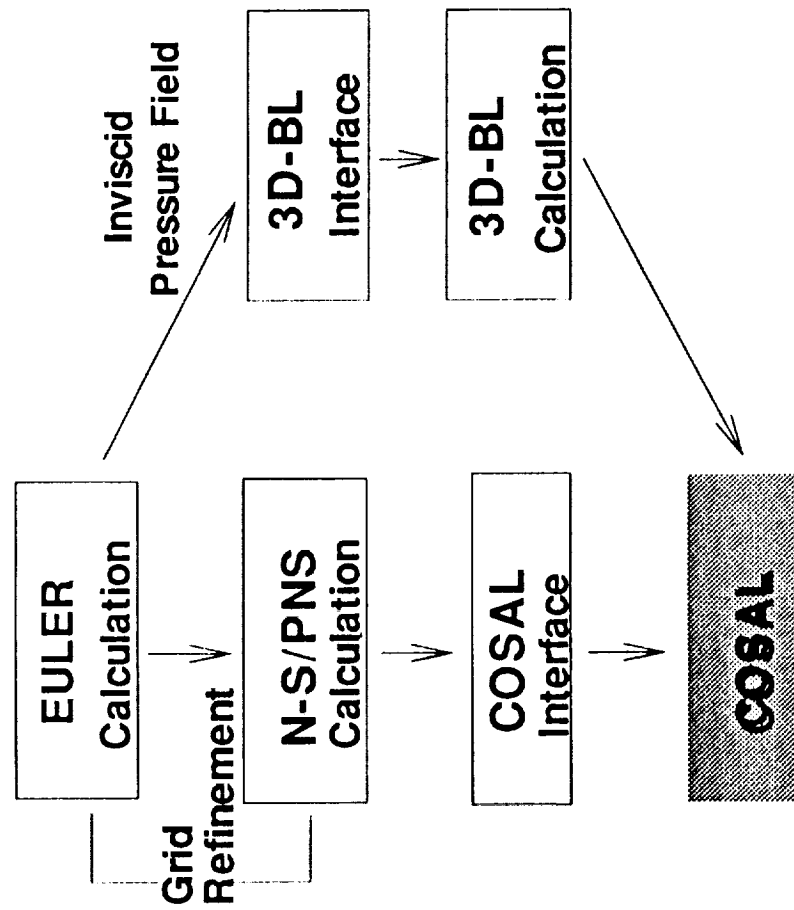
B-L STABILITY

COSAL Modified for 3D Compr. Flows

Depending on the complexity of the geometry, one of the two routes could be followed. For simpler (conical or infinite swept wing type) geometries, a cost-effective way is to run a 3D boundary-layer calculation and feed it directly to the COSAL linear stability analysis.

For more complex bodies such as the F16XL wing, a TLNS calculation is necessary. Grid refinement based on solution on coarse meshes may be required. Once a grid-converged N-S solution is obtained, an interface program is required to process the solution and output it into boundary-layer oriented coordinates suitable for the linear stability analysis.

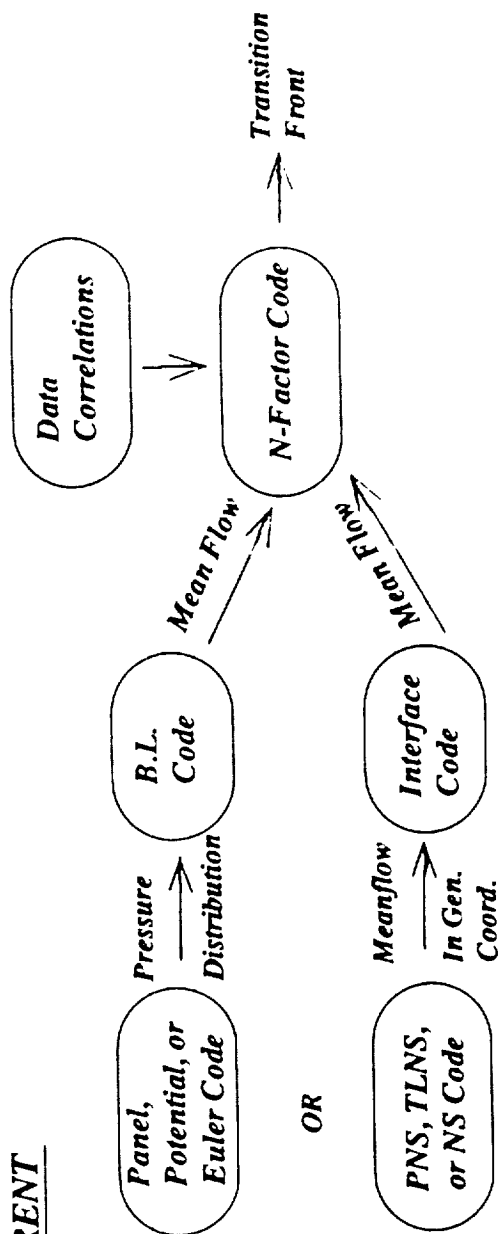
PRESENT APPROACH for B-L Stability Analysis



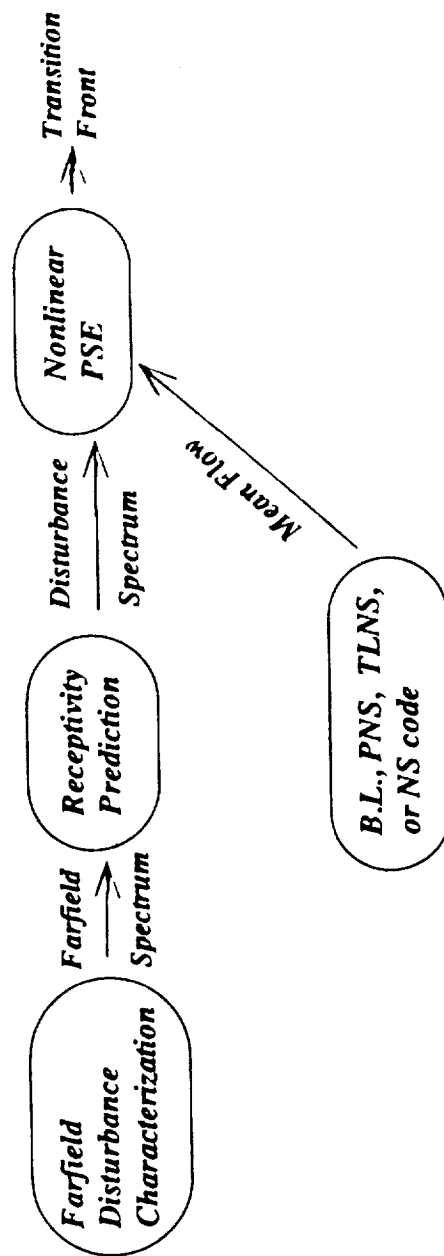
In order to improve the transition prediction procedure, a future methodology would be to include modeling of the far-field disturbances and receptivity mechanisms and use a more general analysis such as the non-linear Parabolised Stability Equations (PSE). The inputs from the mean-flow solution remain the same in present and future methods. This talk will focus on the meanflow issue.

LAMINAR FLOW CONTROL METHODOLOGY

CURRENT

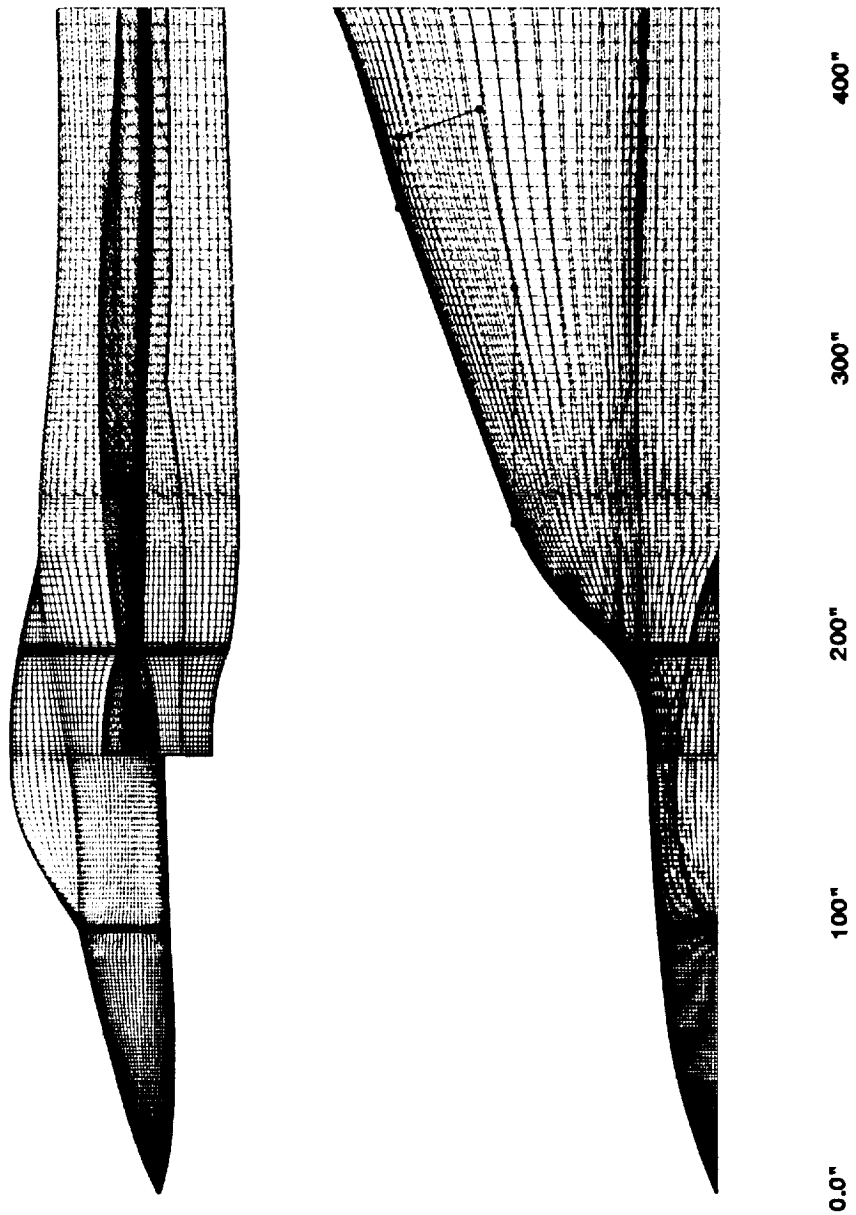


FUTURE



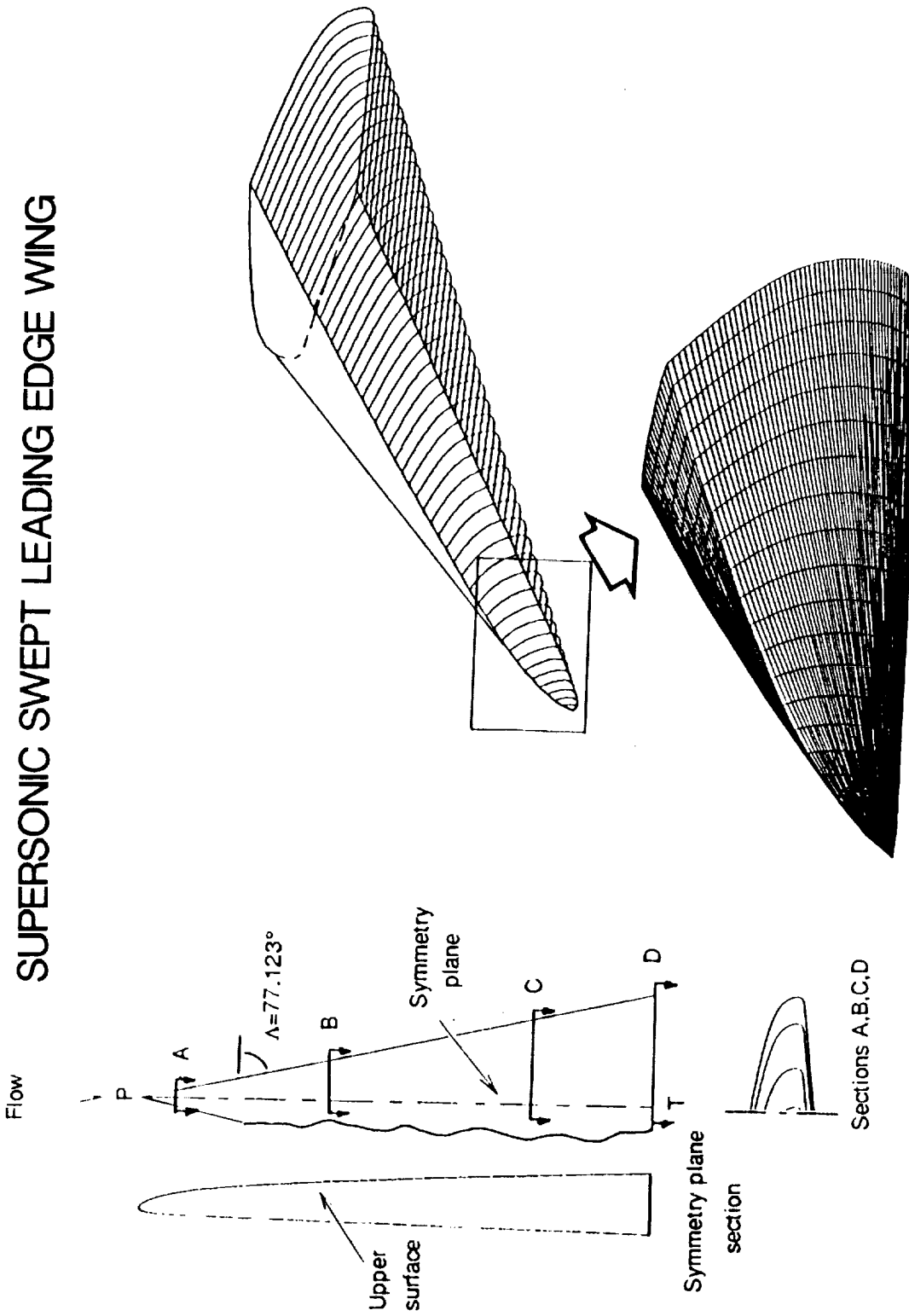
The first case discussed is the flow calculation on the F16XL wing. The figure shows the surface grid description of the body comprising of about 20,000 points. The glove location on the wing is also shown. Velocity and temperature profiles in the wing upper region are of interest from boundary-layer stability point of view.

F16XL SURFACE GRID AND LFC GLOVE LOCATION

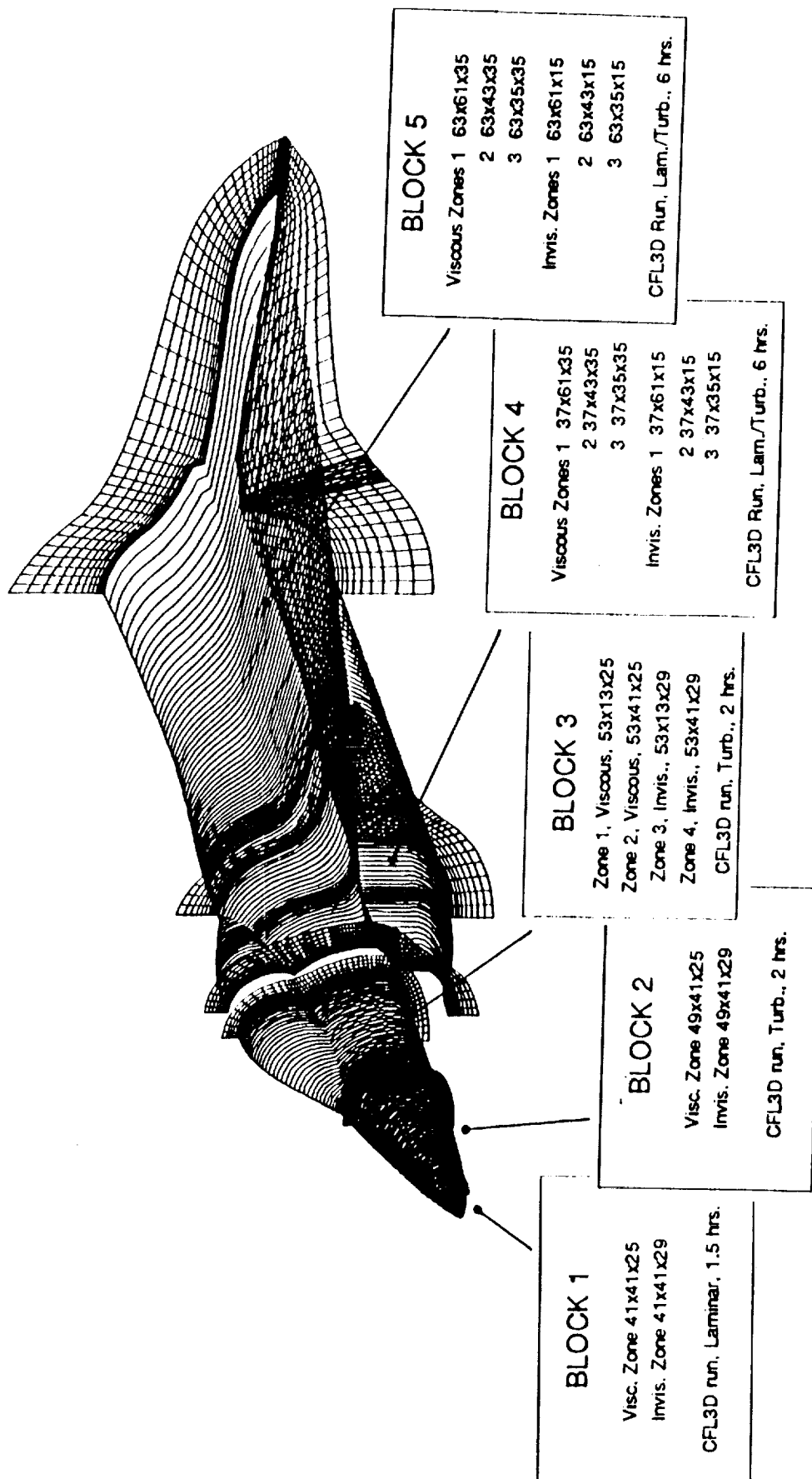


The second case is a wind-tunnel model of a swept wing leading edge region, planned to be tested under low free-stream turbulence conditions. This is a 15" long symmetric model at a higher sweep angle and Mach number compared to the F16XL leading edge.

SUPERSONIC SWEEPED LEADING EDGE WING



In order to compute the entire F16XL configuration, and at the same time to keep computer job sizes at reasonable levels, computation is performed in blocks. Within each block, a globally-iterated computation is performed using the program CFL3D. Between blocks, information is passed from upstream to downstream, which is correct for supersonic flow. A complete run on a grid of 1 million points takes up about 15 hours on the CRAY Y-MP. Some blocks can be run together, towards the end of convergence, in order to avoid interpolation errors between blocks.

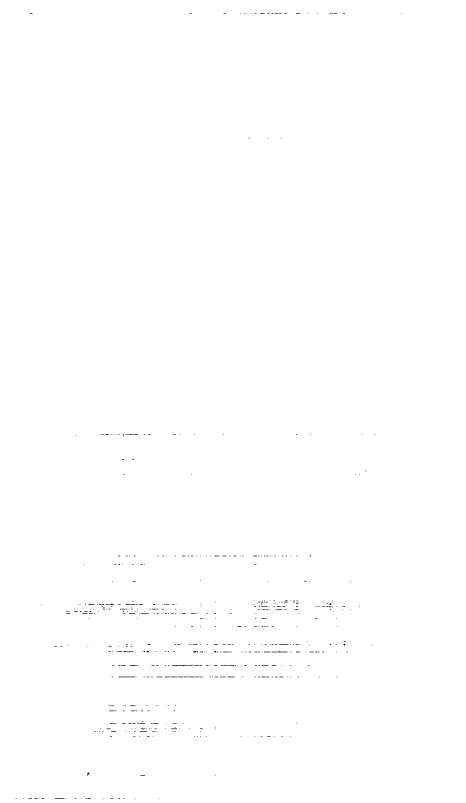


NAVIER-STOKES SOLUTION FOR F16XL GEOMETRY

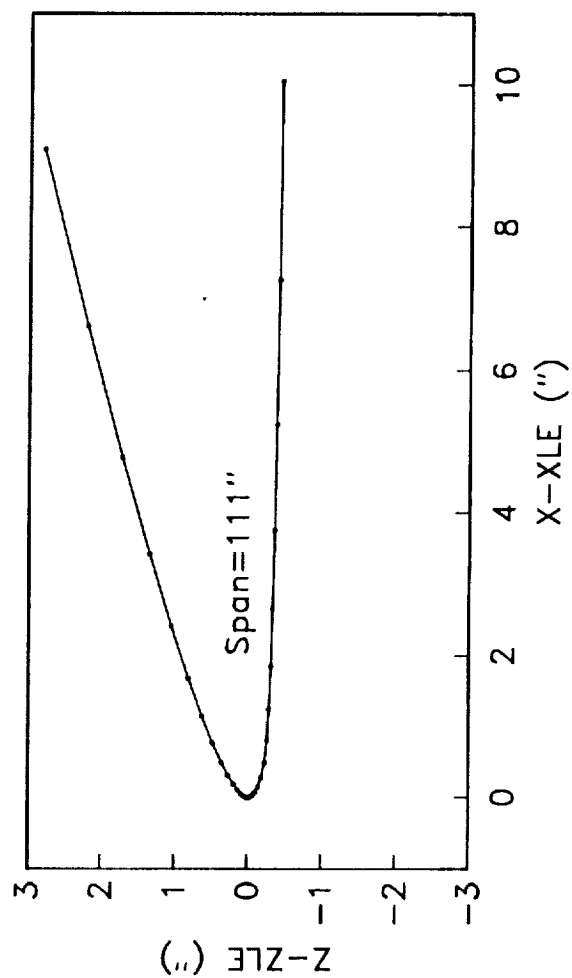
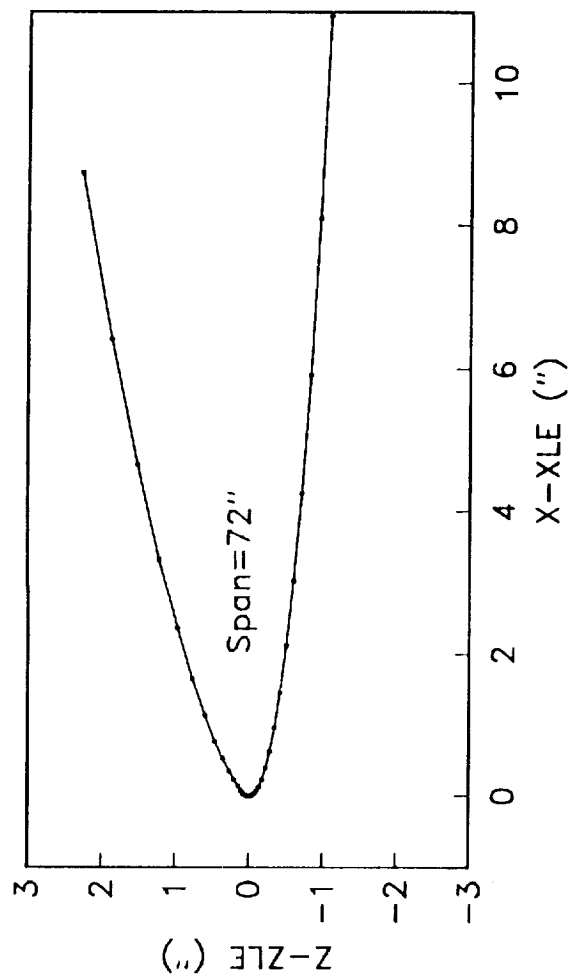
Conditions: $M_\infty = 1.6$, $\alpha = 2^\circ$, Altitude = 44,000 ft.
 No suction, adiabatic wall, laminar flow for $y > 40"$ spanwise

Summary: 1 million grid points, 20,000 surface points
 15 to 20 hrs. Cray Y-MP computation time

The region of interest is the boundary layer over the wing. This figure shows cross-sections of the wing parallel to the fuselage axis. Good resolution is required near the leading edge.

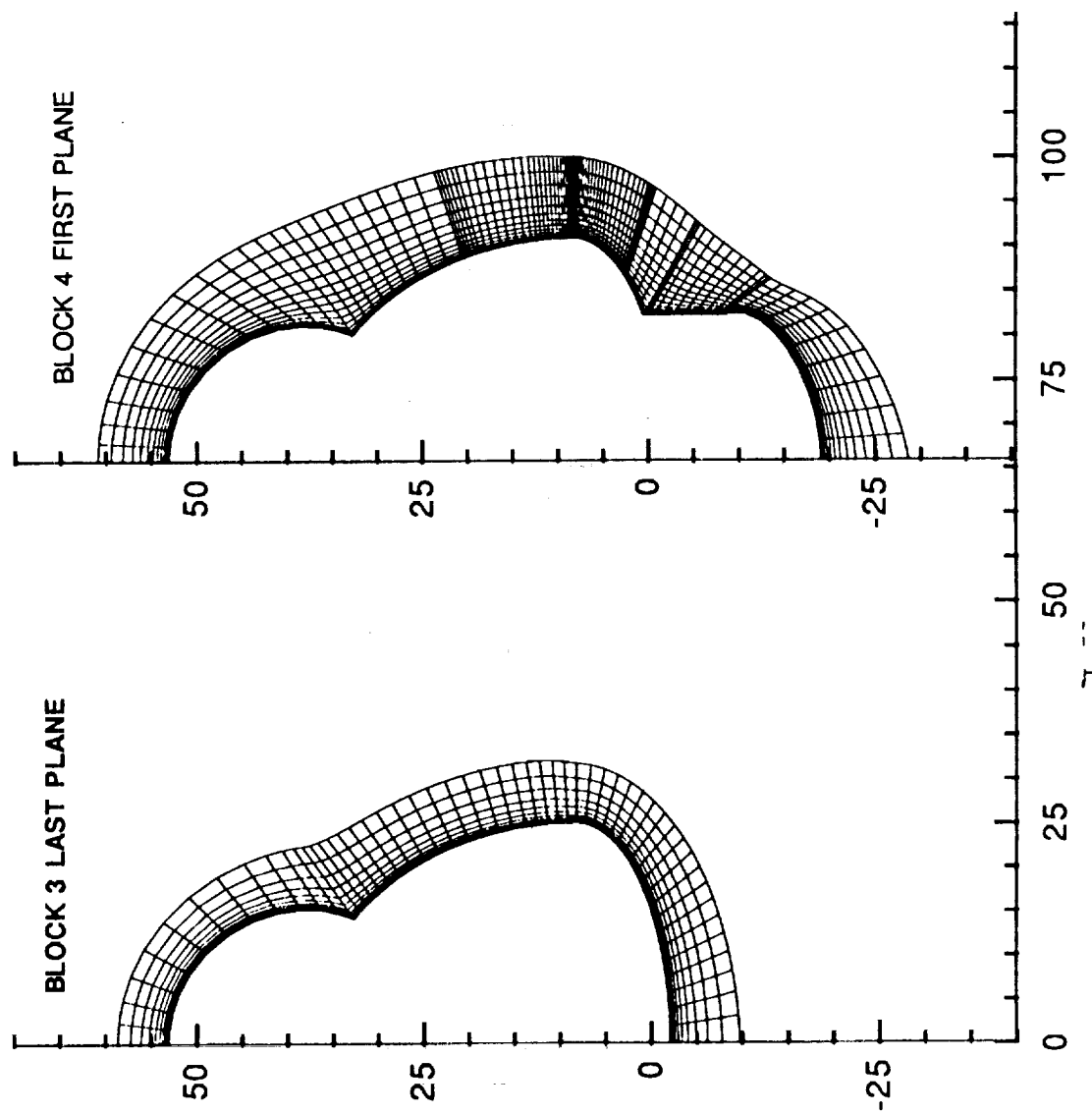


LFC Glove Cross-sections, Inboard & Outboard



This figure shows the viscous zones in the Block 3 — Block 4 interface. The grid clustering in Block 4 is changed to allow enough grid lines to cover the wing area. Solution in Block 3 is interpolated to the Block 4 plane. This assumes that the engine inlet is flow-through type and there is no upstream influence.

BLOCK INTERFACE AT F16XL ENGINE INLET



A list of runs for the F16XL configuration is given here. The conditions correspond to a few selected experimental flight conditions. Euler and Navier-Stokes runs have been made and the results have been applied to the stability analysis code to calculate the n-factors with and without boundary-layer suction.

F16XL CALCULATIONS

- Space Marching Euler (CFL3DE)
 - $M=2$, $\alpha=4^\circ$
 - $M=1.58$, $\alpha=2.019^\circ$ ($M=1.6$, $\alpha=2$ case)
- N-S (CFL3D)
 - $M=1.58$, $\alpha=2.019$, Alt=43,735 ft., without suction
 - $M=1.58$, $\alpha=2.019$, Alt=43,735 ft., with suction
 - $M=1.702$, $\alpha=2.268$, Alt=35,033 ft., turbulent
- B-L STABILITY (COSAL)
 - $M=1.58$, $\alpha=2.019$, Alt=43,735 ft., without suction
 - $M=1.58$, $\alpha=2.019$, Alt=43,735 ft., with suction



This figure shows the pressure coefficient contours on the F16XL upper surface. Euler solution from two space-marching codes are shown. Good agreement has been obtained. This figure also shows the location at which the canopy trailing edge shock will interact with wing boundary layer.

F16XL WING UPPER SURFACE, $M_\infty=2.0$, $\alpha=4^\circ$

Pressure Coefficient

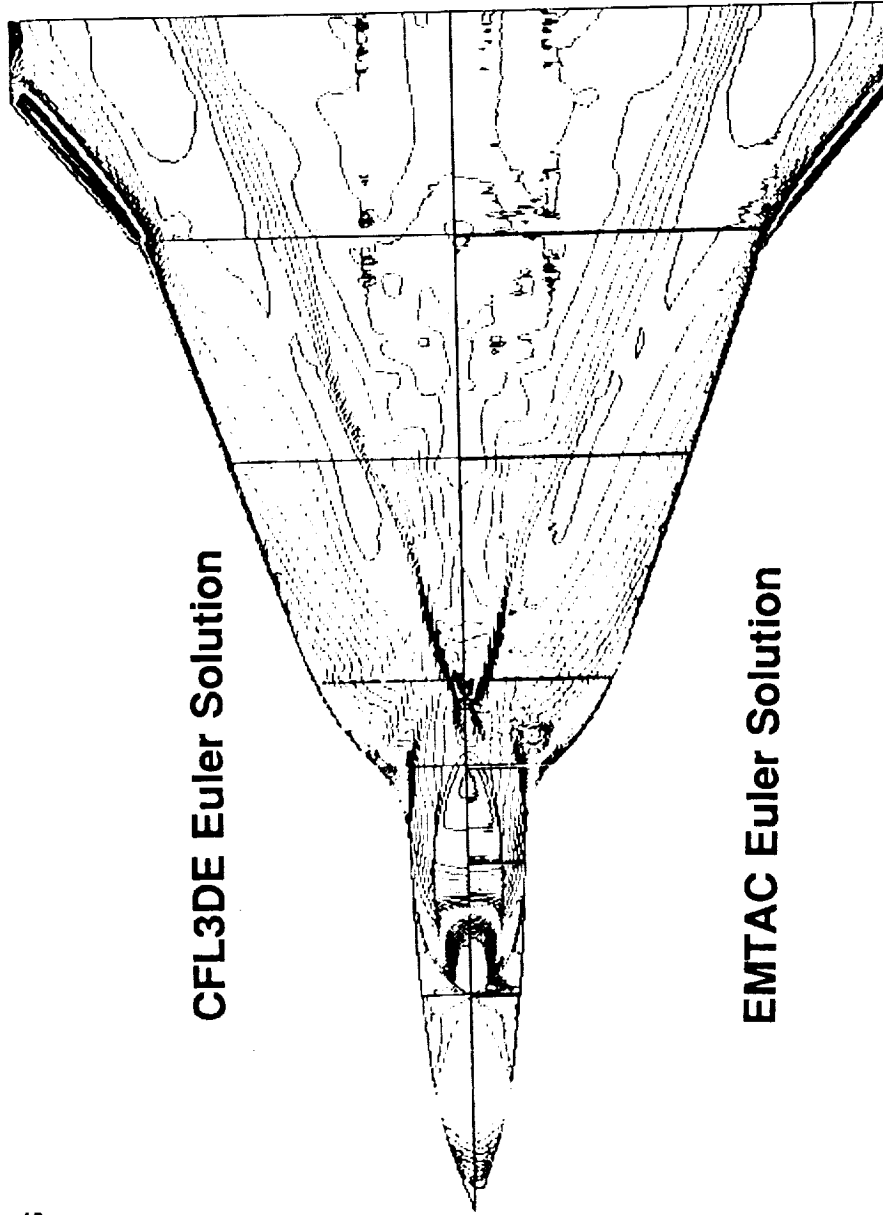
CONTOUR LEVELS

-.20000
 -.18000
 -.16000
 -.14000
 -.12000
 -.10000
 -.08000
 -.06000
 -.04000
 -.02000
 0.00000
 0.02000
 0.04000
 0.06000

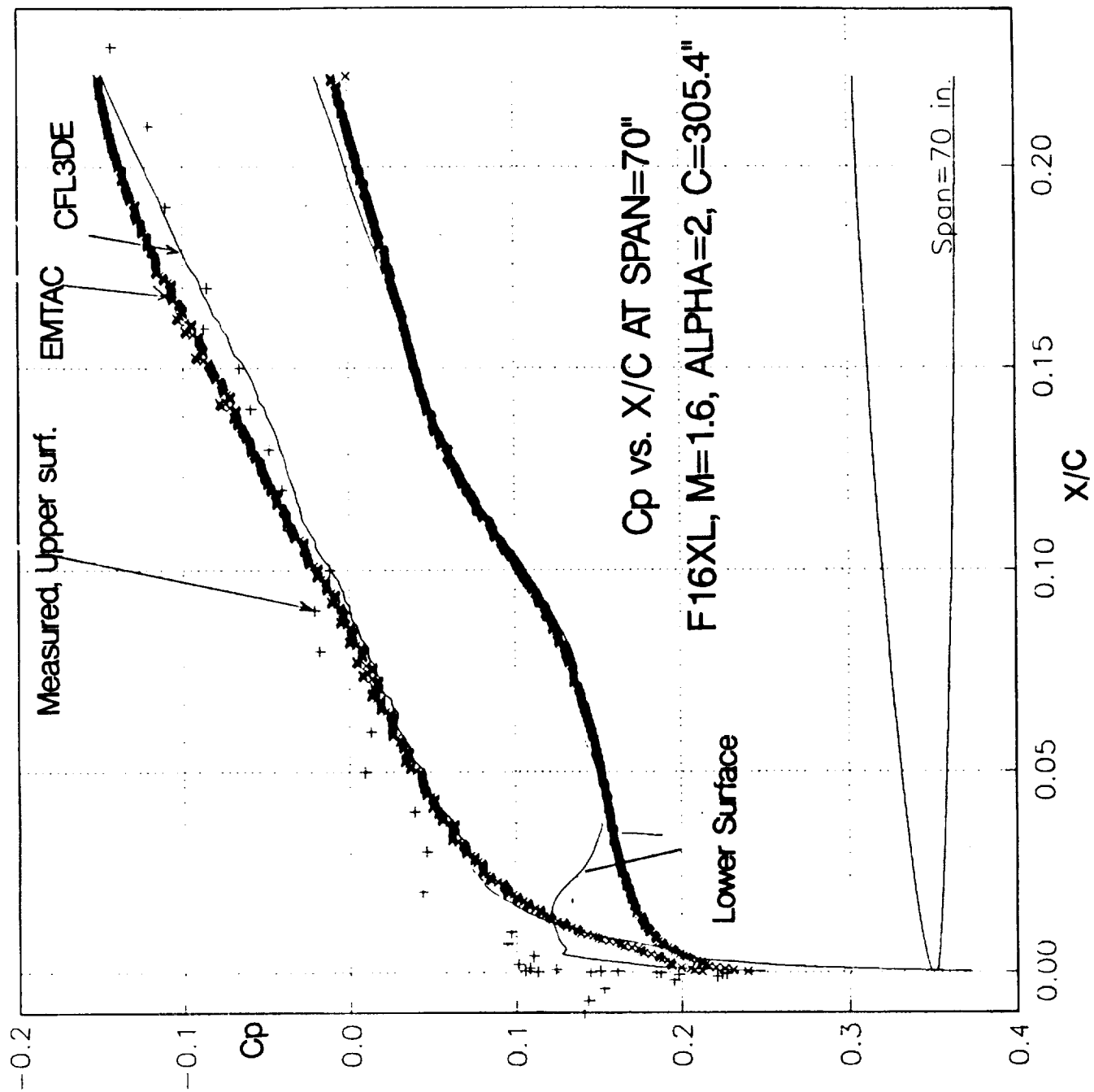
0.10000
 0.16000
 0.18000
 0.20000
 0.22000
 0.24000
 0.26000
 0.28000
 0.30000

CFL3DE Euler Solution

EMTAC Euler Solution

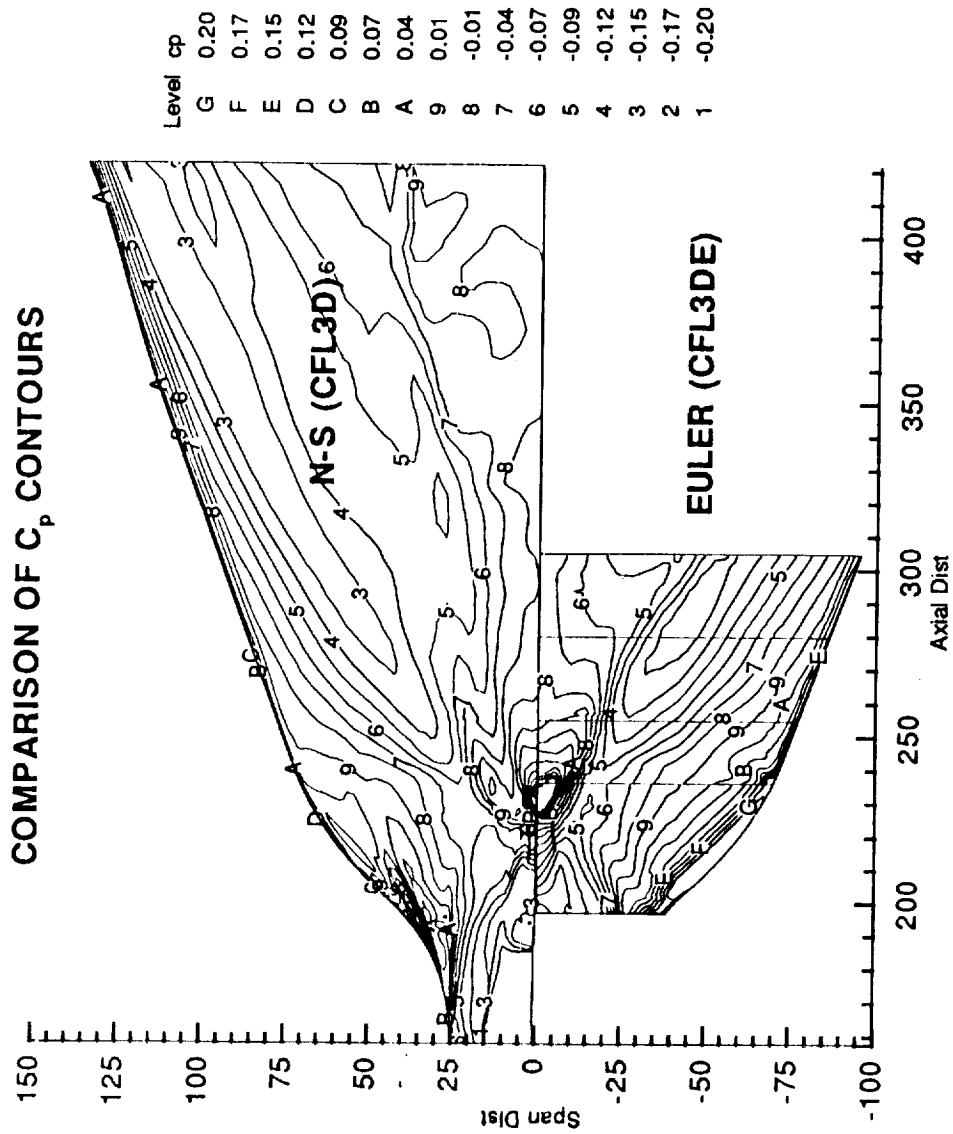


Comparison of C_p values at span of 70" corresponding to the two calculations is shown here. Except for some differences very close to the attachment line, the two results compare well with the measured values which are also shown.



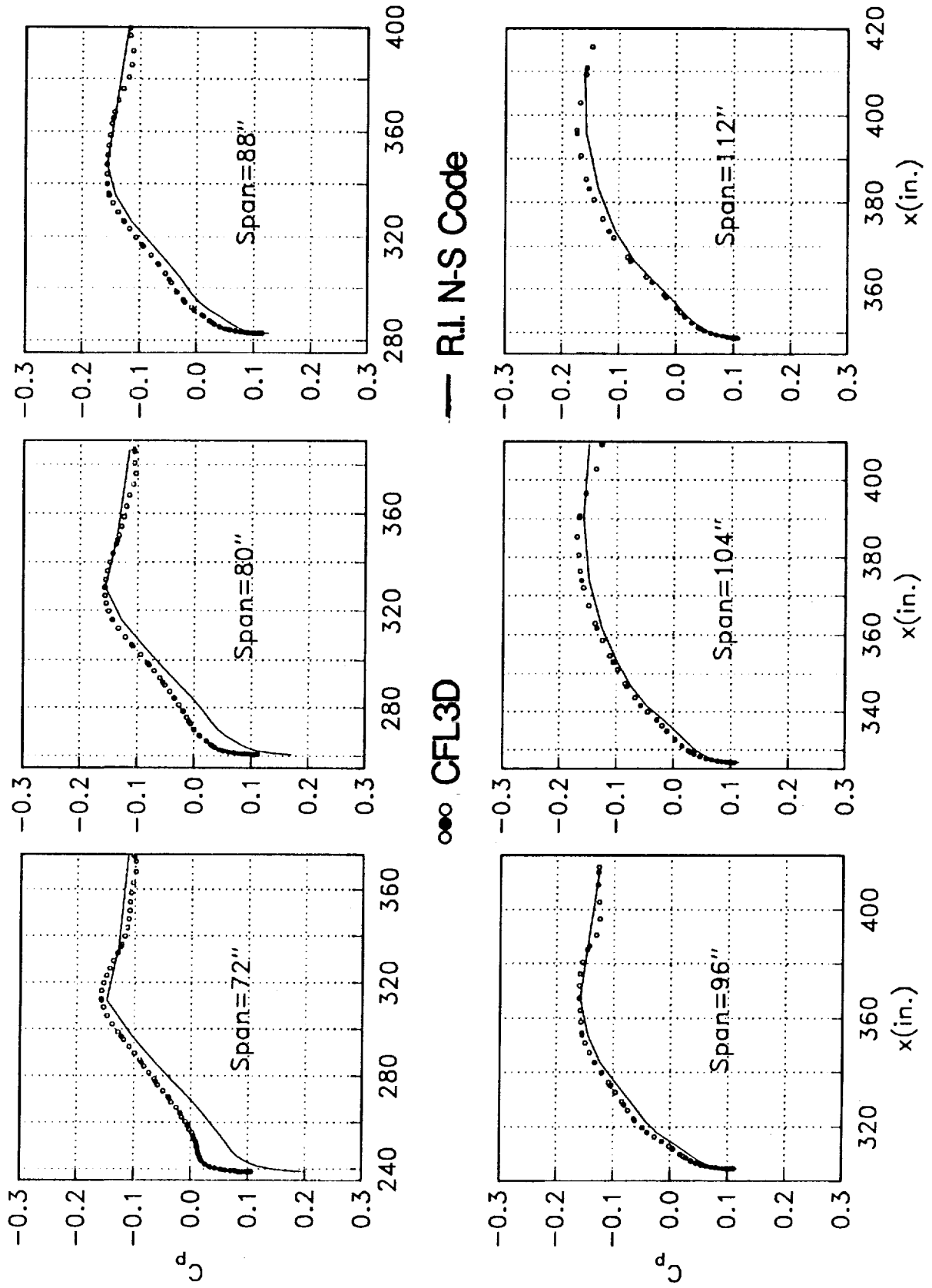
This is a comparison of the surface C_p contours from the Navier-Stokes and Euler calculations. The trends are quite similar, except that the shock off the canopy trailing edge is more diffused in the N-S calculation. The Navier-Stokes calculation also predicts lower values of C_p , or larger acceleration in the leading edge region.

COMPARISON OF C_p CONTOURS



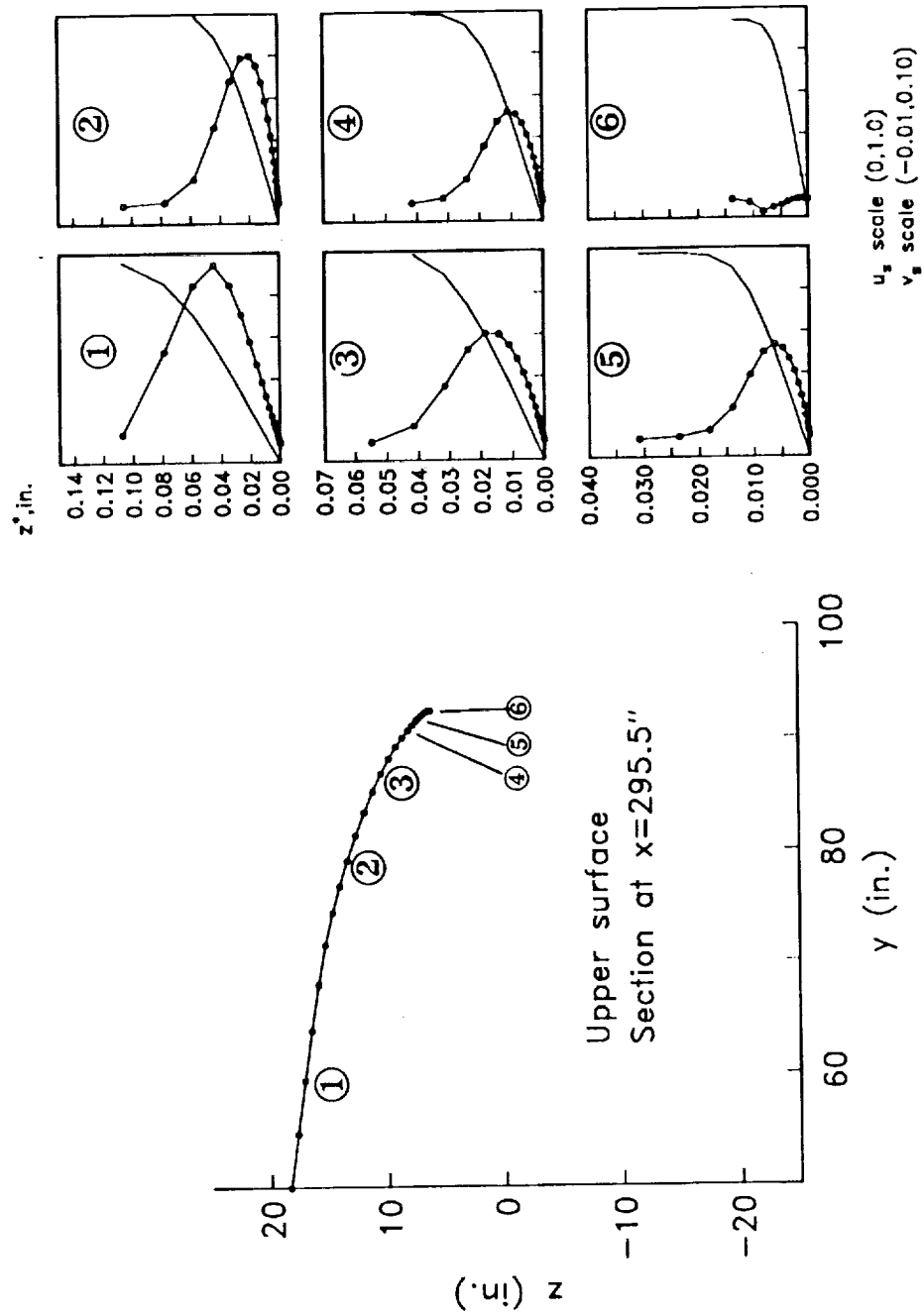
This is a comparison of the surface C_p variation in the chord direction at several span locations on the wing. The symbols correspond to the CFL3D calculation and the solid lines are the results from computation done at Rockwell Int'l. The inboard stations show some differences in the C_p variation near the leading edge. This is presumably resulting from the flow conditions existing in the forward part (fillet area) of the wing. Turbulent flow is assumed in this area of the wing close to the fuselage.

Chordwise Cp Variation, F16XL Upper Surface, M=1.6, Alpha=2°



This figure shows the streamwise and crossflow velocity profiles at a lateral section of the wing at mid-glove location. Station 6 is close to attachment point, showing near-zero crossflow. The crossflow rapidly increases away from this point. A maximum crossflow of about 8% occurs on the glove area, for this section.

F16XL LFC GLOVE MID-SECTION PROFILES



The eventual application of the meanflow solution is in B-L stability analysis. An interface program handles the conversion of the N-S solution to B-L oriented contravariant velocities along surface normals required by the linear stability program.

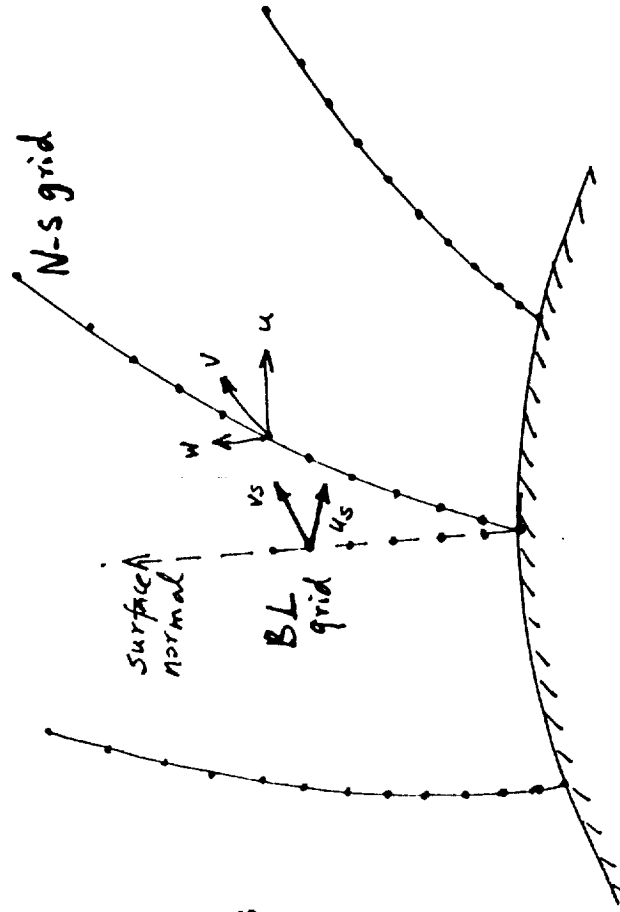
INTERFACE BETWEEN N-S and BL STABILITY PROGRAMS

N-S Solution

- u, v, w Cartesian velocities at N-S grid cell centers

B-L Stability Program

- requires contravariant velocity profiles along surface normals.



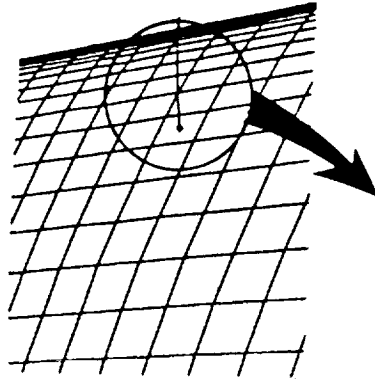
Since the N-S grid is highly clustered within the boundary-layer, certain approximations can be made in the interface program regarding local normals and normal distances. In this program, the boundary layer edge is located by looking at the absolute velocity and its gradient. The Cartesian velocities are then projected in edge streamline direction and an orthogonal crossflow direction.

INTERFACE BETWEEN N-S and BL STABILITY PROGRAMS (Cont'd.)

Approximation

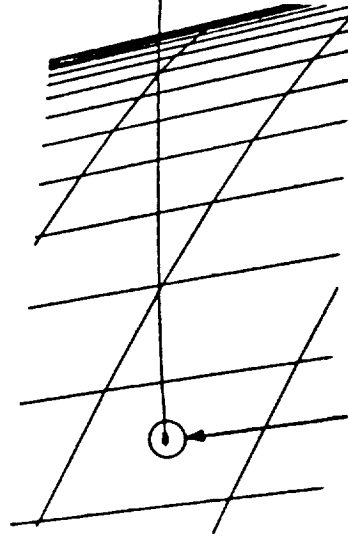
- Viscous solution along a cell center ζ line assumed to be along surface normal, at corresponding normal distances.
- Projection of cell-center points in the viscous layer stays within the corresponding grid cell.

A typical N-S surface grid with a ζ grid line from cell center



Implementation

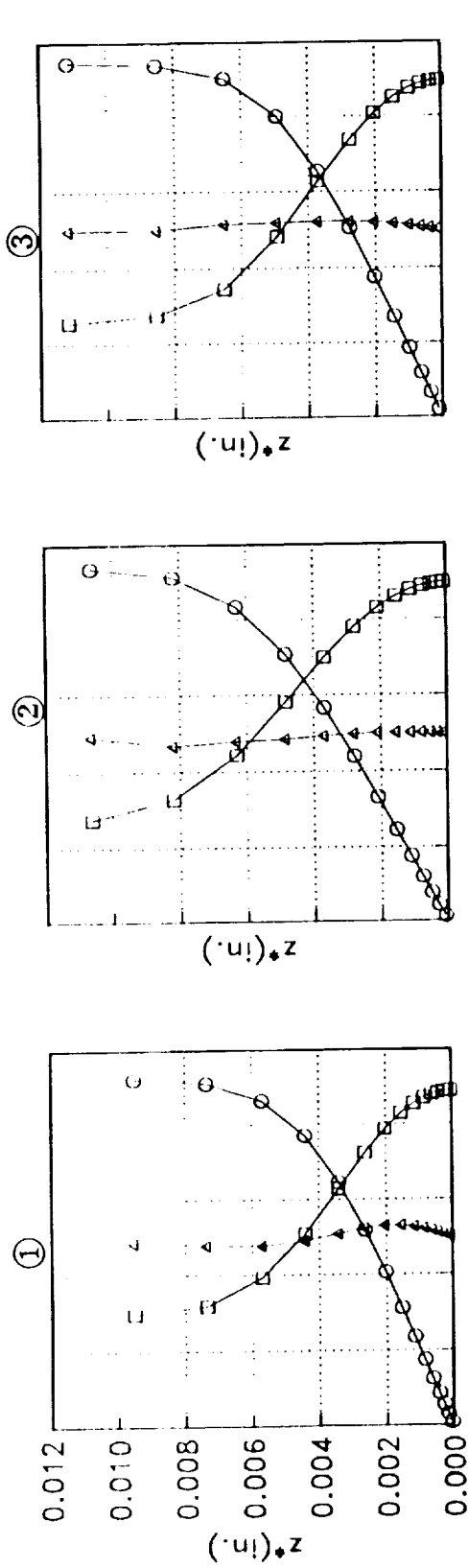
- Calculate normal distances based on cell-center surface normals.
- Locate B-L edge by a criterion such as, $u_{abs} > 0.9$ AND $\delta u_{abs} / \delta \zeta < 0.01$ of maximum in profile.
- Convert (u, v, w) Cartesian velocities to (u_s, v_s) on a body-oriented or edge-streamline-oriented grid.
- Also calculate BL/Transition global quantities such as δ^* , $\delta_{0.99}$, Re_{C-F} , Re_θ , % crossflow.



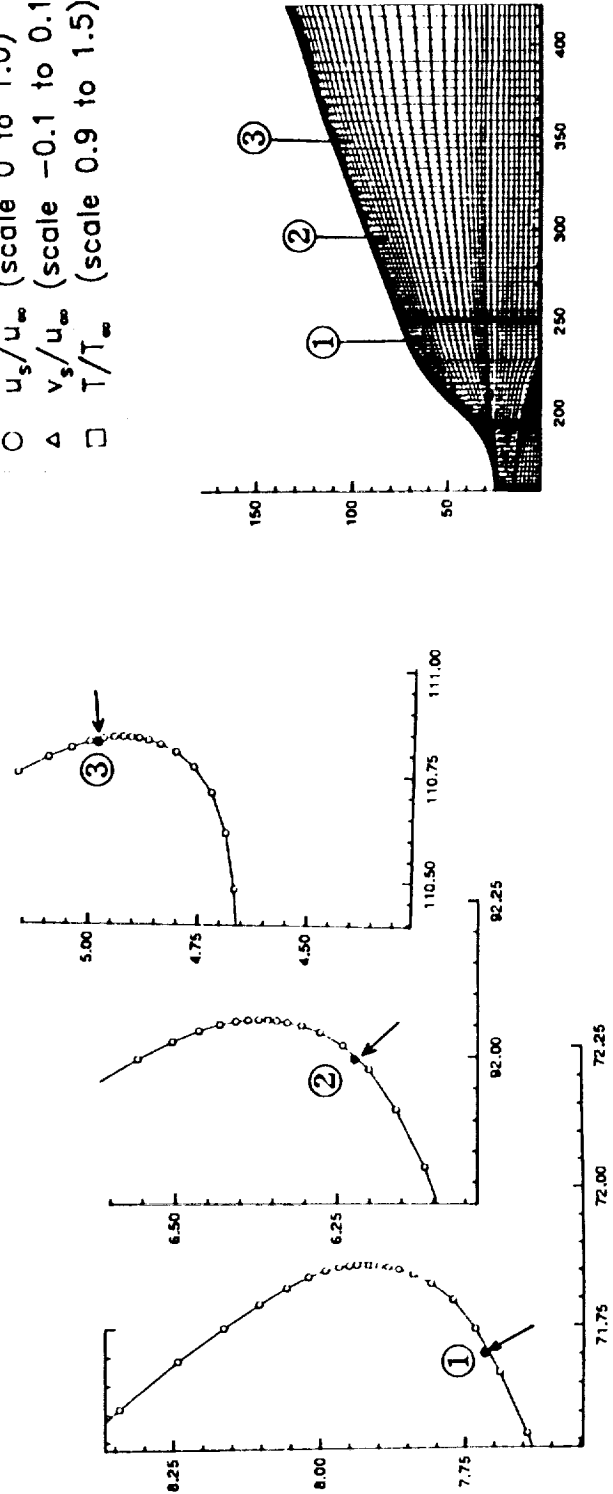
First 20 points off the surface enclosing the boundary layer

The interface program is useful in looking at boundary-layer type of profiles on the wing. This figure shows the location of the attachment line and the velocity and temperature profiles on the attachment line at three lateral sections of the wing.

F16XL ATTACHMENT LINE PROFILES FROM N-S/COSAL INTERFACE

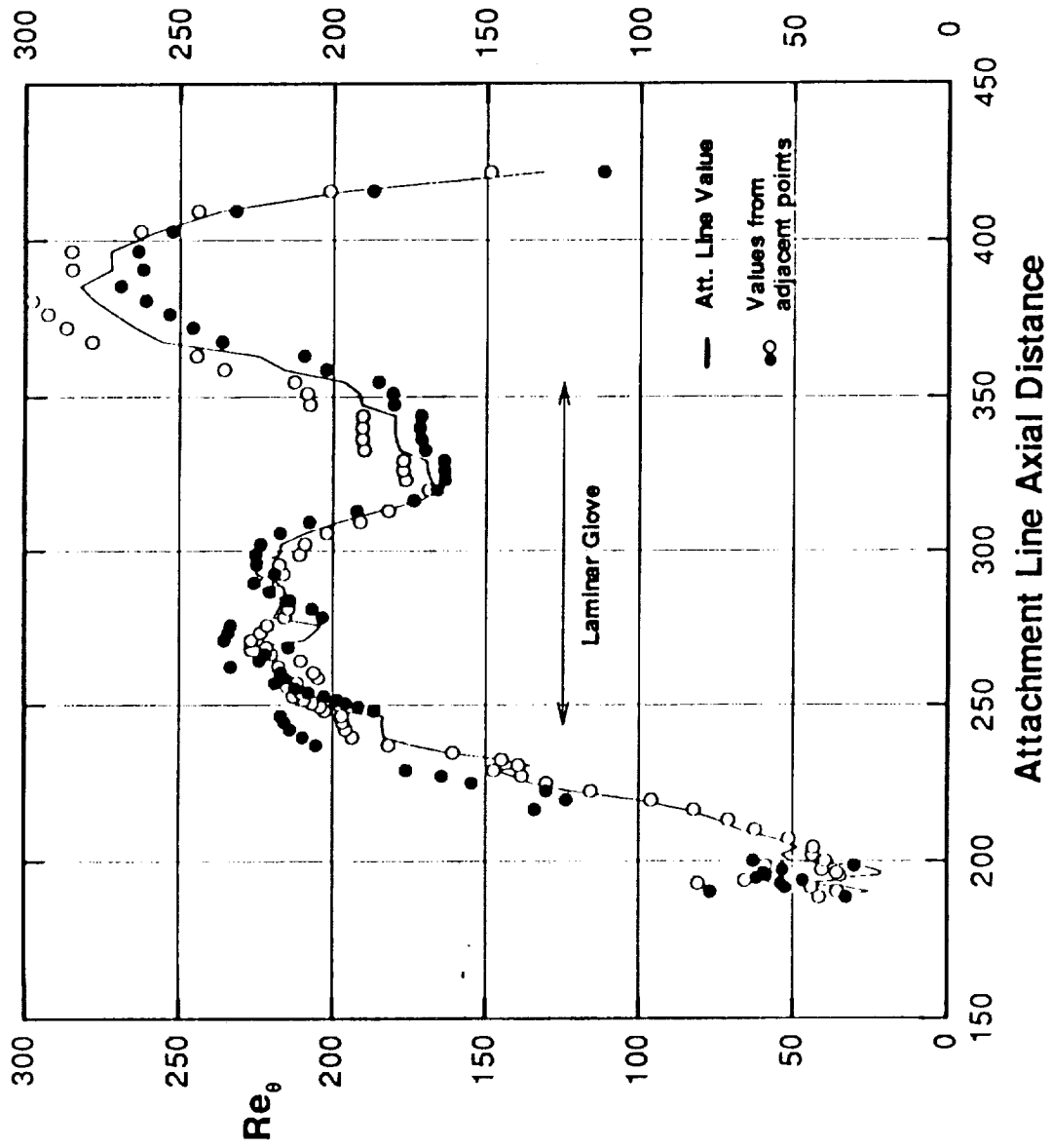


○ u_s/u_∞ (scale 0 to 1.0)
 △ v_s/u_∞ (scale -0.1 to 0.1)
 □ T/T_∞ (scale 0.9 to 1.5)



On the issue of attachment line stability, the momentum thickness Reynolds number is an important parameter. This figure shows the variation of Re_θ along the attachment line. There is a correlation of this value with the location of the attachment point relative to the leading edge.

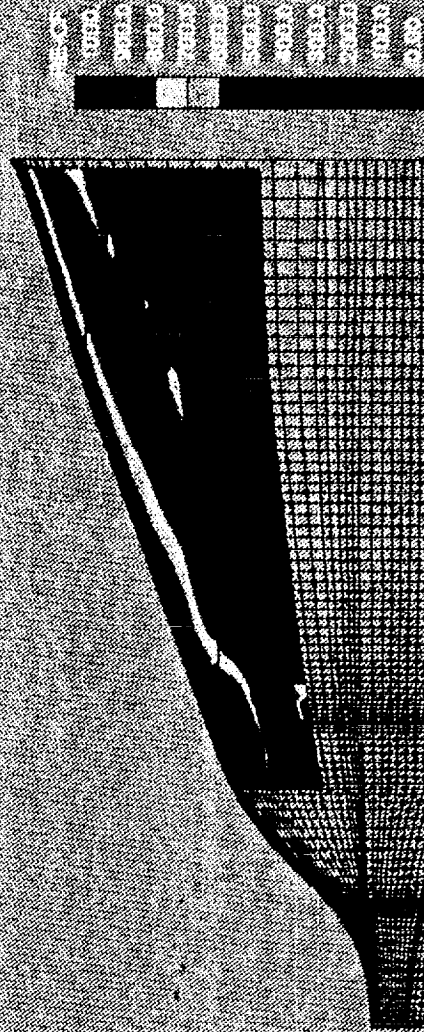
F16XL ATTACHMENT LINE Re_θ VALUES, $M=1.6, \alpha=2, h=44,000$ ft.



The crossflow Reynolds number based on the maximum crossflow and a length scale based on the crossflow profile is an important indication of crossflow instability. This can be calculated from the interface program. The figure shows contours of Re_{CF} on the upper surface of the wing ($M=1.6$, $\alpha=2^\circ$ case) with no suction. Based on a correlation, Re_{CF} of 300 represents the transition location for given freestream conditions.

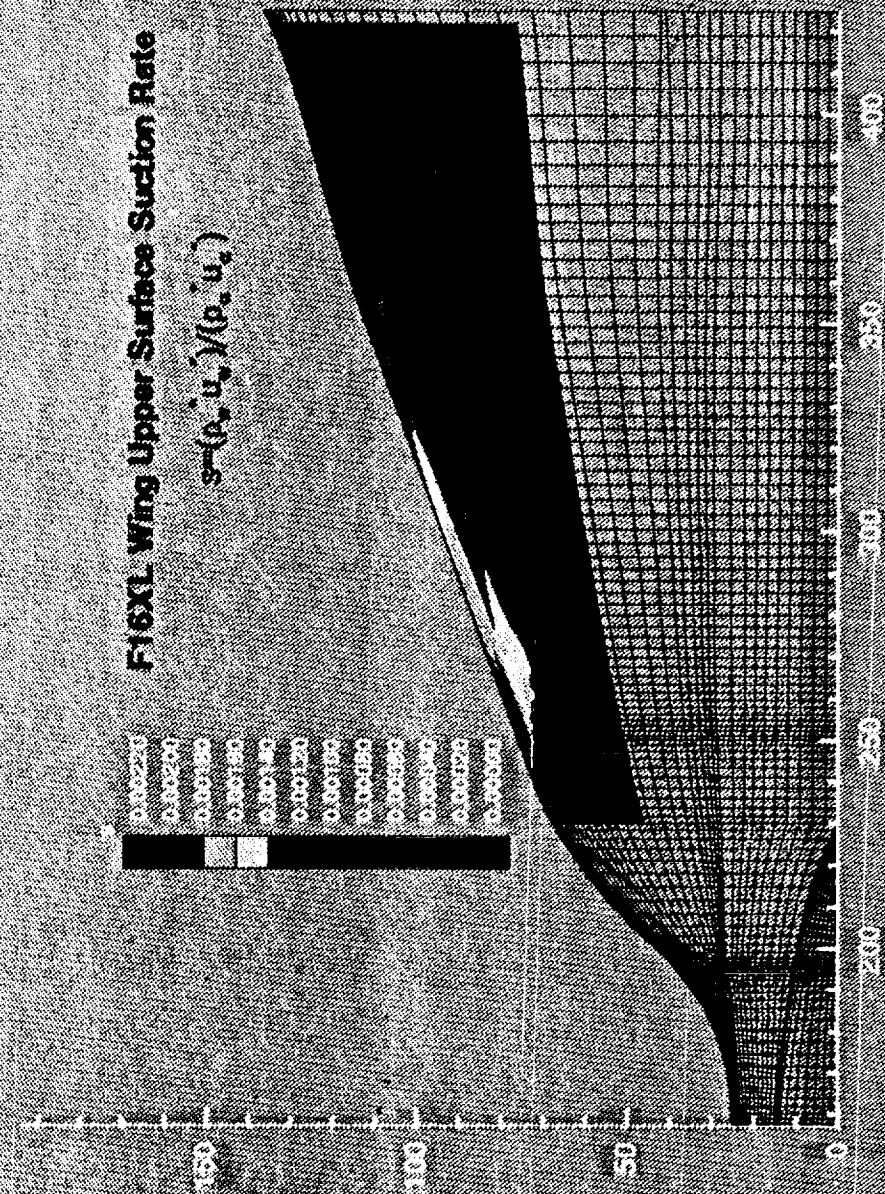
CROSS-FLOW REYNOLDS NUMBER

FIGURE 1-A, $\alpha=2$, CFL3D H-S Results



Red area indicates values > 1000

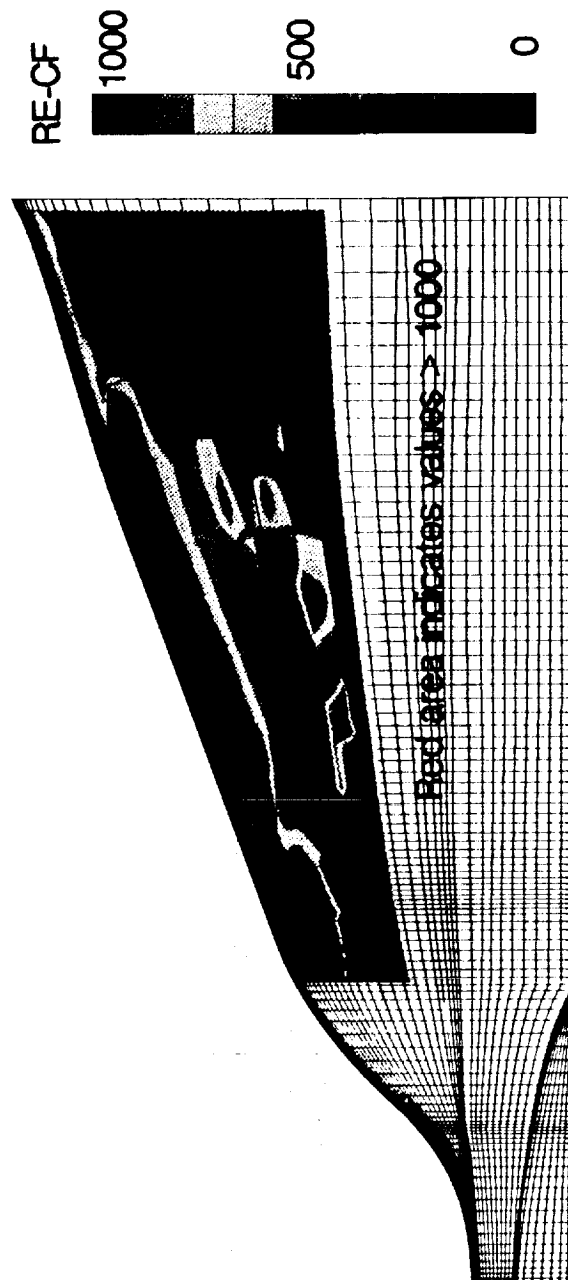
A subsequent calculation was made with suction on the upper surface of the wing. This figure shows the suction rates assumed for the calculation.



The crossflow Reynolds numbers resulting from applying suction are shown here. It can be seen that the transition location based on the Re_{CF} correlation is now further downstream. This indicates that stable laminar flow over a larger area of the LFC glove can be achieved with suction. Optimization of suction rates under different flight conditions and validation with flight measurements are ongoing activities.

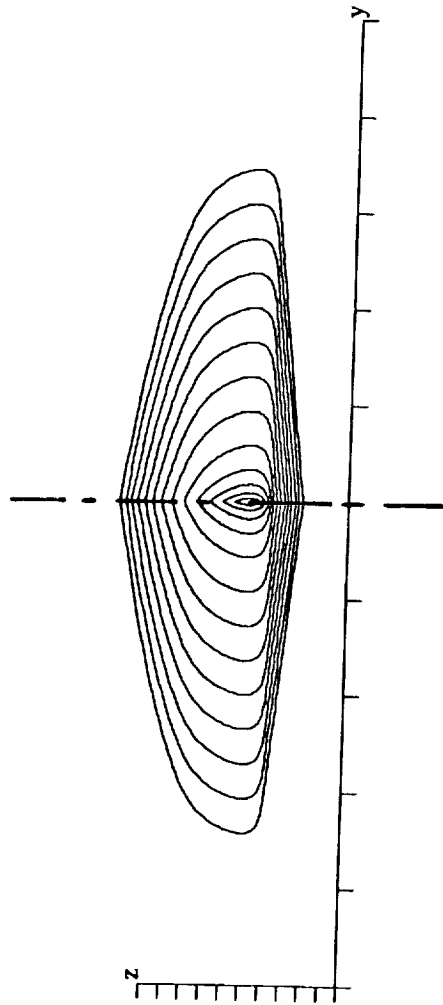
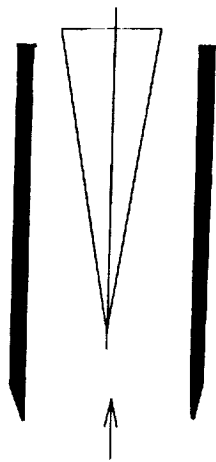
CROSS-FLOW REYNOLDS NUMBER WITH SUCTION ON LFC GLOVE

F16XL, $M=1.6$, $\alpha=2$, CFL3D N-S Results



The second case corresponds to the flow solution past a highly swept leading edge. Tests are planned in the supersonic low-disturbance tunnel at NASA LaRC at $M=3.5$ and different freestream conditions. This figure shows lateral sections of this model viewed from upstream.

77.123 deg. Swept LE MODEL
SS LDPT, $M=3.5$



This is a list of the Euler/N-S calculations on this geometry. More runs will be done during the course of the experiment for validation.

SUPERSONIC SWEPT L.E. CALCULATIONS

Conditions

M = 3.5
p = 39.33 psf
T = 162.3 °R
Re = 2.37 million/ft.

Runs

At $\alpha=0.145^\circ$:

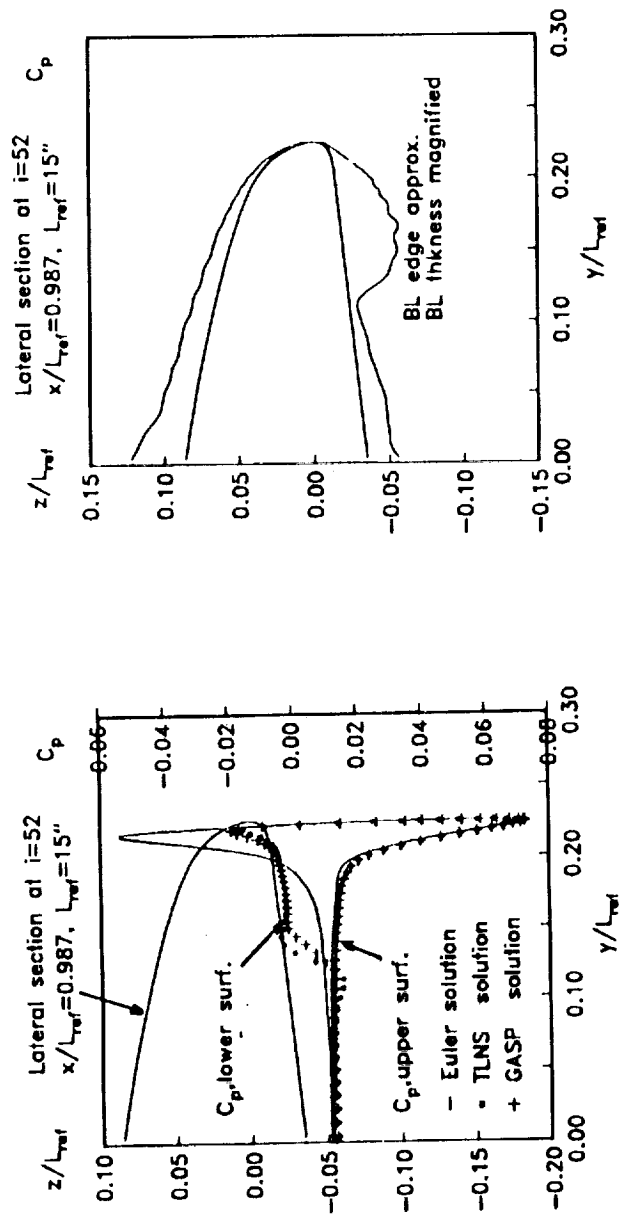
CFL3D Euler Coarse Grid (69x49x37)
TLNS3D Euler Coarse Grid
CFL3D Euler Fine Grid (69x97x37)
CFL3D N-S (69x97x61 grid)
GASP N-S
CFL3D N-S with optimised grid
3D-BL Attachment Ilne Region with Euler Cp

At $\alpha=3.0^\circ$:

CFL3D N-S

This shows a comparison of the C_p variation between Euler and N-S calculation for $\alpha=0.145^\circ$. The location is the near the last axial section of the computational grid. The upper surface C_p compares well, however, the lower surface C_p has a smaller peak in the N-S calculation. This has identified as due to cross-flow separation on the lower surface, resulting in larger boundary layer thickness values on the lower surface as shown.

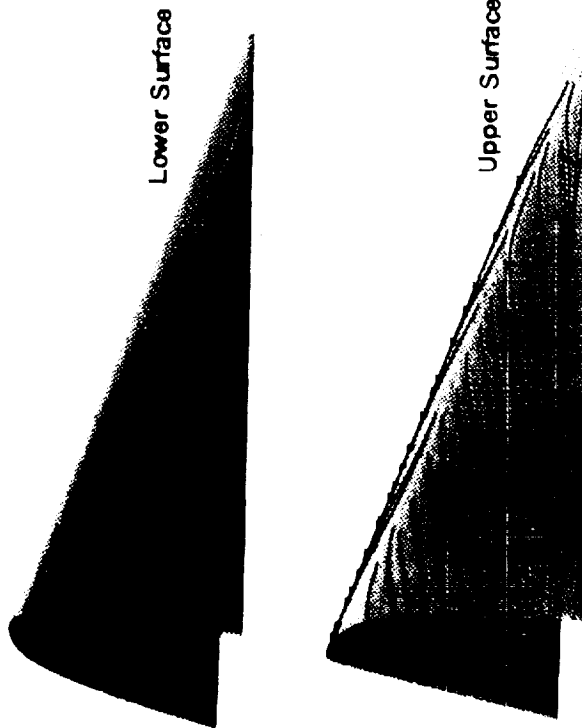
SWEPT WING L.E., Euler/N-S Cp Comparison



This figure shows limiting streamlines on the upper and lower surfaces of the swept leading edge, showing clearly the reversed crossflow on the lower surface.

Swept Leading Edge (F16XL) Limiting Streamlines

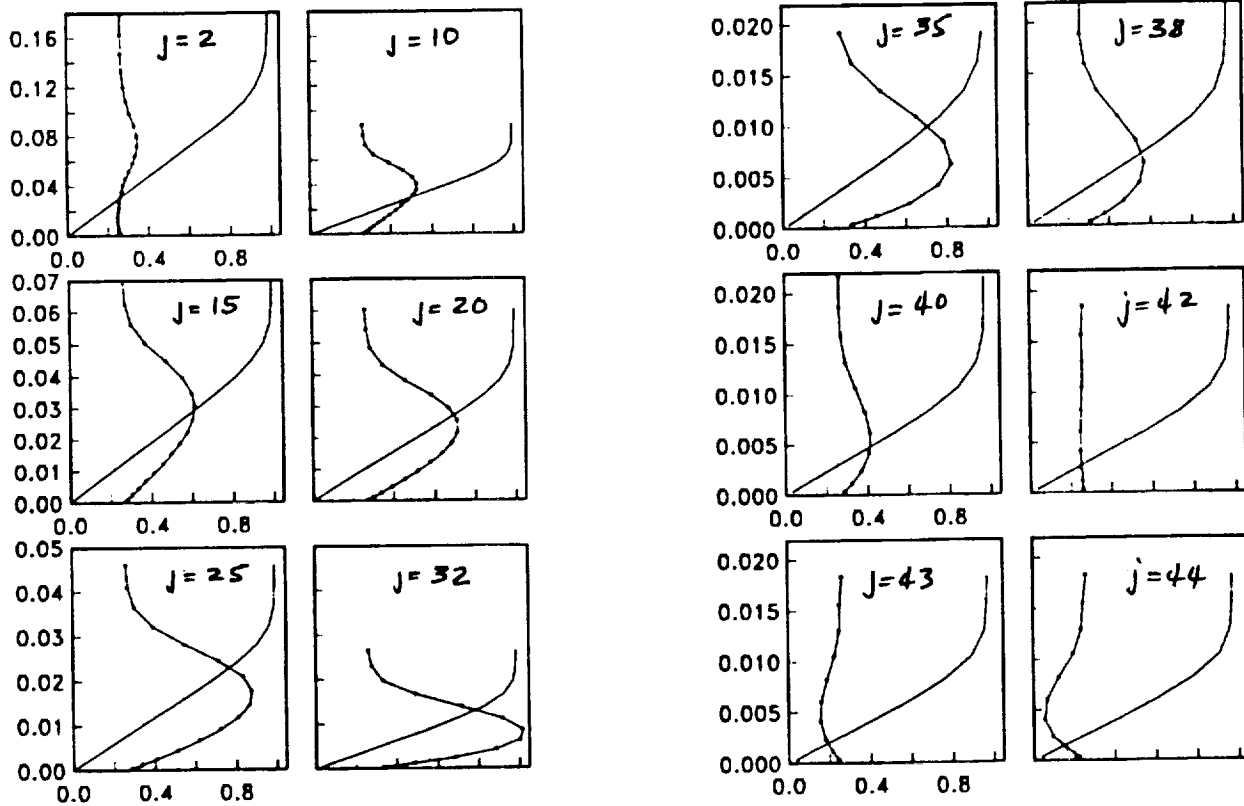
M=3.5, $\alpha=0.145$, $\Lambda=77.1$ deg, TLNS (CFL3D) Results



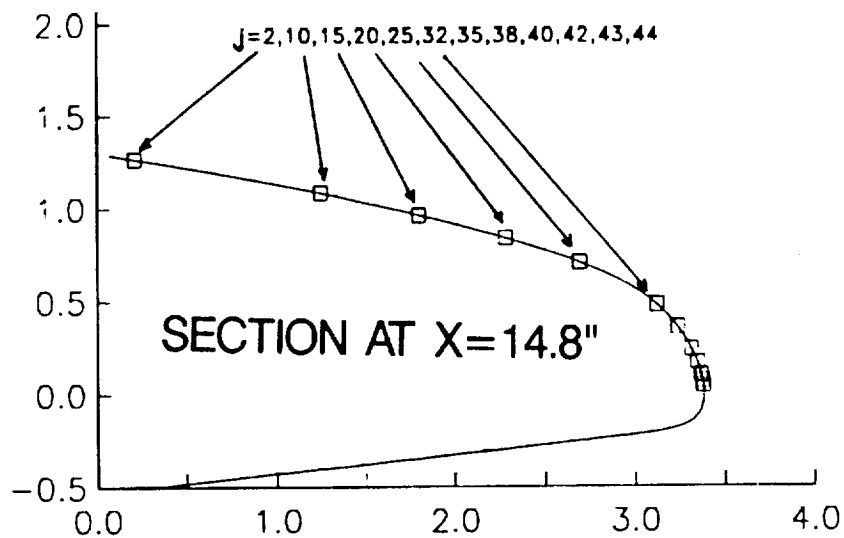
As seen before, the interface program can be used to look at profiles on the body, in streamline oriented coordinates. Shown are the streamwise and crossflow profiles at several locations on the upper surface

The attachment line is at the $j=42$ location, where the crossflow is nearly zero. Maximum crossflow location is at $j=32$. However, there are not points within the boundary-layer at all the profile locations, so a grid refinement was done, subsequent to this calculation

Streamwise and Crossflow Profiles

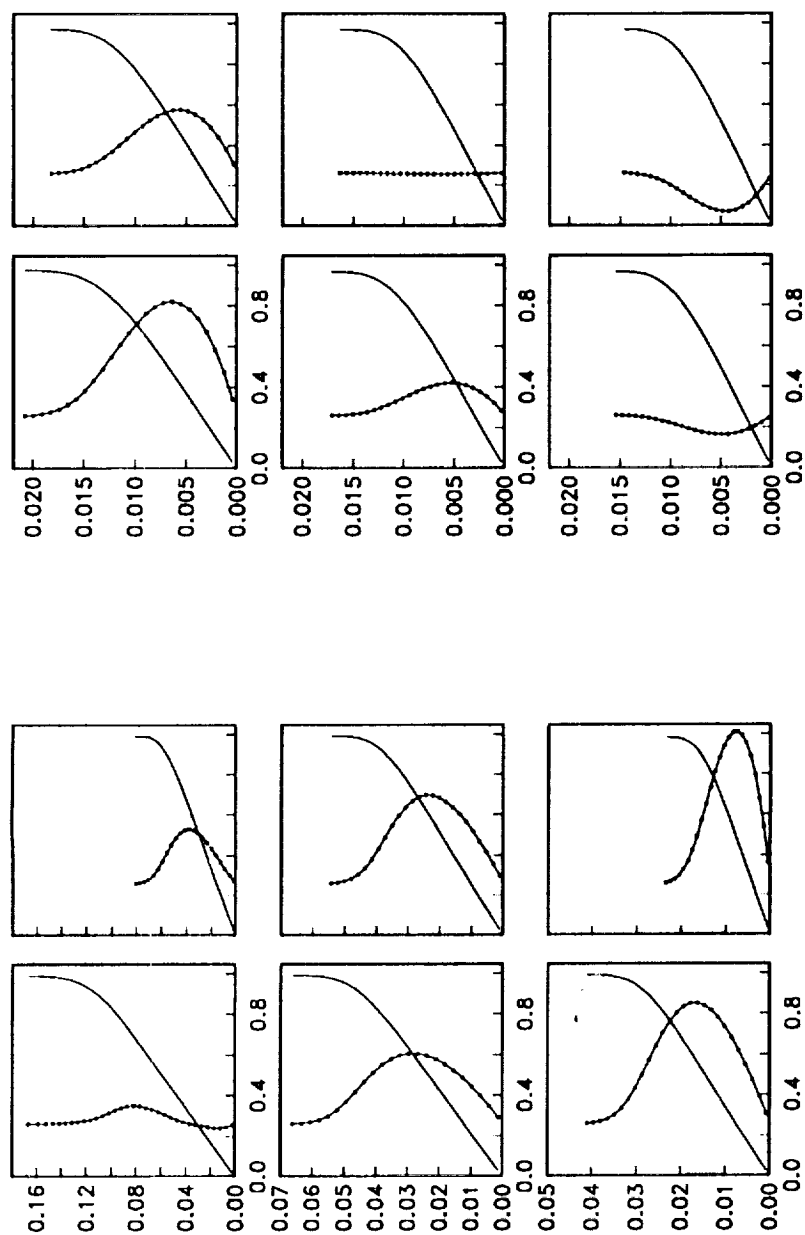


Scales: U_s (0.0,1.05) V_s (-0.03,0.09)



Grid refinement was done to have at least 30 points within the boundary layer, a minimum number required for stability analysis. The resulting profiles are much smoother and can be used directly in the stability analysis.

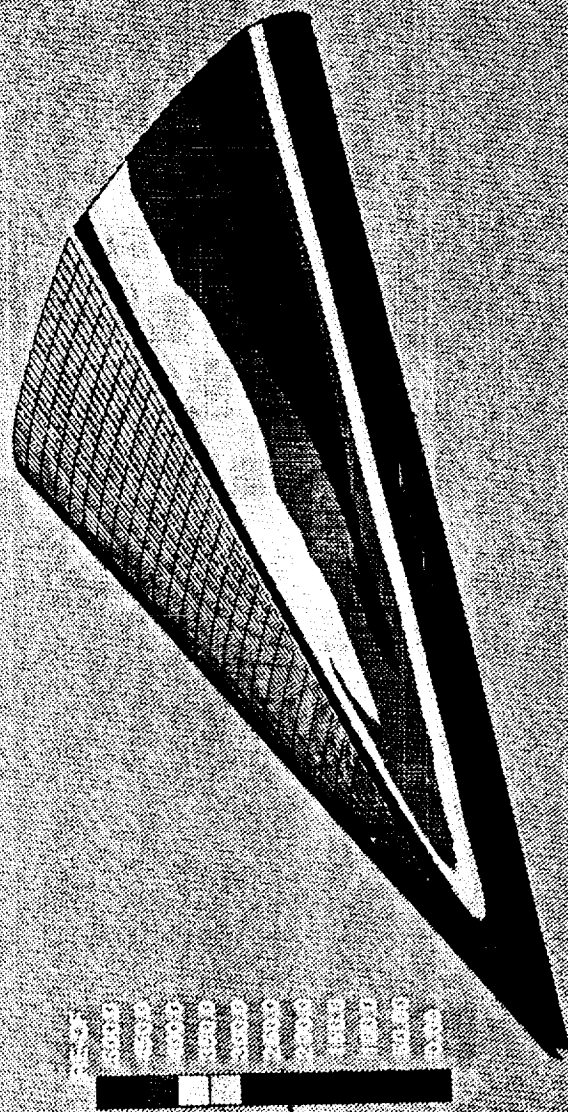
Streamwise and Crossflow Profiles (fine grid)



This figure shows the crossflow Reynolds number on the upper surface for $M=3.5$ $\alpha=0.145^\circ$ case. Correlation indicates that Re_{CF} of 500 is the limit for crossflow instability. This means that, with experimental conditions in the given range, varying conditions of boundary layer stability can be realized in the experiment.

CROSS-FLOW REYNOLDS NUMBER

Swept L.E. Wing, $M=3.5$, $\text{Alpha}=0.145$, CFL3D N-S Results



A set of procedures are now in place to obtain accurate meanflow solutions for supersonic boundary-layer stability analysis. Further validation with experimental measurements are planned.

CONCLUDING REMARKS

- Set of procedures now in place to numerically address the issue of transition in supersonic swept wings.
- Coupling of N-S results to linear stability analysis has been done. If grid resolution in B-L is adequate, accurate profiles for stability analysis can be generated.
- For simpler geometries (cone, ellipsoid, Inf. swept wing), 3D-BL solution is a cheaper alternative and has been implemented.
- Future work:
 - (1) Cross-check mean-flow solution with other codes for F16XL flow (TLNS3D, GASP).
 - (2) Analysis of stability calculation sensitivity to quality of meanflow solution.
 - (3) Validation with experiments for different flight conditions.

THIS PAGE INTENTIONALLY BLANK

Session XIII. Supersonic Laminar Flow Control

omit

Linear Stability Theory and Three-Dimensional Boundary Layer Transition
Robert E. Spall and Mujeeb Malik, High Technology Corporation

PRECEDING PAGE BLANK NOT FILMED

THIS PAGE INTENTIONALLY BLANK

**Linear Stability Theory
and
Three-Dimensional
Boundary Layer Transition**

513-02
11988

**R.E. Spall
M.R. Malik
High Technology Corporation
Hampton, VA**

**Theoretical Flow Physics Branch
NASA Langley Research Center
Hampton, VA**

PRECEDING PAGE BLANK NOT FILMED

The e^N Method for Transition Prediction/LFC Design

The e^N method involves computation of the total amplification of the various instability modes and correlating the transition onset with the most amplified mode.

The general conclusion from various applications of the e^N method is that when fundamental physical effects are properly accounted for, then $N \approx O(9-11)$ is a good predictor of transition for low background disturbances.

The method can also be used to study the effect of various parameters (such as Mach number, pressure gradient, wall heat and mass transfer, etc.) have on transition. However, note the comments on the next page.

THE e^N METHOD FOR TRANSITION PREDICTION/LFC DESIGN

- IN LOW DISTURBANCE ENVIRONMENT, THE e^N METHOD CAN BE USED TO PARAMETERIZE THE EFFECT ON TRANSITION:
 - MACH NUMBER
 - PRESSURE GRADIENT
 - WALL TEMPERATURE
 - WALL MASS TRANSFER
 - SWEEP
 - FLOW HISTORY
 - BODY/STREAMLINE CURVATURE
 - BODY ROTATION/DYNAMICS
 - BLUNTNES
 - FLOW CHEMISTRY
 - ANGLE OF ATTACK
 - REYNOLDS NUMBER(S)
 - SHOCK WAVES

Linear Stability Theory

There are four different instability mechanisms which are important in the stability of boundary layers. These include TS/first mode, second mode, crossflow and Goertler. The second mode is relevant only at Mach numbers above about 4. The first mode further consists of two different mechanisms, namely viscous (such as TS waves) and inviscid instability due to the presence of generalized inflection points in compressible boundary layers or in flows with adverse pressure gradients.

LINEAR STABILITY THEORY

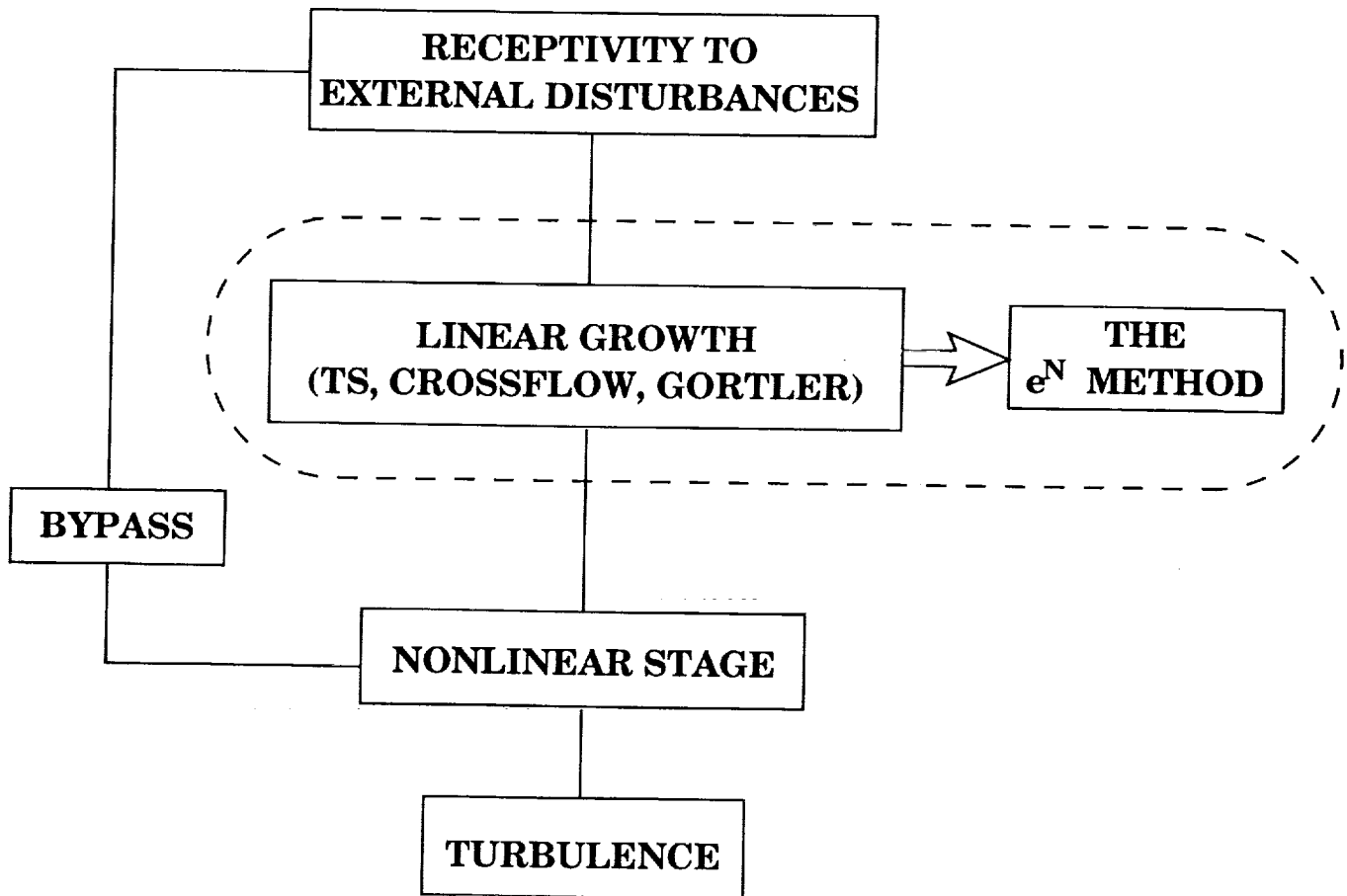
FOUR DIFFERENT INSTABILITY MECHANISMS

- FIRST MODE
 - VISCOUS (TS TYPE)
 - INVISCID RAYLEIGH (DUE TO GENERALIZED INFLECTION POINT)
- SECOND MODE
 - INVISCID INSTABILITY DUE TO SUPERSONIC MEAN FLOW RELATIVE TO DISTURBANCE PHASE VELOCITY ($|U - C|/a > 1$)
- CROSSFLOW
 - INFLECTIONAL INSTABILITY OF THE CROSSFLOW VELOCITY PROFILE
 - PRESENT IN 3-D FLOWS (BODIES AT ANGLE OF ATTACK, ETC.)
- GORTLER
 - CENTRIFUGAL INSTABILITY DUE TO CONCAVE CURVATURE (BODY/STREAMLINE)

Transition Process

Transition is a multi-step process involving receptivity (generation of instability waves), linear stability and non-linear breakdown to turbulence. Ideally, one needs to include all three stages in the transition prediction methodology. In this paper, however, we study some aspects of the linear growth of disturbances in both low and high speed boundary layers. In low disturbance environments, results of linear stability theory may be used to correlate the onset of transition with a wide range of parameters such as pressure gradient, Mach number, curvature, nose bluntness and wall temperature.

TRANSITION PROCESS



e^N Method—Caution

One always has to keep in mind the limitations that the method is subject to. Since the method is based upon linear stability theory, it obviously cannot account for situations where transition is strongly influenced by factors such as elevated levels of external disturbances, distributed roughness and other non-linear interactions. Furthermore, the effects of parameters such as wall cooling on the secondary instability may be different than on the primary instability and, therefore, the effect on transition of a certain parameter may not be the same as on linear stability.

If good experimental data are available, then it is possible to parameterize these effects in the form of correlations. An example is the correlation developed by Mack [1] for low speed flows to account for the effect of turbulence level on the N -factor at transition.

e^N METHOD - CAUTION

- TRANSITION INFLUENCED BY
 - ELEVATED STREAM/WALL DISTURBANCE FIELDS (INCL. PARTICULATES)
 - DISTRIBUTED ROUGHNESS
 - COMBINATION OF NON-LINEAR DISTURBANCE MODES
 - ORGANIZED MEAN VORTICITY (VORTICES)
 - SHOCK WAVES (EMBEDDED/IMPINGING)
- e^N METHOD CANNOT ACCOUNT FOR THESE EFFECTS
 - EMPIRICAL CORRELATIONS POSSIBLE (E.G. $N = -8.43 - 2.4 \ln Tu$, Tu IS TURBULENCE LEVEL, MACK (1977))

Crossflow Reynolds Number Criteria for High-Speed Flows

The value of the crossflow Reynolds number at transition for high-speed flows may be much higher than the upper limit of about 200 for incompressible flows. The value of 200 comes from the correlation of low-speed data, it is necessary to account for the compressibility effect in order to collapse the data from different Mach number flows. This may be achieved in various ways; for example, by defining an effective kinematic viscosity or by computing an effective length scale. Based upon some preliminary studies, we have found that an effective way to account for the compressibility effect is to rescale the characteristic length. Since the boundary-layer thickness δ varies (for adiabatic wall flows) with Mach number as:

$$\delta \propto 1 + \frac{\gamma-1}{2} M_e^2,$$

one way to scale out the Mach number effect is to reduce the crossflow characteristic length scale by a factor $1 + ((\gamma - 1)/2) M_e^2$. Thus the effective crossflow Reynolds number may be defined as:

$$\overline{Re}_{cf} = Re_{cf} / (1 + \frac{\gamma-1}{2} M_e^2) \quad (1)$$

The table below shows the values of \overline{Re}_{cf} along the transition onset trajectory for the Mach 8 flow over a 7° half angle cone at 2° incidence. It can be seen that the maximum value of the scaled crossflow Reynolds number is of $O(200)$, i.e., the same as for incompressible flows.

Experiments performed in the NASA Langley Mach 3.5 quiet tunnel show that the unscaled maximum crossflow Reynolds number at transition could be as high as 500-600. However, the scaled \overline{Re}_{cf} from Eq. (1) would be of $O(200)$. Similar results have been obtained for transition in supersonic flow past swept wings. Therefore, for compressible, adiabatic wall flows, it appears that Eq. (1) provides a reasonable *upper limit* for crossflow Reynolds number. Of course, transition may occur at lower \overline{Re}_{cf} due to the influence of other instability mechanisms. The fact that Re_{cf} is much higher for supersonic flows also implies that compressibility has a stabilizing influence on crossflow instability.

Crossflow Reynolds number criteria for high speed flows

$$\Re_{cf} = \frac{U_n \delta_{0.1}}{v_e}$$

At low speeds correlations show that $\Re_{cf} \approx 200$ represents an upper limit for laminar flow

boundary layer thickness varies as:

$$\delta \propto 1 + \frac{\gamma - 1}{2} M_e^2$$

scale out effect of Mach number by defining:

$$\overline{\Re}_{cf} = \frac{\Re_{cf}}{1 + \frac{\gamma - 1}{2} M_e^2}$$

A range of data up to Mach 8 correlates with $\overline{\Re}_{cf} \approx 200$

Mach 8 Flow Past a 7° Sharp Cone at 2° Incidence
Re/ft= 1 million

Values of Certain Parameters at the Estimated (N=10) Transition Location				
θ°	x (ft)	\Re_{cf}	$\overline{\Re}_{cf}$	f(KHZ)
0	8	0	0	80
48	6	1382	144	40
68	4.7	1690	172	35
110	3.8	2220	213	30
132	3.8	2440	228	20

Linear Stability Calculations for 3-D Boundary Layers

The ability to predict, using analytical tools, the location of boundary-layer transition over aircraft-type configurations is of great importance to designers interested in laminar flow control (LFC). The e^N method has proven to be fairly effective in predicting, in a consistent manner, the location of the onset of transition for simple geometries in low disturbance environments. This method provides a correlation between the most amplified single normal mode and the experimental location of the onset of transition. Studies indicate that values of N between 8 and 10 correlate well with the onset of transition.

For most previous calculations, the mean flows have been restricted to two-dimensional or axisymmetric cases, or have employed simple three-dimensional mean flows (e.g., rotating disk, infinite swept wing, or tapered swept wing with straight isobars). Unfortunately, for flows over general wing configurations, and for nearly all flows over fuselage-type bodies at incidence, the analysis of fully three-dimensional flow fields is required.

In the remainder of this paper we discuss results obtained for the linear stability of fully three-dimensional boundary layers formed over both wing and fuselage-type geometries, and for both high and low speed flows. When possible, transition estimates from the e^N method are compared to experimentally determined locations.

The stability calculations are made using a modified version of the linear stability code COSAL. Mean flows have been computed using both Navier-Stokes and boundary-layer codes.

Linear stability calculations

3D Boundary layers

Low speed flows

- Ellipsoid of revolution of fineness ratio 6:1

Mach number = 0.13

Reynolds number = 6.6×10^6

Angle of attack = 10 degrees

Boundary-layer was computed using analytic metric coefficients and edge velocity conditions

- Cessna Fuselage

Re/ft=1.3 million

Mach number = 0.27

Comparison with experimental of data of Vijgen.

- Flat plate/cylinder configuration

Re/ft = 800,000

$U_\infty = 125.4 \text{ ft/sec}$

Effects of both adverse and favorable pressure gradients

TS and crossflow instability

Linear stability calculations

3D boundary layers

High speed flows

- Analytic Forebody

Mach number = 2.0

Angle of attack = 2 degrees

Boundary layer edge conditions computed using space marching Euler option of CFD code GASP

- F16XL Laminar Flow Control Glove

Mach number = 1.6

Mean flow computed by V. Iyer using Navier-Stokes code CFL3D

- Dagenhart model for NASA Langley “quiet tunnel”

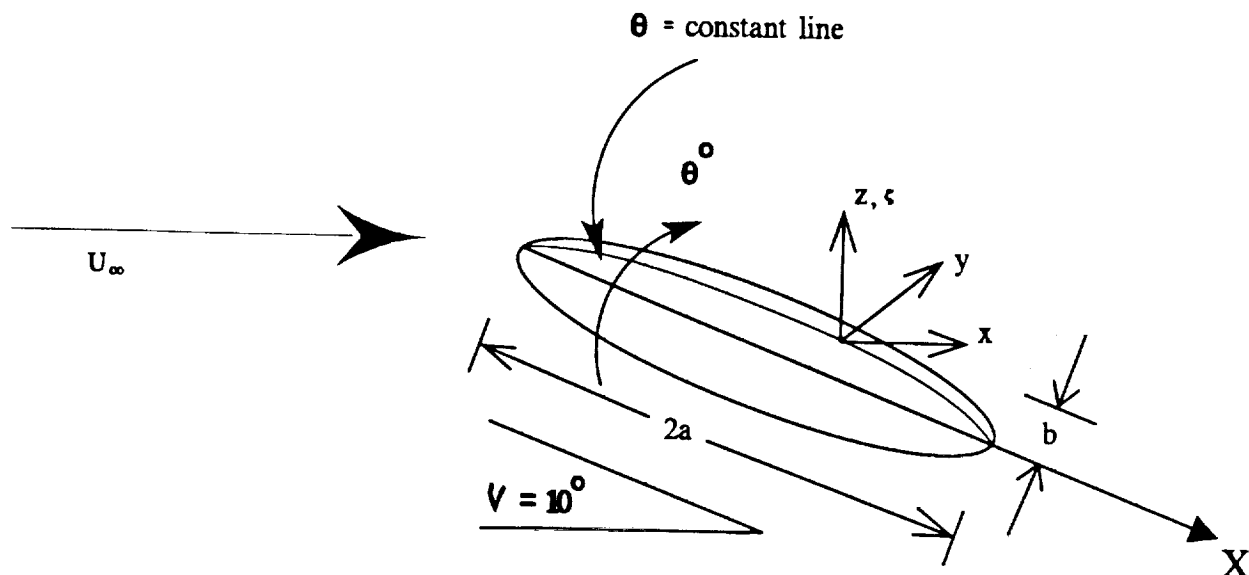
Mach number = 3.5

Mean flow computed by V. Iyer using Navier-Stokes code CFL3D.

Geometry and Coordinate System for Prolate Spheroid

The linear stability of the fully three-dimensional boundary-layer formed over a 6:1 prolate spheroid at 10° is investigated using the linear stability code COSAL. For this case, both Tollmien-Schlichting (TS) and crossflow disturbances are relevant in the transition process. The predicted location of the onset of transition using the e^N method compares favorably with experimental results of Meier and Kreplin [2]. Using a value of $N=10$, the predicted transition location is approximately 10% upstream of the experimentally determined location. Results also indicate that the direction of disturbance propagation is dependent on the type of disturbance, and consequently, on dimensional frequency. Results also indicate that $Re_{cf} = 180$ represents the upper limit for laminar flow (based on $N=10$).

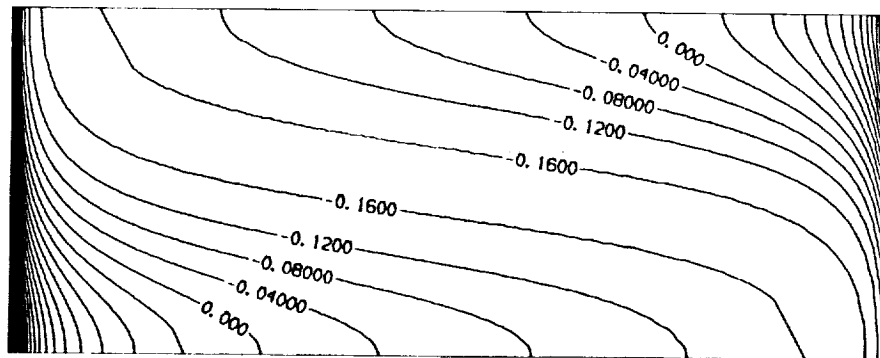
Geometry and coordinate system for prolate spheroid.



Contour Plot of Constant C_p on 6:1 Prolate Spheroid $M=0.132$, angle of attack= 10° , $Re=6.6 \times 10^6$

The analytic inviscid velocity distribution and metric coefficients were used in the solution of the boundary-layer equations. Here we present a contour plot of the distribution of C_p over the ellipsoid. Note that an adverse pressure gradient is encountered at approximately $\xi = -0.9$ on the leeward symmetry line and $\xi = 0.9$ on the windward symmetry line (where $-1.0 \leq \xi \leq 1.0$). This suggests that transition on the leeward symmetry line may take place much sooner than transition on the windward symmetry line, since boundary layers usually become highly unstable in regions of adverse pressure gradient.

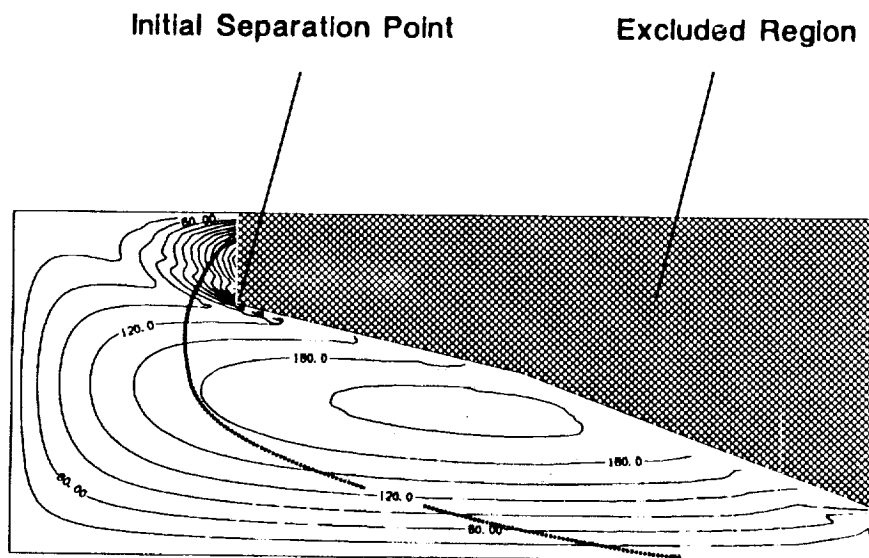
Contour plot of constant C_p on 6:1 prolate spheroid $M=0.132$, $\nu = 10^0$ and $Re = 6.6 \times 10^6$



Contour Plot of Crossflow Reynolds Number

The above figure indicates the boundary-layer computational domain, and also shows contours of constant Crossflow Reynolds numbers. The cross-hatched area has been excluded from the domain of the boundary-layer calculation (due to separation). Also indicated is the location of the initial separation point. Since transition takes place upstream of this point, the exclusion of the region is of no consequence here. The figure indicates a rapid increase in crossflow Reynolds number as the separation point is approached. This results from an increase in the crossflow length scale as the region of adverse pressure gradient is encountered near the leeward symmetry line. Note the occurrence of a local minimum in the crossflow Reynolds number just upstream of the initial separation point.

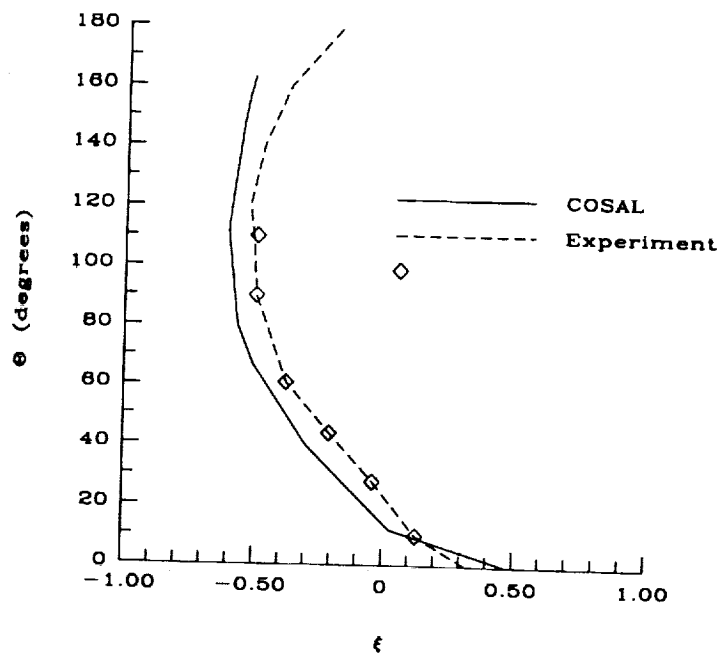
Contour plot of crossflow Reynolds number



Comparison of Theoretical (based on $N=10$) and Experimentally Determined Locations for the Onset of Transition

The transition front obtained using COSAL is compared with the experimental results of Meier and Kreplin [2]. Transition was assumed to occur at $N=10$. The overall agreement between theory and experiment is good. Near the windward edge ($\theta = 0^\circ$), where two-dimensional TS-type disturbances are responsible for transition, the predicted location of transition is about 10% downstream of the experimental results. For the flowfield at $\theta > 20^\circ$, for which instabilities are predominately of the crossflow type, the predicted transition front occurs approximately 10% upstream of the experimental results. The present results might be improved if the displacement thickness were taken into account when calculating the inviscid solution. In addition, the disturbances originating at higher values of θ follow highly curved trajectories, so that wavefront curvature effects may be important. If these effects were included, they would act in a stabilizing manner, and thus tend to shift the computed transition front downstream.

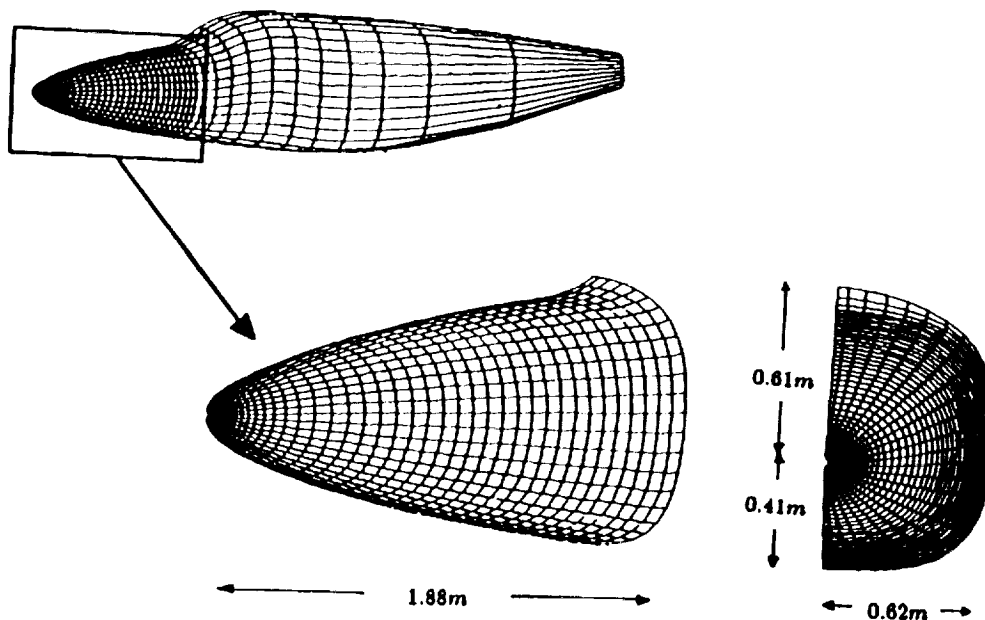
Comparison of theoretical and experimentally determined locations (Meier and Kreplin) for the onset of transition. Theoretical calculations based on a value of $n=10$.



Cessna Forebody Configuration Typical Inviscid Grid

The linear stability of the fully three-dimensional boundary-layer formed over a general aviation fuselage at 0° incidence is investigated. The free stream velocity was taken as 279 ft/sec and the free stream temperature as $T_\infty = 472^\circ \text{ R}$. The unit Reynolds number was 1.3 million. The location of the onset of transition was estimated using the N-factor method. The results are compared with existing experimental data [3] and indicate N-factors of 8.0 on the side of the fuselage and 3.0 near the top. Considerable crossflow exists along the side of the (asymmetric) fuselage, which significantly alters the unstable modes present in the boundary layer. The value of 3.0 along the top may be due to surface waviness, as suggested in Ref [3], where stability calculations using the axisymmetric analog method were performed.

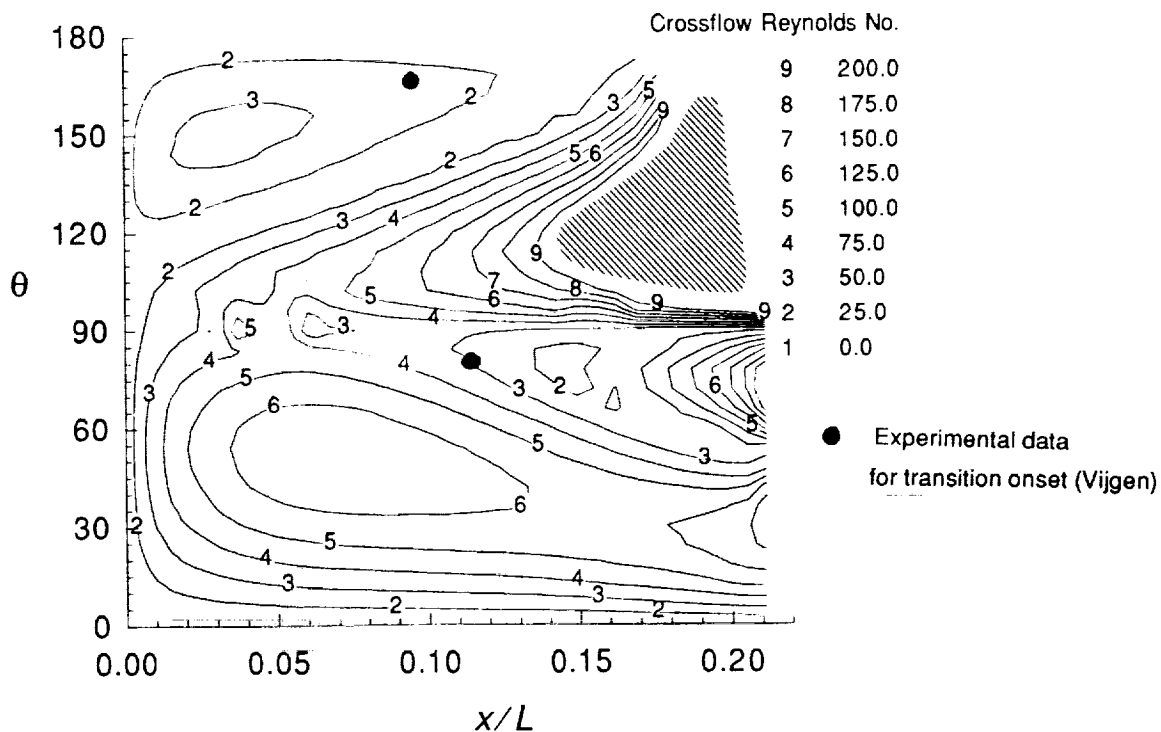
Cessna forebody configuration.
Typical inviscid grid.



Crossflow Reynolds Number Distribution for Cessna Fuselage

N-factors computed using linear stability theory are compared with experimentally determined transition location as given in Vijgen [3]. The contours were obtained from a series of calculations originating along neutral curves (for specific frequencies) at successive circumferential locations. Results for the frequencies which first reach $N=9$ are plotted. These frequencies varies from 1000 Hz in regions of relatively high crossflow, to 1800 Hz in regions of relatively low crossflow. In addition, since the "envelope method" is used, the disturbances which are evaluated at each successive streamwise location represent the most unstable mode. Whether or not this corresponds to the evolution of an actual disturbance within a boundary layer is unknown. The experimental data points, at streamwise points corresponding to transitional flow, are indicated on the figure. The detection of transition onset was determined through surface hot-film anemometry [3]. We also computed a maximum value of $N=3.0$ at the location of the upper experimental data point. This corresponded to a higher frequency than those which first resulted in $N=9$.

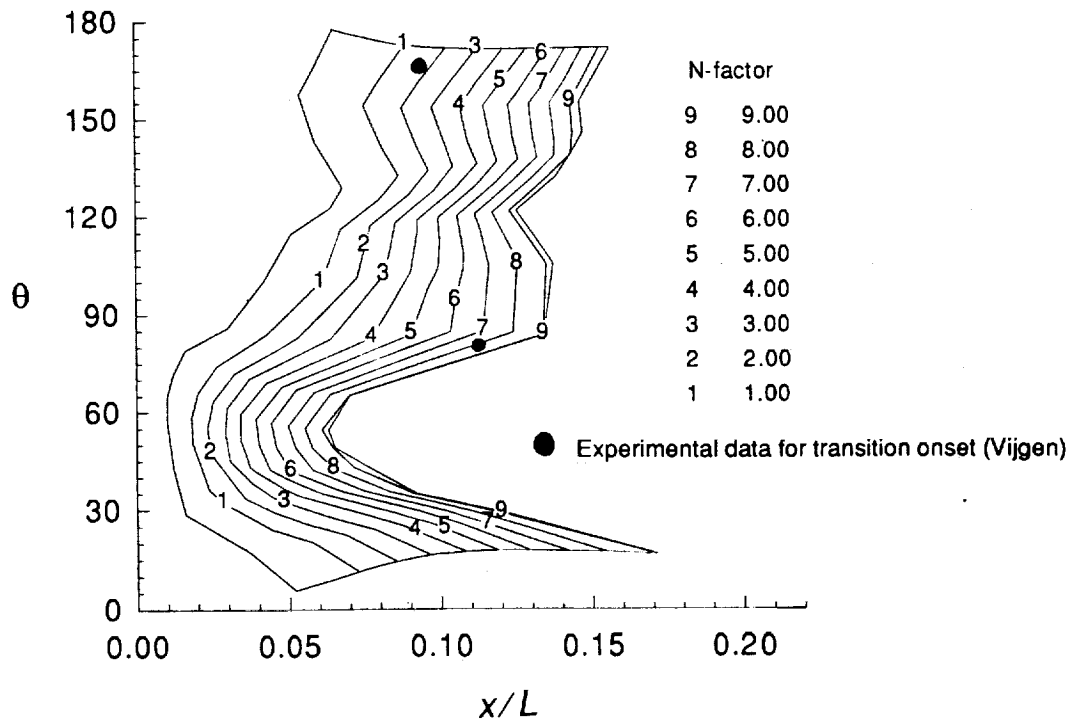
Crossflow Reynolds number distribution for Cessna fuselage. Contours levels over 200 omitted.



Cessna Fuselage
Contours of Constant N-Factors
 $Re/ft=1.3$ million, 0° Incidence

See discussion for previous slide.

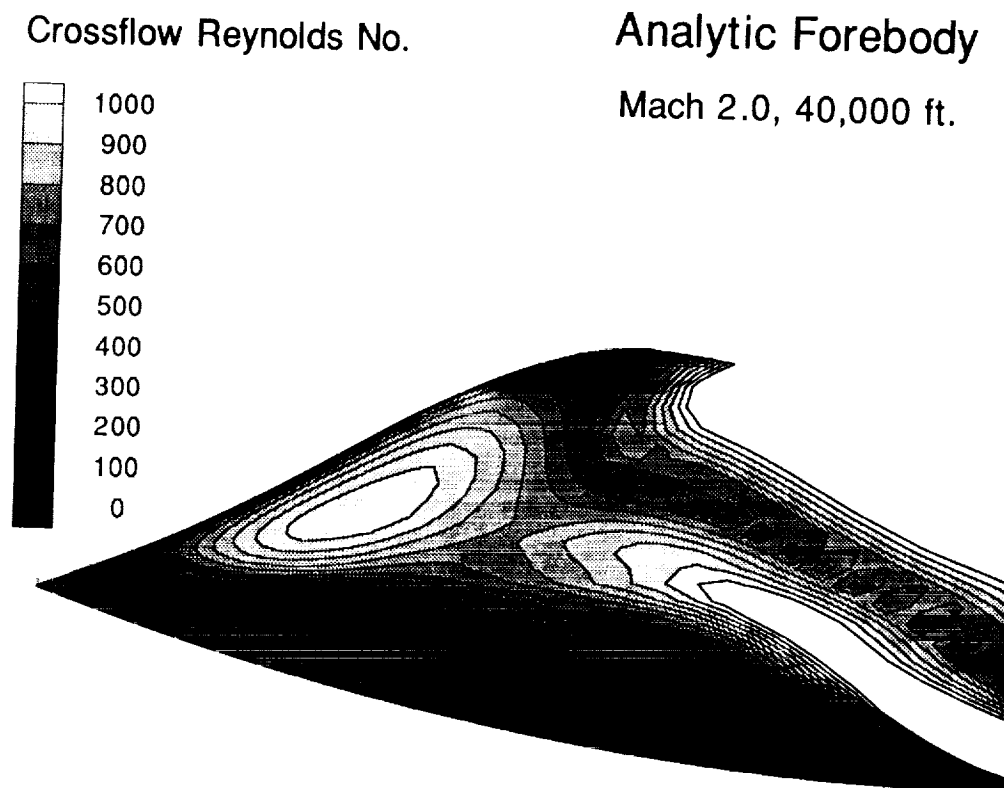
Cessna fuselage
 $Re/ft=1.3$ million, angle of attack = 0°
Contours of constant N-factors.



Crossflow Reynolds Number Distribution for Analytic Forebody

The linear stability of the Mach 2.0 flow over an analytic forebody configuration [4] is investigated. In this case, both first mode and crossflow instabilities are present in the boundary layer. Crossflow Reynolds numbers reach values of over 1000. From the correlation presented earlier, at Mach 2.0, one would expect $Re_{cf} \approx 360$ to represent an upper limit for possible laminar flow. N-factor calculations reveal that along the upper portion of the body, the transition process is likely to be crossflow dominated, since N reaches values of 10 when the crossflow Reynolds number reaches approximately 350. (Note that traces shown in any of the remaining figures represent disturbance trajectories which begin at $N=1$ and terminate at $N=10$.) Over the lower portion of the body, the value of the crossflow Reynolds number is in the range of 50-150 at the location where $N=10$. In this location we conclude that the most amplified disturbances reveal characteristics intermediate between crossflow and first mode instabilities.

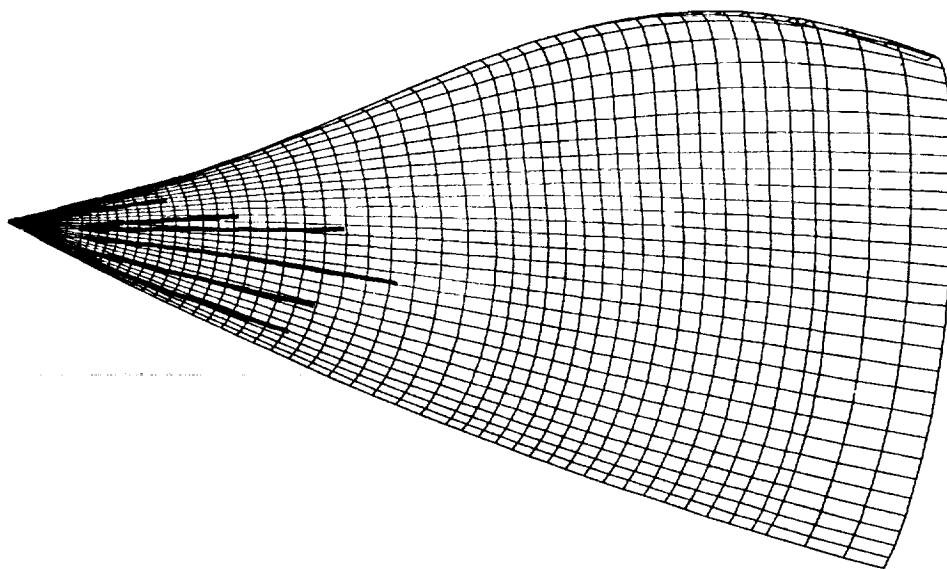
Crossflow Reynolds number distribution for Analytic Forebody. Contour levels above 1,000 omitted.



N-Factor Calculations for Analytic Forebody

See discussion for previous slide.

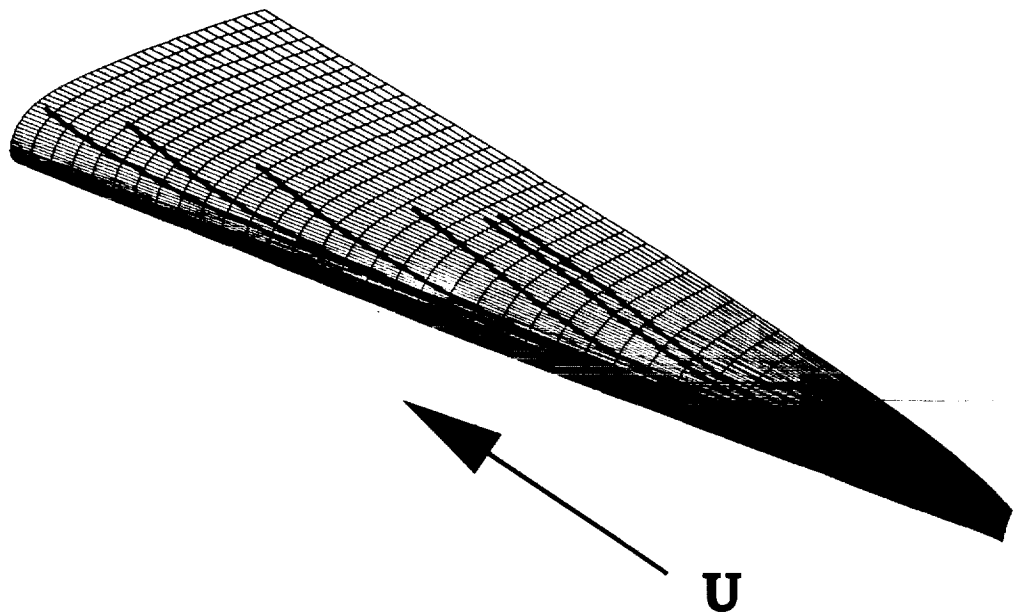
N-factor calculations for Analytic Forebody
Mach 2.0, Altitude=40,000 ft.



N-Factor Calculations for Swept Leading Edge Model for use in LARC Mach 3.5 Quiet Tunnel

Stability calculations for the flow over a highly swept leading edge model to be used for transition studies in the NASA Langley Mach 3.5 Low-disturbance Pilot Tunnel have been performed. The model is a representation of the leading edge of a laminar flow control wing for the F16-XL aircraft [5]. The traces shown in the figure represent disturbances of 40,000 Hz, and the wave angles and wavelengths (not shown) indicate the disturbances are primary of the crossflow type. Additional calculations performed for stationary disturbances resulted in maximum values of $N \approx 6$ at the end of the body.

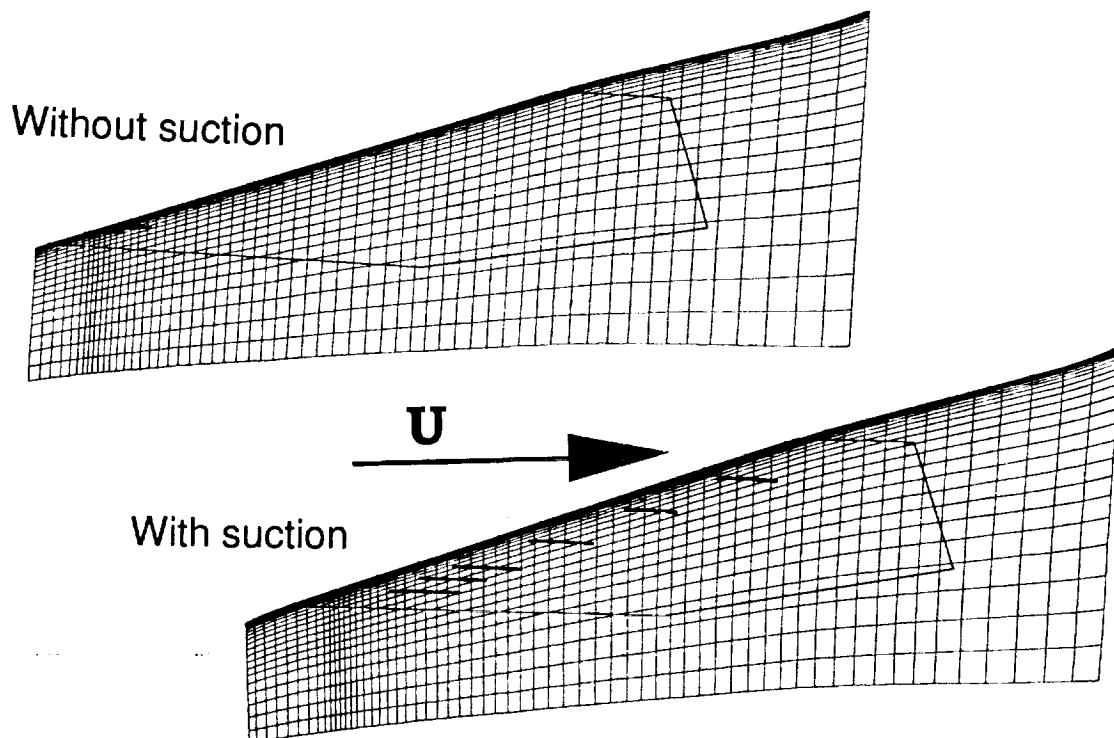
N-factor calculations for swept leading edge model to be utilized for transition studies in LARC Mach 3.5 Quiet Tunnel.



N-Factor Calculations for Laminar Flow Control Glove on F16XL Aircraft

Linear stability/N-factor calculations for the laminar flow glove region for the F16XL fighter aircraft, both with and without boundary-layer suction, have been performed. The results indicate that suction has a stabilizing influence on the boundary layer. The Mach number was 1.6, which indicates an upper limit on the crossflow Reynolds number of ≈ 300 . Contours of constant $Re_{cf} \approx 300$ correlate very well with values of $N=10$ from linear stability theory. To completely laminarize the glove region, surface contouring and/or additional suction will be required.

N-factor calculations for laminar flow control glove
on F16-XL aircraft.



Summary/Conclusions

- ▣ Completed stability calculations for
 - Low Speed:
 - Ellipsoid at incidence
 - General aviation fuselage
 - High Speed:
 - Analytic forebody
 - Leading edge configuration
 - F16XL laminar flow control glove area
- ▣ Linear stability theory/ e^N method offers a viable means towards estimating the location of the onset of transition over a wide speed range for both swept-wing and fuselage-type configurations.
- ▣ Effects of disturbance fields, surface roughness/waviness, etc. not accounted for but may be important (i.e. low value of N on top of Cessna fuselage).
- ▣ For high-speed flows, compressibility corrections allow for the use of a crossflow Reynolds number criterion in establishing an upper limit for laminar flow.

References

1. Mack, L.M., "Transition Prediction and Linear Stability Theory," in AGARD Conference Proceedings No. 224, pp. 1-22, NATO, Paris.
2. Meier, H.U. and Kreplin, H., "Experimental Investigation of the Boundary Layer Transition and Separation on a Body of Revolution," Zeitschrift Fur Flugwissenschaften und Weltraumforschung, Vol. 4, March/April 1980, pp. 65-71.
3. Vijgen, P., Incompressible Boundary-Layer Transition Flight Experiments Over a Nonaxisymmetric Fuselage Forebody and Comparisons with Laminar Boundary-Layer Stability Theory," Doctor of Engineering Dissertation, University of Kansas, December, 1988.
4. Townsend, J.C., Howell, D.T., Collins, I.K. and Hayes, C., "Surface Pressure Data on a Series of Analytic Forebodies at Mach Numbers From 1.7 to 4.5 and Combined Angles of Attack and Slideslip," NASA TM 80062, June 1979.
5. Dagenhart, J.R., Private Communication, Experimental Flow Physics Branch, NASA Langley Research Center, Hampton, VA.

THIS PAGE INTENTIONALLY BLANK

Session XIII. Supersonic Laminar Flow Control

omit

Supersonic HLFC: Potential Benefits and Technology Development Requirements
Frank Neumann, Boeing Commercial Airplane Group

PRECEDING PAGE BLANK NOT FILMED

THIS PAGE INTENTIONALLY BLANK

Supersonic HLFC: Potential Benefits and Technology Development Requirements

*NASA High-Speed Research Workshop
May 16, 1991
Boeing Commercial Airplane Group
Frank Neumann*

N94-33531

514-02
11989.

PRECEDING PAGE BLANK NOT FILMED

2003



THIS PAGE INTENTIONALLY BLANK

Supersonic HLFC: Potential Benefits and Technology Development Requirements

For the last three years Boeing has performed studies on the application of laminar flow control to HSCT configurations.

Large potential net benefits have been identified for laminar flow control, even after accounting for the significant implementation penalties.

However, the technical risks are high at this time, and an early, aggressive technology development program is required if LFC is to be incorporated in a year 2005 HSCT program. This presentation will address the benefits and the required development effort.

Potential Benefits of Laminarization on HSCT

Of all the aerodynamic advances that are being considered for the HSCT, LFC has the largest potential for improving the supersonic Lift/Drag ratio of a given configuration.

Improved L/D leads to reduced fuel consumption, reduced engine size and reduced gross weight; all of which improve economics.

Reduced fuel consumption means reduced emissions.

Reduced aerodynamic heating of the wing fuel tanks reduces tank insulation requirements on long supersonic flights.

Potential Benefits of Laminarization on HSCT

- Largest potential for improvement in L/D
- Reduced gross weight, engine size, and fuel burn improve economics
- Reduced fuel burn means reduced emissions
- Reduced aerodynamic heating
 - Reduced fuel heating rates
 - Possible structural benefits of lowered skin temperatures

HLFC ON HSCT - PAST BOEING/NASA LaRC STUDIES

The majority of the work accomplished to date was sponsored by NASA Langley under three successive tasks beginning in 1988.

The first task led to the identification of laminarization schemes, supersonic cruise performance benefits and research needs.

The second task addressed the use of the suction system to improve high lift performance during low speed climbout.

The third task addressed the use of the suction system to improve Mach 0.9 cruise performance. Also, economics and community noise impact were quantified.

The next three charts summarize the results of the three successive tasks.

HLFC on HSCT

Past Boeing/NASA LaRC Studies

1. Contract NAS1-15325 (FY '88)
 - Laminarization issues
 - Hybrid laminarization schemes
 - Initial performance benefits
 - Identification of research needs
2. Contract NAS1-18377 (FY '89)
 - Low-speed BLC requirements and compatibility with supersonic cruise HLFC system
 - Revised performance and economics
3. Contract NAS1-18377 (FY '90)
 - M = 0.9 cruise HLFC requirements and compatibility with supersonic cruise HLFC system
 - Performance, economics, and community noise

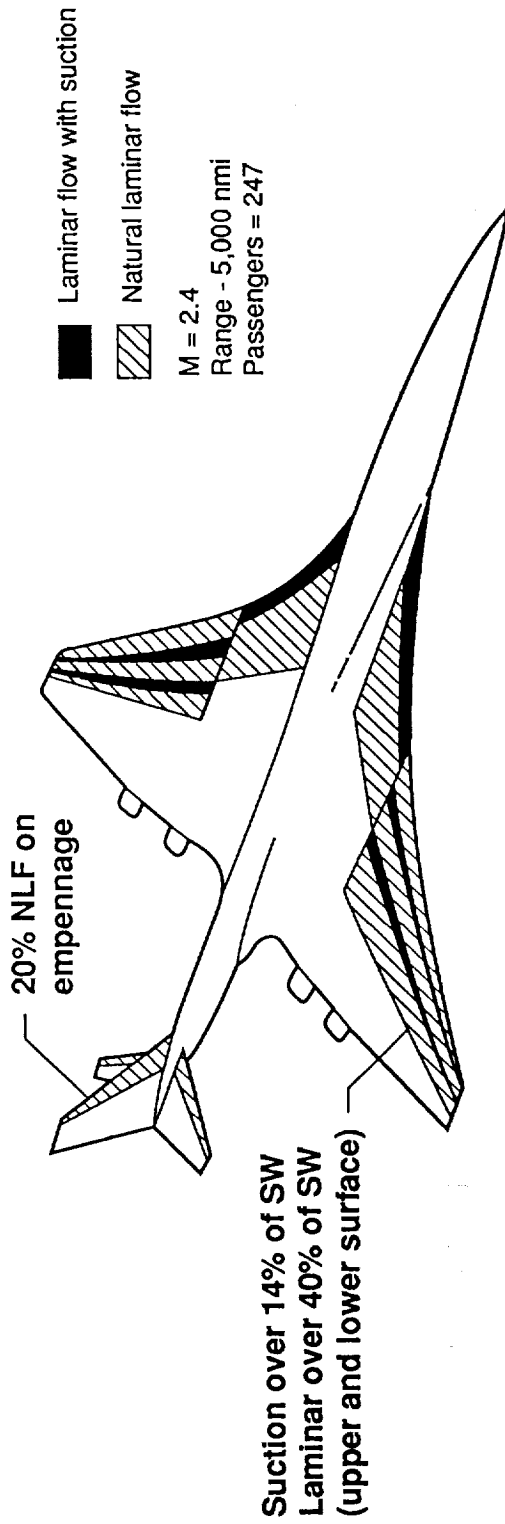
HLFC APPLICATION TO HSCT

The first task defined a HLFC scheme that accomplished a laminar flow run over 40% of the wing surface area; consisting of laminar flow regions with suction, as well as natural laminar flow regions.

The aerodynamic benefit is an impressive supersonic cruise drag reduction of 8.5%. There are significant implementation penalties, as shown. These penalties were identified as a result of indepth design studies. These penalties were accounted for when we determined the net performance benefits of HLFC. The additional maintenance cost is included in the economics. Net benefits are impressive as well.

The economic benefits are due mainly to the reduced fuel consumption.

HLFC Application to HSCCT



Aerodynamic benefit

- Cruise drag reduction: 8.5%

Implementation penalties

- System and structural weight increment: 8,000 lb (2.7% of OEW)
- System fuel displacement: 38,000 lb (10.3% of available fuel volume)
- Engine power extraction: 1,185 HP (0.4% TSFC penalty)
- Suction air momentum drag: 0.45 counts (0.4% of cruise drag)

Performance benefits

- MTOW reduction 5.5%
- OEW reduction 1.7%
- Engine size reduction 8.5%
- Block fuel reduction 10.0%

Economic benefit

- 18% reduction in surcharge required for 12% ROI

CRUISE HLFC/LOW SPEED BLC COMPATIBILITY

The achievement of laminar flow on HSCT upper and lower wing surfaces requires the elimination of steps, gaps and discontinuities.; hence a desire to eliminate moveable high lift devices on the leading edge.

Studies were performed on a wing with no leading edge devices on the inboard wing and simple hinged leading edge flaps on the outboard wing.

The supersonic HLFC suction system was employed in a low speed BLC mode to retain attached flow to yield high lift/drag ratios during high lift conditions; so important for low noise over the community.

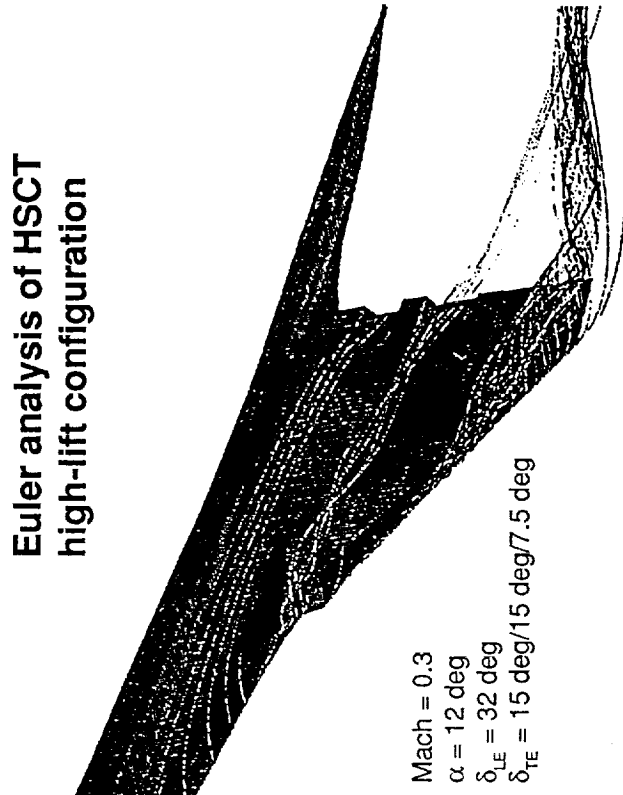
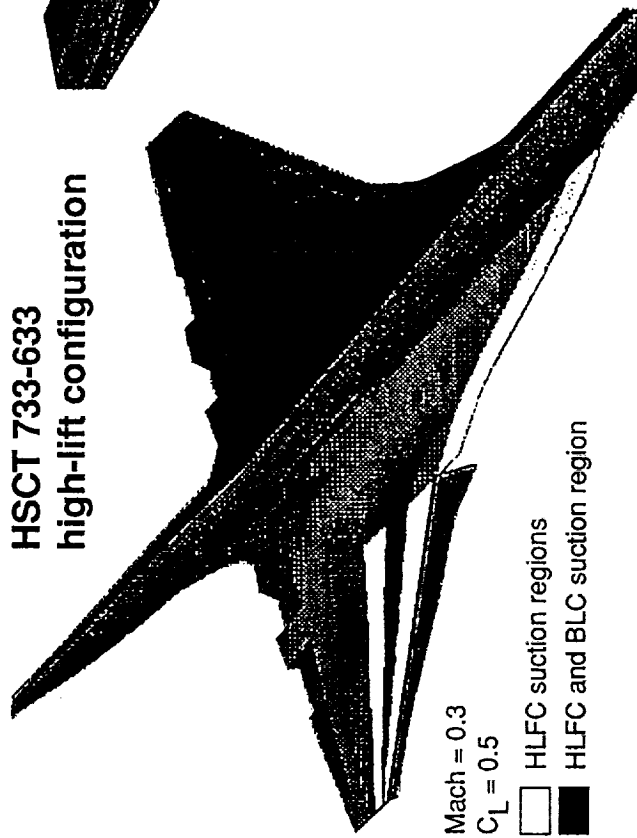
Engineering studies showed that the supersonic HLFC system can be operated at low speed to provide high lift suction BLC on the inboard wing leading edge and on the outboard wing leading edge flap hingeline.

Aerodynamic simulations showed the potential for achieving attached flow with the use of high lift suction BLC and corresponding improvements in lift/drag ratio of 10%.

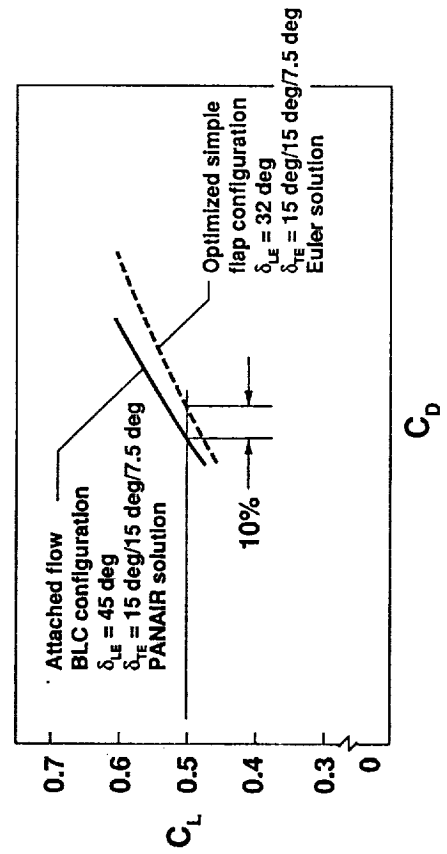
The improvement in lift/drag ratio ,in turn, reduces community noise to the same level that was achieved previously with full-span leading edge flaps, before HLFC was added.

Hence the added cost of the HLFC system is partly offset by a simpler high-lift flap system.

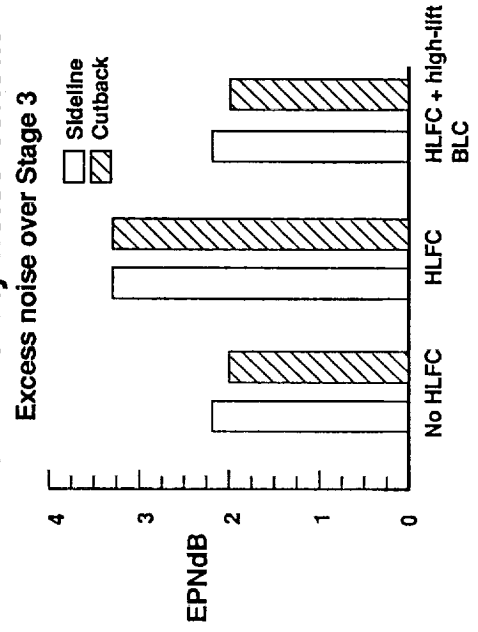
Cruise HLFc/Low-Speed High-Lift BLC Compatibility



High-lift benefit



Community noise benefit



IMPACT OF M 0.9 HLFC AND HIGH LIFT BLC

The illustrations in the upper half of the Figure show the operation of the suction system in the three modes investigated: mach 2.4 cruise, mach 0.9 cruise and mach 0.3 high-lift BLC. Using the suction system during mach 0.9 cruise showed only minor benefits. The primary reason being that drag benefits due to changing wing camber through leading edge flap deflection outweigh the drag benefits due to laminar flow; which can only be achieved with flaps retracted.

Essentially no change occurred in airplane MTOW and block fuel, as indicated by the small differences between the second and third bars in the barcharts.

Figure 1: Comparison of cruise lift and fuel consumption for the 1080-860TF, 1080-860TR, and 1080-861.

Legend:
 Laminar flow with suction (Solid black)
 Natural laminar flow (Hatched)

Airfoil Cross-Sections:
 - **M = 0.3 High lift/BLC:** Shows BLC suction on the upper surface.
 - **M = 0.9 Cruise HLFC:** Shows HLFC on the upper surface.
 - **M = 2.4 Cruise HLFC:** Shows HLFC on the upper surface.

Bar Charts (MTOW in '000 lb):

- Design mission supersonic (~5,000-nmi range):**
 - 1080-861 No HLFC: ~285
 - 1080-860TR HLFC: ~255 (5.6% Block fuel)
 - 1080-860TF HLFC subsonic and supersonic + high-lift BLC: ~250 (10.03% Block fuel)
- Mixed mode mission subsonic and supersonic (~3,450-nmi range):**
 - 1080-861 No HLFC: ~190
 - 1080-860TR HLFC: ~175 (7.45% Block fuel)
 - 1080-860TF HLFC subsonic and supersonic + high-lift BLC: ~170 (7.54% Block fuel)

CONCLUSIONS TO DATE

Read words on chart

This concludes the first part of the presentation. The second part focuses on the R&D effort required to mature the LFC technology to the level where it could be considered for incorporation into the HSCT.

Conclusions to Date

Implementation studies on HSCT show:

- Net benefits in terms of reduced MTOW, OEW, fuel burn, engine size, and fuel heating rates are impressive
- Performance benefits outweigh cost penalties for HLFC system and maintenance to yield significant net economic benefit
- Benefits increase with increasing design range
- Annual fuel savings are five times greater than on subsonic aircraft
- Significant R&D effort needed in aerodynamics, structures, manufacturing, and systems technologies to attain level of practical implementation

REQUIREMENTS FOR PRODUCTION COMMITMENT

Before any airplane manufacturer commits a high risk technology, like laminar flow control, to a production program, a demanding set of requirements must be satisfied.

For example, we must have in hand hard data that prove not only that we can make an efficient design but also that this design is producible, certifiable and cost effective to own and operate.

To do that we must have in hand the capability to predict performance benefits and penalties, the airplane's useful life, production costs and schedules, maintenance and repair costs, to name but a few. These are reasonable requirements, given the uncertainties of a complex new system like HLFC.

The task before us is to define and perform a risk reduction program at the conclusion of which we will have met the majority of these requirements.

Requirements for Production Commitment

Must have in hand:

- Capability for making an efficient, producible, certifiable, cost-effective design
- Capability to predict performance benefits and penalties
- Design criteria and allowables
- Capability for predicting the airplanes' useful life
- Capability for predicting production cost and schedules
- Capability for predicting maintenance and repair costs
- Satisfactory production processes
- Production facility requirements
- Airline acceptance

HSCT - HLFC RISK REDUCTION PROGRAM

Illustrated here is a typical risk reduction program. A step-by-step systematic approach to develop the critical technologies, and to reduce the technical risk. With each successive step the risk is gradually reduced until it reaches the low risk level required for incorporation into the HSCT, prior to configuration freeze.

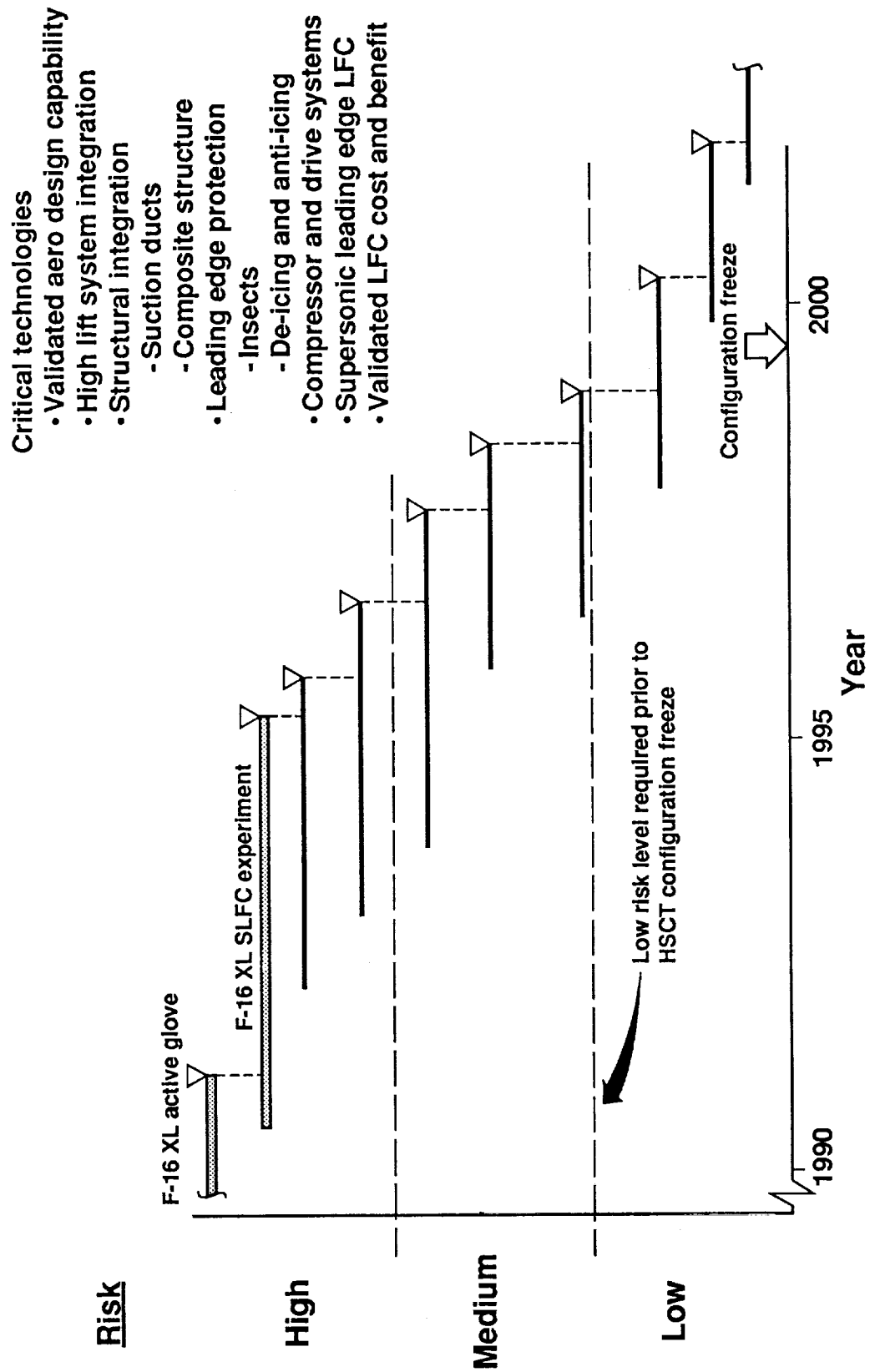
The F-16XL supersonic aerodynamic experiment is but one important element; it does not address many of the other critical technology issues, such as high lift system integration, structural integration, compressor and drive system, that will be required on the HSCT.

The message here is that: 1) a lot of work needs to be done in a relatively short time, 2) the F-16XL experiment needs to be accelerated, and 3) other critical technologies need to be developed in parallel.

In the following charts we will give you our views on the required development program.

HSCT-LFC

Risk Reduction Program



FUTURE DIRECTIONS IN LAMINAR FLOW APPLICATIONS

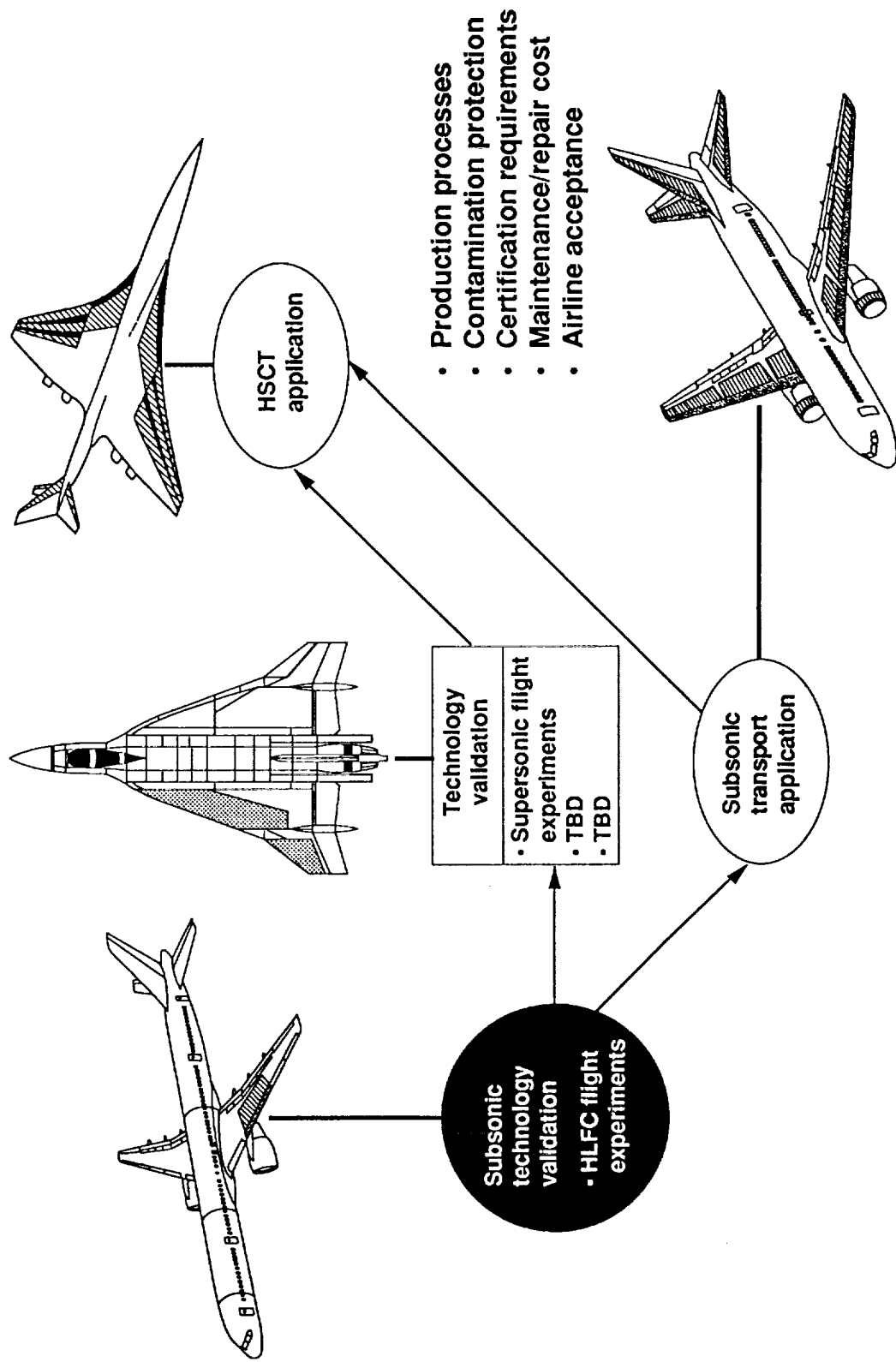
We believe fantastic progress has been made towards applying laminar flow control to commercial transport by the very successful 757 HLFC flight experiment. For example, we have successfully drilled millions of holes with laser beams, formed and bonded large titanium panels and achieved longer laminar runs than predicted with reduced suction requirements.

More development will be required and is being planned to prepare for subsonic transport application of HLFC.

The supersonic technology validation program has to clear similar hurdles, because many of the integration problems are unique to the HSCT application.

However, in many cases the subsonic transport application will pave the way for supersonic application. For example, the experience gained in titanium perforation processes, contamination protection, certification, maintenance, repair and airline acceptance will be transferrable to HSCT.

Future Directions in Laminar Flow Applications



SUPERSONIC HLFC DEVELOPMENT PLANNING

We would like to offer to you our recommendations for a NASA/Industry risk reduction program, that would develop HLFC technology for possible incorporation into a year 2005 HSCT program, year 2000 configuration freeze.

Supersonic HLFC Development Planning

- Define a NASA/industry risk reduction program that would develop HLFC technology for possible incorporation in a year 2005 HSCT program (year 2000 configuration freeze)
- Near-term workshop at Langley to coordinate the planning process

PLANNING GROUND RULES

The plan was laid out using the ground rules summarized in this chart

read chart

Planning Ground Rules

- Satisfy requirements for production commitment by 1999 (prior to configuration freeze)
- Address technical issues first—do not pace development by availability of people and resources
- Schedule for most rapid technical progress possible
- F-16XL aircraft available for flight experiments

PLAN ELEMENTS

We have addressed:

read chart

We have yet to address:

Priorities and decision gates

Resource estimates

Plan Elements

- Technology development
 - Aerodynamics
 - Systems
 - Structures
 - Manufacturing
 - HSCT airplane design studies
 - Hardware demonstrations
 - Ground
 - Flight
-
- Priorities and decision gates (TBD)
 - Resource estimates (TBD)

AERODYNAMIC TECHNOLOGY

The objectives of the risk reduction program in aerodynamic technology, in broad terms, are summarized here:

We need to improve and validate prediction methods for transition and suction requirements in order to meet the next objective:

Optimization of airfoil and wing design, considering laminar flow requirements, to achieve maximum drag reduction with the least amount of suction.

The achievement of laminar flow and high-lift must go hand in hand. The objective is to develop and validate a laminar flow/high-lift compatible aerodynamic system.

Aerodynamic Technology

Objectives:

- Improve and validate prediction methods for transition and suction requirements
- Optimize airfoil/wing design, considering laminar flow requirements
- Validate laminar flow/high-lift compatibility
- Understand HLFC impact upon HSCT stability and control

LAMINAR FLOW/HIGH - LIFT INTEGRATION

As pointed out earlier, studies at Boeing to date indicate that an aerodynamic concept for achievement of laminar flow and high-lift might use the following approach:

- 1) on the subsonic, inboard portion of the wing-a blunt leading edge without flaps. At high angles-of-attack attached flow is maintained through suction BLC at the leading edge
- 2) on the supersonic, outboard portion of the wing- a sharp leading edge with simple hinged flaps. At high angles-of-attack attached flow is maintained through suction BLC at the hingeline.

The technical issues to be solved during the risk reduction program are:

read chart

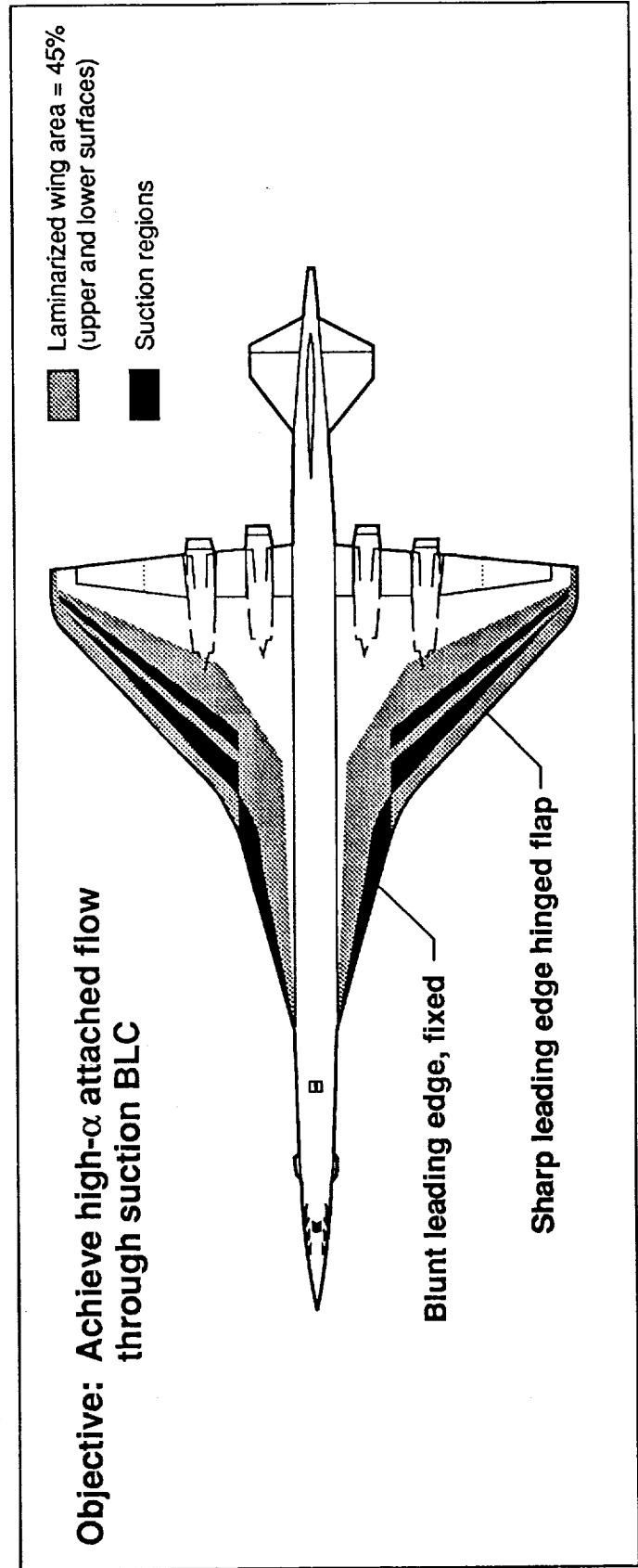
We are proposing incremental modifications of F-16 XL aircraft-beyond the planned extended suction glove experiment- for HLFC and high-lift compatibility experiments.

Laminar Flow/High Lift Integration

Issues:

- Leading edge radius and camber
- Suction for LFC and separation control
- Impact of hinge lines, steps, and gaps
- Insect protection, anti-ice, de-ice
- Subsystem design
- Subsystems compatibility

~~Q.S.~~



F 16-XL MODIFICATIONS FOR HLFC AND HIGH-LIFT EXPERIMENTS

We do not expect the HSCT wing planform to have the F-16 XL "S" curve in the apex region. We propose supersonic HLFC experiments on the F-16XL, depicted on the left of the Figure, which would eliminate the "S" curve by extending the suction glove to the side of the fuselage. In addition, a suction glove could be added to the supersonic, sharp leading edge, outboard wing for follow-on experiments

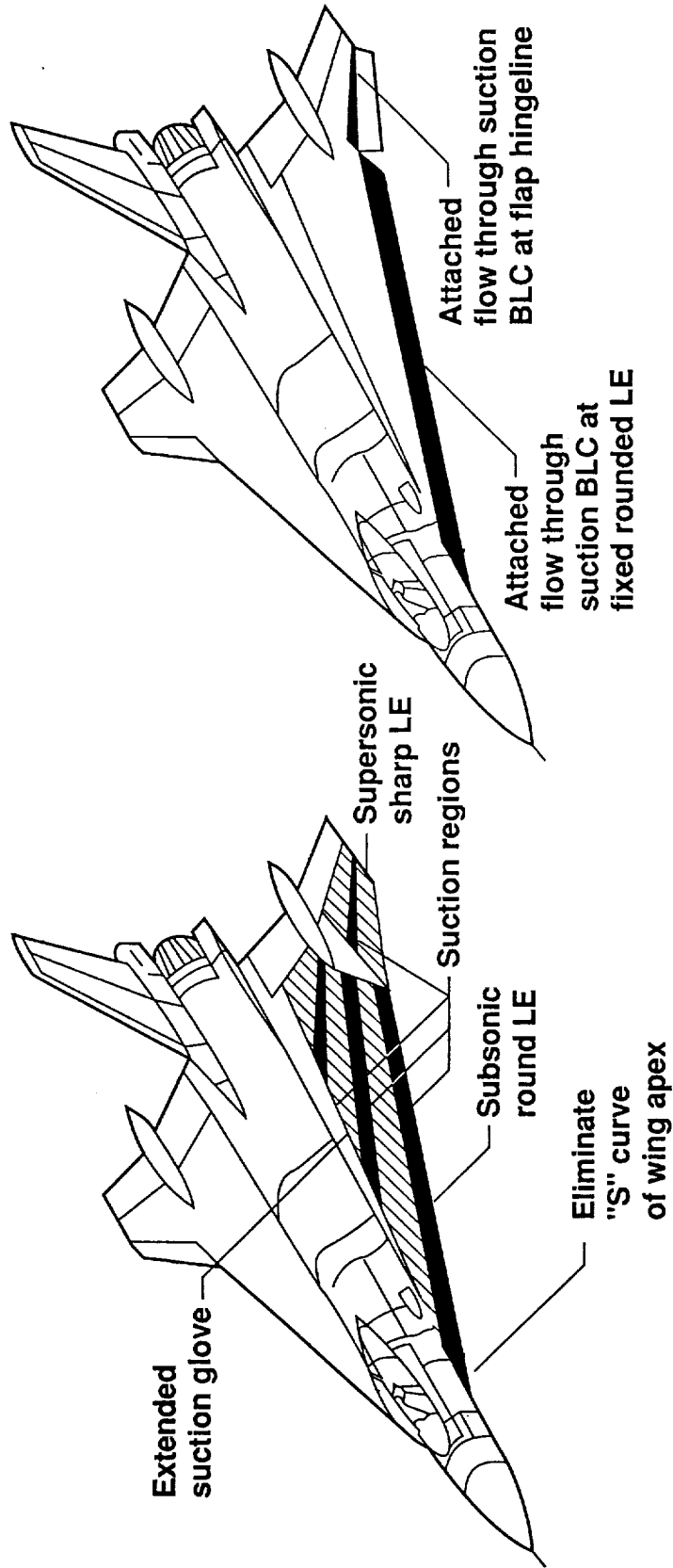
Flight demonstration of the modified glove and suction system in the high-lift mode is illustrated on the right side of the Figure. The HLFC suction system would be designed and operated in the high-lift BLC mode to demonstrate the ability to maintain attached flow.

C-27

F-16 XL Modifications for HLFC and High-Lift Experiments

HLFC mode  High-lift BLC mode

Establish technology compatibility



INTEGRATED SCHEDULE-HLFC/HIGH-LIFT EXPERIMENT

Here is our view of an integrated schedule for HLFC/high-lift experiments.

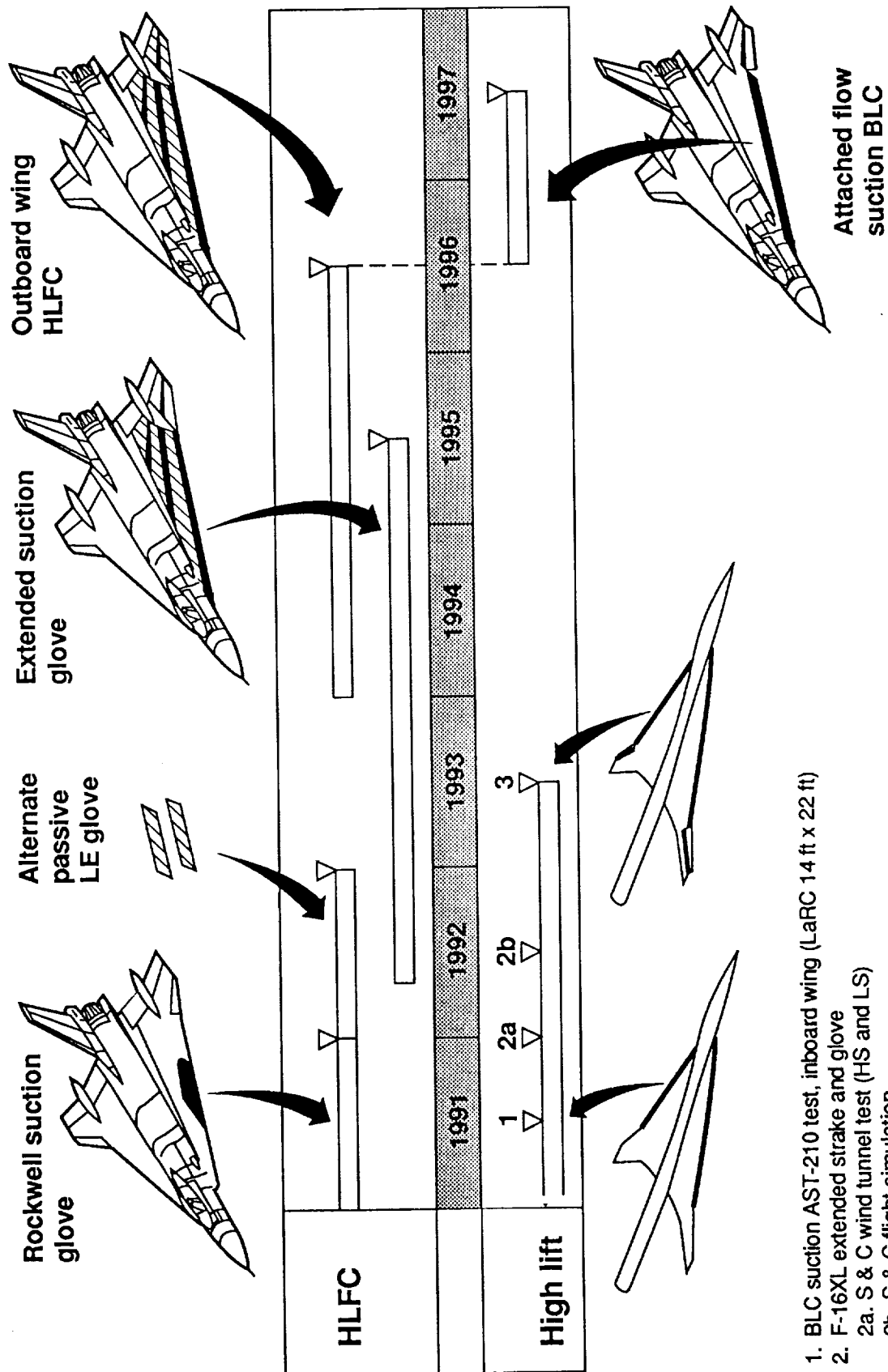
Some of the experiments are already planned by NASA, but they remain to be finalized and accelerated. HLFC experiments include:

- additional experiments on ship 1
- experiments with alternate passive gloves
- F-16 XL extended suction glove experiments, and
- additional proposed experiments to laminarize the outboard wing, and the elimination of the "S" curve, in case that cannot be accomplished in connection with the planned extended suction glove experiment.

A high-lift experiment already planned is a BLC suction test on the inboard wing of a modified AST-210 model (milestone 1). A BLC suction test on the inboard & outboard wing of the same model (milestone 3) should also be conducted.

Milestone 2a indicates the need for F-16 XL high speed and low speed wind tunnel tests with the extended suction glove; and milestone 2b indicates the need for flight simulations.

Integrated Schedule, HLFC/High-Lift Experiment



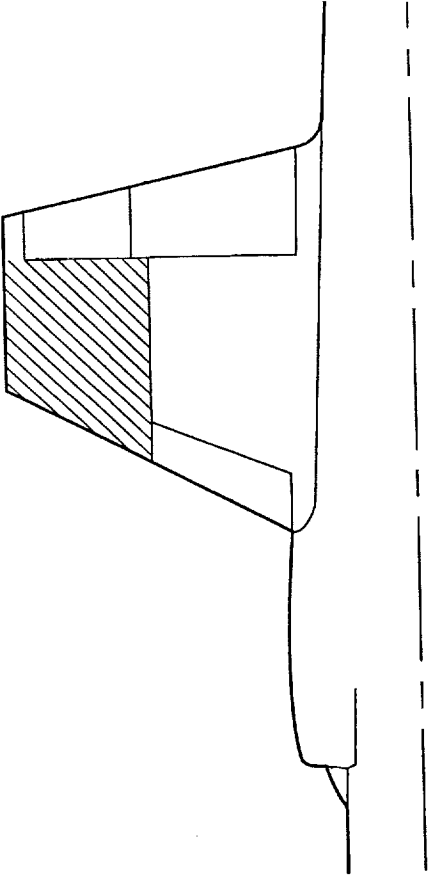
1. BLC suction AST-210 test, inboard wing (LaRC 14 ft x 22 ft)
2. F-16XL extended strake and glove
 - 2a. S & C wind tunnel test (HS and LS)
 - 2b. S & C flight simulation
3. BLC suction AST-210 test, inboard and outboard wing (LaRC 14 ft x 22 ft)

ADDITIONAL AERODYNAMIC EXPERIMENTS

We have identified the need for at least three additional aerodynamic experiments:

- 1) a high speed pressure model test for the purpose of validating CFD codes for wing cp prediction.
- 2) a high speed test of an HSCT model where the wing has been optimized for HLFC. Comparison with test data for a baseline non-HLFC wing design would yield the incremental drag due-to-lift and wave drag, if any.
- 3) a flight test on the F-104 supersonic leading edge wing (in case that cannot be accomplished on the F-16 XL) for the purpose of obtaining 3D supersonic boundary layer transition data to calibrate boundary layer stability codes.

Additional Aerodynamic Experiments

Experiment	Purpose
High-speed pressure model test (LaRC unitary plan)	Validate CFD codes for wing C_p prediction
High-speed test of HSCT model with wing optimized for HLFC (LaRC unitary plan)	Determine impact on drag due to lift and wave drag
F-104 laminar flow flight test 	NLF and HLFC tests on supersonic leading-edge wing to calibrate stability codes

SUB-SYSTEMS TECHNOLOGY

The challenge facing us in the sub-systems technology area is to minimize the penalties associated with providing the HLFC capability. Hence, the objective is to integrate the HLFC system functions with other system functions on HSCT as much as possible.

To meet this objective the following major issues need to be addressed through design, analyses and experiments:

- 1) flow control to provide optimum flow distribution for LFC, high-lift BLC, anti-ice and insect protection. The former two will be accomplished through appropriate suction control. The latter two can be accomplished, possibly, through "glycol-sweating". All four using the same flutes and skin perforations.
- 2) another issue is the integration of the extensive ducting system with load carrying wing structure to minimize the parasitic weight increment.
- 3) an intriguing idea is to integrate the air cycle machinery for the LFC and the Environmental Control System (ECS) to minimize system duplication, power extraction and power transmission losses. It is expected that novel integrated system architectures can be evolved as we intensify our studies on HSCT during the coming years.

Ground test requirements will need to be defined to demonstrate the new multi-function subsystem capability. Appropriate hardware-in-the-loop ground tests will need to be designed and conducted with support from suppliers.

Subsystems Technology

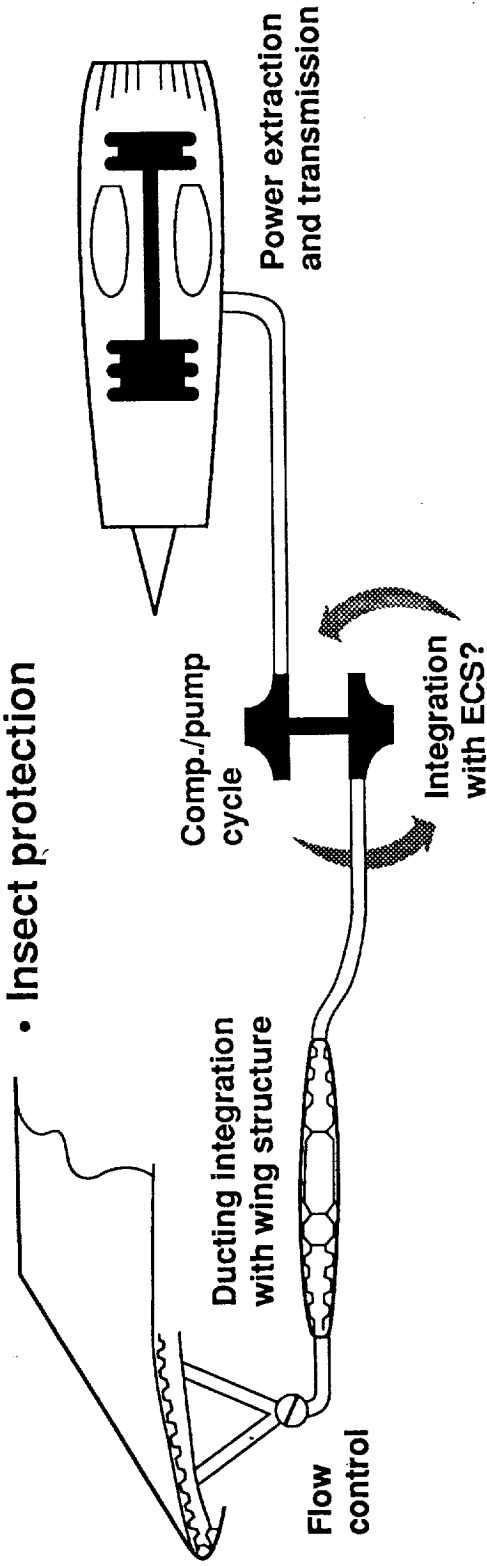
Objective:

- Integrate HLFC system requirements with other system functions on HSCT to minimize implementation penalties

Issues:

Optimum flow distribution

- LFC function
- High-lift BLC
- Anti-ice
- Insect protection



Integrated system architecture trades				Detail plan for integrated system ground test			F-16XL flight test			Integrated system ground test complete	
1992	1993	1994	1995	1996	1997	1998	HLFC	BLC	high lift	Integrated system test buildup	1998
▽		▽	▽	▽	▽	▽				▽	

STRUCTURES AND MANUFACTURING TECHNOLOGY

A substantial risk reduction program will be required in structures and manufacturing technology. Whereas on subsonic applications like 757, the suction panels and ducting are located in the wing leading edge region, on the HSCT the suction panels and ducting may have to coexist with wing fuel tanks. On the outboard wing, in addition, these systems have to be integrated into thin, highly loaded primary wing structure.

Hence, the objectives of the risk reduction program will be to validate the integration of the HLFC system with primary wing structure; and to establish weight and cost parameters.

The proposed approach is to build a multi-cell wing box section representative of the outboard wing with suction panels in the fuel tank area. Perform ground tests to validate static and fatigue performance, functional compatibility of the HLFC - and fuel systems, and to demonstrate maintenance and repair approaches.

Some of the intermediate steps along the way are illustrated on the schedule.

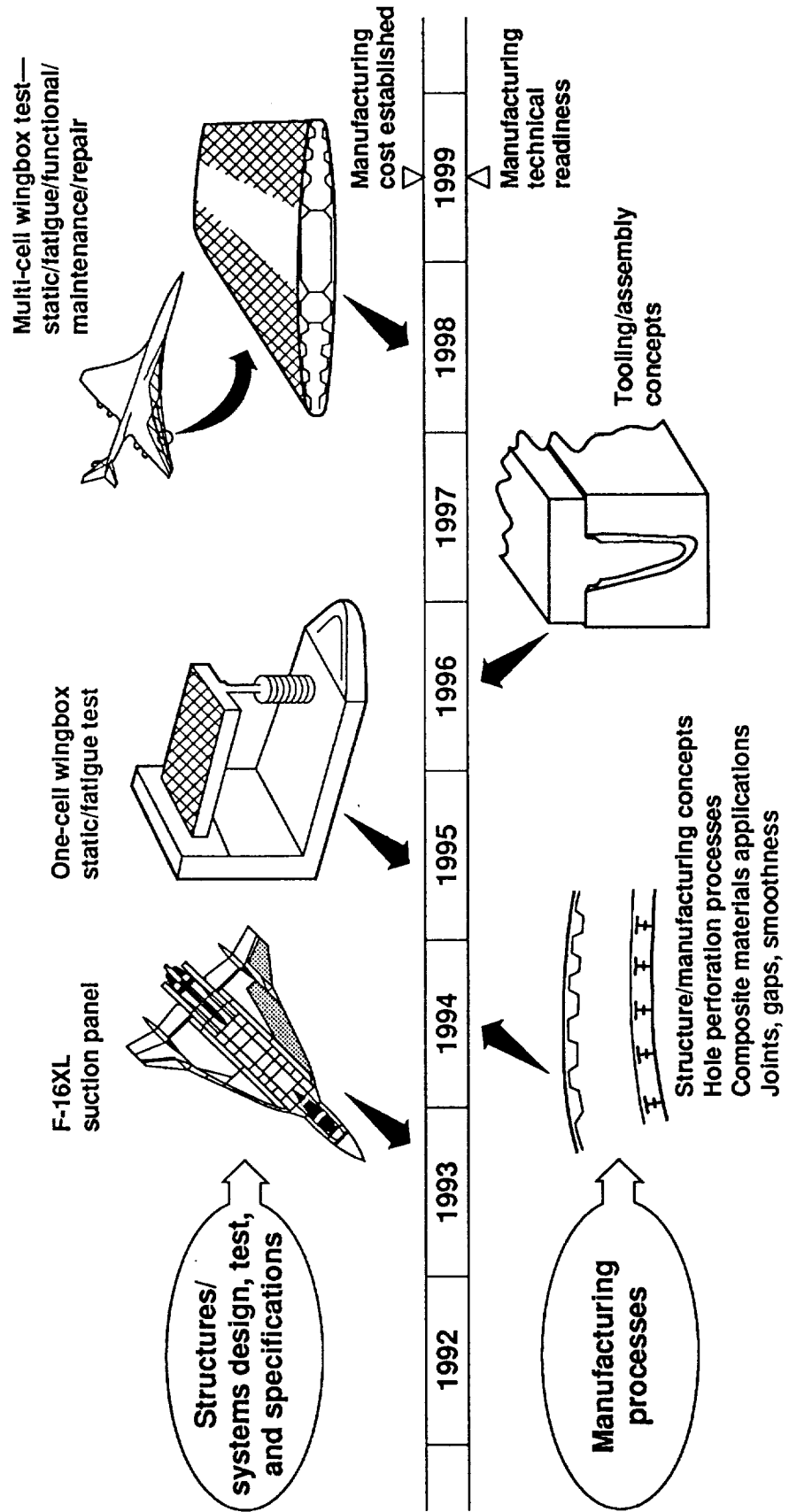
Structures and Manufacturing Technology

Objective:

- Validate integration of HLFC with primary wing structure
- Establish weight and cost parameters

Approach:

- Build a multi-cell wing box section with suction belts in tank area
- Ground test – static/fatigue/functional/maintenance



HSCT AIRPLANE DESIGN STUDIES

The objectives of concurrent airplane design studies are to develop the best possible HSCT configuration that derives maximum benefits from incorporation of HLFC.

In addition, airplane design studies are essential for:

- providing a focus and direction for HLFC technology development
- and to evaluate net performance and economic benefits

Earlier during this presentation we showed the benefits of HLFC on the initial HSCT concept which is illustrated in the Figure.

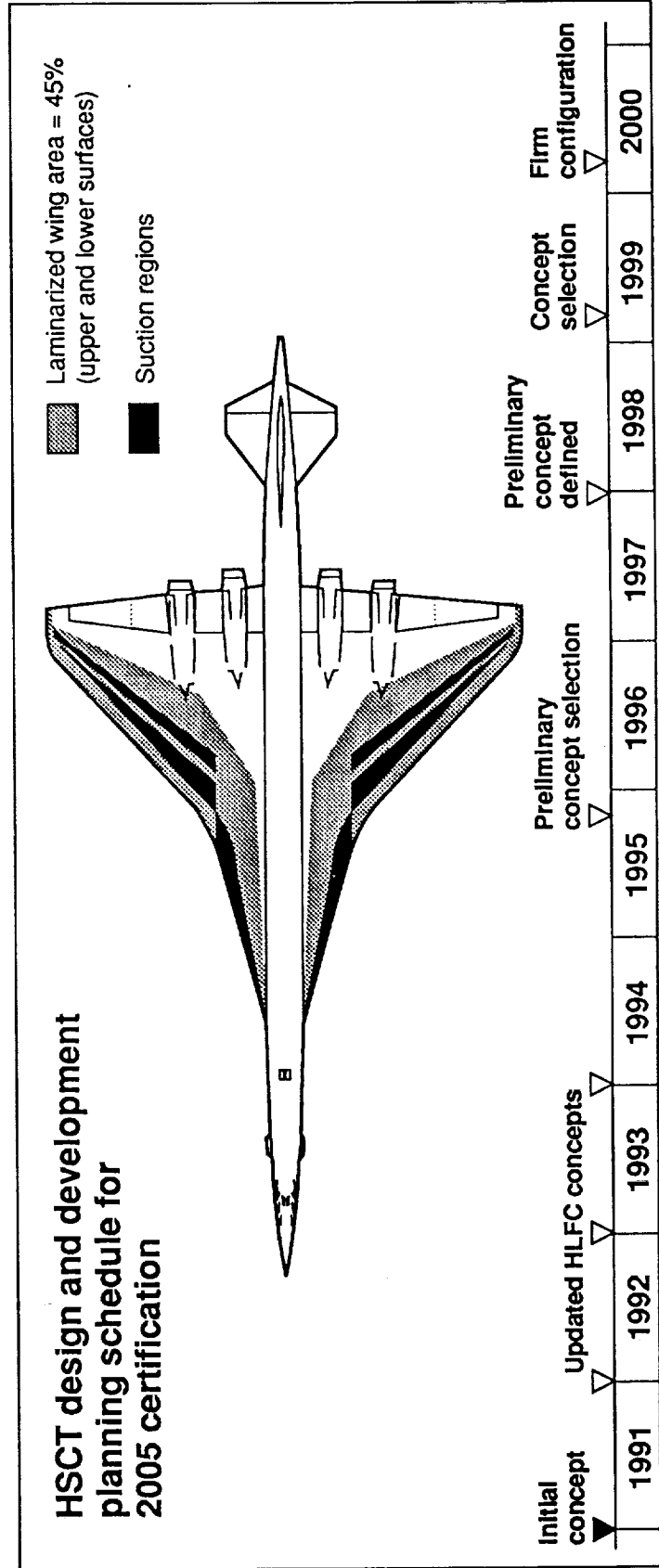
Currently, we are investigating HLFC on an updated HSCT configuration, which has a smaller supersonic leading edge outboard wing panel. Comparing results of the two studies will provide guidance on how to tailor configuration elements, such as the wing, for further improvements of the HSCT configuration

Key HSCT program decision gates relating to airplane concept selection, according to the current Boeing schedule, will occur between 1995 and 1999. If HLFC is to be aboard the selected airplane concept, risk reduction programs as outlined on the previous charts must have been completed successfully during that time period.

HSCT Airplane Design Studies

Objectives:

- Provide focus and direction for HLFC research
- Develop and evaluate HLFC integration concepts (Aero, Structures, Systems, Manufacturing)
- Minimize HLFC implementation penalties
- Develop best HSCT configuration with HLFC
- Evaluate net performance and economic benefits



SUMMARY AND RECOMMENDATIONS

Results of HLFC studies to date have shown that the technology has very high leverage on improving HSCT economic viability.

However, technical risk is high at this time, and an aggressive risk reduction program is required. The elements of the required risk reduction program have been outlined in this paper.

It is recommended that a NASA/Industry study group be formed and tasked to prepare a plan for such a risk reduction program by the end of 1991.

F-16 XL experiments have been identified that offer opportunities for accelerated validation of HLFC benefits

Summary and Recommendations

- LFC is a high-leverage technology for HSCT
- Technical risk is high; an aggressive risk reduction program is required to meet HSCT program schedule
- A NASA/industry study group should prepare a program plan in 1991
- F-16XL experiments offer an opportunity for accelerated validation of LFC benefits

THIS PAGE INTENTIONALLY BLANK

REPORT DOCUMENTATION PAGE			Form Approved OMB No. 0704-0188	
Public reporting burden for this collection of information is estimated to average 1 hour per response, including the time for reviewing instructions, searching existing data sources, gathering and maintaining the data needed, and completing and reviewing the collection of information. Send comments regarding this burden estimate or any other aspect of this collection of information, including suggestions for reducing this burden, to Washington Headquarters Services, Directorate for Information Operations and Reports, 1215 Jefferson Davis Highway, Suite 1204, Arlington, VA 22202-4302, and to the Office of Management and Budget, Paperwork Reduction Project (0704-0188), Washington, DC 20503.				
1. AGENCY USE ONLY (Leave blank)		2. REPORT DATE April 1992	3. REPORT TYPE AND DATES COVERED Conference Publication	
4. TITLE AND SUBTITLE First Annual High-Speed Research Workshop			5. FUNDING NUMBERS WU 537-01-22-01	
6. AUTHOR(S) Allen H. Whitehead, Jr., Compiler				
7. PERFORMING ORGANIZATION NAME(S) AND ADDRESS(ES) NASA Langley Research Center Hampton, VA 23665-5225			8. PERFORMING ORGANIZATION REPORT NUMBER	
9. SPONSORING/MONITORING AGENCY NAME(S) AND ADDRESS(ES) National Aeronautics and Space Administration Washington, DC 20546-0001			10. SPONSORING/MONITORING AGENCY REPORT NUMBER NASA CP-10087, Part 4	
11. SUPPLEMENTARY NOTES				
12a. DISTRIBUTION / AVAILABILITY STATEMENT LIMITED DISTRIBUTION until April 30, 1994 Subject Category 02			12b. DISTRIBUTION CODE	
13. ABSTRACT (Maximum 200 words) This publication is in four volumes and represents the compilation of papers presented at the First Annual High-Speed Research Workshop held in Williamsburg, Virginia, on May 14-16, 1991. This NASA-sponsored workshop provided a national forum for presenting and discussing important technology issues related to the definition of an economically viable, and environmentally compatible High-Speed Civil Transport. The Workshop and this publication are organized into 13 sessions, with Session 1 presenting NASA and Industry overviews of the High-Speed Civil Transport Program. The remaining sessions are developed around the technical components of NASA's Phase I High-Speed Research Program, which addresses the environmental issues of atmospheric emissions, community noise and sonic boom. Because of the criticality of the materials and structures technology area, and the long-term nature of the supporting research requirements, a session was added in this area to capture the ongoing work at NASA Lewis and NASA Langley and within industry.				
14. SUBJECT TERMS atmospheric science, high lift, laminar flow control, sonic boom, aeroacoustics, supersonic transport, ozone, community noise			15. NUMBER OF PAGES 415	
			16. PRICE CODE	
17. SECURITY CLASSIFICATION OF REPORT Unclassified	18. SECURITY CLASSIFICATION OF THIS PAGE Unclassified	19. SECURITY CLASSIFICATION OF ABSTRACT	20. [REDACTED]	

NSN 7540-01-280-5500

*U.S. GOVERNMENT PRINTING OFFICE: 1992-627-0646028

Standard Form 298 (Rev. 2-89)
Prescribed by ANSI Std. Z39-18
298-102

PRECEDING PAGE BLANK NOT FILMED

SECRET